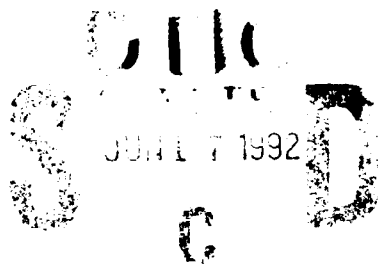


WL-TR-91-3022

**AD-A251 659**



# **FINITE ELEMENT ANALYSIS OF FREE-EDGE DELAMINATION IN LAMINATED COMPOSITE SPECIMENS**

R.S. Sandhu, W.E. Wolfe, R.L. Sierakowski, C.C. Chang and H.R. Chu  
Department of Civil Engineering  
The Ohio State University  
1960 Kenny Road  
Columbus, Ohio 43212

June 18, 1991

Final Report for Period July 1985 - June 1990

Approved for public release; distribution unlimited

FLIGHT DYNAMICS DIRECTORATE  
WRIGHT LABORATORY  
AIR FORCE SYSTEMS COMMAND  
WRIGHT-PATTERSON AIR FORCE BASE, OHIO 45433-6553

**92-15749**

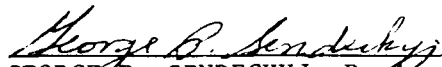


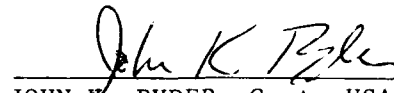
## NOTICE

When Government drawings, specifications, or other data are used for any purpose other than in connection with a definitely Government-related procurement, the United States Government incurs no responsibility or any obligation whatsoever. The fact that the Government may have formulated or in any way supplied the said drawings, specifications, or other data, is not to be regarded by implication, or otherwise in any manner construed, as licensing the holder, or any other person or corporation; or as conveying any rights or permission to manufacture, use, or sell any patented invention that may in any way be related thereto.

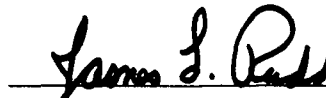
This report is releasable to the National Technical Information Service (NTIS). At NTIS, it will be available to the general public, including foreign nations.

This technical report has been reviewed and is approved for publication.

  
GEORGE P. SENDECKYJ, Project Engineer  
Fatigue, Fracture and Reliability Gp  
Structural Integrity Branch

  
JOHN K. RYDER, Capt, USAF  
Technical Manager  
Fatigue, Fracture and Reliability Gp  
Structural Integrity Branch

FOR THE COMMANDER

  
JAMES L. RUDD, Chief  
Structural Integrity Branch  
Structures Division

If your address has changed, if you wish to be removed from our mailing list, or if the addressee is no longer employed by your organization, please notify WL/FIBEC, WPAFB, OH 45433-6553 to help us maintain a current mailing list.

Copies of this report should not be returned unless return is required by security considerations, contractual obligations, or notice on a specific document.

# REPORT DOCUMENTATION PAGE

Form Approved  
OMB No. 0704-0188

1. REPORT SECURITY CLASSIFICATION Unclassified			1b. RESTRICTIVE MARKINGS None			
2. SECURITY CLASSIFICATION AUTHORITY			3. DISTRIBUTION / AVAILABILITY OF REPORT  Approved for public release; distribution unlimited			
3. DECLASSIFICATION / DOWNGRADING SCHEDULE						
PERFORMING ORGANIZATION REPORT NUMBER(S)			5. MONITORING ORGANIZATION REPORT NUMBER(S) WL-TR-91-3022			
4. NAME OF PERFORMING ORGANIZATION The Ohio State University Research Foundation		6b. OFFICE SYMBOL (If applicable) OSURF	7a. NAME OF MONITORING ORGANIZATION Flight Dynamics Directorate (WL/FIBEC) Wright Laboratory			
4. ADDRESS (City, State, and ZIP Code) 1960 Kenny Road Columbus, Ohio 43212			7b. ADDRESS (City, State, and ZIP Code) Wright-Patterson Air Force Base Dayton, Ohio 45433-6553			
5. NAME OF FUNDING / SPONSORING ORGANIZATION Flight Dynamics Directorate		8b. OFFICE SYMBOL (If applicable) WL/FIBEC	9. PROCUREMENT INSTRUMENT IDENTIFICATION NUMBER Contract No. F33615-85-C-3213			
5. ADDRESS (City, State, and ZIP Code) Wright-Patterson Air Force Base Dayton, Ohio 45433-6553			10. SOURCE OF FUNDING NUMBERS			
			PROGRAM ELEMENT NO. 61102F	PROJECT NO. 2302	TASK NO. N1	WORK UNIT ACCESSION NO. 02
1. TITLE (Include Security Classification) Finite Element Analysis of Free-Edge Delamination in Laminated Composite Specimens						
2. PERSONAL AUTHOR(S) R.S. Sandhu, W.E. Wolfe, R.L. Sierakowski, C.C. Chang and H.R. Chu						
3a. TYPE OF REPORT Final	13b. TIME COVERED FROM 7/1/85 to 6/30/90	14. DATE OF REPORT (Year, Month, Day) 1991, June 18	15. PAGE COUNT 176			
6. SUPPLEMENTARY NOTATION						
7. COSATI CODES			18. SUBJECT TERMS (Continue on reverse if necessary and identify by block number)			
FIELD	GROUP	SUB-GROUP	Composite Laminates      Finite Element Method Delamination			
9. ABSTRACT (Continue on reverse if necessary and identify by block number)						
<p>A mixed-type finite element formulation based on minimization of potential energy, and ensuring continuity of displacements as well as tractions, is developed to analyze the free-edge delamination problem in composite laminate coupons under uniform longitudinal strain. In this model, compatible cubic interpolation functions, originally proposed by Felippa for plate bending analysis, were used for defining the displacement field within each element. To ensure traction continuity, the nodal displacement components and their gradients normal to element boundary were transformed to a mixed set of degrees of freedom through appropriate displacement-traction relationships. Thus, for global assembly, the nodal degrees of freedom include interlaminar traction components at the corner nodes, as well as traction components at the mid-side nodes of each element. This ensures continuity of displacement and traction along interelement boundaries as well as across laminate interfaces. Also, traction-free boundary conditions can be specified in a point-wise sense. (continued)</p>						
0. DISTRIBUTION / AVAILABILITY OF ABSTRACT <input checked="" type="checkbox"/> UNCLASSIFIED/UNLIMITED <input type="checkbox"/> SAME AS RPT. <input type="checkbox"/> DTIC USERS			21. ABSTRACT SECURITY CLASSIFICATION Unclassified			
2a. NAME OF RESPONSIBLE INDIVIDUAL George P. Sendeckyj			22b. TELEPHONE (Include Area Code) 513-255-6104	22c. OFFICE SYMBOL WL/FIBEC		

UNCLASSIFIED

---

SECURITY CLASSIFICATION OF THIS PAGE

19. ABSTRACT (continued)

The procedure is verified by application to four-ply laminate specimens. The displacement and stress fields from the continuous traction finite element procedure are compared with solutions by Pagano's procedure which is based on a totally different theoretical approach.

Application of the proposed method to multilayer coupons is shown to be successful in modeling some failure phenomena observed in the experiments. The method has potential for obtaining accurate estimates of stresses in laminated composites and, hence, for better understanding of damage and failure mechanisms.

## FOREWORD

The research reported herein was supported by the Air Force System Command/ASD under Grant No. F33615-85-C-3213 to the Ohio State University. Dr. George P. Sendeckyj of Wright Laboratory/Flight Dynamics Directorate was the Program Manager. The report summarizes the work done from July 1, 1985 to June 30, 1990. At the Ohio State University, the research was carried out, under the supervision of the Professors Ranbir S. Sandhu, and William E. Wolfe, by graduate research associate Cherrng-Chi Chang up to December 1987, and later by graduate research associate Han-Ru Chu. The work by C. C. Chang formed part of his dissertation for the degree of Doctor of Philosophy at the Ohio State University. Revision by H. R. Chu corrected some errors and added further studies on performance of the procedures developed during the research.

The Instruction and Research Computer Center (IRCC) at The Ohio State University and the Ohio Supercomputer Center (OSC) provided the computational and documentation facilities.



Accession For	
NTIS	<input checked="" type="checkbox"/>
DTIC TAB	<input type="checkbox"/>
Unannounced	<input type="checkbox"/>
Justification	
By	
Distribution/	
Availability Codes	
Avail and/or	
Dist	Special
A-1	

## CONTENTS

<b>FOREWORD</b> .....	iii
<b>SECTION I: INTRODUCTION</b> .....	1
<b>SECTION II: REVIEW OF EARLIER WORK</b> .....	6
Introduction .....	6
Analytical Approach .....	7
Approximate Elasticity Solution .....	7
Modified Higher Order Theory .....	8
Galerkin's Method .....	8
Perturbation Technique .....	9
Boundary Layer Theory .....	9
Reissner's Variational Principle .....	10
Global-local Model .....	10
Finite Difference Method .....	11
Pseudo Two-dimensional Analysis .....	11
Three-dimensional Analysis .....	11
Finite Element Method .....	12
Displacement Method .....	12
Stress Method .....	13
Hybrid Assumed Stress Model .....	14
Summary and Research Motivation .....	14
<b>SECTION III: VARIATIONAL FORMULATION AND FINITE ELEMENT                 APPROXIMATION IN LINEAR ELASTICITY</b> .....	17
Introduction .....	17
Boundary Value Problem .....	18
A Variational Principle .....	19
Variational Principle for Finite Element Approximation .....	20
Linear Operator with Adjoint Splitting .....	21
Principle of Minimum Potential Energy .....	23
Assumed Displacement Finite Element Formulation .....	26

<b>SECTION IV: CONTINUOUS STRAIN FINITE ELEMENT INTERPOLATION</b>	<b>32</b>
Introduction	32
Interpolation Functions of Continuous Strain Elements	33
LCCT-12 Element	34
LCCT-11 and LCCT-9 Elements	36
Quadrilateral Elements	38
Application to the Free-Edge Stress Problem	40
Finite Element Formulation	42
Higher Order Elements	43
 <b>SECTION V: CONTINUOUS TRACTION FINITE ELEMENT PROCEDURE FOR COMPOSITE LAMINATES</b>	 <b>46</b>
Introduction	46
Derivation of Displacement-Stress Transformation	47
Corner Nodes	47
Mid-side Nodes	53
Finite Element Formulation	64
Calculation of Stresses	67
Boundary Conditions of a Quadrant of the Delamination Specimen	68
Boundary Conditions Along Lines of Symmetry	68
Traction-Free Boundary Conditions	70
 <b>SECTION VI: ANALYSIS OF FREE-EDGE DELAMINATION IN LAMINATE COMPOSITE SPECIMENS</b>	 <b>73</b>
Introduction	73
Four-Ply Laminates	74
Angle-Ply Laminate	76
Cross-Ply Laminate	82
Effect of Traction-Free Edge on the Solutions	92
Effect of Mesh Refinement	96
Free-Edge Delamination in Multi-Ply Laminate Specimens	104
Analysis of $[(\theta/-\theta)_m/90_{n/2}]_s$ Laminates	104
Numerical Evaluation	105
Analytical-Experimental Correlation	139
Delamination of $[(\theta/-\theta)_2/90]_s$ Laminate	141
Anisotropic Strength and Failure Criteria	143
Onset of Material Damage	148
 <b>SECTION VII: DISCUSSION</b>	 <b>159</b>

REFERENCES . . . . .	164
----------------------	-----

Appendix A: DERIVATION OF COMPATIBLE CUBIC INTERPOLATION FUNCTIONS . . . . .	168
---	-----

LIST OF SYMBOLS . . . . .	178
---------------------------	-----



## FIGURES

1.	Comparison of Z-stress at the Interface of 45/-45 Layers . . . . .	3
2.	Assembly of the LCCT-12 Plane Elasticity Element . . . . .	35
3.	Compatible Triangular Elements . . . . .	37
4.	Quadrilateral Elements formed from (a) LCCT-12 (b) LCCT-11 (c) LCCT-9 . . . . .	39
5.	Geometry and Loading of Symmetric Laminates . . . . .	41
6.	Free-Edge Stress LCCT-12 Element . . . . .	44
7.	Components of Traction Vector Acting on an Arbitrary Plane N . . . . .	54
8.	Local and Global Cartesian Coordinates . . . . .	58
9.	Numbering of Nodal Points in LCCT-12 Element . . . . .	60
10.	144-Element Mesh . . . . .	75
11.	Distribution of X-stress Along Center of Top Layer (45 degree) . . . . .	77
12.	Distribution of XY-stress Along Center of Top Layer (45 degree) . . . . .	78
13.	Distribution of XZ-stress Along 45/-45 Interface . . . . .	79
14.	Through-Thickness Distribution of XZ-stress at the Free-Edge of [45/-45] <sub>s</sub> Laminate . . . . .	80
15.	Axial Displacement Across Top Surface of [45/-45] <sub>s</sub> Laminate . . . . .	81
16.	Through-Thickness Distribution of Axial Displacement at the Free-Edge of [45/-45] <sub>s</sub> Laminate . . . . .	83
17.	Distribution of Z-stress Along Central Plane of [0/90] <sub>s</sub> Laminate . . . . .	84
18.	Distribution of Z-stress Along 0/90 Interface . . . . .	85
19.	Effect of Mesh Refinement on the Z-stress Distribution Along 0/90 Interface . . . . .	86
20.	Through-Thickness Distribution of Z-stresss at the Free-Edge of [0/90] <sub>s</sub> Laminate . . . . .	87
21.	Distribution of YZ-stress Along the 0/90 Interface . . . . .	89

22.	Through-Thickness Distribution of YZ-stress Along the Free-Edge of [0/90] <sub>s</sub> Laminate . . . . .	90
23.	Transverse Displacement Across Top Surface of [0/90] <sub>s</sub> Laminate . . . . .	91
24.	Distribution of XZ-stress Along +45/-45 Interface--Effect of Traction- Free-Edge . . . . .	93
25.	Distribution of Z-stress Along 0/90 Interface--Effect of Traction-Free- Edge . . . . .	94
26.	Axial Displacement Across Top Surface of [45/-45] <sub>s</sub> Laminate--Effect of Traction-Free-Edge . . . . .	95
27.	80-Element Model . . . . .	97
28.	Distribution of XZ-stress Along +45/-45 Interface--Effect of Mesh Refinement . . . . .	98
29.	Distribution of Z-stress Along +45/-45 Interface--Effect of Mesh Refinement . . . . .	99
30.	Distribution of Z-stress Along 0/90 Interface--Effect of Mesh Refinement . . . . .	100
31.	Distribution of YZ-stress Along 0/90 Interface--Effect of Mesh Refinement . . . . .	102
32.	Through-Thickness Distribution of Z-stress at the Free-Edge of [0/90] <sub>s</sub> Laminate--Effect of Mesh Refinement . . . . .	103
33.	Finite Element Meshes . . . . .	106
34.	Distribution of Z-stress at Mid-plane for Width of 10 Plies of Specimen A . . . . .	107
35.	Distribution of Z-stress at Mid-plane for Width of 10 Plies of Specimen B . . . . .	108
36.	Distribution of Z-stress at Mid-plane for Width of 10 Plies of Specimen C . . . . .	109
37.	Distribution of Z-stress at Mid-plane for Width of 10 Plies of Specimen D . . . . .	110
38.	Through-Thickness Stress Distributions at the Free-Edge of Specimen A Based on the Continuous Traction Q-23 Element . . . . .	113
39.	Through-Thickness Stress Distributions at the Free-Edge of Specimen B Based on the Continuous Traction Q-23 Element . . . . .	114

40.	Through-Thickness Stress Distributions at the Free-Edge of Specimen C Based on the Continuous Traction Q-23 Element . . . . .	115
41.	Through-Thickness Stress Distributions at the Free-Edge of Specimen D Based on the Continuous Traction Q-23 Element . . . . .	116
42.	Distribution of Z-stress at Mid-plane for Width of 10 Plies Based on the Continuous Traction Q-23 Element . . . . .	117
43.	Through-Thickness Z-stress Distributions of Specimen A Based on the Continuous Traction Q-23 Element . . . . .	118
44.	Through-Thickness Stress Distributions at the Free-Edge of Specimen A with Further Refinement on the free-edge . . . . .	119
45.	Through-Thickness Stress Distributions at $y=0.495$ of Specimen A with Further Refinement on the free-edge . . . . .	120
46.	Stresses at the Mid-plane of the Free-edge as a Function of Fiber Orientation for $[(\theta/-\theta)_{\pm 90}]_5$ Laminate . . . . .	121
47.	Through-Thickness Z-stress Distribution at the Free-Edge of Specimen A Based on the Continuous Traction Q-23 Element . . . . .	122
48.	Through-Thickness Stress Distributions at the Free-Edge of Specimen A with Further Refinement both on the Free-edge and on the 90-degree Layer . . . . .	123
49.	Through-Thickness Stress Distributions at $y=0.495$ of Specimen A with Further Refinement both on the Free-edge and on the 90-degree Layer . . . . .	124
50.	Distribution of YZ-stress at the Center of 90-degree Layer for Width of 8 Plies of Specimen A . . . . .	125
51.	Distribution of YZ-stress at the Center of 90-degree Layer for Width of 8 Plies of Specimen B . . . . .	126
52.	Distribution of YZ-stress at the Center of 90-degree Layer for Width of 8 Plies of Specimen C . . . . .	127
53.	Distribution of YZ-stress at the Center of 90-degree Layer for Width of 8 Plies of Specimen D . . . . .	128
54.	Through-Thickness Distribution of YZ-stress at the Center of the Second Element From the Free-Edge for Specimen A . . . . .	129
55.	Through-Thickness Distribution of YZ-stress at the Center of the Second Element From the Free-Edge for Specimen B . . . . .	130

56.	Through-Thickness Distribution of YZ-stress at the Center of the Second Element From the Free-Edge for Specimen C . . . . .	131
57.	Through-Thickness Distribution of YZ-stress at the Center of the Second Element From the Free-Edge for Specimen D . . . . .	132
58.	Finite Element Models of A, B and C Laminate Specimens . . . . .	135
59.	Finite Element Models D Laminate Specimen . . . . .	136
60.	100-Element Model . . . . .	142
61.	Ratio of Stress-to-Strength Tensor for $[(\pm 5)_2/90]_5$ Laminate under Transverse Cracks Loading . . . . .	150
62.	Ratio of Stress-to-Strength Tensor for $[(\pm 15)_2/90]_5$ Laminate under Transverse Cracks Loading . . . . .	151
63.	Ratio of Stress-to-Strength Tensor for $[(\pm 25)_2/90]_5$ Laminate under Transverse Cracks Loading . . . . .	152
64.	Ratio of Stress-to-Strength Tensor for $[(\pm 35)_2/90]_5$ Laminate under Transverse Cracks Loading . . . . .	153
65.	Ratio of Stress-to-Strength Tensor for $[(\pm 45)_2/90]_5$ Laminate under Transverse Cracks Loading . . . . .	154
66.	Ratio of Stress-to-Strength Tensor for $[(\pm 5)_2/90]_5$ Laminate under Delamination Loading . . . . .	157
67.	Ratio of Stress-to-Strength Tensor for $[(\pm 25)_2/90]_5$ Laminate under Delamination Loading . . . . .	158
A.1	Triangular, Local and Global Cartesian Coordinates . . . . .	169
A.2	X-Y Projected Dimensions . . . . .	170
A.3	Intrinsic Dimensions . . . . .	171

## TABLES

1.	Comparison of Various Methods for Solving the FED Problems . . . . .	16
2.	Comparisons of Delamination Tendency for Various Speimens . . . . .	134
3.	Comparisons of Maximum Transverse Deformation for Various Specimens . . . . .	138
4.	Experimental Results for Various Laminate Specimens . . . . .	140
5.	Test Results for $[(\pm \theta)_2/90]_s$ Laminate . . . . .	149
6.	Comparison of Pagano's Theory and Continuous Traction Q-23 Element . . . .	161

## SECTION I

### INTRODUCTION

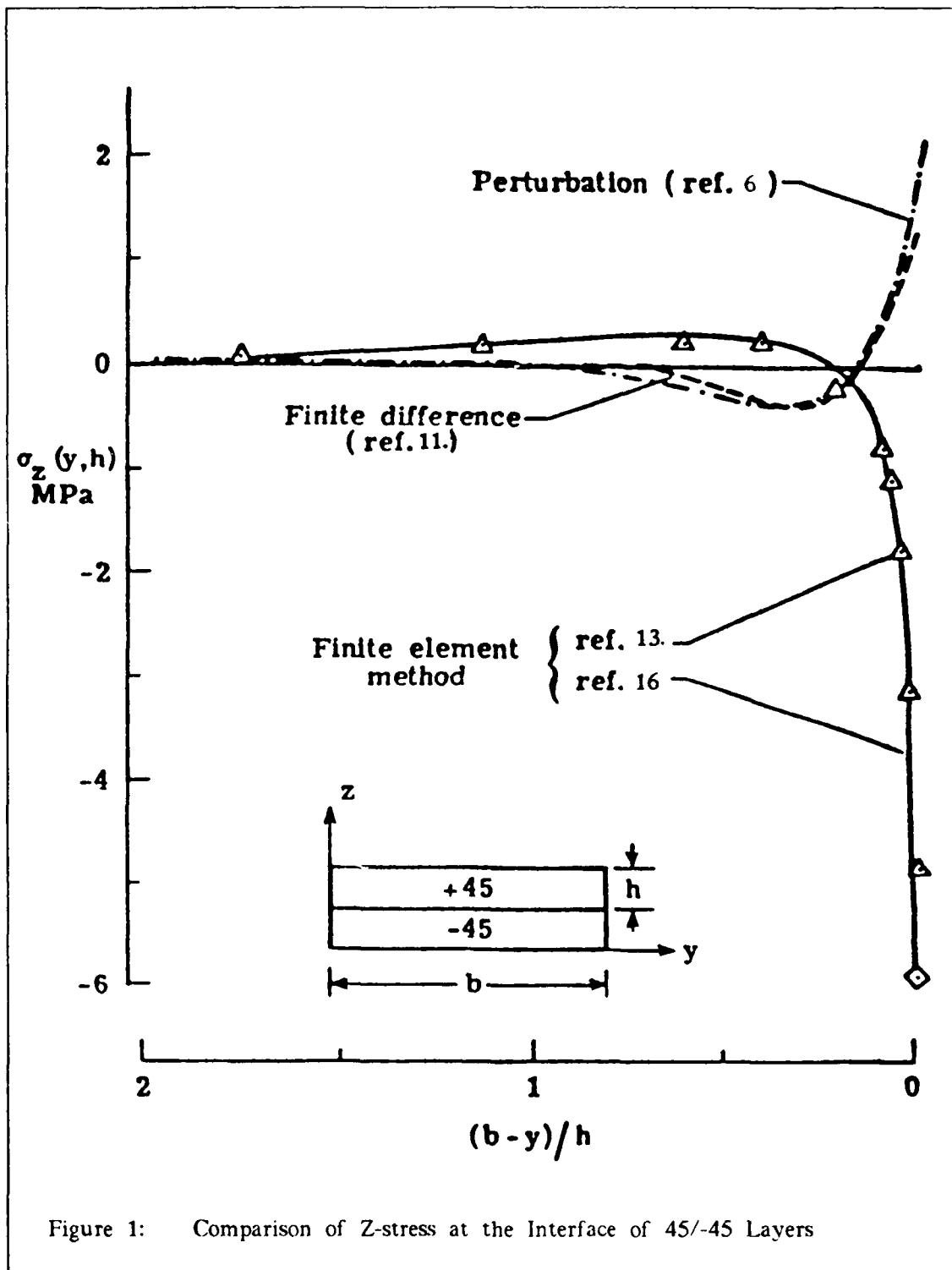
The increasing use of composite materials in structural applications, such as automobiles, aircraft and space structures, is characterized by their high strength (stiffness)-to-weight ratio, low maintenance costs and the flexibility in tailoring the stiffness and strength to design requirements. As fiber reinforced laminates have played a more important role in high performance structures for the last 2 decades, the need to have accurate stress and failure analysis become apparent for design or repair purpose.

Recent development in the analysis of composite laminate coupons under uniform extension indicated that the high interlaminar stresses near the free-edge are mainly responsible for delamination failure [1]. Before delamination can be predicted on the basis of a stress-based failure criterion, it is essential that a highly reliable estimate of interlaminar stresses be available for the given situation. However, it has been difficult to obtain solutions for the stress field because of the anisotropy as well as heterogeneity of the material, and the difficulty of satisfying traction-free boundary condition in a solution procedure based on the displacement formulation.

Considerable research efforts have been devoted to the study of such free-edge delamination problem. These can be classified as analytical and numerical approaches. The analytical solutions are based upon simple elastic approximation [2,3], modified higher order theory [4], Galerkin method [5], Perturbation technique [6], Boundary layer

theory [7], Reissner's variational principle [8,9], Global-local model [10] etc., while the numerical solutions are based on finite difference [11,12] and finite element methods including displacement [13-16], stress [17] and hybrid [18,19] formulations. It was found that some of the solution techniques were only applicable under certain conditions. For this reason, a complete stress distribution was usually hard to obtain. Although results calculated from various approaches have demonstrated similarities in some cases, discrepancies do exist in the magnitude as well as sign of the computed interlaminar stresses near the free-edge of laminate coupons. (One example is shown in Figure (1) in which significant difference was observed for  $\sigma_z$  stress distribution along the interface of  $[45/-45]_s$  laminate based on various solution techniques [19]. Apparently, one possible source of these discrepancies is that, in these methods, the continuity conditions for displacements and tractions across laminate interfaces along with traction-free boundary condition along free-edges characteristic of the real life situation, can only be approximated to a limited extent. However, the credibility of various methods in predicting the  $\sigma_z$  distribution shown in Figure (1) will be judged later.

Due to the presence of singular interlaminar stresses near the laminate free-boundary, edge delamination associated with various types of damage modes, such as fiber breakage, matrix cracking, fiber-matrix debonding, etc., are observed to occur under incremental loading. Delamination can be simply interpreted as separation of laminae from each other in the laminate, and can occur under static, impact or fatigue loading conditions. For the case of a symmetric laminate under inplane loading, the strain components are essentially uniform throughout the laminate. Due to the free-edge effect the out-of-plane interlaminar stresses, however, may be sufficiently





large to damage the matrix material, which bonds adjacent plies together, and cause delamination.

Two generic approaches are available for investigating damage modes in composite materials. The first approach involves a detailed stress analysis used in conjunction with a failure criterion to predict, and measure experimentally, the onset of fiber fracture, matrix cracking and delamination. This can be referred to as the strength characterization approach. In the second approach, classical linear elastic fracture mechanics can be applied to characterize matrix cracking and the delamination process. Delamination has usually been isolated from the other damage modes and treated as a stable crack growth [20-25], and the basic character of the strain energy release rate has been widely used to predict the kinematic behavior of delamination. However, experiments [26] have indicated that delamination usually does not produce a clean surface between the adjacent plies; instead it is associated with other types of damage such as matrix cracking and fiber breakage. Thus, use of linear elastic fracture mechanics approach to study delamination growth seems to be inappropriate. Meanwhile, due to the irregular occurrence of various damage modes in the form of different cracking patterns, use of anisotropic strength and failure criteria is apparently superior to the fracture mechanic approach for the determination of damage characteristics such as type of failure mode, damage zone and crack growth behavior including delamination.

The primary objective of the present research was to develop a finite element model with a sound theoretical background, which could accurately and efficiently predict the complete stress field of the free-edge stress problem in composite laminates without resorting to any special singularity elements. The next was to incorporate

various commonly known macroscopic failure criteria into the finite element computational procedure to evaluate the performance of various criteria on the determination of onset of matrix cracking and delamination in the composite laminate specimens under uniform extension. In Section II, a review of analytical and numerical methods related to the free-edge stress problem is presented. Section III contains the theoretical foundation of the finite element formulation including basic variational principles. Section IV describes a continuous strain finite element model based on a compatible cubic interpolation function. A continuous traction finite element procedure for analysis of free-edge delamination specimens is developed in Section V. In Section VI, analysis of free-edge effect as well as onset of delamination in various types of laminated specimens are presented. Section VII contains discussion of the proposed finite element models for analysis of free-edge delamination specimens. Derivation of Felippa's compatible cubic interpolation function is summarized in the Appendix.

## SECTION II

### REVIEW OF EARLIER WORK

#### 2.1 Introduction

The problem of calculating interlaminar stresses near the free-edges of a layered composite under uniform inplane extension has been investigated by many researchers. Most approximate solutions [2-7,10-19] are based upon elasticity theory and treat the problem as a generalized plane strain case. This is because first of all, the classical and even many of the refined laminate theories, are single-layer theories which do not account for local effects such as geometric and material discontinuities, and the presence of a free-edge; secondly, use of discrete layered theory is very uneconomical and impractical from the computational stand point. An effective modulus formulation [27] in which each layer is characterized as a homogeneous, anisotropic material has been widely used [1-19]. A complex state of stress with high gradients has been noticed [19] in the neighborhood of the free-edge due to the presence of interlaminar stresses to keep the laminae in a state of equilibrium. In order to have a precise prediction of delamination behavior, an accurate estimate for the near-field stress distribution is essential. However, due to the singular nature of the boundary-layer stress field [19], an exact solution is currently unavailable, and discrepancies exist in the magnitude and even the sign of the computed interlaminar stresses near the free-edge (Figure 1) based on various approximate theories.

## 2.2 Analytical Approach

Except for Pagano's [8] approximate theory based on Reissner's variational principle and Pagano and Soni's [10] Global-local model, most analytical solutions discussed in this section are obtained by using various engineering methods to solve the displacement-equilibrium equations under certain assumptions. Thus, these can be regarded as approximate solutions based upon elasticity theory.

### 2.2.1 Approximate Elasticity Solution

Investigations of the free edge problem was carried out by Puppo and Evensen [2] using a composite model essentially consisting of a set of anisotropic layers separated by isotropic adhesive layers. It was assumed that the isotropic layers, developed only interlaminar shear stresses, acting as an adhesive between the anisotropic layers. It was reported that a sharp rise of the interlaminar shear stress could be observed in finite width laminates. However, the simplicity of these elastic formulations precluded calculation of the transverse normal stress, and the problem became more complicated when more layers were involved.

In an attempt to approximate the interlaminar normal stress, a simplified formula was developed by Pagano and Pipes [1]. The strategy was to use solutions along the longitudinal mid-plane of the laminate based upon classical laminated plate theory. one could then compute the force and moment resultants caused by the interlaminar stresses on any plane  $z=\text{constant}$  through consideration of static equilibrium. The maximum interlaminar normal stress at the free-edge could then be expressed in terms of the transverse stress in the  $y$ -direction calculated from the laminated plate theory.

Another approximate elasticity solution proposed by Pipes and Pagano [3] was based upon displacement-equilibrium equations for an anisotropic elastic medium. Assuming

the transverse stresses in the  $y$ -,  $z$ - directions to vanish, the equations were written in terms of the single variable  $U$  (axial displacement function). This yielded components of displacement, strain as well as remaining stress fields in the form of sinusoidal-hyperbolic series. However, violation of stress equilibrium in the transverse directions as well as neglect of the interlaminar normal stress constituted major drawbacks of this scheme.

## 2.2.2 Modified Higher Order Theory

Pagano [4] derived another approximate method for determination of distribution of the interlaminar normal stress along the mid-plane of a symmetric, finite width laminate. The approach was based upon a modified version of a higher order theory proposed by Whitney and Sun [28], which recognized the effect of shear deformation through the inplane rotations as well as the thickness strain implemented in the assumed displacement field. However, like the approximate theories discussed previously, none of them were able to determine the complete stress field near the free-edge.

## 2.2.3 Galerkin's Method

Due to the fact that high stress gradients occurring near the free-edge are difficult to estimate by numerical approaches, Wang and Dickson [5] applied the extended Galerkin's approach, in which interlaminar stresses and displacements of each layer satisfying geometrical boundary conditions were represented as series of Legendre polynomials. The final solution was reached by requiring the satisfaction of continuity conditions at each interface as well as stress boundary conditions at exterior planes. Due to the completeness of Legendre polynomials, convergence of solutions could be expected.

## 2.2.4 Perturbation Technique

In an effort to obtain more accurate free-edge stress intensities, a perturbation technique was applied by Hsu and Herakovich [6] to solve the three coupled dimensionless partial differential equations based upon a displacement formulation of the elastic problem. It showed that the perturbation solution provided a smooth continuous stress distribution in the vicinity of the free-edge. However, this solution had the limitation that the shear stress distribution was a function of both laminate thickness-to-width ratio and a problem-dependent parameter. Although the latter could be chosen such that the maximum values of shear stress field did not exceed elastic limits, the accuracy of the calculated stresses was suspect.

## 2.2.5 Boundary Layer Theory

A boundary layer theory for laminated composites in plane stress was developed by Tang and Levy [7] from the three-dimensional theory of anisotropic elasticity. By expanding the stresses, displacements, body forces and surface tractions in power series of the half-thickness of a lamina in the equations of equilibrium, compatibility and boundary conditions, a sequence of systems of equations was obtained. The complete solution was obtained by combining solutions of the interior domain based on the classical lamination theory and those from boundary layer and matching a set of appropriate boundary conditions. This formulation indeed provided a way to obtain analytical solution for estimating interlaminar normal as well as shear stress distribution.

## 2.2.6 Reissner's Variational Principle

In order to have displacement as well as stress continuity, a mixed formulation is sometimes used. Unlike the elastic approximations discussed previously, Pagano [8] developed an approximate theory for a general composite laminate based upon an application of Reissner's variational principle. In this theory, the inplane stresses are considered linear in the thickness coordinate while the transverse stresses derived from equilibrium consideration are cubic. If a laminate or a single lamina is viewed as an assembly of  $N$  sheets, each having a finite thickness and required to satisfy force and moment equilibrium, the analysis led to a set of  $23N$  algebraic and ordinary differential equations which had to be solved simultaneously. Based upon the assumption that the stress field is independent of the longitudinal axis, Pagano [9] further specialized the theory to the free-edge problem by reducing the stress field determination to the solution of a one-dimensional problem. Despite the relative accuracy of this theory resulting from the improvement of smoothness for both displacement and traction fields at interfaces between adjacent layers, a major drawback was that its application was limited at most to six sublayers.

## 2.2.7 Global-local Model

Pagano [10] introduced a global-local model, which was able to define detailed response functions in a particular, predetermined region of interest while representing the remainder of the domain by effective properties, that reduced the number of variables in a given problem. In this model, for the global region of the laminate, potential energy has been utilized, and the displacement components were based upon the assumption given by Whitney and Sun [28]. The Reissner variational principle described in [8], however, was applied for the local region in which a thickness

distribution of stress field satisfying equilibrium equation within each layer was assumed. A variational principle was then used to derive the governing equations of equilibrium for the whole system. It was reported that the global-local model could effectively solve the same class of free-edge stress problem as described in [8] and had wider range of applicability.

## 2.3 Finite Difference Method

### 2.3.1 Pseudo Two-dimensional Analysis

Pipes and Pagano [11] used the classical theory of linear elasticity to formulate the problem of free-edge delamination of a strip under uniform axial strain. Allowing for material symmetries and uniform extension, the transverse components of displacement were assumed to be independent of the longitudinal coordinate. The three coupled elliptic equations for the displacement functions were solved using a finite difference solution technique to approximate the interlaminar stresses. Delamination was assumed to be primarily due to the high shear stress near the free-edge and the interlaminar stress field was found to be an edge effect which was restricted to a boundary region approximately equal to the laminate thickness.

### 2.3.2 Three-dimensional Analysis

A three-dimensional finite difference analysis was carried out by Altus, Rotem and Shmueli [12] to examine the free-edge stress field. The displacement equilibrium equation was solved by using central difference method while for displacement or traction-free boundary conditions as well as interfacial continuity conditions, either forward or backward difference scheme was applied. Convergence of the solution was



expected providing a reasonable displacement field was assumed initially. Although a complete stress field was available due to three-dimensional characteristics, an iteration scheme could be a serious inconvenience.

## 2.4 Finite Element Method

In order to more effectively evaluate the high gradient stress field at the free-edge of laminated composites, the popular finite element method has been applied by numerous investigators.

### 2.4.1 Displacement Method

Wang and Crossman [13] used a very fine, constant strain triangular element grid to model the laminate boundary region through a cross-section. The functional dependence of the assumed displacement field was of the same type as in Pipes and Pagano's analysis [11]. To overcome the difficulty of computational storage and time limitation, the solution process adopted the so-called "sky-line" matrix storage scheme. The results indicated that the interlaminar as well as inplane stress singular behavior was highly localized in angle-ply laminated composite. A simplified method for calculating interlaminar stress was proposed [14] wherein the stresses at the desired layer-interface were evaluated by substructuring the laminate with fewer number of effective layers. This reduced the number of laminar interfaces and facilitated finite element calculation within fewer elements.

A quasi-three-dimensional finite element analysis was carried out by Raju and Crew [15] using eight-noded isoparametric elements. In order to approximate the stress singularities, polar mesh was introduced near the intersection of interface and free-edge, associated with a so-called log-linear procedure to relate the steep gradient stress with

the radial distance from the singular point in the logarithmic coordinate. One major drawback of this scheme is that the power of singularity has to be determined by solutions calculated from finer polar mesh near the interface of the free-edge.

Whitcomb, Raju and Goree [16] further pointed out that the disagreement for both magnitude and sign of the interlaminar normal stress distribution among various numerical methods could be attributed to the unsymmetric stress tensor at the singularity. In their approach too, the problem was modeled by eight-noded isoparametric elements. It was concluded that finite element displacement models were capable of giving accurate stress distributions everywhere except in the region within two elements of a stress singularity.

In summary, we observe that in the conventional displacement-based finite element formulation, evaluation of shear as well as normal stresses required expensive mesh refinement near the boundary region to approximate the singular stress field. Even then the actual stress distribution along the free-edge was generally not sufficiently accurate.

## 2.4.2 Stress Method

Rybicki [17] used a three-dimensional equilibrium finite element analysis procedure, based upon minimization of complementary energy, to solve the free-edge stress problem. Due to the fact that the assumed stress state in the analysis did not contain singular term, a finite rise in interlaminar normal and shear stresses near the interface corner was observed for angle-ply layup. However, this method involved very large matrices and was computationally expensive, and even at that did not yield a continuous stress field.

### 2.4.3 Hybrid Assumed Stress Model

In Pian's hybrid model [29], stress equilibrium in the interior of the elements as well as displacement continuity along interelement boundaries are ensured, but the interelement stress continuity is satisfied only in a weighted integral sense. Following Pian's formulation, Spilker [18] developed a special hybrid element for the edge-stress problem. In his work, the assumed stress field was made to satisfy exactly the continuity of traction across interlayer boundaries as well as traction-free conditions along exterior planes of the laminate. This was found to be effective for study of cross-ply laminates having a relatively simple stress field. It is difficult to extend this procedure to angle-ply laminates because in these the complete stress field has to be considered.

A special formulation of a singular composite-edge element was developed by Wang and Yuan [19] based on the Boundary Layer theory [30] and the variational principle of a modified hybrid functional. In the analysis, the singular hybrid element was used in conjunction with displacement-based eight-noded isoparametric elements, and it was reported to give satisfactory stress distribution near the free-edge. This method is excellent for determining possible growth of delamination but would be awkward to use to predict occurrence of delamination in an intact specimen. This is because sometimes, it is hard to find the place in which stress singularity may occur.

## 2.5 Summary and Research Motivation

The analytical and numerical solutions discussed above for the free-edge stress problem are summarized in Table (1). Some conclusions can be made at this point.

1. Generally speaking, an analytical solution for the complete stress field is extremely difficult. The solution procedure for the case of a multi-layer system is not currently available.
2. Use of a finite difference technique suffers from geometric limitations. Calculation of stresses at the interfaces or laminate boundaries needs to apply additional techniques, such as iteration scheme. Even then the solution generally lacks credibility.
3. Conventional displacement-based finite element methods are incapable of predicting accurate stress fields particularly along element boundaries. Stress equilibrium approach is apparently impractical. Use of hybrid element does improve stress calculation but is applicable only to some special cases. Application of singular element near the free-edge boundary apparently makes the analysis too subjective. In order to have reliable predictions of displacement and stress fields, it is necessary that the free-edge stress model be able to approximate the real life situation as closely as possible. In other words, the displacement and stress continuity conditions along with traction-free boundary condition have to be exactly satisfied. Considering also the generality and effectiveness of the analysis, the displacement-based finite element approach with higher order interpolation function could conceivably be superior to the other approximate theories.

Table 1: Comparison of Various Methods for Solving the FED Problems

Ref	Author	method of analysis	calculated stresses
2	Puppo & Evensen	Elastic approximation	$\sigma_x \sigma_y \tau_{xz} \tau_{xy}$
3	Pipes & Pagano	Approximate elastic solution	$\sigma_x \tau_{xy} \tau_{yz} \tau_{yz}$
4	Pagano	Modified higher order theory	$\sigma_z$
5	Wang & Dickson	Extended Galerkin's approach	$\sigma_z \tau_{yz}$
6	Hsu & Herakovich	Perturbation technique	$\sigma_z \tau_{xz} \tau_{yz}$
7	Tang & Levy	Boundary Layer theory	$\sigma_x \sigma_y \sigma_z \tau_{yz} \tau_{xz} \tau_{xy}$
8	Pagano	Reissner's variational principle--mixed method	$\sigma_x \sigma_y \sigma_z \tau_{yz} \tau_{xz} \tau_{xy}$
10	Pagano & Soni	Global-local model	$\sigma_x \sigma_y \sigma_z \tau_{yz} \tau_{xz} \tau_{xy}$
11	Pipes & Pagano	Finite difference method	$\sigma_x \sigma_y \sigma_z \tau_{yz} \tau_{xz} \tau_{xy}$
13	Wang & Crossman	Finite element method: constant strain triangle	$\sigma_x \sigma_y \sigma_z \tau_{yz} \tau_{xz} \tau_{xy}$
16	Whitcomb et al.	Finite element method: 8-noded isoparametric element	$\sigma_x \sigma_y \sigma_z \tau_{yz} \tau_{xz} \tau_{xy}$
17	Rybicki	Finite element method: equilibrium stress approach	$\sigma_x \sigma_y \sigma_z \tau_{yz} \tau_{xz} \tau_{xy}$
18	Spilker	Finite element method: hybrid assumed stress model	$\sigma_y \sigma_z \tau_{yz}$
19	Wang & Yuan	Finite element method: Singular hybrid element	$\sigma_x \sigma_y \sigma_z \tau_{yz} \tau_{xz} \tau_{xy}$

### SECTION III

## VARIATIONAL FORMULATION AND FINITE ELEMENT APPROXIMATION IN LINEAR ELASTICITY

### 3.1 Introduction

In this section, a variational formulation of three-dimensional elasticity is described and its use as the basis of a finite element approximation is discussed. The treatment essentially follows that in reference [31]. Variational formulation has been used as the basis for direct methods of obtaining approximate solutions to boundary value and initial boundary value problems. Traditionally, the approximation space is generated by complete orthonormal sets consisting of eigenfunctions of self-adjoint operators. The functions which are used to approximate the field variables are required to satisfy certain continuity requirements over the whole domain. The finite element method, however, offers an alternative route for generating the sequence of finite dimensional approximation spaces. The region under consideration is subdivided into a finite number of discrete elements, and the field variables are represented by functions which follow the same continuity condition only piecewise within each element. Some significant differences between the finite element method and the traditional direct methods include [31]

1. The base functions have local support and are nonorthogonal.
2. The sequence of approximation spaces is ordered by refinement
3. The local support functions may have only limited smoothness

The support of each base function is confined to the neighborhood of a nodal point and extends over the elements of the finite element approximation sharing that point. Across interelement boundaries within the support and at the boundary of the support, the function may have only limited smoothness. In a sequence of refinements, additional nodal points, elements and base functions are introduced. The base functions associated with each nodal point change with refinement, including a monotonic decrease in support. Additional discontinuities might be introduced at each refinement. Variational formulations and solution procedure for direct methods based on the finite element approach must allow for these peculiarities of finite element approximation spaces.

### 3.2 Boundary Value Problem

Consider an open connected region  $R$  in an euclidean space.  $\partial R$  is the boundary of  $R$  and  $\bar{R}$  its closure. A typical boundary value problem on  $\bar{R}$  is defined by the set of equations

$$Au = f \quad \text{on } R \quad (1)$$

$$Cu = g \quad \text{on } \partial R \quad (2)$$

where  $A$  is the field operator and  $C$  is the boundary operator such that

$$A : D_R \rightarrow V_R \quad (3)$$

$$C : D_{\partial R} \rightarrow V_{\partial R} \quad (4)$$

$V_R, V_{\partial R}$  are linear vector spaces whose elements are defined on the regions indicated by the subscripts.  $D_R, D_{\partial R}$  are dense subsets in  $V_R, V_{\partial R}$ , and denote the domains of  $A, C$  respectively.  $D_{\partial R}$  is the extension of  $D_R$  i.e. any element  $u \in D_R$  has a unique extension in  $D_{\partial R}$  and every element in  $D_{\partial R}$  is the extension of an element (not

necessarily unique) in  $D_R$ . For given  $f \in V_R$ ,  $g \in V_{\partial R}$ , the boundary value problem consists of determining  $u \in D_R$  along with its extension in  $D_{\partial R}$  such that (1) and (2) are satisfied.

### 3.3 A Variational Principle

Let the linear operator  $A$  be self-adjoint, i.e. there exists a nondegenerate, linear Gateaux differentiable, bilinear mapping  $B_R : D_R \times V_R \rightarrow S$ , where  $S$  is a linear vector space, such that

$$B_R(u, Av) = B_R(v, Au) + C_{\partial R}(v, u) \quad u, v \in D_R \cap V_R \quad (5)$$

Here,  $C_{\partial R}(v, u)$  are quantities associated with the boundary  $\partial R$ . Magri [32] has shown that such a bilinear mapping can be constructed for every linear operator  $A$ . If the boundary operator  $C$  is consistent [33] with the field operator  $A$ , i.e., there exists a nondegenerate, linear Gateaux differentiable, bilinear mapping  $B_{\partial R} : D_{\partial R} \times V_{\partial R} \rightarrow S$ , such that

$$C_{\partial R}(v, u) = B_{\partial R}(v, Cu) - B_{\partial R}(u, Cv) \quad (6)$$

then, the linear Gateaux differential of

$$\Omega(u) = B_R(u, Au - 2f) + B_{\partial R}(u, Cu - 2g) \quad (7)$$

vanishes if and only if (1), (2) are satisfied. Sandhu and Salaam [33] further pointed out that even if the boundary condition is homogeneous, i.e.  $g = 0$ , the quantity  $B_{\partial R}(u, Cu)$  in (7) must be included if the variational principle is to hold for the path of Gateaux differentiation not satisfying homogeneous boundary conditions. This is important for approximation in finite element spaces where the variation is introduced as change in the nodal point value of the field variable and, consequently, the path of variation may not satisfy the boundary condition or internal smoothness.



### 3.4 Variational Principle for Finite Element Approximation

In the finite element method, the region  $R$  is approximated by a set of elements  $\{R_e; e=1,2,\dots,m\}$  such that

$$R_e \cap R_f = \emptyset \quad \text{if } e \neq f \quad (8)$$

$$\lim_{m \rightarrow \infty} \bigcup_{e=1}^m \bar{R}_e = \bar{R} \quad (9)$$

The field variables are approximated by functions which may not be sufficiently smooth. However, over each element, adequate smoothness is assured. If  $R_e$  represents the interior of the  $e$ -th element and  $\partial R_e$  its boundary, we have [34]

$$B_{R_e}(u, Av) = B_{R_e}(v, Au) + C_{\partial R_e}(v, u) \quad (10)$$

and

$$C_{\partial R_e}(v, u) = B_{\partial R_e}(v, Cu) - B_{\partial R_e}(u, Cv) \quad (11)$$

Further define

$$\Omega(u) = \sum_{e=1}^m [B_{R_e}(u, Au - 2f) + B_{\partial R \cap \partial R_e}(u, Cu - 2g)] + B_{\partial R_e^i}(u, (Cu)') \quad (12)$$

where  $\partial R_e^i$  represents interior boundaries of elements and a prime denotes a jump. The Gateaux differential

$$\Delta_v \Omega(u) = 2 \sum_{e=1}^m [B_{R_e}(v, Au - f) + B_{\partial R \cap \partial R_e}(v, Cu - g)] + 2 B_{\partial R_e^i}(v, (Cu)') \quad (13)$$

vanishes if and only if (1), (2) are satisfied over each element and  $(Cu)'$  vanishes, i.e.  $Cu$  is continuous across interelement boundaries. If there are actual discontinuities in the interior of  $R$ , let

$$(Cu)' = g' \quad \text{over } \partial R^i \quad (14)$$

where  $g'$  is specified over  $\partial R^i$ . Then, if the union of intersection of element boundaries covers  $R^i$ , the functional in (12) may be redefined as

$$\Omega(u) = \sum_{e=1}^m [B_{R_e}(u, Au - 2f) + B_{\partial R \cap \partial R_e}(u, Cu - 2g)] + B_{\partial R^i_e}(u, (Cu)' - 2g') \quad (15)$$

### 3.5 Linear Operator with Adjoint Splitting

Many physical problems can be written in the form of

$$Au = Fu + TETu = f \quad \text{on } R \quad (16)$$

where

$$F: W_R \rightarrow V_R \quad (17)$$

$$T: W_R \rightarrow X_R \quad (18)$$

$$E: X_R \rightarrow Y_R \quad (19)$$

$$T^*: Y_R \rightarrow V_R \quad (20)$$

$T^*$  is the adjoint of  $T$ , i.e.  $B_R, \bar{B}_R$  such that

$$B_R(u, Tv) = \bar{B}_R(v, T^*u) + C_{\partial R}(v, u) \quad (21)$$

Here  $B_R: W_R \times X_R \rightarrow S$  and  $\bar{B}_R: W_R \times V_R \rightarrow S$ .  $S$  is a linear vector space and  $B_R, \bar{B}_R$  are continuous non-degenerate bilinear mappings.  $E, F$  are symmetric, i.e.

$$B_R(u, Ev) = B_R(v, Eu) \quad (22)$$

$$\bar{B}_R(u, Fv) = \bar{B}_R(v, Fu) \quad (23)$$

Introducing  $\epsilon, \sigma$  through the equations

$$Tu - \epsilon = 0 \quad \text{on } R \quad (24)$$

$$E\epsilon - \sigma = 0 \quad \text{on } R \quad (25)$$

(16) can be written as

$$Fu + T^* \sigma = f \quad \text{on } R \quad (26)$$

Combining (24) through (26), these constitute the coupled system

$$\begin{pmatrix} F & 0 & T^* \\ 0 & E & -1 \\ T & -1 & 0 \end{pmatrix} \begin{pmatrix} u \\ \epsilon \\ \sigma \end{pmatrix} = \begin{pmatrix} f \\ 0 \\ 0 \end{pmatrix} \quad \text{on } R \quad (27)$$

If the inverse of  $E$  exists, let  $G=E^{-1}$ . Then, combining (24), (25)

$$Tu - G\sigma = 0 \quad \text{on } R \quad (28)$$

(26) and (28) are the coupled system

$$\begin{pmatrix} F & T \\ T & -G \end{pmatrix} \begin{pmatrix} u \\ \sigma \end{pmatrix} = \begin{pmatrix} f \\ 0 \end{pmatrix} \quad \text{on } R \quad (29)$$

(29) is referred to as the complementary form.

For an operator with adjoint splitting, let the boundary conditions on  $u, \sigma$  be

$$C_1 u = g_1 \quad \text{on } S_1 \quad \partial R \quad (30)$$

$$C_2 \sigma = g_2 \quad \text{on } S_2 \quad \partial R \quad (31)$$

The discontinuity conditions are

$$(C_1 u)' = g'_1 \quad \text{on } S_1^i \quad (32)$$

$$(C_2 \sigma)' = g'_2 \quad \text{on } S_2^i \quad (33)$$

where  $S_1^i$  and  $S_2^i$  are interior surfaces imbedded in the intersection of finite element boundaries.  $C_1, C_2$  consistent with  $T, T^*$  implies the existence of bilinear mapping  $B_{S_1^e}, B_{S_2^e}$  such that

$$B_{R_e}(u, Tv) = B_{R_e}(v, T^*u) + B_{S_2^e}(v, C_2 u) - B_{S_1^e}(u, C_1 v) \quad (34)$$

where  $S_2^e, S_1^e$  are complementary subsets of boundary  $\partial R_e$  of element  $e$ .

The function governing variational formulation of (27) for finite element approximation is

$$\begin{aligned}\Omega(u, \epsilon, \sigma) = & \sum_{e=1}^m [\bar{B}_{R_e}(u, Fu + T^* \sigma - 2f) + B_{R_e}(\epsilon, E\epsilon - \sigma) + B_{R_e}(\sigma, Tu - \epsilon) + B_{\partial R_e \cap S_1}(\sigma, C_1 u - 2g_1)] \\ & + [B_{\partial R_e \cap S_2}(u, C_2 \sigma - 2g_2)] + B_1^1(\sigma, (C_1 u)' - 2g_1') + B_2^1(u, (C_2 \sigma)' - 2g_2')\end{aligned}\quad (35)$$

It is important to note that even if there are no interior discontinuities in the physical problem or the specified boundary conditions are homogeneous, the boundary and the discontinuity terms must be included to accommodate the nature of the finite element approximation space [32].

### 3.6 Principle of Minimum Potential Energy

The field equations for isothermal quasi-static deformation of anisotropic, linear elastic solids, assuming no initial stresses and strains, are:

a) Equilibrium of stresses

$$\sigma_{i,j} + f_j = 0 \quad \text{on } R \quad (36)$$

b) Kinematics

For small deformation, the strain-displacement relationship is

$$u_{(i,j)} = \epsilon_{ij} \quad \text{on } R \quad (37)$$

c) Constitutive relations

$$\sigma_{ij} = E_{ijkl} \epsilon_{kl} \quad (38)$$

on an open bounded connected set  $R$  contained in the three-dimensional Euclidean space  $E$ . Here  $u_i$ ,  $f_i$ ,  $\epsilon_{kl}$ ,  $\sigma_{ij}$ ,  $E_{ijkl}$  are, respectively, the components of the displacement vector, the body force vector, the infinitesimal strain tensor, the symmetric Cauchy stress tensor and the isothermal elasticity tensor. The range of indices is 1, 2, 3 and

summation on repeated indices is implied. A subscript following a comma denotes partial differentiation with respect to the coordinate, in the reference frame, defined by the subscript. Parantheses around subscripts denote the symmetric part of the quantity.

Let the functions  $u_i, \epsilon_{ij}, \sigma_{ij}$  satisfy the continuity and differentiability properties required in the equations of elasticity over every subregion  $R_i$ . Then, admitting  $(u_i, \epsilon_{ij}, \sigma_{ij})$  as the 15-tuple of dependent variables, components of vectors and tensors being regarded as ordered subsets in an n-tuple, (36)-(38) can be written as [33]

$$\begin{pmatrix} 0 & 0 & \frac{-1}{2}(\delta_{ik} \frac{\partial}{\partial j} + \delta_{jk} \frac{\partial}{\partial i}) \\ 0 & E_{ijkl} & -1 \\ \frac{1}{2}(\delta_{ki} \frac{\partial}{\partial l} + \delta_{li} \frac{\partial}{\partial k}) & -1 & 0 \end{pmatrix} \begin{pmatrix} u_i \\ \epsilon_{kl} \\ \sigma_{ij} \end{pmatrix} = \begin{pmatrix} f_k \\ 0 \\ 0 \end{pmatrix} \quad \text{on } R \quad (39)$$

Consistent boundary conditions for the problem are

$$-n_j u_i = -n_j \hat{u}_i \quad \text{on } S_1 \quad (40)$$

$$\sigma_{ij} n_i = \hat{t}_j \quad \text{on } S_2 \quad (41)$$

where the  $n_j$  are components of a unit normal to the boundary  $S$ , and the jump conditions are

$$(\sigma_{ij} n_i)' = g'_{2j} \quad \text{on } S_2^i \quad (42)$$

$$-(n_j u_i)' = -g'_{1ji} \quad \text{on } S_1^i \quad (43)$$

Setting up the problem in inner product space, i.e.  $B_R(u,v) = \int_R u v dR$ , and defining

$$B_R(u,v) = \sum_{e=1}^m B_R(u,v)_{R_e} \quad (44)$$

The basic functional corresponding to (35), allowing for relaxed continuity, is [33]

$$\Omega_1(u_i, \epsilon_{kl}, \sigma_{ij}) = \int_R (\epsilon_{ij} E_{ijkl} \epsilon_{kl} - u_i \sigma_{ij,j} - 2 \epsilon_{ij} \sigma_{ij} - 2 u_i f_i + u_{i,j} \sigma_{ij}) dR$$

$$\begin{aligned}
& + \int_{S_2} u_j (\sigma_{ij} n_i - 2t_j) dS - \int_{S_1} \sigma_{ij} n_j (u_i - 2\hat{u}_i) dS + \int_{S_2} u_j ((\sigma_{ij} n_i)' - 2g'_{2j}) dS \\
& - \int_{S_1^i} \sigma_{ij} ((n_j u_i)' - 2g'_{1ji}) dS
\end{aligned} \tag{45}$$

In using (45) as the basis for finite element approximations, it is not necessary for the interpolants to satisfy any boundary conditions or interelement continuity. For no jump discontinuities,  $g'_{1ji}$  and  $g'_{2j}$  vanish. However, it is important to retain the terms containing  $(\sigma_{ij} n_i)'$ ,  $(n_j u_i)'$  in the formulation.

Using symmetry property of the operator matrix, i.e.

$$\begin{aligned}
\int_R \sigma_{ijj} u_i dR &= - \int_R \sigma_{ij} u_{i,j} dR + \int_S \sigma_{ij} n_j u_i dS + \int_{S_1^i} \sigma_{ij} (n_j u_i)' dS \\
&+ \int_{S_2^i} u_j (\sigma_{ij} n_i)' dS
\end{aligned} \tag{46}$$

to eliminate the term containing  $\sigma_{ijj}$  from (45), the functional can be written as

$$\begin{aligned}
\Omega_2(u_i, \epsilon_{ij}, \sigma_{ij}) &= \int_R \epsilon_{ij} E_{ijkl} \epsilon_{kl} dR + 2 \int_R \sigma_{ij} (u_{i,j} - \epsilon_{ij}) dR - 2 \int_R u_i f_i dR \\
&- 2 \int_{S_2} u_i t_i dS - 2 \int_{S_1} \sigma_{ij} n_j (u_i - \hat{u}_i) dS - 2 \int_{S_1^i} \sigma_{ij} (n_j u_i)' dS
\end{aligned} \tag{47}$$

$\Omega_2$  is the modified variational principle with three independent fields proposed by Prager [35]. If  $u_i$ ,  $\epsilon_{ij}$  are restricted to satisfy the last of (39), the strain-displacement relations, Prager's modified principle of total energy theory is obtained

$$\begin{aligned}
\Omega_3 &= \int_R \epsilon_{ij} E_{ijkl} \epsilon_{kl} dR - 2 \int_R u_i f_i dR - 2 \int_{S_2} u_i t_i dS - 2 \int_{S_1} \sigma_{ij} n_j (u_i - \hat{u}_i) dS \\
&- 2 \int_{S_1^i} \sigma_{ij} (n_j u_i)' dS
\end{aligned} \tag{48}$$

(48) was also proposed by Pian and Tong [29] and is the basis of their hybrid method with assumed displacement field. If the displacement field,  $u_i$ , is further restricted to satisfy the displacement boundary condition (40) on  $S_1$ ,  $\Omega_3$  reduces to

$$\Omega_4 = \int_R \epsilon_{ij} E_{ijkl} \epsilon_{kl} dR - 2 \int_R u_i f_i dR - 2 \int_{S_2} u_i t_i dS - 2 \int_{S_1} \sigma_{ij} (n_j u_i)' dS \quad (49)$$

If the finite element interpolations are chosen to identically satisfy displacement continuity across  $S_1$ , the last term in  $\Omega_4$  vanished and (49) becomes

$$\Omega_5 = \int_R \epsilon_{ij} E_{ijkl} \epsilon_{kl} dR - 2 \int_R u_i f_i dR - 2 \int_{S_2} u_i t_i dS \quad (50)$$

The vanishing of the variation of  $\Omega_5$  with respect to the displacement components  $u_i$  implies the satisfaction of equilibrium equations (36). This functional corresponds to the classical principle of minimum potential energy which is customarily used as the basis of the finite element displacement formulation of the elastostatics problems.

### 3.7 Assumed Displacement Finite Element Formulation

For the boundary value problem stated in (1) and (2), the solutions  $u$  to the forcing functions  $f$  in general belong to  $L_2$ , the space of square integrable function.  $L_2$  is a separable Hilbert space. However,  $u$  may be contained in a subset  $D$  of  $L_2$  such that  $A$ , the linear operator, is defined on  $D$ . We assume that  $D$  is dense in  $L_2$ . If the set of functions  $\{\phi_k, k=1,2,\dots,\infty\}$  is a basis in  $D$ , then any function  $u \in L_2$  can be expressed as an infinite sum:

$$u = \sum_{k=1}^{\infty} a_k \phi_k \quad (51)$$

A scheme to generate approximate solutions is to use a finite set of terms in the infinite sum above. Thus, as an approximation

$$\underline{u} = \sum_{k=1}^n a_k \phi_k \quad (52)$$

The approximation process consists of an appropriate choice of  $n$ ,  $\phi_k$  and the coefficient  $a_k$ . Several alternative procedures are available. The finite element method is a special process of selection of finite subset of the basis  $\{\phi_k\}$ . The coefficients  $a_k$  are generally evaluated by requiring the approximate solution to satisfy a variational principle.

The finite element idealization essentially partitions the spatial region  $R$  into a finite number of nontrivial discrete elements or subregions. The geometry of the elements is defined by a set of points in space called the nodal points of the system. Over an element  $m$ , let an approximation to  $u$  be  $u_n^m$  such that

$$u_n^m = \sum_{k=1}^n a_k^m \phi_k \quad (53)$$

or in matrix form, dropping the subscript  $n$ ,

$$u^m = \{\phi^m\}^T \{a^m\} \quad (54)$$

where  $\{\phi^m\}^T$  is a row vector consisting of  $\phi_k^m$  as its elements and  $\{a^m\}$  is a column vector of coefficients  $a_k^m$ . Evaluating the function, and its derivatives up to a certain order at nodal points, yields

$$\{u_i^m\} = [\phi_i^m]^T \{a^m\} \quad (55)$$

where  $\{u_i^m\}$  is the vector of nodal point values of the function and its derivatives up to the order selected, and  $[\phi_i^m]^T$  is the matrix of base functions evaluated at each nodal



point. The rows and columns of  $[\phi_i^m]^T$  are linearly independent. If square, the matrix is invertible. Hence, we can write

$$\{a^m\} = ([\phi_i^m]^T)^{-1} \{u_i^m\} = [A]^{-1} \{u_i^m\} \quad (56)$$

where  $A = [\phi_i^m]^T$

Substituting (56) into (54)

$$u^m = [\phi^m]^T [A]^{-1} \{u_i^m\} = [\phi^m]^T \{u_i^m\} \quad (57)$$

where  $[\phi^m]$  can now be regarded as a set of interpolation functions relating nodal point values of a function and its derivatives up to a preselected order, to the value at an arbitrary point within the element  $m$  [36].

In applying the potential energy functional shown in (50),  $\epsilon_{ij}$  is assumed to satisfy the strain-displacement relationship, and the displacement field should satisfy the prescribed displacement boundary condition on  $S_1$ . Vanishing of the variation would imply satisfaction of the equilibrium equations. As stated previously, in the finite element method, the displacement  $u$  is approximated by interpolation functions and generalized displacements at a finite number of nodal points of each element. The interpolation function must be chosen in such a way that when the nodal point displacements for two adjacent elements are compatible, the displacements along the common boundary are compatible. Meanwhile, the interpolation function must also satisfy the requirement that the first derivatives of the displacement field exist.

Based on (57), the assumed displacement over an element can be rewritten in matrix form as

$$\{\underline{u}^m\} = [\phi_q^m | \phi_r^m]^T \begin{Bmatrix} q^m \\ r^m \end{Bmatrix} \quad (58)$$

where  $q^m$  is the column matrix of generalized displacements at boundary nodes of element  $m$  which determines the inter-element continuity, and  $r^m$  is the column matrix of generalized displacements at nodal points either at the boundary or at the interior of element  $m$  but which do not affect the interelement continuity requirements. The corresponding strain distribution is

$$\{\epsilon^m\} = [\phi_{eq}^m | \phi_{er}^m]^T \begin{Bmatrix} q^m \\ r^m \end{Bmatrix} \quad (59)$$

where  $\phi_{eq}^m$  and  $\phi_{er}^m$  are obtained by differentiating  $\phi_q^m$  and  $\phi_r^m$  with respect to the spatial coordinates. Substituting (59) into (50) and expressing in the finite element discretized form, we have [37]

$$\begin{aligned} \Omega_5 = & \sum_{m=1}^M \left( \int_{R_m} \begin{Bmatrix} q \\ r \end{Bmatrix}^T [\phi_{eq}^m | \phi_{er}^m] [E^m] [\phi_{eq}^m | \phi_{er}^m]^T \begin{Bmatrix} q \\ r \end{Bmatrix} dR_m - 2 \int_{R_m} \begin{Bmatrix} q \\ r \end{Bmatrix}^T [\phi_q^m | \phi_r^m] [\phi_t^m]^T \{f\} dR_m \right. \\ & \left. - 2 \int_{S_2 \cap \partial R_m} \begin{Bmatrix} q \\ r \end{Bmatrix}^T [\phi_q^m | \phi_r^m] [\phi_t^m]^T \{t\} dR_m \right) \quad (60) \end{aligned}$$

where

- $[E^m]$  = matrix of elastic constants for element  $m$
- $[\phi_f^m]$  = matrix of interpolation functions for the body forces in element  $m$
- $[\phi_t^m]$  = matrix of interpolation functions for the prescribed tractions on the surface  $S_m$  of element  $m$

The summation sign in (60) implies the direct stiffness assembly procedure, and the

vector  $\begin{Bmatrix} q \\ r \end{Bmatrix}$  is the vector of global displacements.  $\Omega_5$  can also be written as

$$\begin{aligned} \Omega_5 = & \sum_{m=1}^M (\{q^m\}^T [K_{qq}^m] \{q^m\} + 2 \{r^m\}^T [K_{rq}^m] \{q^m\} + \{r^m\}^T [K_{rr}^m] \{r^m\} \\ & - 2 \{F_q^m\}^T \{q^m\} - 2 \{F_r^m\}^T \{r^m\}) \quad (61) \end{aligned}$$

where

$$K_{qq} = \int_{R_m} [\phi_{eq}^m][E^m][\phi_{eq}^m]^T dR_m \quad (62)$$

$$K_{rq} = \int_{R_m} [\phi_{er}^m][E^m][\phi_{eq}^m]^T dR_m \quad (63)$$

$$K_{rr} = \int_{R_m} [\phi_{eq}^m][E^m][\phi_{er}^m]^T dR_m \quad (64)$$

$$F_q = \int_{R_m} [\phi_q^m][\phi_r^m]^T \{f^m\} dR_m + \int_{S_2 \cap S_m} [\phi_q^m][\phi_t^m]^T \{t^m\} dS_m \quad (65)$$

$$F_r = \int_{R_m} [\phi_r^m][\phi_r^m]^T \{f^m\} dR_m + \int_{S_2 \cap S_m} [\phi_r^m][\phi_t^m]^T \{t^m\} dS_m \quad (66)$$

The displacements  $\{r^m\}$  in element  $m$  are independent of displacements,  $\{r^i\}$ , for  $i \neq m$ .

The stationarity condition with respect to their variations yields

$$[K_{rq}^m]\{q^m\} + [K_{rr}^m]\{r^m\} - \{F_r^m\} = 0 \quad (67)$$

Solving (67) for  $\{r^m\}$  yields

$$\{r^m\} = [K_{rr}^m]^{-1}(\{F_r^m\} - [K_{rq}^m]\{q^m\}) \quad (68)$$

Substituting (68) into (61) yields

$$\Omega_5 = \sum_{m=1}^M (\{q^m\}^T [K^m] \{q^m\} - \{F^m\}^T \{q^m\} + C_m) \quad (69)$$

where  $[K^m]$  and  $\{F^m\}$  are, respectively, the element stiffness matrix and the equivalent nodal forces defined by

$$[K^m] = [K_{qq}^m] - [K_{rq}^m]^T [K_{rr}^m]^{-1} [K_{rq}^m] \quad (70)$$

$$\{F^m\} = \{F_q^m\} - [K_{rq}^m]^T [K_{rr}^m]^{-1} \{F_r^m\} \quad (71)$$

$$C_m = -\{F_r^m\} [K_{rr}^m]^{-1} \{F_r^m\} = \text{constant} \quad (72)$$

$\Omega_s$  in (69) is given in terms of the generalized displacements  $\{q\}$  which are not independent for different elements. Using global coordinates, (69) can be written as

$$\Omega_s = \{q\}^T [K] \{q\} - 2 \{q\}^T \{F\} + C'_m \quad (73)$$

Taking the variation of this discretized form of the functional yields the system of algebraic equations

$$[K] \{q\} = \{F\} \quad (74)$$

which can be solved for the unknown nodal displacement  $\{q\}$ . The matrix  $[K]$  is positive definite, symmetric and banded. The process of eliminating the generalized coordinates,  $\{r\}$ , from each element is called the static-condensation process [38]. The introduction of these terms, which do not interfere with interelement compatibility, results in an improvement in the satisfaction of the equilibrium equations within each element. However, the satisfaction of the equilibrium equations along the interelement boundary is still governed by the degrees of compatibility supplied by the interpolation functions for the generalized displacements,  $\{q\}$ . The solution obtained represents an underestimate of the true solution in the sense of energy [39].

## SECTION IV

### CONTINUOUS STRAIN FINITE ELEMENT INTERPOLATION

#### 4.1 Introduction

In the finite element method, the displacement field is approximated by interpolation functions and generalized displacements at a finite number of nodal points which also define the geometry of the elements. To ensure continuous strain across interelement boundaries, it is sufficient that the interpolation functions be such that the displacement components as well as their first derivatives along the common boundary are continuous.

Tocher and Hartz [40] pointed out that for plate bending analysis, continuity of slopes of the plate displacement surface is necessary. The compatible cubic interpolation functions developed by Tocher [40] and by Clough and Felippa [41], among others, satisfy this requirement. For plate bending, the generalized displacements used were  $w$ , the transverse displacement of the plate and its derivatives  $w_x, w_y$ . Here, the subscripts  $x$  or  $y$  denote partial differentiation with respect to the independent variables  $x, y$ . Applying the same displacement interpolation scheme to the plane elasticity problems [40], the corresponding generalized displacements were  $u, u_x, u_y, v, v_x, v_y$ , the in-plane displacements and their first derivatives at each node. Thus, continuity of strain between adjacent elements was ensured.

Instead of using a local Cartesian coordinate system in the derivation of the cubic polynomial with nine coefficients for each displacement component in Tocher and Hartz's work, triangular coordinates were used in the present fully compatible quadrilateral element, following Felippa's [42] work on plate bending analysis. This simplified the generation of various matrix relationships for the constituent triangular elements. Tocher's [40] element used incomplete cubic polynomials. Felippa's elements were based on complete cubic polynomials and were therefore selected for application to the free-edge problems. These elements include Tocher's formulation as specialization. Cubic expansion of the 9-degree-of-freedom conforming triangular element (LCCT-9) for both in plane displacement components as used by Tocher [40] was extended to quadrilateral element designated Q-15. Quadrilateral elements, Q-19 and Q-23, assembled from LCCT-11 and LCCT-12 triangular elements introduced by Felippa [42], were also redeveloped for the plane elasticity problems. The continuous strain elements were used to analyze a pseudo two-dimensional free-edge stress problem similar to that of Pipes and Pagano [11] for composite laminate coupons under uniform extension.

## 4.2 Interpolation Functions of Continuous Strain Elements

In the following, Felippa's [41,42] approach for deriving the plate bending interpolation functions is summarized. We use the same element name as Felippa's and start with  $u$  instead of  $w$  for the plane elasticity problems. Similar derivations applied to the displacement component  $v$ .

#### 4.2.1 LCCT-12 Element

A complete cubic polynomial in two variables is defined by ten independent coefficients. The values of  $u$ , the  $x$ -direction displacement of the plane stress body and its derivatives  $u_x, u_y$  at the three vertices of a triangle yields nine independent quantities. To ensure continuity of derivative  $u_n$  across element boundaries, it is necessary that  $u_n$  be known at some points other than the vertices along each of the three edges. It is convenient to introduce mid side nodes on each of the three edges. This element then has twelve independent quantities against the minimum of ten needed to completely define a cubic polynomial.

In order to use a cubic polynomial with continuous first derivatives in the interior as well as on the element boundaries, Felippa proposed that the element be made up of three subtriangles as illustrated in Figure (2). Each subtriangle has three vertices and one mid-side node to supply the ten independent quantities for defining the cubic polynomial interpolation in its interior. The point  $O$  could be any interior point. However, for simplicity of formulation, the centroid is generally used [41].

The nodal displacement degrees of freedom to be considered in the stiffness matrix of the complete element (Figure 2) include the values of the in-plane displacement components,  $u_i, v_i$  along with their first derivatives  $u_{x_i}, u_{y_i}, v_{x_i}, v_{y_i}$  ( $i=1,2,3$ ) about the  $x$  and  $y$  axes at each corner as well as the normal slopes at the three mid-side nodes about axes perpendicular to these sides respectively, viz.  $u_{n_4}, u_{n_5}, u_{n_6}$ , and  $v_{n_4}, v_{n_5}, v_{n_6}$ . After forming the expression of the cubic displacement patterns in the three subelements, because of the common displacements imposed at the nodes, the in-plane displacements of two adjacent subelements are identical along their juncture line. To establish continuity of  $u_n$  along the edges of the subelements, it is sufficient that  $u_n$

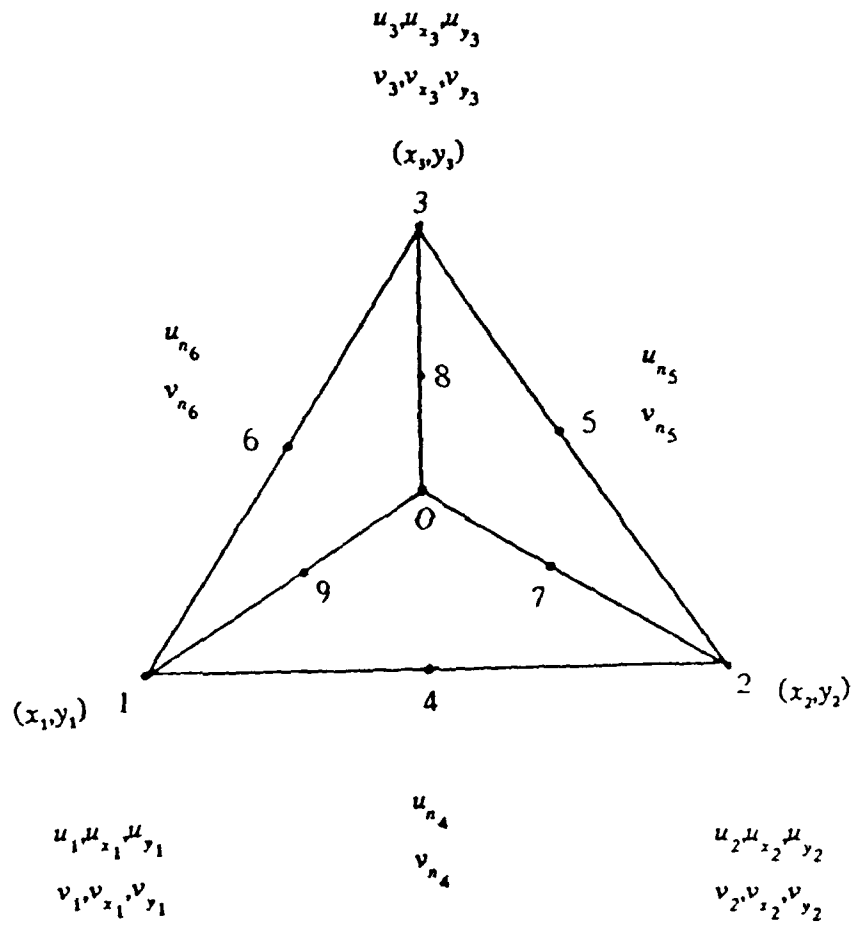


Figure 2: Assembly of the LCCT-12 Plane Elasticity Element

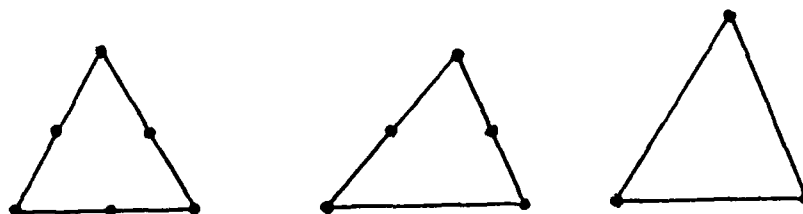


evaluated at points 7, 8, 9, mid-points of these edges, from adjacent subtriangles be the same. These three conditions were used to evaluate the in-plane displacement  $u$ , and its derivatives  $u_x$ ,  $u_y$  at the interior point  $O$ . With the interior point thus condensed out, Felippa [41] obtained a set of interpolation functions for the LCCT-12 element. These define a piecewise cubic polynomial interpolation such that the in-plane displacements and their first derivatives are continuous both in the interior of the element and along the entire boundary of the complete triangular element. A more detailed derivation procedure and the complete listing of the cubic interpolation functions are given in Appendix.

#### 4.2.2 LCCT-11 and LCCT-9 Elements

Assembly of three subtriangles results in the LCCT-12 element (Figure 3a). However, the mid-side nodal points in this element are not desirable for programming. They complicate the mesh generation procedure, increase the band-width of the assembled equation systems, and require special identification in calculation of the stiffness matrix. To overcome these difficulties, it may be desirable to develop a special element without external midpoints. This can be accomplished by assuming the normal slope to vary linearly along one or more sides [42].

With the elimination of one mid-side node, the five-node element is designated as LCCT-11 (Figure 3b). Further imposing linear slope variation constraints on three sides gives a triangle with three nodal points and results in LCCT-9 element as illustrated in Figure 3(c). The LCCT-9 element is identical to the Tocher and Hartz [40] element.



(a) LCCT-12

(b) LCCT-11

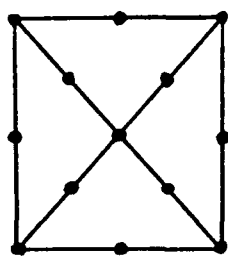
(c) LCCT-9

Figure 3: Compatible Triangular Elements

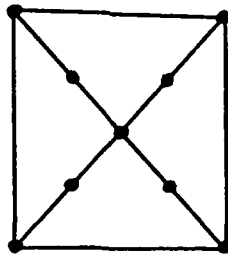
### 4.2.3 Quadrilateral Elements

Elements of quadrilateral shape can be set up as assemblages of triangular elements. Figure (4) shows quadrilateral elements built up from four LCCT-12, LCCT-11 and LCCT-9 elements. The quadrilateral element in Figure 4(a) has a total of 23 degrees of freedom for each variable and was designated by Felippa as Q-23. Using four LCCT-11 or LCCT-9 triangles, the Q-19 and Q-15 elements as shown in Figures 4(b), 4(c) respectively are realized.

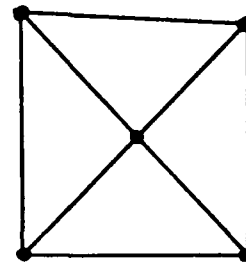
The quadrilateral element has interior nodal points not connected to the other quadrilateral element in a finite element mesh. These points can be eliminated through a local condensation process. Thus, the final quadrilateral element has 24 degrees of freedom, corresponding to the two in-plane displacement components and their first derivatives with respect to spatial coordinates  $x$  and  $y$  at the four corners of the elements and an additional eight degrees of freedom corresponding to the normal derivatives of each of the displacement components at the mid-side nodes. Assuming that the normal derivatives vary linearly along the edges of the quadrilateral, the mid-side nodes can be dropped. This reduces the Q-23 to Felippa's Q-19 element with 12 degrees of freedom for each of the displacement components. It is a fully compatible quadrilateral element, having a continuous cubic variation of displacement and quadratic variation of strain both in the interior of the element and along the entire boundary of the element, as well as a linear variation of normal slope along all external edges. We note however that LCCT-9 and LCCT-11 do not use a complete cubic polynomial. For this reason, Felippa's LCCT-12 element based on complete cubic interpolation was considered an improvement upon Tocher's [40] LCCT-9.



(a) Q-23



(b) Q-19



(c) Q-15

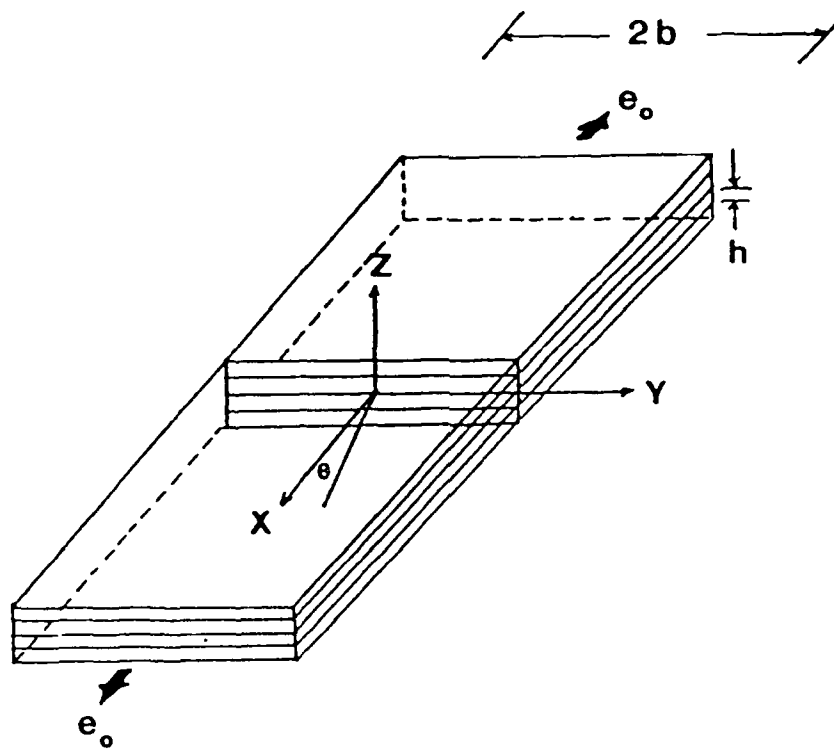
Figure 4:    Quadrilateral Elements formed from (a) LCCT-12 (b) LCCT-11 (c) LCCT-9

### 4.3 Application to the Free-Edge Stress Problem

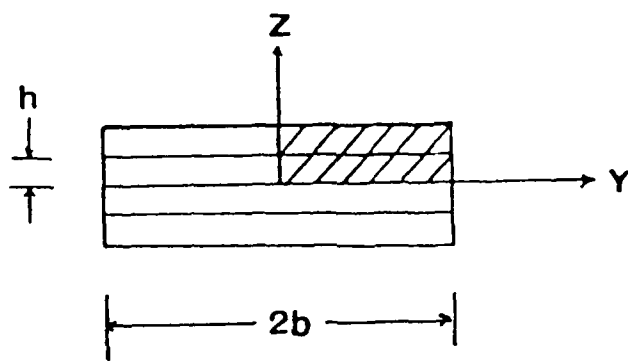
Figure (5) shows a symmetric laminated composite coupon under a state of uniform axial strain. In this case, away from the ends, the transverse  $x \approx \text{constant}$  plane displacement fields can be assumed to be independent of  $x$ . These assumptions imply the following form for the three components of displacement [11].

$$\begin{aligned}u(x,y,z) &= e_x x + U(y,z) \\v(x,y,z) &= V(y,z) \\w(x,y,z) &= W(y,z)\end{aligned}\tag{75}$$

where  $e_x$  is the uniform in plane strain in the  $x$ -direction and  $u$ ,  $v$ ,  $w$  are components of displacement along  $x$ ,  $y$  and  $z$  axes respectively.



(a) Symmetric Laminate



(b)  $x=\text{constant}$  Plane

Figure 5: Geometry and Loading of Symmetric Laminates

### 4.3.1 Finite Element Formulation

The constitutive relationship for linear elastic anisotropic material obeys the generalized Hooke's law

$$\sigma_i = C_{ij} \epsilon_j \quad i, j = 1, 2, \dots, 6 \quad (76)$$

where  $\epsilon_i$  is namely the uniform extensional strain  $e_o$ . Based upon the minimum potential energy principle (50) and substituting various interpolation functions for displacement, body force and traction fields appearing in the governing functional (60), a nodal force-displacement relation within each element is expressed as

$$K_{ij} u_j = R_i \quad (77)$$

where  $R_i$  represents the resultant external nodal force,  $K_{ij}$  is the element stiffness matrix which can be written as

$$K_{ij} = \int_V B_{im} C_{mn} B_{nj} dV \quad m, n = 1, 2, \dots, 6 \quad (78)$$

The range of  $i, j$  depends upon the 'degree of freedom' of the element,  $B$  is the displacement transformation matrix and  $V$  is the domain of the element.

Because of the longitudinal extensional strain is specified as constant, the corresponding term in the stiffness matrix can be separated from the rest and (78) rewritten as

$$K_{ij} u_j = R_i - R_i^o \quad (79)$$

where the range of summation on  $m, n$  is now 2, 3, ..., 6 and  $R_i^o$  is the element residual force due to uniform in-plane strain  $e_o$ , i.e.

$$R_i^o = \int_V B_{im} C_{m1} e_o dV \quad (80)$$

After forming the system stiffness matrix and nodal force vectors, the displacement components can be obtained by solving the resulting set of linear equations in the standard manner.

### 4.3.2 Higher Order Elements

For the free-edge stress problem, due to the fact that dependence of the longitudinal displacement on the longitudinal coordinate  $x$  is made explicit, the three displacement components are completely defined by three functions of two independent transverse coordinates  $y$  and  $z$  as shown in (75). Thus, the compatible cubic interpolation functions used for plane elasticity problems can be extended to the pseudo two-dimensional model of a laminate coupon, and a continuous strain field along both in-plane and transverse directions ensured.

Figure (6) shows the nodal displacement degrees of freedom considered in the stiffness matrix for the complete triangular element. These included the values of the in-plane displacement components  $u$ ,  $v$ , the transverse displacement  $w$ , along with the first derivatives  $u_y$ ,  $u_z$ ,  $v_y$ ,  $v_z$ ,  $w_y$ ,  $w_z$  about the  $y$  and  $z$  axes at each corners  $i=1,2,3$  as well as the normal slopes at the three mid-side nodes, viz.  $u_{n_4}$ ,  $u_{n_5}$ ,  $u_{n_6}$ ,  $v_{n_4}$ ,  $v_{n_5}$ ,  $v_{n_6}$ ,  $w_{n_4}$ ,  $w_{n_5}$ ,  $w_{n_6}$ . This is the LCCT-12 element but with total of 36 degrees of freedom. Further assuming the normal slope to vary linearly along one or all three sides, the LCCT-11 and LCCT-9 elements, with total of 33 and 27 degrees of freedom respectively, are obtained as specializations.

As described for plane elasticity, quadrilateral elements, designated as Q-23, Q-19 and Q-15, were set up as assemblage of four LCCT-12, LCCT-11 and LCCT-9 respectively. After eliminating the interior nodal points through a local condensation process, the final quadrilateral element, Q 23, had 36 degrees of freedom, corresponding



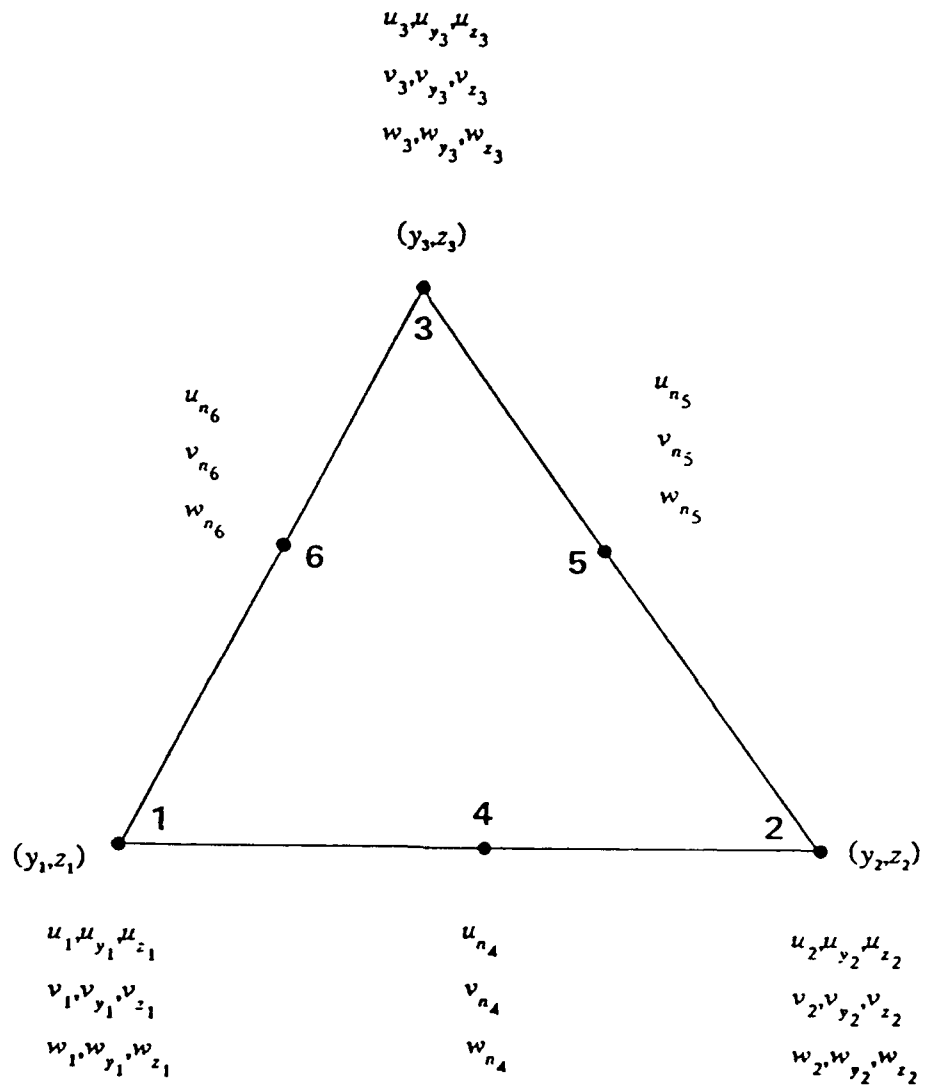


Figure 6: Free-Edge Stress LCCT-12 Element

to the three displacement components and their first derivatives with respect to the spatial coordinates  $y$  and  $z$  at the four corners of the element and an additional 12 degrees of freedom corresponding to the normal derivative of each of the displacement components at the mid-side nodes. It is a fully compatible quadrilateral element, having a continuous cubic variation of displacement and quadratic variation of strain not only within the elements as well as along element boundaries, but also across laminate interfaces.

## SECTION V

### CONTINUOUS TRACTION FINITE ELEMENT PROCEDURE FOR COMPOSITE LAMINATES

#### 5.1 Introduction

In the continuous strain Q-23 element developed for the free-edge stress problem, both displacement and strain are continuous along interelement as well as interlaminar boundaries. However, the tractions calculated across the interfaces between differently oriented layers are discontinuous due to different orientation of adjacent plies. Also, traction-free boundary conditions associated with the finite-width laminate coupon cannot be satisfied. In order to remedy these two defects and make the numerical model more representative of the real situation, it was necessary to ensure interelement as well as interlaminar continuities of tractions and the traction-free boundary condition along the free-edge. To accomplish this, nodal point degrees of freedom must include some components of stress and exclude normal gradients of displacement which will be different across interelement boundaries. This was implemented by transforming the displacements and their normal gradients at each of the nodal points of the Q-23 element to a mixed set of degrees of freedom which would be continuous across interelement boundaries. These included both displacement and interlaminar traction components. Appropriate displacement-stress relationships derived from the constitutive laws were used. For this element, traction-free boundary condition could be satisfied in a point-wise sense.

The continuous traction Q-23 element still has cubic variation of displacement over the element and retains continuity of displacements across interelement as well as interlaminar boundaries. The strains as well as stresses vary quadratically within each subtriangle of the constituent LCCT-12 elements of the quadrilateral. However, certain components of strain are not continuous across interelement boundaries but interelement tractions are. This correctly allows for possible differences in orientation of adjacent laminae. If adjacent layers have the same stress-strain relationships due to identical orientation, stress continuity will imply strain continuity as well.

## 5.2 Derivation of Displacement-Stress Transformation

In the Q-23 element analysis, the number of nodal degrees of freedom is different for the corner nodal points and the midside nodes. For this reason, derivation of transformation matrices for displacements and their gradients at the corners of the LCCT-12 element, and for normal gradients of displacement at the midside nodes on the element boundaries, is discussed separately in the following sections.

### 5.2.1 Corner Nodes

The strain-stress relationship for an orthotropic material expressed in the  $x-y-z$  coordinate system is

$$\epsilon_i = S_{ij} \sigma_j \quad i,j=1,2,\dots,6 \quad (81)$$

or in matrix form

$$\begin{Bmatrix} \epsilon_x \\ \epsilon_y \\ \epsilon_z \\ \gamma_{yz} \\ \gamma_{xz} \\ \gamma_{xy} \end{Bmatrix} = \begin{bmatrix} \bar{S}_{11} & \bar{S}_{12} & \bar{S}_{13} & 0 & 0 & \bar{S}_{16} \\ \bar{S}_{12} & \bar{S}_{22} & \bar{S}_{23} & 0 & 0 & \bar{S}_{26} \\ \bar{S}_{13} & \bar{S}_{23} & \bar{S}_{33} & 0 & 0 & \bar{S}_{36} \\ 0 & 0 & 0 & \bar{S}_{44} & \bar{S}_{45} & 0 \\ 0 & 0 & 0 & \bar{S}_{45} & \bar{S}_{55} & 0 \\ \bar{S}_{16} & \bar{S}_{26} & \bar{S}_{36} & 0 & 0 & \bar{S}_{66} \end{bmatrix} \begin{Bmatrix} \sigma_x \\ \sigma_y \\ \sigma_z \\ \tau_{yz} \\ \tau_{xz} \\ \tau_{xy} \end{Bmatrix} \quad (82)$$

where  $\bar{S}_{ij}$  are components of the compliance matrix for monoclinic materials which have symmetry with respect to x-y plane (Figure 2) and are defined as [43]

$$\begin{aligned} \bar{S}_{11} &= S_{11}m^4 + (2S_{12} + S_{66})m^2n^2 + S_{22}n^4 \\ \bar{S}_{12} &= (S_{11} + S_{22} - 2S_{12} - S_{66})m^2n^2 + S_{12} \\ \bar{S}_{13} &= S_{13}m^2 + S_{23}n^2 \\ \bar{S}_{16} &= [2S_{11}m^2 - 2S_{22}n^2 + (2S_{12} + S_{66})(n^2 - m^2)]mn \\ \bar{S}_{22} &= S_{11}n^4 + (2S_{12} + S_{66})m^2n^2 + S_{22}m^4 \\ \bar{S}_{23} &= S_{13}n^2 + S_{23}m^2 \\ \bar{S}_{26} &= [2S_{11}n^2 - 2S_{22}m^2 + (2S_{12} + S_{66})(m^2 - n^2)]mn \\ \bar{S}_{33} &= S_{33} \\ \bar{S}_{36} &= 2(S_{13} - S_{23})mn \\ \bar{S}_{44} &= S_{44}m^2 + S_{55}n^2 \\ \bar{S}_{45} &= -S_{44}mn + S_{55}mn \\ \bar{S}_{55} &= S_{44}n^2 + S_{55}m^2 \\ \bar{S}_{66} &= 4(S_{11} + S_{22} - 2S_{12} - S_{66})m^2n^2 + S_{66} \end{aligned} \quad (83)$$

where  $m = \cos\theta'$ ,  $n = \sin\theta'$ , and

$$\begin{aligned}
S_{11} &= \frac{1}{E_{11}}, S_{12} = -\frac{\nu_{21}}{E_{22}}, S_{13} = -\frac{\nu_{31}}{E_{33}} \\
S_{21} &= -\frac{\nu_{12}}{E_{11}}, S_{22} = \frac{1}{E_{22}}, S_{23} = -\frac{\nu_{32}}{E_{33}} \\
S_{31} &= -\frac{\nu_{13}}{E_{11}}, S_{32} = -\frac{\nu_{23}}{E_{22}}, S_{33} = \frac{1}{E_{33}} \\
S_{44} &= \frac{1}{G_{23}}, S_{55} = \frac{1}{G_{13}}, S_{66} = \frac{1}{G_{12}}
\end{aligned} \tag{84}$$

$\theta'$  is angle of ply from global axis  $x$  to material axis 1, and  $E_{kk}$ ,  $G_{ij}$ ,  $\nu_{ij}$  ( $i,j,k=1,2,3$ ) are moduli of elasticity, shear moduli, Poisson's ratios, respectively, in material coordinates.

Replacing the strain components by their corresponding displacement gradients, for small strain theory, and rearranging the constitutive relation, (82) becomes

$$\begin{Bmatrix} u_x \\ v_y \\ u_y \\ w_z \\ w_y + v_z \\ u_z \end{Bmatrix} = \begin{bmatrix} \bar{S}_{11} & \bar{S}_{12} & \bar{S}_{16} & \bar{S}_{13} & 0 & 0 \\ \bar{S}_{12} & \bar{S}_{22} & \bar{S}_{26} & \bar{S}_{23} & 0 & 0 \\ \bar{S}_{16} & \bar{S}_{26} & \bar{S}_{66} & \bar{S}_{36} & 0 & 0 \\ \bar{S}_{13} & \bar{S}_{23} & \bar{S}_{36} & \bar{S}_{33} & 0 & 0 \\ 0 & 0 & 0 & 0 & \bar{S}_{44} & \bar{S}_{45} \\ 0 & 0 & 0 & 0 & \bar{S}_{45} & \bar{S}_{55} \end{bmatrix} \begin{Bmatrix} \sigma_x \\ \sigma_y \\ \tau_{xy} \\ \sigma_z \\ \tau_{yz} \\ \tau_{xz} \end{Bmatrix} \tag{85}$$

or symbolically

$$\begin{Bmatrix} \epsilon_1 \\ \epsilon_2 \end{Bmatrix} = \begin{bmatrix} D_{11} & D_{12} \\ D_{21} & D_{22} \end{bmatrix} \begin{Bmatrix} \sigma_1 \\ \sigma_2 \end{Bmatrix} \tag{86}$$

where

$$\begin{aligned}
\{\epsilon_1\} &= \begin{Bmatrix} u_x \\ v_y \\ u_y \end{Bmatrix}, \quad \{\epsilon_2\} = \begin{Bmatrix} w_z \\ w_y + v_z \\ u_z \end{Bmatrix} \\
\{\sigma_1\} &= \begin{Bmatrix} \sigma_x \\ \sigma_y \\ \tau_{xy} \end{Bmatrix}, \quad \{\sigma_2\} = \begin{Bmatrix} \sigma_z \\ \tau_{yz} \\ \tau_{xz} \end{Bmatrix}
\end{aligned} \tag{87}$$

and

$$\begin{aligned}
 [D_{11}] &= \begin{bmatrix} \bar{S}_{11} & \bar{S}_{12} & \bar{S}_{16} \\ \bar{S}_{12} & \bar{S}_{22} & \bar{S}_{26} \\ \bar{S}_{16} & \bar{S}_{26} & \bar{S}_{66} \end{bmatrix}, & [D_{12}] &= \begin{bmatrix} \bar{S}_{13} & 0 & 0 \\ \bar{S}_{23} & 0 & 0 \\ \bar{S}_{36} & 0 & 0 \end{bmatrix} \\
 [D_{21}] &= \begin{bmatrix} \bar{S}_{13} & \bar{S}_{23} & \bar{S}_{36} \\ 0 & 0 & 0 \\ 0 & 0 & 0 \end{bmatrix}, & [D_{22}] &= \begin{bmatrix} \bar{S}_{33} & 0 & 0 \\ 0 & \bar{S}_{44} & \bar{S}_{45} \\ 0 & \bar{S}_{45} & \bar{S}_{55} \end{bmatrix}
 \end{aligned} \tag{88}$$

To relate the interlaminar strain components  $\{\epsilon_j\}$  to their corresponding interlaminar stress components  $\{\sigma_j\}$ ,  $\{\sigma_1\}$  was eliminated through a static condensation process. This yields

$$\{\epsilon\} = [S] \{\sigma_2\} \tag{89}$$

where

$$\{\epsilon'\} = \{\epsilon_2\} - [D_{21}] [D_{11}]^{-1} \{\epsilon_1\} \tag{90}$$

$$[S] = [D_{22}] - [D_{21}] [D_{11}]^{-1} [D_{12}] \tag{91}$$

The inverse of  $[D_{11}]$ , namely, the compliance matrix in plane stress case, can be written explicitly as

$$[D_{11}]^{-1} = \begin{bmatrix} \bar{Q}_{11} & \bar{Q}_{12} & \bar{Q}_{16} \\ \bar{Q}_{12} & \bar{Q}_{22} & \bar{Q}_{26} \\ \bar{Q}_{16} & \bar{Q}_{26} & \bar{Q}_{66} \end{bmatrix} \tag{92}$$

where

$$\begin{aligned}
\bar{Q}_{11} &= Q_{11}m^4 + 2(Q_{12} + 2Q_{66})m^2n^2 + Q_{22}n^4 \\
\bar{Q}_{12} &= (Q_{11} + Q_{22} - 4Q_{66})m^2n^2 + Q_{12}(m^4 + n^4) \\
\bar{Q}_{16} &= -mn^3Q_{22} + m^3nQ_{11} - mn(m^2 - n^2)(Q_{12} + 2Q_{66}) \\
\bar{Q}_{22} &= Q_{11}n^4 + 2(Q_{12} + 2Q_{66})m^2n^2 + Q_{22}m^4 \\
\bar{Q}_{26} &= -m^3nQ_{22} + mn^3Q_{11} + mn(m^2 - n^2)(Q_{12} + 2Q_{66}) \\
\bar{Q}_{66} &= (Q_{11} + Q_{22} - 2Q_{12})m^2n^2 + Q_{66}(m^2 - n^2)^2
\end{aligned} \tag{93}$$

with

$$\begin{aligned}
Q_{11} &= \frac{E_{11}}{1 - \nu_{21}\nu_{12}}, \quad Q_{22} = \frac{E_{22}}{1 - \nu_{12}\nu_{21}} \\
Q_{12} &= \frac{\nu_{12}E_{22}}{1 - \nu_{12}\nu_{21}}, \quad Q_{66} = G_{12}
\end{aligned} \tag{94}$$

Substituting (92) into (91) and (90), (89) could be expressed as

$$\begin{Bmatrix} w_z - B_1u_x - B_2v_y - B_3u_y \\ w_y + v_z \\ u_z \end{Bmatrix} = \begin{Bmatrix} \bar{S}_{33} - X & 0 & 0 \\ 0 & \bar{S}_{44} & \bar{S}_{45} \\ 0 & \bar{S}_{45} & \bar{S}_{55} \end{Bmatrix} \begin{Bmatrix} \sigma_z \\ \tau_{yz} \\ \tau_{xz} \end{Bmatrix} \tag{95}$$

where

$$B_1 = \bar{S}_{13}\bar{Q}_{11} + \bar{S}_{23}\bar{Q}_{12} + \bar{S}_{36}\bar{Q}_{16} \tag{96}$$

$$B_2 = \bar{S}_{13}\bar{Q}_{12} + \bar{S}_{23}\bar{Q}_{22} + \bar{S}_{36}\bar{Q}_{26} \tag{97}$$

$$B_3 = \bar{S}_{13}\bar{Q}_{16} + \bar{S}_{23}\bar{Q}_{26} + \bar{S}_{36}\bar{Q}_{66} \tag{98}$$

and

$$X = B_1\bar{S}_{13} + B_2\bar{S}_{23} + B_3\bar{S}_{36} \tag{99}$$

The gradients of displacement appearing in the expression for interlaminar strains were then written in terms of interlaminar stresses using (95), i.e.

$$u_z = \bar{S}_{45}\tau_{yz} + \bar{S}_{55}\tau_{xz} \tag{100}$$

$$v_z = (w_y + v_z) - w_y = \bar{S}_{44}\tau_{yz} + \bar{S}_{45}\tau_{xz} - w_y \tag{101}$$



$$\begin{aligned}
w_z &= (w_z - B_1 u_x - B_2 v_y - B_3 u_x) + B_1 u_x + B_2 v_y + B_3 u_x \\
&= (\bar{S}_{33} - X) \sigma_z + B_1 u_x + B_2 v_y + B_3 u_x
\end{aligned} \tag{102}$$

Combining (100)-(102) with the rest of the displacement nodal degrees of freedom,  $u$ ,  $v$ ,  $w$ ,  $u_y$ ,  $v_y$ ,  $w_y$ , and noting that  $u_x = e_o$ , the applied strain loading, the generalized displacement components at the corner nodes of the LCCT-12 element were related to a mixed set of degrees of freedom as follows:

$$\begin{Bmatrix} u \\ v \\ w \\ u_y \\ v_y \\ w_y \\ u_z \\ v_z \\ w_z \end{Bmatrix} = \begin{bmatrix} 1 & 0 & 0 & 0 & 0 & 0 & 0 & 0 & 0 \\ 0 & 1 & 0 & 0 & 0 & 0 & 0 & 0 & 0 \\ 0 & 0 & 1 & 0 & 0 & 0 & 0 & 0 & 0 \\ 0 & 0 & 0 & 1 & 0 & 0 & 0 & 0 & 0 \\ 0 & 0 & 0 & 0 & 1 & 0 & 0 & 0 & 0 \\ 0 & 0 & 0 & 0 & 0 & 1 & 0 & 0 & 0 \\ 0 & 0 & 0 & 0 & 0 & 0 & \bar{S}_{55} & \bar{S}_{45} & 0 \\ 0 & 0 & 0 & 0 & 0 & -1 & \bar{S}_{45} & \bar{S}_{44} & 0 \\ 0 & 0 & 0 & B_3 & B_2 & 0 & 0 & 0 & \bar{S}_{33} - X \end{bmatrix} \begin{Bmatrix} u \\ v \\ w \\ u_y \\ v_y \\ w_y \\ \tau_{xz} \\ \tau_{yz} \\ \sigma_z \end{Bmatrix} + \begin{Bmatrix} 0 \\ 0 \\ 0 \\ 0 \\ 0 \\ 0 \\ 0 \\ 0 \\ B_1 e_o \end{Bmatrix} \tag{103}$$

or symbolically

$$\{r\} = [G]\{r'\} + \{R\} \tag{104}$$

$B_1$ ,  $B_2$ ,  $B_3$ , and  $X$  occurring in (103) have been defined by (96) through (99). Thus, at each of the three corners in the LCCT-12 element, we have three displacement components  $u$ ,  $v$ ,  $w$  along with three inplane strain components,  $u_y$ ,  $v_y$ ,  $w_y$ , and three interlaminar stress components  $\tau_{xz}$ ,  $\tau_{yz}$ ,  $\sigma_z$ .

### 5.2.2 Mid-side Nodes

In order to have traction continuity across interelement as well as interlaminar boundaries, it is necessary that the three traction components calculated at the mid-side nodes on the common boundary from two adjacent elements be the same. This was accomplished by transforming the displacement normal gradients associated with each of the mid-side nodes in the LCCT-12 element to three boundary traction components through the following relationships.

Let  $x_i$  and  $x'_i$  be two right-handed Cartesian coordinate systems having the same origin. Then the traction vector  $T_i$  on the plane with normal direction  $N_i$  has components  $t_i$  and  $t'_i$  in the two systems. The two components are related through the following transformation [44]

$$t'_i = l_{ij} t_j \quad (105)$$

with

$$l_{ij} = e'_i \cdot e_j \quad (106)$$

where  $e'_i$ ,  $e_j$  are unit vectors in the two coordinate systems. The traction vector can also be expressed in terms of stress components, that is

$$t_i = \sigma_{ij} n_j \quad (107)$$

with

$$n_j = \cos(e_j, N) \quad (108)$$

Substituting (107) into (105)

$$t'_i = l_{ij} t_j = l_{ij} \sigma_{kj} n_k \quad (109)$$

For the free-edge stress problem defined in a pseudo two-dimensional space [11], the traction vector  $T$  at any point on the element surface can be decomposed into three components,  $t_i$ ,  $i=1,2,3$ , in the  $x'_i$  coordinate system. Figure (7) shows these

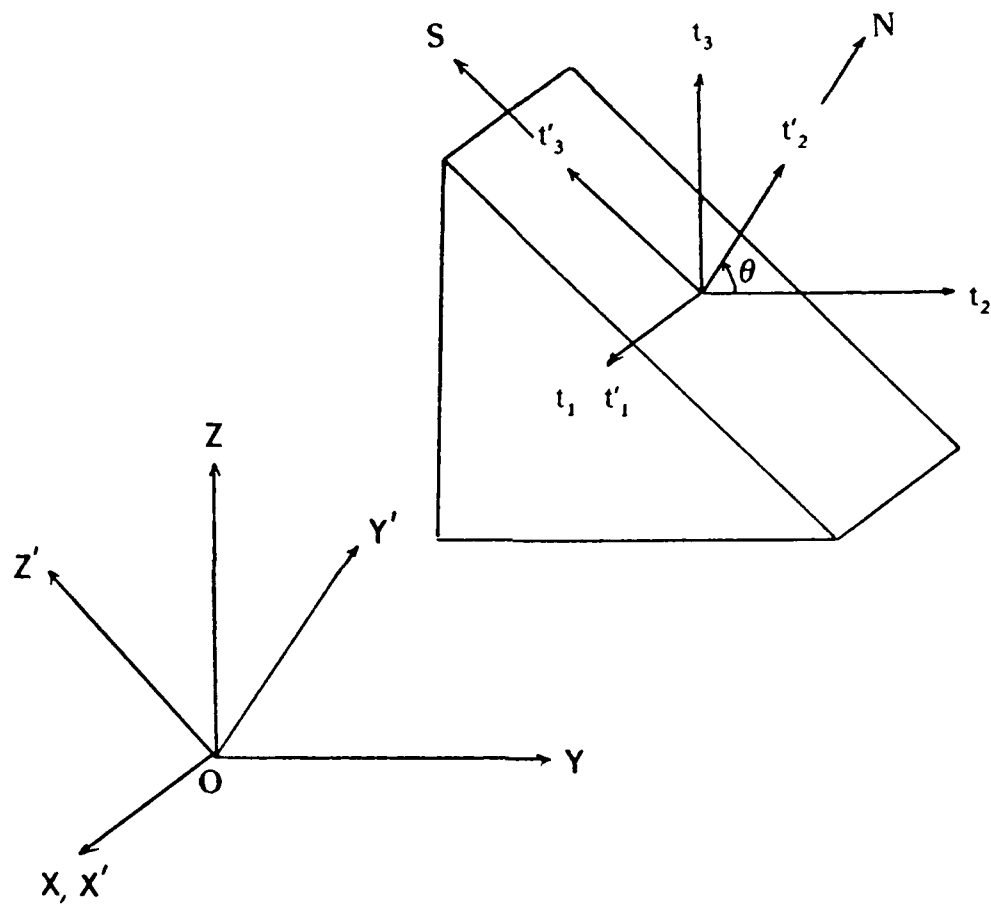


Figure 7: Components of Traction Vector Acting on an Arbitrary Plane  $N$

three traction components which indeed can be regarded as the out-of-plane shearing stress  $\sigma_{nx}$ , the normal stress  $\sigma_{nn}$ , and the in-plane shearing stress  $\sigma_{ns}$ . The relation between  $x_i$  and  $x'_i$  coordinates as shown in Figure (7) yields

$$\begin{aligned} l_{11}=1, l_{12}=0, l_{13}=0 \\ l_{21}=0, l_{22}=m, l_{23}=n \\ l_{31}=0, l_{32}=-n, l_{33}=m \end{aligned} \quad (110)$$

and

$$n_1=0, n_2=m, n_3=n \quad (111)$$

where  $m=\cos\theta$ ,  $n=\sin\theta$  and  $\theta$  is the angle between these two coordinates. Substituting the above quantities into (109), we have

$$t'_1 = \sigma_{nx} = m\tau_{xy} + n\tau_{xz} \quad (112)$$

$$t'_2 = \sigma_{nn} = m^2\sigma_y + 2mn\tau_{yz} + n^2\sigma_z \quad (113)$$

$$t'_3 = \sigma_{ns} = (m^2 - n^2)\tau_{yz} + mn(\sigma_z - \sigma_y) \quad (114)$$

Here, for interlaminar stresses acting on the element boundary are nothing but the traction field,  $\sigma_{nx}$ ,  $\sigma_{nn}$ ,  $\sigma_{ns}$  expressed in (112)-(114) indeed represent the three traction components as illustrated in Figure (7).

The stress-strain relationship for the orthotropic lamina expressed in the x-y-z laminate coordinate system is

$$\begin{bmatrix} \sigma_x \\ \sigma_y \\ \sigma_z \\ \tau_{yz} \\ \tau_{xz} \\ \tau_{xy} \end{bmatrix} = \begin{bmatrix} \bar{C}_{11} & \bar{C}_{12} & \bar{C}_{13} & 0 & 0 & \bar{C}_{16} \\ \bar{C}_{12} & \bar{C}_{22} & \bar{C}_{23} & 0 & 0 & \bar{C}_{26} \\ \bar{C}_{13} & \bar{C}_{23} & \bar{C}_{33} & 0 & 0 & \bar{C}_{36} \\ 0 & 0 & 0 & \bar{C}_{44} & \bar{C}_{45} & 0 \\ 0 & 0 & 0 & \bar{C}_{45} & \bar{C}_{55} & 0 \\ \bar{C}_{16} & \bar{C}_{26} & \bar{C}_{36} & 0 & 0 & C_{66} \end{bmatrix} \begin{bmatrix} \epsilon_x \\ \epsilon_y \\ \epsilon_z \\ \gamma_{yz} \\ \gamma_{xz} \\ \gamma_{xy} \end{bmatrix} \quad (115)$$

where  $\bar{C}_{ij}$  is the stiffness matrix for monoclinic symmetry with respect to x-y plane and is defined as [43]

$$\begin{aligned}
\bar{C}_{11} &= C_{11}m^4 + 2(C_{12} + 2C_{66})m^2n^2 + C_{22}n^4 \\
\bar{C}_{12} &= (C_{11} + C_{22} - 4C_{66})m^2n^2 + C_{12}(m^4 + n^4) \\
\bar{C}_{13} &= C_{13}m^2 + C_{23}n^2 \\
\bar{C}_{22} &= C_{11}n^4 + 2(C_{12} + 2C_{66})m^2n^2 + C_{22}m^4 \\
\bar{C}_{23} &= C_{13}n^2 + C_{23}m^2 \\
\bar{C}_{33} &= C_{33} \\
\bar{C}_{16} &= -C_{25}mn^3 + C_{14}m^3n - (C_{12} + 2C_{66})mn(m^3 - n^3) \\
\bar{C}_{26} &= -C_{25}m^3n + C_{14}mn^3 + (C_{12} + 2C_{66})mn(m^3 - n^3) \\
\bar{C}_{36} &= (C_{13} - C_{23})mn \\
\bar{C}_{44} &= C_{44}m^2 + C_{55}n^2 \\
\bar{C}_{45} &= (C_{55} - C_{44})mn \\
\bar{C}_{55} &= C_{55}m^2 + C_{44}n^2 \\
\bar{C}_{66} &= (C_{11} + C_{22} - 2C_{12})m^2n^2 + C_{66}(m^2 - n^2)^2
\end{aligned} \tag{116}$$

where, with  $m = \cos\theta'$ ,  $n = \sin\theta'$ , again  $\theta'$  is angle between the global axis x to material axis 1, and

$$\begin{aligned}
C_{11} &= \frac{(1 - \nu_{23}\nu_{32})E_{11}}{\Delta}, \quad C_{12} = \frac{(\nu_{21} + \nu_{31}\nu_{23})E_{11}}{\Delta} \\
C_{22} &= \frac{(1 - \nu_{31}\nu_{13})E_{22}}{\Delta}, \quad C_{13} = \frac{(\nu_{31} + \nu_{21}\nu_{31})E_{11}}{\Delta} \\
C_{33} &= \frac{(1 - \nu_{12}\nu_{21})E_{33}}{\Delta}, \quad C_{23} = \frac{(\nu_{32} + \nu_{12}\nu_{13})E_{22}}{\Delta} \\
C_{44} &= G_{23}, \quad C_{55} = G_{13}, \quad C_{66} = G_{12}
\end{aligned} \tag{117}$$

with

$$\Delta = 1 - \nu_{12}\nu_{21} - \nu_{23}\nu_{32} - \nu_{31}\nu_{13} - 2\nu_{21}\nu_{32}\nu_{13} \tag{118}$$

(112)-(114) along with (115), gives

$$\begin{aligned}
\begin{Bmatrix} \sigma_{ns} \\ \sigma_{nn} \\ \sigma_{ns} \end{Bmatrix} &= \begin{Bmatrix} m\bar{C}_{66} & m\bar{C}_{26} & n\bar{C}_{45} & n\bar{C}_{55} & n\bar{C}_{45} \\ m^2\bar{C}_{26}+n^2\bar{C}_{36} & m^2\bar{C}_{22}+n^2\bar{C}_{23} & 2mn\bar{C}_{44} & 2mn\bar{C}_{45} & 2mn\bar{C}_{44} \\ (\bar{C}_{36}-\bar{C}_{26})mn & (\bar{C}_{23}-\bar{C}_{22})mn & (m^2-n^2)\bar{C}_{44} & (m^2-n^2)\bar{C}_{45} & (m^2-n^2)\bar{C}_{44} \end{Bmatrix} \\
&\quad \begin{Bmatrix} u_y \\ v_y \\ w_y \\ u_z \\ v_z \\ w_z \end{Bmatrix} + \begin{Bmatrix} m\bar{C}_{16}e_o \\ (m^2\bar{C}_{12}+n^2\bar{C}_{13})e_o \\ (\bar{C}_{13}-\bar{C}_{12})mne_i \end{Bmatrix} \quad (119)
\end{aligned}$$

(119) is the general relationship between traction components at the element mid side nodes and the corresponding displacement gradients. It is different for each element midside node.

In order to relate the displacement gradients at the mid-point to the mixed nodal degrees of freedom at the two ends defining the element surface, let  $j$  and  $k$  denote the first and second cyclic permutations of  $i=1,2,3$  (i.e.  $j=2,3,1$  and  $k=3,1,2$ ), the projected dimensions and the corresponding boundary length are defined as (see Appendix A)

$$a_i = y_k - y_j, \quad b_i = z_k - z_j, \quad l_i = \sqrt{a_i^2 + b_i^2} \quad (120)$$

Also, if the outward normal is defined as positive (Figure 8), the relation between local and global Cartesian Coordinates is [42]

$$\begin{Bmatrix} s_i \\ n_i \end{Bmatrix} = \frac{1}{l_i} \begin{Bmatrix} a_i & -b_i \\ -b_i & -a_i \end{Bmatrix} \begin{Bmatrix} y-y_j \\ z-z_j \end{Bmatrix} \quad (121)$$

Considering (121) and using chain rule of differentiation, we have

$$u_{y_{i+3}} = \left( \frac{\partial u}{\partial y} \right)_{i+3} = \frac{\partial u}{\partial s_i} \frac{\partial s_i}{\partial y} + \frac{\partial u}{\partial n_i} \frac{\partial n_i}{\partial y} = \frac{a_i}{l_i} u_{s_{i+3}} - \frac{b_i}{l_i} u_{n_{i+3}} \quad (122)$$

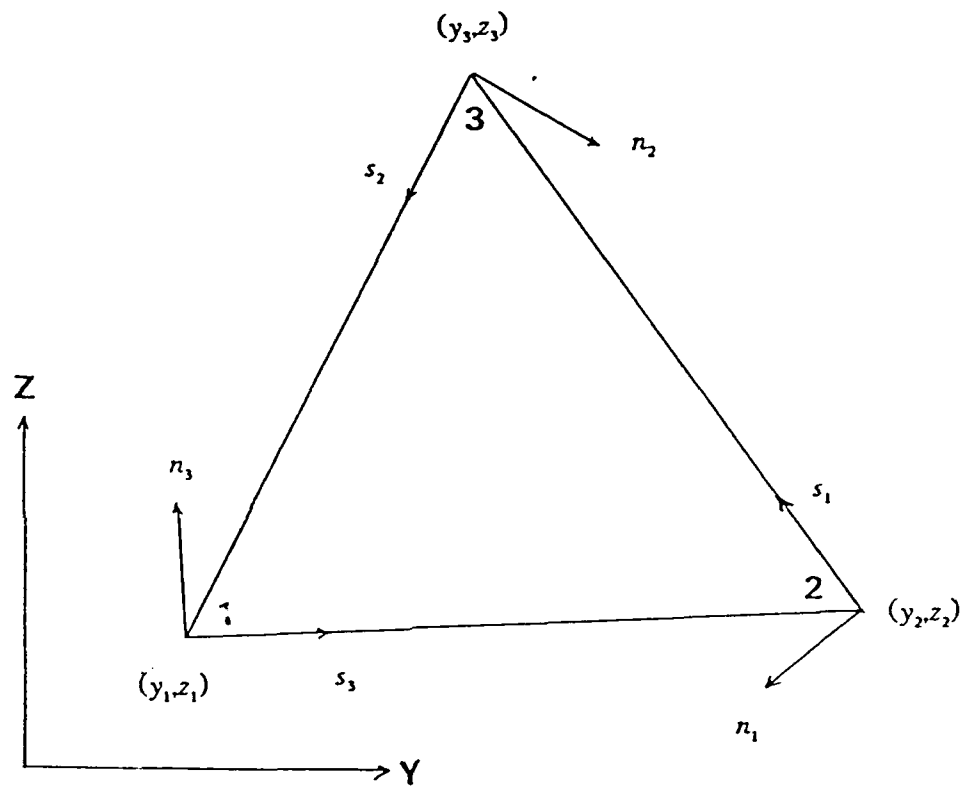


Figure 8: Local and Global Cartesian Coordinates

$$u_{z_{i+3}} = \left( \frac{\partial u}{\partial z} \right)_{i+3} = \frac{\partial u}{\partial s_i} \frac{\partial s_i}{\partial z} + \frac{\partial u}{\partial n_i} \frac{\partial n_i}{\partial z} = -\frac{b_i}{l_i} u_{s_{i+3}} - \frac{a_i}{l_i} u_{n_{i+3}} \quad (123)$$

where  $u_{s_{i+3}}$  ( $i=1,2,3$ ) denotes the tangential derivatives of  $u$  at one of the mid-side nodes (Figure 9), which can be further interpolated from the displacements and their gradients at the two ends of the corresponding element boundary, i.e.

$$u_{s_{i+3}} = -\frac{3}{2l_i} u_j - \frac{a_i}{4l_i} u_{y_j} + \frac{b_i}{4l_i} u_{z_j} + \frac{3}{2l_i} u_k - \frac{a_i}{4l_i} u_{y_k} + \frac{b_i}{4l_i} u_{z_k} \quad (124)$$

Recalling (100), we have

$$u_{z_j} = \bar{S}_{ss} \tau_{xz_j} + \bar{S}_{4s} \tau_{yz_j} \quad (125)$$

$$u_{z_k} = \bar{S}_{ss} \tau_{xz_k} + \bar{S}_{4s} \tau_{yz_k} \quad (126)$$

Substituting (124), (125) and (126) into (122) and (123), we can express  $u_j$ ,  $u_k$  at each of the element mid-side nodes in terms of their corresponding normal derivatives  $u_n$ , as well as the mixed nodal degrees of freedom at the two ends defining the segment. That is

$$\begin{aligned} u_{y_{i+3}} = & -\frac{3a_i}{2l_i^2} u_j - \frac{a_i^2}{4l_i^2} u_{y_j} + \frac{a_i b_i}{4l_i^2} \bar{S}_{ss} \tau_{xz_j} + \frac{a_i b_i}{4l_i^2} \bar{S}_{4s} \tau_{yz_j} \\ & + \frac{3a_i}{2l_i^2} u_k - \frac{a_i^2}{4l_i^2} u_{y_k} + \frac{a_i b_i}{4l_i^2} \bar{S}_{ss} \tau_{xz_k} + \frac{a_i b_i}{4l_i^2} \bar{S}_{4s} \tau_{yz_k} - \frac{b_i}{l_i} u_{n_{i+3}} \end{aligned} \quad (127)$$

$$\begin{aligned} u_{z_{i+3}} = & \frac{3b_i}{2l_i^2} u_j + \frac{a_i b_i}{4l_i^2} u_{y_j} - \frac{b_i^2}{4l_i^2} \bar{S}_{ss} \tau_{xz_j} - \frac{b_i^2}{4l_i^2} \bar{S}_{4s} \tau_{yz_j} \\ & - \frac{3b_i}{2l_i^2} u_k + \frac{a_i b_i}{4l_i^2} u_{y_k} - \frac{b_i^2}{4l_i^2} \bar{S}_{ss} \tau_{xz_k} - \frac{b_i^2}{4l_i^2} \bar{S}_{4s} \tau_{yz_k} - \frac{a_i}{l_i} u_{n_{i+3}} \end{aligned} \quad (128)$$

Following the same procedure and considering (103), the transformation equations for  $v_y$ ,  $v_z$ ,  $w_y$ ,  $w_z$  at each of the element mid side nodes are



△ : Numbering for Element Assembly

○ : Numbering for Mid-Point Transformation

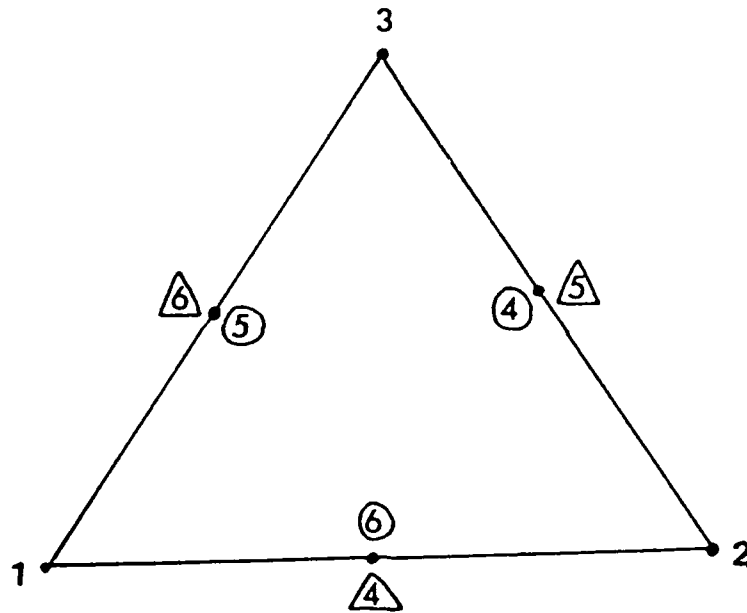


Figure 9: Numbering of Nodal Points in LCCT-12 Element

$$\begin{aligned}
v_{y_{i+3}} = & -\frac{3a_1}{2l_1^2}v_j - \frac{a_1^2}{4l_1^2}v_{y_j} - \frac{a_1b_1}{4l_1^2}w_{y_j} + \frac{a_1b_1}{4l_1^2}\bar{S}_{45}\tau_{xz_j} + \frac{a_1b_1}{4l_1^2}\bar{S}_{44}\tau_{yz_j} \\
& + \frac{3a_1}{2l_1^2}v_k - \frac{a_1^2}{4l_1^2}v_{y_k} - \frac{a_1b_1}{4l_1^2}w_{y_k} + \frac{a_1b_1}{4l_1^2}\bar{S}_{45}\tau_{xz_k} + \frac{a_1b_1}{4l_1^2}\bar{S}_{44}\tau_{yz_k} - \frac{b_1}{l_1}v_{n_{i+3}}
\end{aligned} \quad (129)$$

$$\begin{aligned}
v_{z_{i+3}} = & \frac{3b_1}{2l_1^2}v_j + \frac{a_1b_1}{4l_1^2}v_{y_j} + \frac{b_1^2}{4l_1^2}w_{y_j} - \frac{b_1^2}{4l_1^2}\bar{S}_{45}\tau_{xz_j} - \frac{b_1^2}{4l_1^2}\bar{S}_{44}\tau_{yz_j} \\
& - \frac{3b_1}{2l_1^2}v_k + \frac{a_1b_1}{4l_1^2}v_{y_k} + \frac{b_1^2}{4l_1^2}w_{y_k} - \frac{b_1^2}{4l_1^2}\bar{S}_{45}\tau_{xz_k} - \frac{b_1^2}{4l_1^2}\bar{S}_{44}\tau_{yz_k} - \frac{a_1}{l_1}v_{n_{i+3}}
\end{aligned} \quad (130)$$

$$\begin{aligned}
w_{y_{i+3}} = & -\frac{3a_1}{2l_1^2}w_j - \frac{a_1^2}{4l_1^2}w_{y_j} + \frac{a_1b_1}{4l_1^2}B_3u_{y_j} + \frac{a_1b_1}{4l_1^2}B_2v_{y_j} + \frac{a_1b_1}{4l_1^2}(\bar{S}_{33}-X)\sigma_{z_j} + \frac{3a_1}{2l_1^2}w_k \\
& - \frac{a_1^2}{4l_1^2}w_{y_k} + \frac{a_1b_1}{4l_1^2}B_3u_{y_k} + \frac{a_1b_1}{4l_1^2}B_2v_{y_k} + \frac{a_1b_1}{4l_1^2}(\bar{S}_{33}-X)\sigma_{z_k} + \frac{a_1b_1}{2l_1^2}B_1e_0 - \frac{b_1}{l_1}w_{n_{i+3}}
\end{aligned} \quad (131)$$

$$\begin{aligned}
w_{z_{i+3}} = & \frac{3b_1}{2l_1^2}w_j + \frac{a_1b_1}{4l_1^2}w_{y_j} - \frac{b_1^2}{4l_1^2}B_3u_{y_j} - \frac{b_1^2}{4l_1^2}B_2v_{y_j} - \frac{b_1^2}{4l_1^2}(\bar{S}_{33}-X)\sigma_{z_j} - \frac{3b_1}{2l_1^2}w_k \\
& + \frac{a_1b_1}{4l_1^2}w_{y_k} - \frac{b_1^2}{4l_1^2}B_3u_{y_k} - \frac{b_1^2}{4l_1^2}B_2v_{y_k} - \frac{b_1^2}{4l_1^2}(\bar{S}_{33}-X)\sigma_{z_k} - \frac{b_1^2}{2l_1^2}B_1e_0 - \frac{a_1}{l_1}w_{n_{i+3}}
\end{aligned} \quad (132)$$

Substituting (127)-(132) into (119), the relation between the surface traction components at each of the element mid-side nodes and the corresponding displacement normal gradients is

$$\begin{Bmatrix} \sigma_{nx} \\ \sigma_{nn} \\ \sigma_{ns} \end{Bmatrix}_{i+3} = [T_1]_i \begin{Bmatrix} u_n \\ v_n \\ w_n \end{Bmatrix}_{i+3} + [T_2]_i \{r'\}_{i+3} + \{T_3\}_i \quad (133)$$

where

$$[T_1] = \begin{bmatrix} m^2\bar{C}_{66} + n^2\bar{C}_{55} & m^2\bar{C}_{26} + n^2\bar{C}_{45} \\ m^3\bar{C}_{26} + mn^2\bar{C}_{36} + 2mn^2\bar{C}_{45} & m^3\bar{C}_{22} + mn^2\bar{C}_{23} + 2mn^2\bar{C}_{44} \\ (\bar{C}_{36} - \bar{C}_{26})m^2n + (m^2n - n^3)\bar{C}_{45} & (\bar{C}_{23} - \bar{C}_{22})m^2n + (m^2n - n^3)\bar{C}_{44} \\ (\bar{C}_{45} + \bar{C}_{36})mn & \\ 2m^2n\bar{C}_{44} + m^2n\bar{C}_{23} + n^3\bar{C}_{33} & \\ (m^3 - mn^2)\bar{C}_{44} + (\bar{C}_{33} - \bar{C}_{23})mn^2 & \end{bmatrix} \quad (134)$$

$$\{T\}_{1 \times 6} = \{u_1, v_1, w_1, u_2, v_2, w_2, \tau_{xz1}, \tau_{yz1}, \sigma_{z1}, u_3, v_3, w_3, u_4, v_4, w_4, \tau_{xz4}, \tau_{yz4}, \sigma_{z4}\}^T \quad (135)$$

$$\{T\}_1 = \begin{bmatrix} \frac{1}{2}\bar{C}_{44}mn^3B_1 - \frac{1}{2}\bar{C}_{66}m^3B_1 + m\bar{C}_{16} \\ \bar{C}_{44}m^2n^3B_1 - \frac{1}{2}(m^4\bar{C}_{23} + m^2n^2\bar{C}_{33})B_1 + m^2\bar{C}_{12} + n^2\bar{C}_{13} \\ \frac{1}{2}\bar{C}_{44}(m^3n - mn^3)B_1 - \frac{1}{2}(\bar{C}_{33} - \bar{C}_{23})m^3nB_1 + (\bar{C}_{13} - \bar{C}_{12})mn \end{bmatrix} e_0 \quad (136)$$

with

$$m = -\frac{b_1}{l_1}, \quad n = -\frac{a_1}{l_1} \quad (137)$$

and  $[T_1]$  is the product of the transformation matrix shown in (119) with the following matrix  $[TA]$

$$\begin{aligned}
[TA] = & \begin{bmatrix}
-\frac{3a_1}{2l_1^2} & 0 & 0 & -\frac{a_1^2}{4l_1^2} & 0 & 0 & \frac{a_1 b_1}{4l_1^2} S_{33} & \frac{a_1 b_1}{4l_1^2} S_{43} & 0 \\
0 & -\frac{3a_1}{2l_1^2} & 0 & 0 & -\frac{a_1^2}{4l_1^2} & -\frac{a_1 b_1}{4l_1^2} & \frac{a_1 b_1}{4l_1^2} S_{43} & \frac{a_1 b_1}{4l_1^2} S_{44} & 0 \\
0 & 0 & -\frac{3a_1}{2l_1^2} & \frac{a_1 b_1}{4l_1^2} B_3 & \frac{a_1 b_1}{4l_1^2} B_2 & -\frac{a_1^2}{4l_1^2} & 0 & 0 & \frac{a_1 b_1}{4l_1^2} (S_{33} - X) \\
\frac{3b_1}{2l_1^2} & 0 & 0 & \frac{a_1 b_1}{4l_1^2} & 0 & 0 & -\frac{b_1^2}{4l_1^2} S_{33} & -\frac{b_1^2}{4l_1^2} S_{43} & 0 \\
0 & \frac{3b_1}{2l_1^2} & 0 & 0 & \frac{a_1 b_1}{4l_1^2} & -\frac{b_1^2}{4l_1^2} & -\frac{b_1^2}{4l_1^2} S_{43} & -\frac{b_1^2}{4l_1^2} S_{44} & 0 \\
0 & 0 & \frac{3b_1}{2l_1^2} & -\frac{b_1^2}{4l_1^2} B_3 & -\frac{b_1^2}{4l_1^2} B_2 & \frac{a_1 b_1}{4l_1^2} & 0 & 0 & -\frac{b_1^2}{4l_1^2} (S_{33} - X)
\end{bmatrix} \\
& \begin{bmatrix}
\frac{3a_1}{2l_1^2} & 0 & 0 & -\frac{a_1^2}{4l_1^2} & 0 & 0 & \frac{a_1 b_1}{4l_1^2} S_{33} & \frac{a_1 b_1}{4l_1^2} S_{43} & 0 \\
0 & \frac{3a_1}{2l_1^2} & 0 & 0 & -\frac{a_1^2}{4l_1^2} & -\frac{a_1 b_1}{4l_1^2} & \frac{a_1 b_1}{4l_1^2} S_{43} & \frac{a_1 b_1}{4l_1^2} S_{44} & 0 \\
0 & 0 & \frac{3a_1}{2l_1^2} & \frac{a_1 b_1}{4l_1^2} B_3 & \frac{a_1 b_1}{4l_1^2} B_2 & -\frac{a_1^2}{4l_1^2} & 0 & 0 & \frac{a_1 b_1}{4l_1^2} (S_{33} - X) \\
-\frac{3b_1}{2l_1^2} & 0 & 0 & \frac{a_1 b_1}{4l_1^2} & 0 & 0 & -\frac{b_1^2}{4l_1^2} S_{33} & -\frac{b_1^2}{4l_1^2} S_{43} & 0 \\
0 & -\frac{3b_1}{2l_1^2} & 0 & 0 & \frac{a_1 b_1}{4l_1^2} & -\frac{b_1^2}{4l_1^2} & -\frac{b_1^2}{4l_1^2} S_{43} & -\frac{b_1^2}{4l_1^2} S_{44} & 0 \\
0 & 0 & -\frac{3b_1}{2l_1^2} & -\frac{b_1^2}{4l_1^2} B_3 & -\frac{b_1^2}{4l_1^2} B_2 & \frac{a_1 b_1}{4l_1^2} & 0 & 0 & -\frac{b_1^2}{4l_1^2} (S_{33} - X)
\end{bmatrix}
\end{aligned}
\tag{138}$$

Rearranging (133), the displacement stress transformtions for the normal displacement gradients at each of the mid side nodes in the TCT12 element are

$$\begin{Bmatrix} u_n \\ v_n \\ w_n \end{Bmatrix}_{i+3} = [T_1]_i^{-1} \begin{Bmatrix} \sigma_{xx} \\ \sigma_{yy} \\ \sigma_{xy} \end{Bmatrix}_{i+3} - [T_1]_i^{-1} [T_2]_i \{r\}_{i+3} - [T_1]_i^{-1} [T_3]_i \{S\}_i \quad (139)$$

or symbolically,

$$\{r\}_{i+3} = [H]_i \{r'\}_{i+3} + [L]_i \{r\}_{i+3} + \{S\}_i \quad (140)$$

where

$$[H]_i = [T_1]_i^{-1} \quad (141)$$

$$[L]_i = -[T_1]_i^{-1} [T_2]_i \quad (142)$$

$$\{S\}_i = -[T_1]_i^{-1} [T_3]_i \{S\}_i \quad (143)$$

Here,  $[H]_i$  denotes the transformation matrix which directly related the normal slope quantities at the mid-point,  $i+3$ , to the corresponding surface traction components.  $[L]_i$  can be regarded as the coupling matrix between the normal gradients and the mixed degrees of freedom associated with the nodal points,  $j$  and  $k$ , at the two ends of the boundary.  $\{S\}_i$  is the local effect resulting from the applied uniform loading  $e_0$ .

### 5.3 Finite Element Formulation

The discretized form of (73) can be rewritten as

$$\Omega = \sum_{m=1}^M \left( \frac{1}{2} \{q^m\}^T [K^m] \{q^m\} - \{q^m\}^T \{F^m\} \right) \quad (144)$$

where  $[K^m]$  is the element stiffness matrix,  $\{F^m\}$  denotes the nodal force including the local effect due to the uniform in-plane strain loading as shown in (80) for the free-edge stress problem.  $\{q^m\}$  is the set of generalized nodal displacement components within the element  $m$ , and  $M$  denotes the total number of elements.

In order to have both displacement and traction continuity along interelement as well as interlaminar boundaries, assuming (144) is based on continuous strain cubic displacement interpolation as in LCCT-12 described in 4.3.2, the displacement-stress transformation matrices derived in the previous section were imposed on the generalized degrees of freedom. Combining (104) and (140), the generalized displacement components in the LCCT-12 element were transformed to the mixed type degrees of freedom as follows:

$$\{q^m\} = [T^m] \{q^d\} + \{P^m\} \quad (145)$$

where

$$[T^m] = \begin{bmatrix} [G] & 0 & 0 & 0 & 0 & 0 \\ 0 & [G] & 0 & 0 & 0 & 0 \\ 0 & 0 & [G] & 0 & 0 & 0 \\ [L]_3 & [L]_3 & 0 & [H]_3 & 0 & 0 \\ 0 & [L]_1 & [L]_1 & 0 & [H]_1 & 0 \\ [L]_2 & 0 & [L]_2 & 0 & 0 & [H]_2 \end{bmatrix} \quad (146)$$

$$\{P^m\} = \{\{R\}, \{R\}, \{R\}, \{S\}_3, \{S\}_1, \{S\}_2\}^T \quad (147)$$

$$\{q^m\} = \{u_1, v_1, w_1, u_{y1}, v_{y1}, w_{y1}, u_{z1}, v_{z1}, w_{z1}, u_2, v_2, w_2, u_{y2}, v_{y2}, w_{y2}, u_{z2}, v_{z2}, w_{z2}, \\ u_3, v_3, w_3, u_{y3}, v_{y3}, w_{y3}, u_{z3}, v_{z3}, w_{z3}, u_4, v_4, w_4, u_{y4}, v_{y4}, w_{y4}, u_5, v_5, w_5\}^T \quad (148)$$

$$\{q^m\} = \{u_1, v_1, w_1, u_{y1}, v_{y1}, w_{y1}, \tau_{xz1}, \tau_{yz1}, \sigma_{z1}, u_2, v_2, w_2, u_{y2}, v_{y2}, w_{y2}, \tau_{xz2}, \tau_{yz2}, \sigma_{z2}, u_3, v_3, w_3, \\ u_{y3}, v_{y3}, w_{y3}, \tau_{xz3}, \tau_{yz3}, \sigma_{z3}, \sigma_{nx6}, \sigma_{ny6}, \sigma_{nz6}, \sigma_{nx4}, \sigma_{ny4}, \sigma_{nz4}, \sigma_{nx5}, \sigma_{ny5}, \sigma_{nz5}\}^T \quad (149)$$

Each of the  $[L]_i$  matrices in (146) was divided into two parts to match the mixed degrees of freedom in (149). In the finite element computation, this transformation was implemented during the formation of each of the subtriangular element stiffness matrix and load vector corresponding to the LCCT-12 element. Thus, due to

appearance of displacement and interlaminar traction components at the corners of the triangle as well as traction components at the mid-side nodes, a cubic variation of displacement and a quadratic variation of traction were ensured along element boundary. More importantly, both fields are continuous across the common boundary between two contiguous triangular elements. Substituting (145) into (144), we have

$$\begin{aligned}\Omega &= \sum_{m=1}^M \left( \frac{1}{2} \{q^{(m)}\}^T [T^{(m)}]^T + \{P^{(m)}\}^T \right) [K^{(m)}] ([T^{(m)}] \{q^{(m)}\} + \{P^{(m)}\}) - (\{q^{(m)}\}^T [T^{(m)}]^T + \{P^{(m)}\}^T) \{F^{(m)}\}) \\ &= \sum_{m=1}^M \left( \frac{1}{2} \{q^{(m)}\}^T [T^{(m)}]^T [K^{(m)}] [T^{(m)}] \{q^{(m)}\} + \frac{1}{2} \{q^{(m)}\}^T [T^{(m)}]^T [K^{(m)}] \{P^{(m)}\} + \frac{1}{2} \{P^{(m)}\}^T [K^{(m)}] [T^{(m)}] \{q^{(m)}\} \right. \\ &\quad \left. + \frac{1}{2} \{P^{(m)}\}^T [K^{(m)}] \{P^{(m)}\} - \{q^{(m)}\}^T [T^{(m)}]^T \{F^{(m)}\} - \{P^{(m)}\}^T \{F^{(m)}\} \right) \quad (150)\end{aligned}$$

or

$$\Omega = \sum_{m=1}^M \left( \frac{1}{2} \{q^{(m)}\}^T [\bar{K}^{(m)}] \{q^{(m)}\} - \{q^{(m)}\}^T \{\bar{R}^{(m)}\} + C^{(m)} \right) \quad (151)$$

where

$$[\bar{K}^{(m)}] = [T^{(m)}]^T [K^{(m)}] [T^{(m)}] \quad (152)$$

$$\{\bar{R}^{(m)}\} = [T^{(m)}]^T \{F^{(m)}\} - [T^{(m)}]^T [K^{(m)}] \{P^{(m)}\} \quad (153)$$

$$C^{(m)} = \frac{1}{2} \{P^{(m)}\}^T [K^{(m)}] \{P^{(m)}\} - \{P^{(m)}\}^T \{F^{(m)}\} = \text{constant} \quad (154)$$

Using global coordinates, (151) could be written as

$$\Omega = \frac{1}{2} \{q'\}^T [\bar{K}] \{q'\} - \{q'\}^T \{\bar{R}\} + C_m \quad (155)$$

Taking the variation of (155) with respect to  $\{q'\}$  yields the system generalized nodal force-displacement equilibrium equations

$$[\bar{K}] \{q'\} = \{\bar{R}\} \quad (156)$$

The displacement as well as interlaminar stress components were then obtained by solving the resulting set of linear equations in the standard manner.

#### 5.4 Calculation of Stresses

Solutions of the finite element system gives the three displacement components, their tangential gradients along the element edges, rotation about the longitudinal axis and interlaminar stress field at the corner nodes of the Q-23 element, along with the boundary traction components at the center point of each of the Q-23 element surfaces. To retrieve the rest of the displacement components at each corner node, the transformation matrix used in (104) was reapplied to the calculated nodal point solution. Having found the complete displacement gradients and hence strains, the inplane stress components at the corner nodes of the Q-23 element could then be computed using (115).

The interlaminar or interelement stress components at the mid-point of each element boundary are merely the traction components directly produced by the solution of the continuous traction Q-23 element provided a rectangular mesh is used in the analysis. For determining the rest of the stress components, the normal displacement gradients at mid-side nodes were recovered from the nodal point solution using (140). Furthermore, the displacement and their gradients along the edge at the mid-point were interpolated from the previously computed displacement components at the two ends of the segment. Having transformed these displacement gradients from local to global Cartesian coordinates, calculation of the remaining strain and stress components at the mid-side of each of the element boundaries is direct.



## 5.5 Boundary Conditions of a Quadrant of the Delamination Specimen

For the free-edge delamination specimen, because of symmetries in the laminate, only one quadrant of an  $x=\text{constant}$  plane was considered (Figure 2). Along the boundary, either displacements or tractions are specified at each point.

### 5.5.1 Boundary Conditions Along Lines of Symmetry

Symmetry of loading as well as geometry about the mid-plane implies that the displacement functions satisfy the following condition

$$U(y,-z)=U(y,z) \quad (157)$$

$$V(y,-z)=V(y,z) \quad (158)$$

$$W(y,-z)=-W(y,z) \quad (159)$$

Using chain rule of differentiation,

$$-U_z(y,-z)=U_z(y,z) \quad (160)$$

$$-V_z(y,-z)=V_z(y,z) \quad (161)$$

$$W_y(y,-z)=-W_y(y,z) \quad (162)$$

Setting  $z=0$  in (5.79)-(5.82), we have

$$W(y,0)=0 \quad (163)$$

$$W_y(y,0)=U_z(y,0)=V_z(y,0)=0 \quad (164)$$

From (5.84),  $\gamma_{xz}(y,0)=\gamma_{yz}(y,0)=0$ , and consequently, for the layered orthotropic material,

$$\tau_{xz}(y,0)=\tau_{yz}(y,0)=0 \quad (165)$$

Also

$$(W_y - V_z)(y,0) = 0$$

Invariance under a rotation of 180 degree about the z-axis through the center of the specimen implies

$$U(-y,z)=-U(y,z) \quad (166)$$

$$V(-y,z)=-V(y,z) \quad (167)$$

$$W(-y,z)=W(y,z) \quad (168)$$

(166) and (167) lead immediately to

$$U(0,z)=V(0,z)=0 \quad (169)$$

for all  $z$ , and consequently

$$U_y(0,z)=V_y(0,z)=0 \quad (170)$$

By chain rule of differentiation, (166) yields

$$-W_y(-y,z)=W_y(y,z) \quad (171)$$

Hence, for  $y=0$

$$W_y(0,z)=0 \quad (172)$$

(170) and (172) imply  $\gamma_{xz}(0,z)=\gamma_{yz}(0,z)=0$ . Hence, for the layered orthotropic material,

$$\tau_{xz}(0,z)=\tau_{yz}(0,z)=0 \quad (173)$$

Also

$$(W_y - V_y)(0,z) = 0$$

Combining (163), (164), (165), (169), (172) and (173), along with  $U(0,0)=0$  in order to prevent rigid-body displacement of the laminate, the continuous traction finite element model for a quadrant laminate under consideration should satisfy the following conditions along lines of symmetry

$$U(0,0)=U(0,z)=V(0,z)=W(y,0)=W_y(y,0)=W_y(0,z)=0 \quad (174)$$

$$\tau_{xz}(y,0)=\tau_{yz}(y,0)=\tau_{xz}(0,z)=\tau_{yz}(0,z)=0 \quad (175)$$

### 5.5.2 Traction-Free Boundary Conditions

The traction free boundary conditions associated with one quadrant of the laminated specimen are

$$\tau_{xz}(y,H)=\tau_{yz}(y,H)=\sigma_z(y,H)=0 \quad (176)$$

at the top surface, along with

$$\sigma_x(B,z)=\tau_{xy}(B,z)=\tau_{xz}(B,z)=0 \quad (177)$$

at the lateral free edge. Here  $2B$  and  $2H$  denote the total width and thickness respectively of the laminated specimen. Using the continuous traction Q 23 model, traction-free boundary conditions shown in (176) can be identically satisfied for nodal points on the top surface. However, due to the lack of inplane stress components as nodal degrees of freedom, only the last condition shown in (177) can be specified at those element corner nodes along the lateral free-edge. To completely satisfy the traction-free condition along the lateral free-edge, the following device was developed.

In order to enforce the remaining two inplane stress-free conditions in (177), it is necessary to express these in terms of nodal point degrees of freedom. This results in a linear relationship between the degrees of freedom at nodal points on the free edge. The stress free condition can be written explicitly as

$$\sigma_x=0=\bar{C}_{12}e_x+\bar{C}_{23}w_z+\bar{C}_{22}v_x+\bar{C}_{26}u_x \quad (178)$$

$$\tau_{xy}=0=\bar{C}_{16}e_x+\bar{C}_{36}w_z+\bar{C}_{26}v_x+\bar{C}_{66}u_x \quad (179)$$

or symbolically

$$\begin{Bmatrix} 0 \\ 0 \end{Bmatrix} = \begin{bmatrix} \bar{C}_{12} & \bar{C}_{23} & \bar{C}_{22} & \bar{C}_{26} \\ \bar{C}_{16} & \bar{C}_{36} & \bar{C}_{26} & \bar{C}_{66} \end{bmatrix} \begin{Bmatrix} e_x \\ w_z \\ v_x \\ u_x \end{Bmatrix} \quad (180)$$

where  $\bar{C}_{ij}$  are components of the stiffness matrix defined by (116). Solving above equation, the inplane strain components  $u_y, v_y$  can be expressed in terms of interlaminar normal strain  $w_z$ , by

$$\begin{Bmatrix} v_y \\ u_y \end{Bmatrix} = \begin{bmatrix} I_{11} & I_{12} \\ I_{21} & I_{22} \end{bmatrix} \begin{Bmatrix} e_o \\ w_z \end{Bmatrix} \quad (181)$$

where

$$\begin{aligned} I_{11} &= \frac{1}{\alpha} (\bar{C}_{26}\bar{C}_{16} - \bar{C}_{66}\bar{C}_{11}) \\ I_{12} &= \frac{1}{\alpha} (\bar{C}_{26}\bar{C}_{36} - \bar{C}_{66}\bar{C}_{12}) \\ I_{21} &= \frac{1}{\alpha} (\bar{C}_{26}\bar{C}_{12} - \bar{C}_{22}\bar{C}_{16}) \\ I_{22} &= \frac{1}{\alpha} (\bar{C}_{26}\bar{C}_{23} - \bar{C}_{22}\bar{C}_{36}) \end{aligned} \quad (182)$$

and

$$\alpha = \bar{C}_{22}\bar{C}_{66} - \bar{C}_{26}^2 \quad (183)$$

Substituting (102) into (181) for  $w_z$ , we can further relate  $u_y$  and  $v_y$  to the interlaminar normal stress component  $\sigma_z$  through the following linear relationships

$$u_y = p_1 \sigma_z + p_2 e_o \quad (184)$$

$$v_y = q_1 \sigma_z + q_2 e_o \quad (185)$$

where

$$p_1 = \frac{1}{\beta} [I_{22}(\bar{S}_{33} - X)] \quad (186)$$

$$p_2 = \frac{1}{\beta} (I_{11}I_{22}B_2 - I_{12}I_{21}B_2 + I_{22}B_1 + I_{21}) \quad (187)$$

$$q_1 = \frac{1}{\beta} [I_{12}(\bar{S}_{33} - X)] \quad (188)$$

$$q_2 = \frac{1}{\beta} (I_{12}I_{21}B_3 - I_{11}I_{22}B_3 + I_{12}B_1 + I_{11}) \quad (189)$$

and

$$\beta = 1 - l_{22}B_3 - l_{12}B_2 \quad (190)$$

Again,  $B_1$ ,  $B_2$ ,  $B_3$  and  $X$  occurring in (186) through (190) have been defined by (96)-(99). Thus, the variables associated with the nodal points of the free-edge in the lateral continuous traction Q-23 element are no longer independent but related through (184) and (185). Incorporating these linear relationships in the displacement-stress transformations shown in (104) and (140) for elements on the lateral boundary implies satisfaction of the traction free boundary conditions (177). The transformation becomes

$$\begin{Bmatrix} u \\ v \\ w \\ u_y \\ v_y \\ w_y \\ u_z \\ v_z \\ w_z \end{Bmatrix} = \begin{bmatrix} 1 & 0 & 0 & 0 & 0 & 0 & 0 & 0 & 0 \\ 0 & 1 & 0 & 0 & 0 & 0 & 0 & 0 & 0 \\ 0 & 0 & 1 & 0 & 0 & 0 & 0 & 0 & 0 \\ 0 & 0 & 0 & 0 & 0 & 0 & 0 & 0 & p_1 \\ 0 & 0 & 0 & 0 & 0 & 0 & 0 & 0 & q_1 \\ 0 & 0 & 0 & 0 & 0 & 1 & 0 & 0 & 0 \\ 0 & 0 & 0 & 0 & 0 & 0 & \bar{S}_{55} & \bar{S}_{45} & 0 \\ 0 & 0 & 0 & 0 & 0 & -1 & \bar{S}_{45} & \bar{S}_{44} & 0 \\ 0 & 0 & 0 & 0 & 0 & 0 & 0 & 0 & r_1 \end{bmatrix} \begin{Bmatrix} u \\ v \\ w \\ u_y \\ v_y \\ w_y \\ \tau_{xz} \\ \tau_{yz} \\ \sigma_z \end{Bmatrix} + \begin{Bmatrix} 0 \\ 0 \\ 0 \\ p_2 e_o \\ q_2 e_o \\ 0 \\ 0 \\ 0 \\ r_2 e_o \end{Bmatrix} \quad (191)$$

where

$$r_1 = \bar{S}_{33} - X + B_2 q_1 + B_3 p_1 \quad (192)$$

$$r_2 = B_1 + B_2 q_2 + B_3 p_2 \quad (193)$$

## SECTION VI

### ANALYSIS OF FREE-EDGE DELAMINATION IN LAMINATE COMPOSITE SPECIMENS

#### 6.1 Introduction

Continuous traction finite element formulation developed in the previous section was applied to obtain an approximation to displacement as well as stress fields in a free-edge delamination specimen. The analysis consisted of two parts. The first consisted of solving four-ply symmetric laminates. The purpose was to examine the credibility of the continuous traction finite element model by comparing the numerical solutions with those from Pagano's analysis based on a generalization of Reissner's theory. At the same time, the deficiency in using the continuous strain free-edge stress model described in Section IV was examined. The second part consisted of studying of edge delamination tendency in two classes of multi-ply laminates subjected to longitudinal loading. For laminate specimens with stacking sequence of  $[(\theta/-\theta)_m/90_n]_2$ , displacement and stress fields calculated from the continuous traction Q-23 element were compared with those obtained using an overlay procedure with constant strain elements [45] and with experimental observation [46]. For the  $[(\theta/-\theta)_2/90]_2$  laminate specimens, the continuous traction finite element code was used in conjunction with some well known anisotropic failure criteria [47-50] to predict the onset of transverse cracking and the onset of edge delamination in various laminate specimens observed in experimental data [51]. The purpose was to evaluate the

suitability of these failure criteria for application to the free-edge delamination problem. Because of symmetries in the laminates, only one quadrant (Figure 2) was considered in each case.

## 6.2 Four-Ply Laminates

In this section, analysis of two long symmetric laminate strips made of graphite epoxy materials, with fiber orientations of  $[45\ 45]$  and  $[0\ 90]$  under uniform inplane strain in the longitudinal direction is described. The relation between laminate width and thickness was  $2b=16h$  following [8]. In the analysis, each ply was idealized as a homogeneous, elastic orthotropic material. For comparison purpose, the material properties assumed here following Pagano's work [8]

$$E_{11}=20\times 10^6 \text{ psi}$$

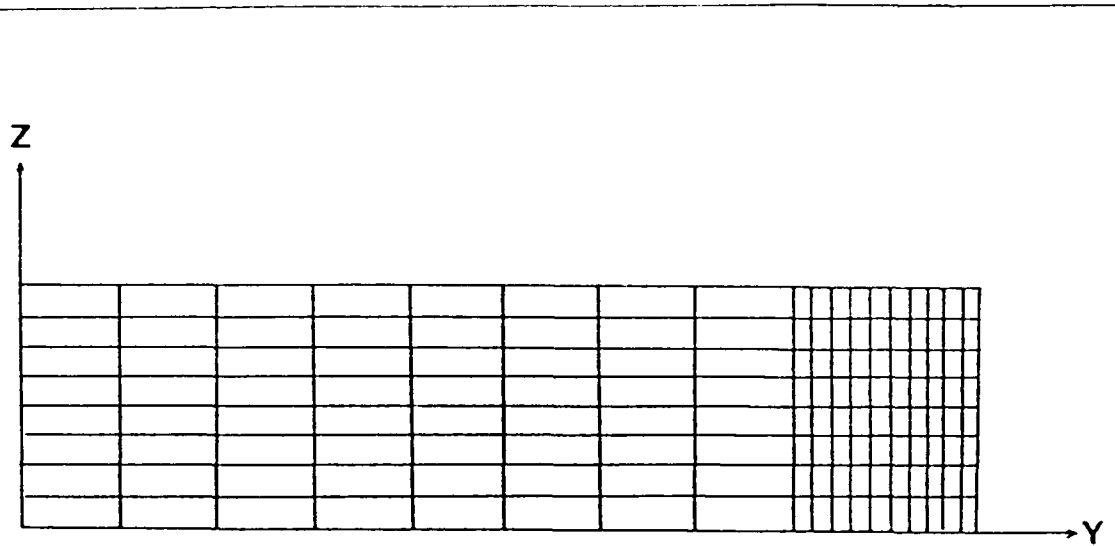
$$E_{22}=E_{33}=2.1\times 10^6 \text{ psi}$$

$$G_{12}=G_{13}=G_{23}=0.85\times 10^6 \text{ psi}$$

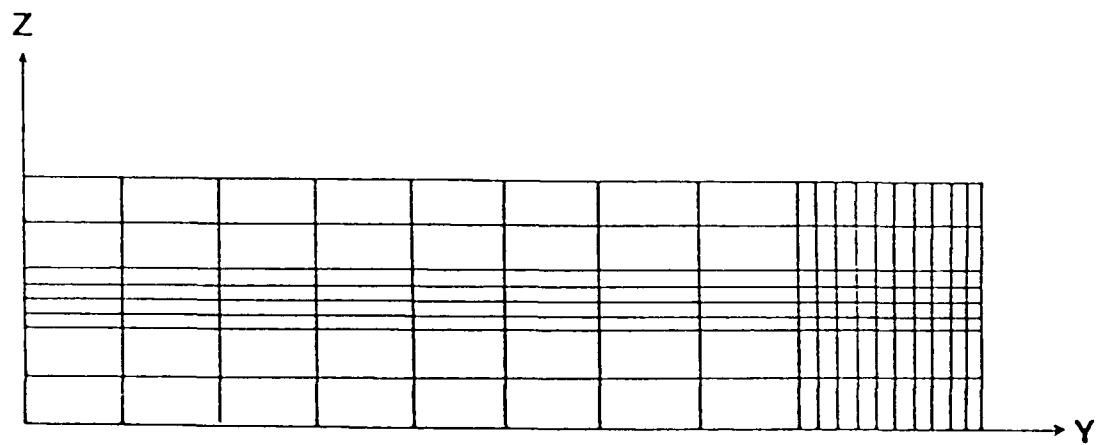
$$\nu_{12}=\nu_{13}=\nu_{23}=0.21$$

The subscripts 1, 2 and 3 correspond to the longitudinal transverse and thickness directions respectively. A 144-element model as shown in Figure (10a) was used to discretize a typical  $x=\text{constant}$  plane. Numerical results based on the continuous traction  $Q_{23}$  and continuous strain  $Q_{23}$  elements were compared with Pagano's [8] analytical solution.

Figures (11) through (23) illustrate comparisons for both stress and displacement fields at specific locations for the angle-ply and cross-ply laminates using different solution techniques. The value of  $N$  in these figures corresponds to the number of sublayers used in Pagano's theory. Thus,  $N=6$  indicates that each physical layer of thickness  $h$  was modeled by three sublayers each of thickness  $h/3$ , while  $N=2$  denotes



(a)



(b)

Figure 10: 144-Element Mesh



that each physical layer is treated as a unit [8]. Also, the calculated displacements and stresses were normalized by the applied uniform strain loading  $\epsilon_0$  which has been taken as unit in the present analysis.

### 6.2.1 Angle-Ply Laminate

Figures (11) and (12) show the distribution of  $\sigma_x$  and  $\tau_{xy}$  along the width of the laminate at the center line of the top (45 degree) layer. The results obtained using the continuous traction Q-23 element agreed quite well with those of Pagano's N-6 solutions across the entire width of the laminate.

A comparison of the shear stress ( $\tau_{xz}$ ) distribution along the interface of the 45/-45 layers (Figure 13), indicated that the continuous traction Q-23 solution had sharp rise toward the free-edge similar to Pagano's solution with N=6. Satisfactory agreement was observed between these two solutions for stress across the width except at the free-edge boundary where continuous traction Q-23 somewhat underestimated the singular stress. Figure (14) shows the through-thickness stress distribution of  $\tau_{xz}$  calculated from both continuous strain and continuous traction Q-23 elements at the free-edge of the laminate. Very close agreement was generally observed between these two solutions throughout the thickness. Also, at the interface of the 45/-45 layers, continuity of the interlaminar shear stress was ensured for both cases. This is because of the rotational symmetry about z-axis in the particular angle-ply laminate considered. The singular behavior of  $\tau_{xz}$ , which is highly localized at the interface between 45/-45 layers, is noticeable. The distribution of  $\sigma_z$  along the interface between 45° and -45° plies, which was not indicated in [8], will be discussed in the next section.

For the axial displacement distribution across the width of the top surface, continuous traction Q-23 results compared well with Pagano's N-6 solution (Figure 15).

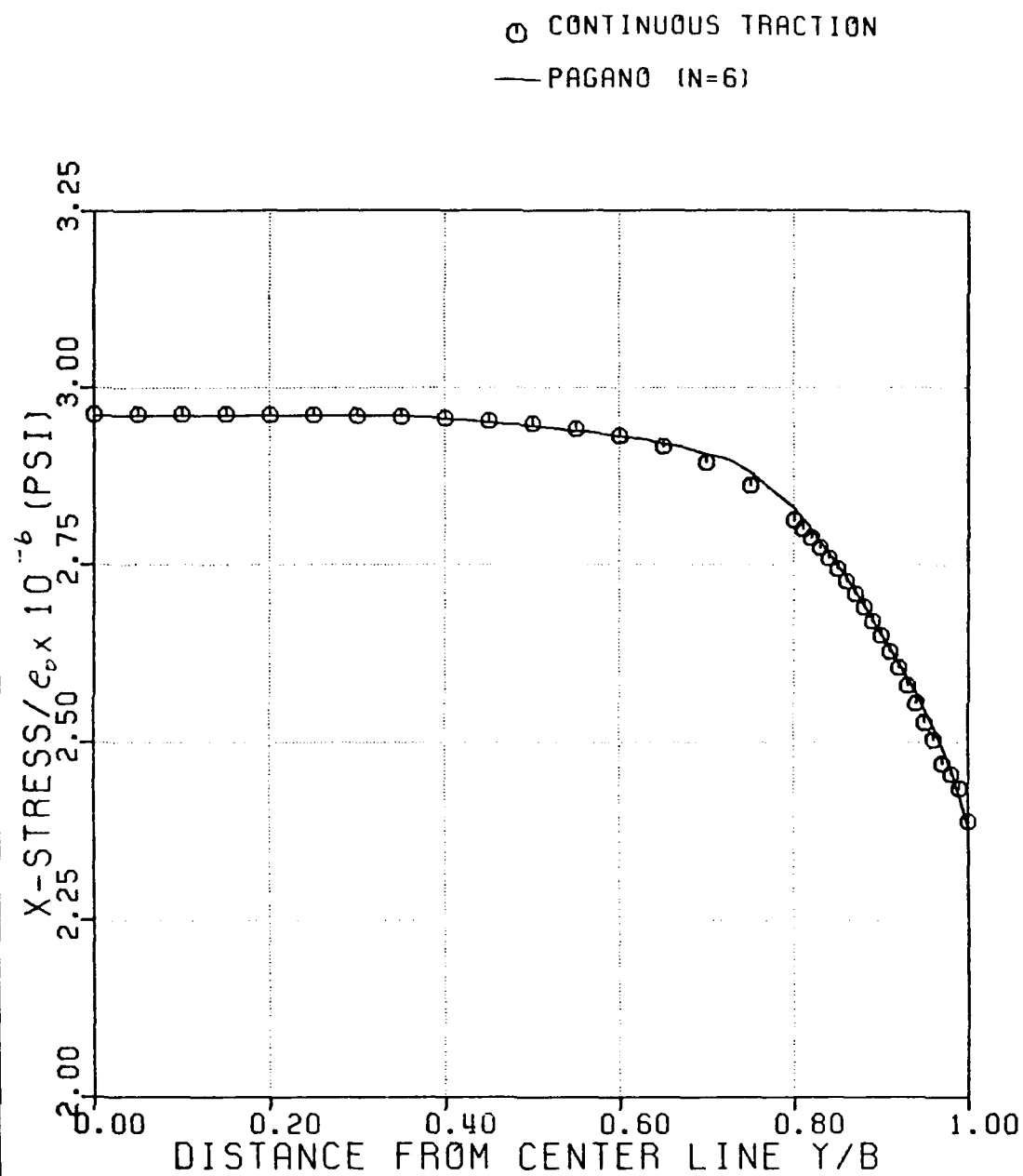
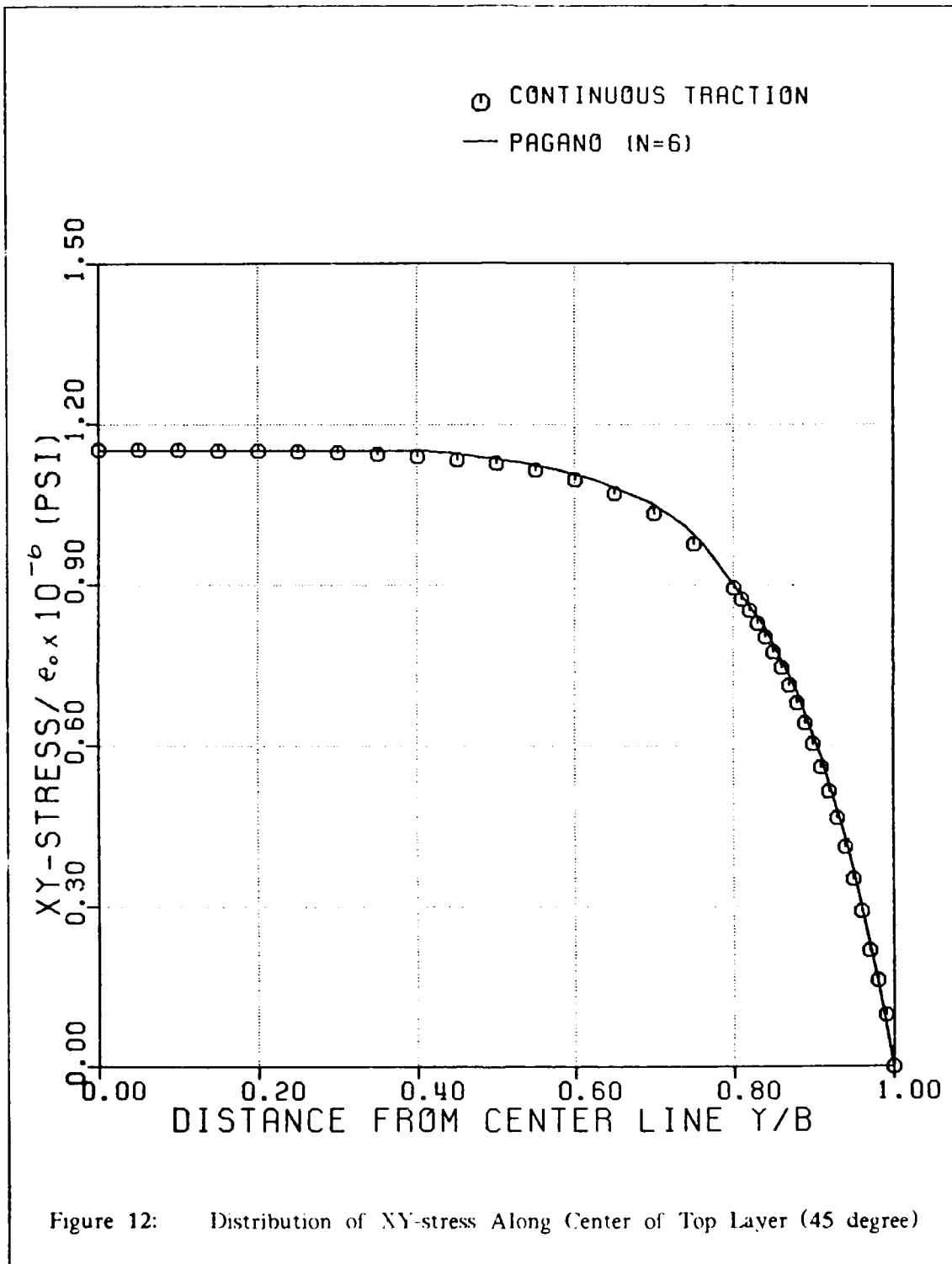
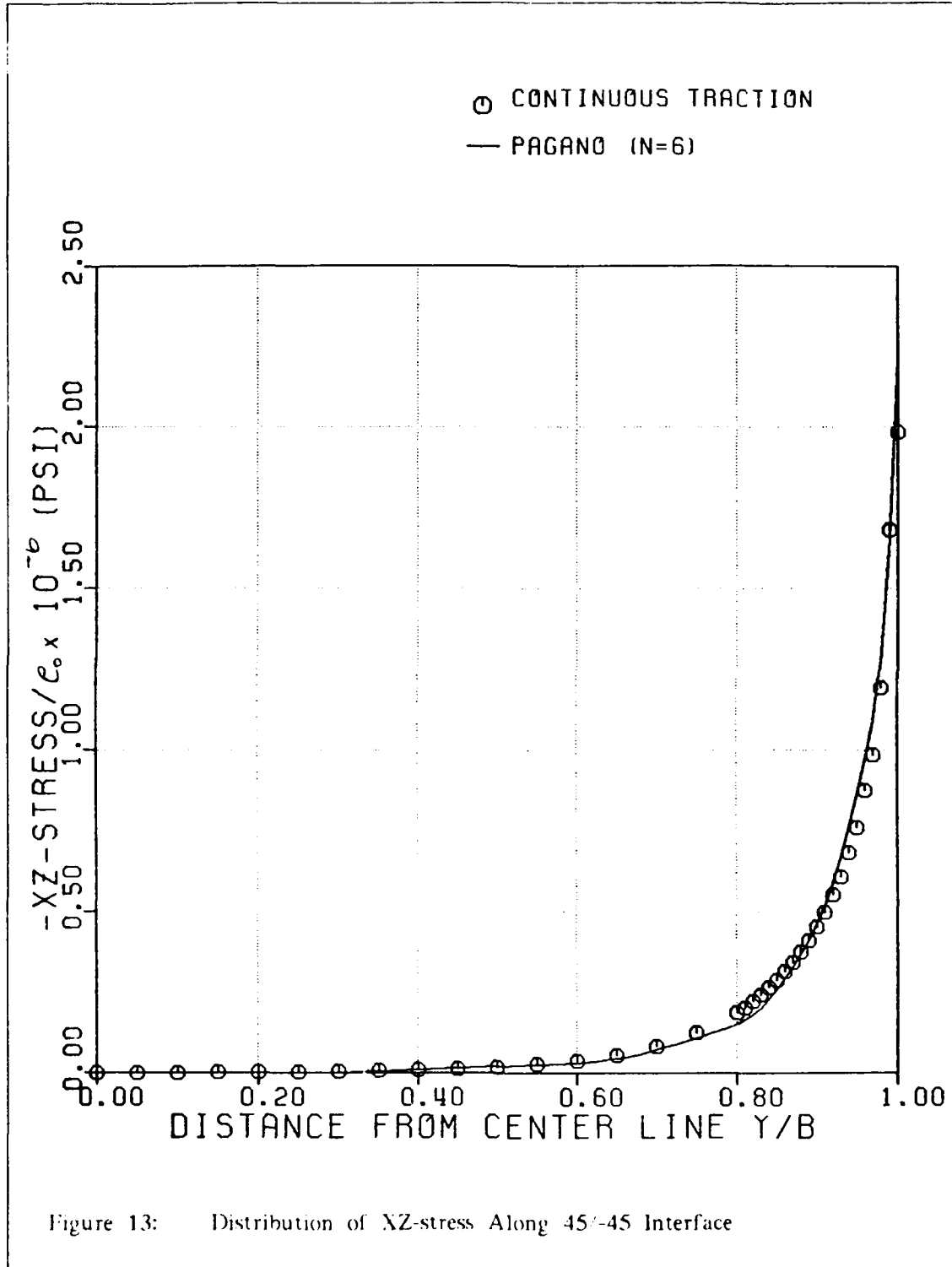
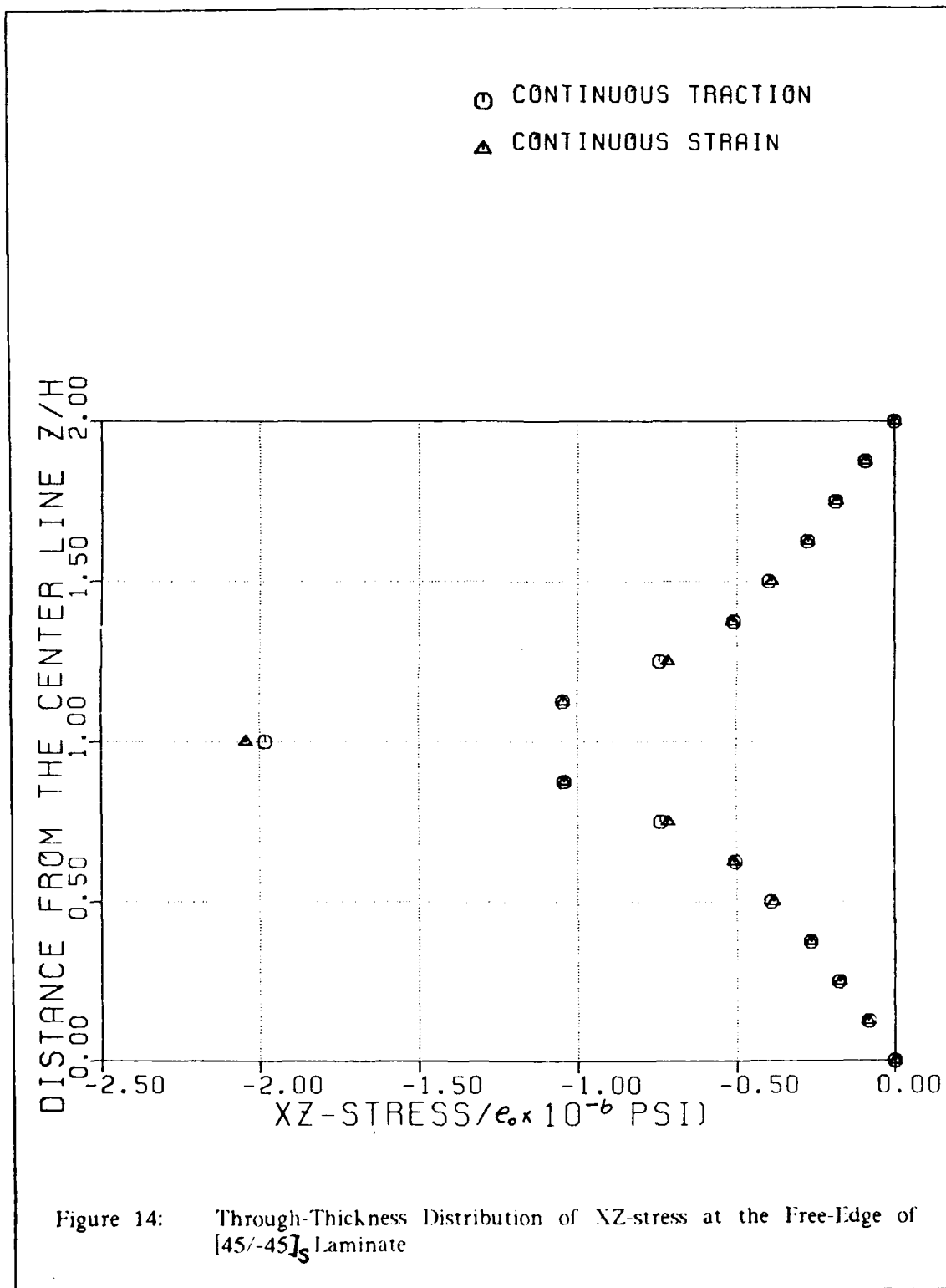


Figure 11: Distribution of X-stress Along Center of Top Layer (45 degree)







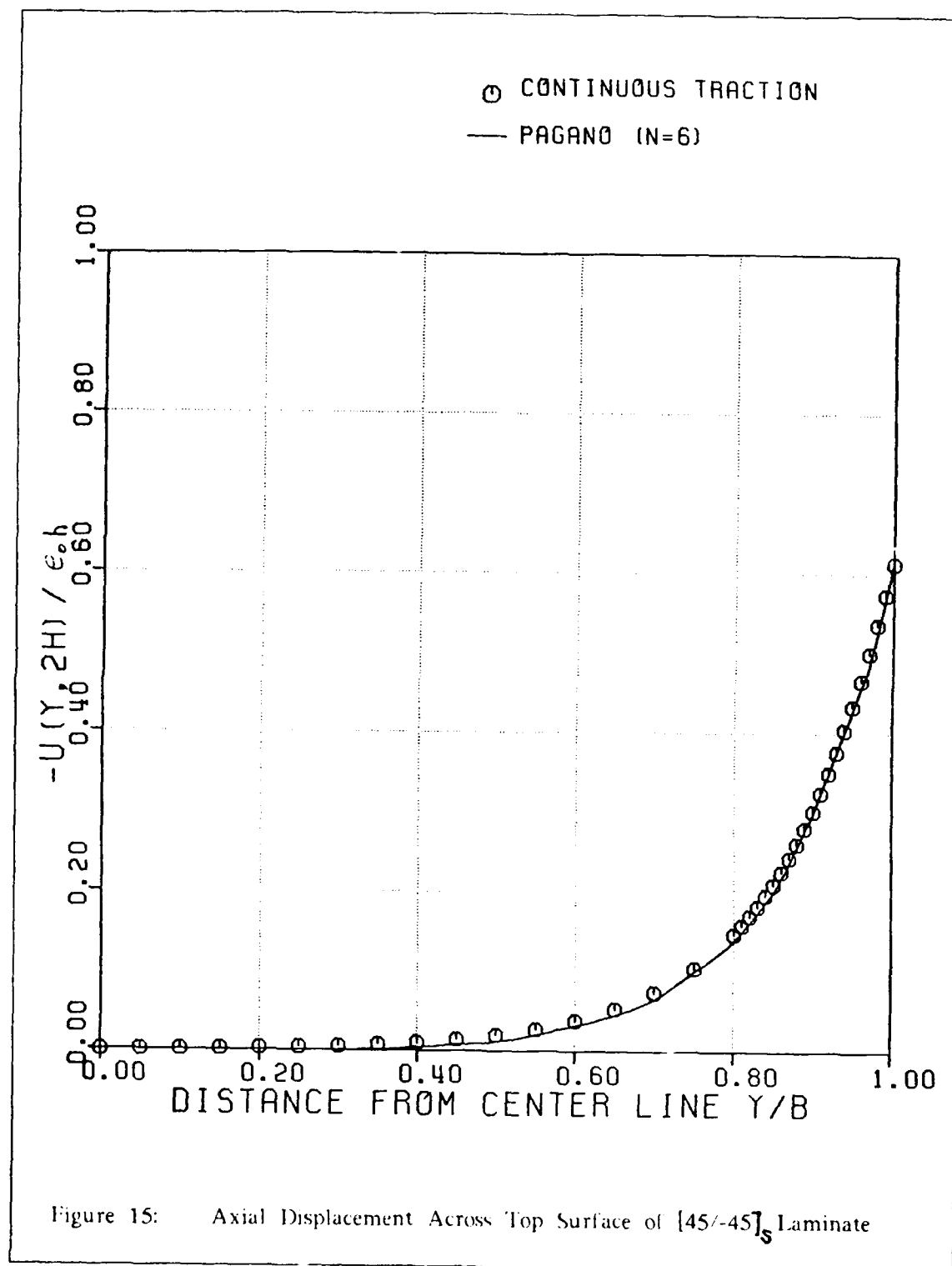


Figure (16) shows the through-thickness distribution of axial displacement based on continuous strain as well as continuous traction Q-23 elements at the free-edge of the laminate. Again, these two solutions matched well throughout.

### 6.2.2 Cross-Ply Laminate

Distribution of  $\sigma_x$  along the width on the central plane of the  $[0/90]_x$  laminate, shown in Figure (17), indicates a sharp rise near the free-edge boundary. Solutions obtained from the continuous traction Q-23 element nearly coincided with Pagano's  $N \times 6$  solution over the entire width of the laminate.

Figure (18) shows the variation of  $\sigma_x$  along the interface between the 0° and 90° plies. Due to the presence of the discontinuity in elastic properties, a singular stress behavior would be expected at the free-edge. On the contrary, result from the continuous traction Q-23 element had a steeper gradient than that of Pagano's theory. Apparently, one possible reason for this discrepancy is that, in Pagano's analysis, each physical layer could be modeled by at most three sub-layers. However, in the finite element analysis, the thickness was divided into eight elements. If a coarser discretization were to be used, say  $4 \times 18$ ,  $\sigma_x$  calculated from the continuous traction Q-23 element would possibly agree quite well with Pagano's solution at the free edge interface. Figure (19) shows the influence of through the thickness refinement of mesh on  $\sigma_x$ . Figure (20) shows through-the thickness distribution of  $\sigma_x$  at the free-edge of the laminate. In the vicinity of the interface, the continuous traction Q-23 element, enforcing continuity of  $\sigma_x$  at the interface between differently oriented layers, gave a stress distribution quite different from that given by the continuous strain Q-23 analysis. Away from the interface the two sets of results were close. Also, the interlaminar stress  $\sigma_z$  was observed to have a maximum value in the interior

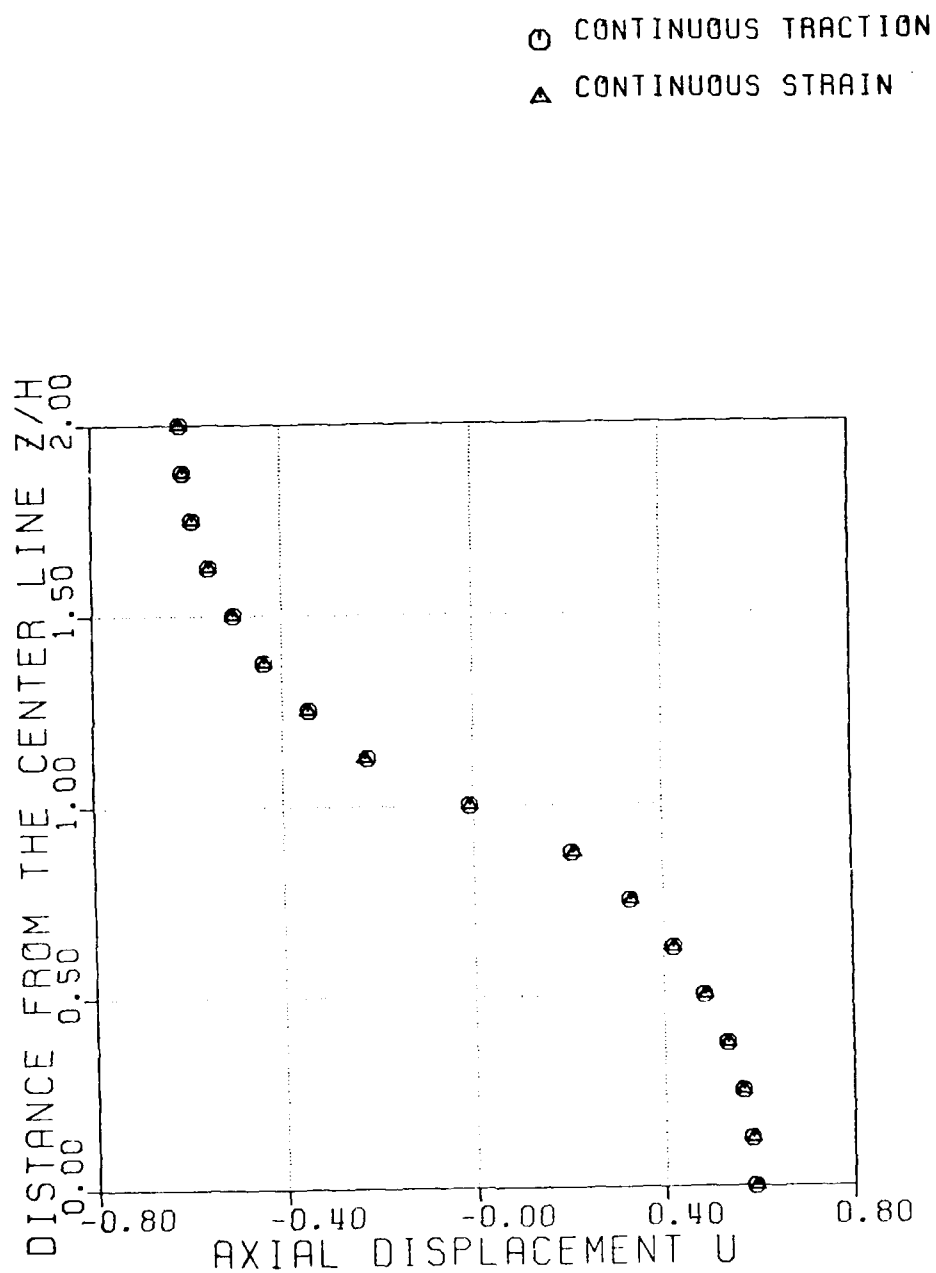
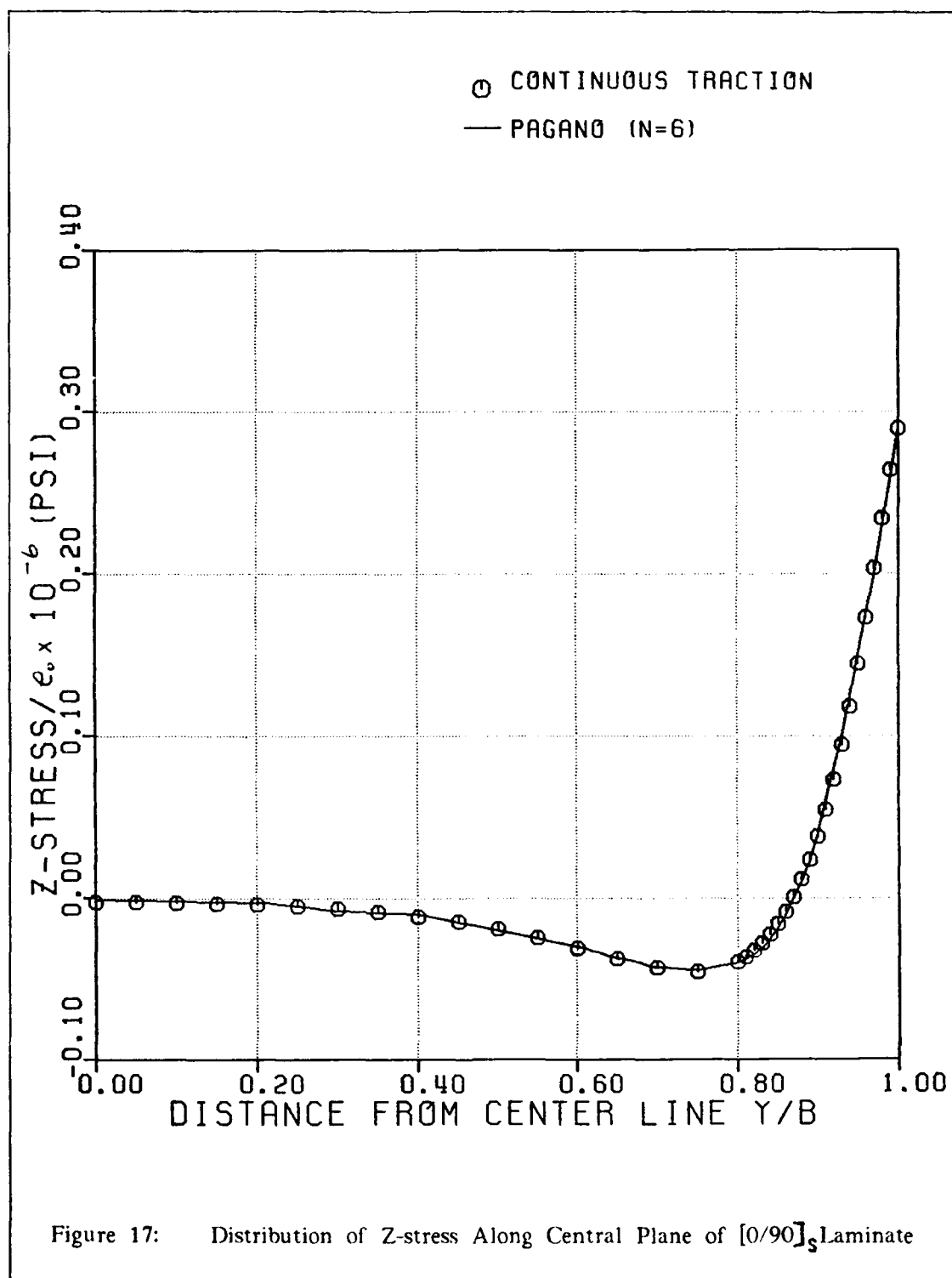
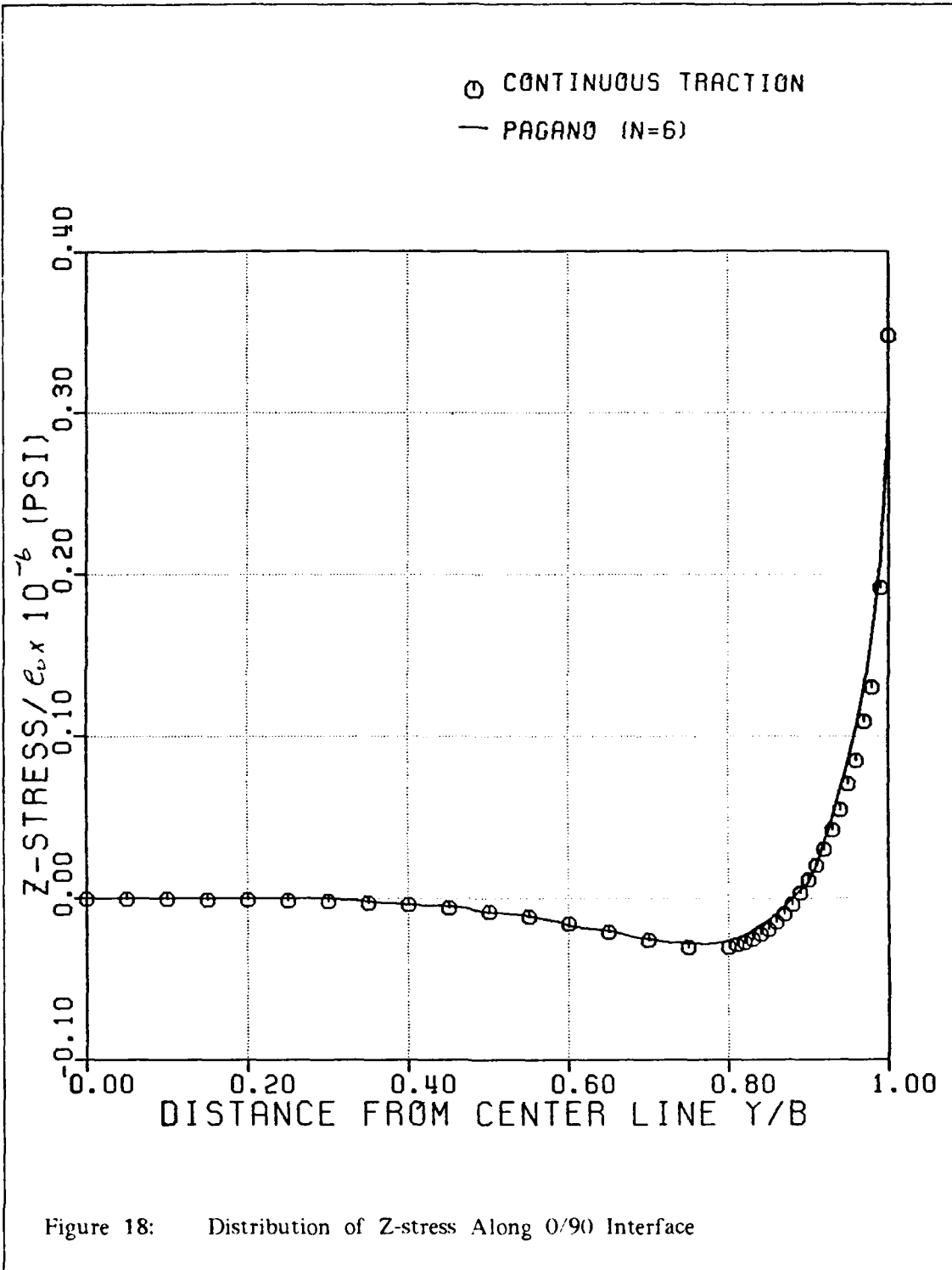


Figure 16: Through-Thickness Distribution of Axial Displacement at the Free-Edge of  $[45/-45]_s$  Laminate







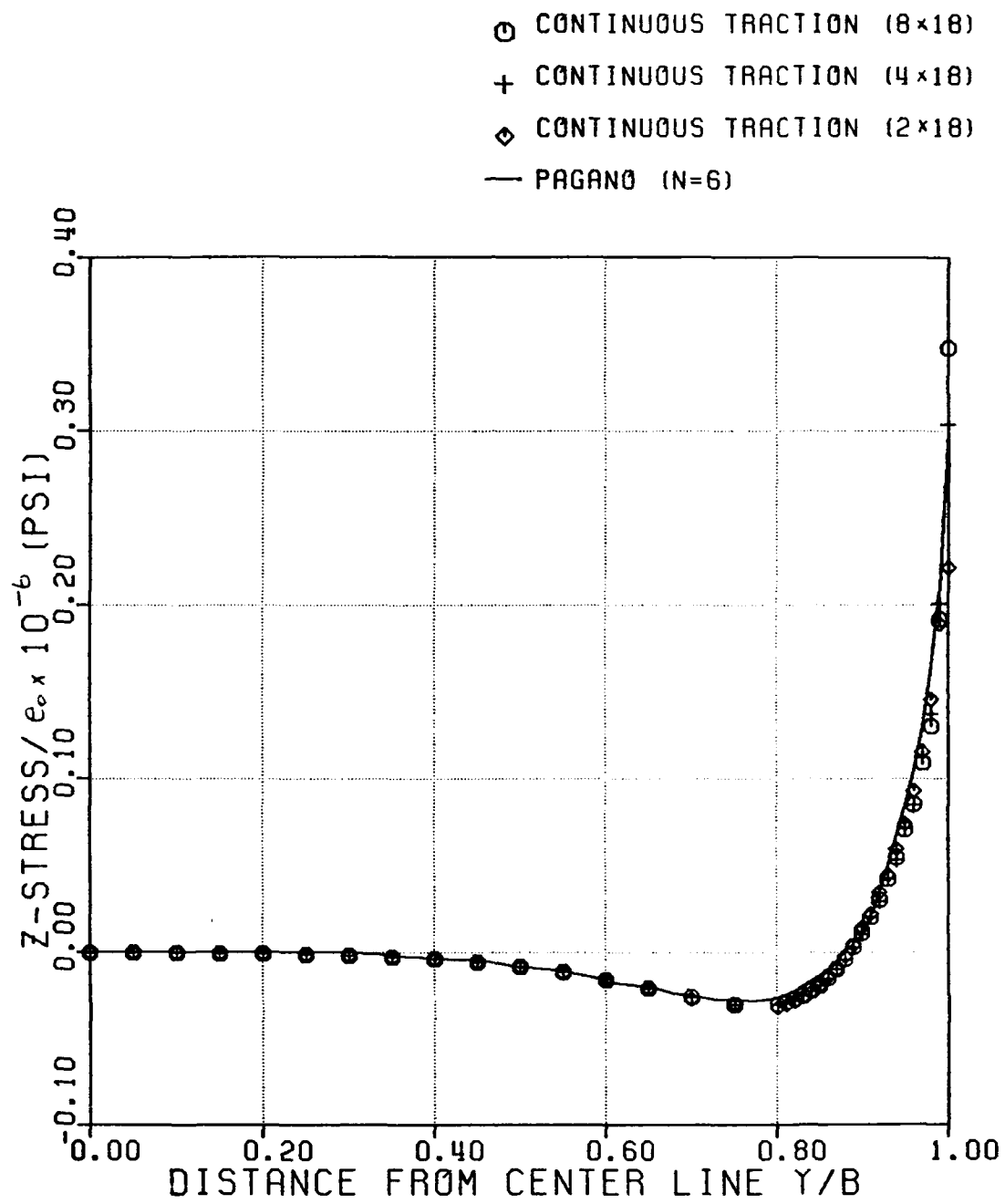


Figure 19: Effect of Mesh Refinement on the Z-stress Distribution Along 0/90 Interface

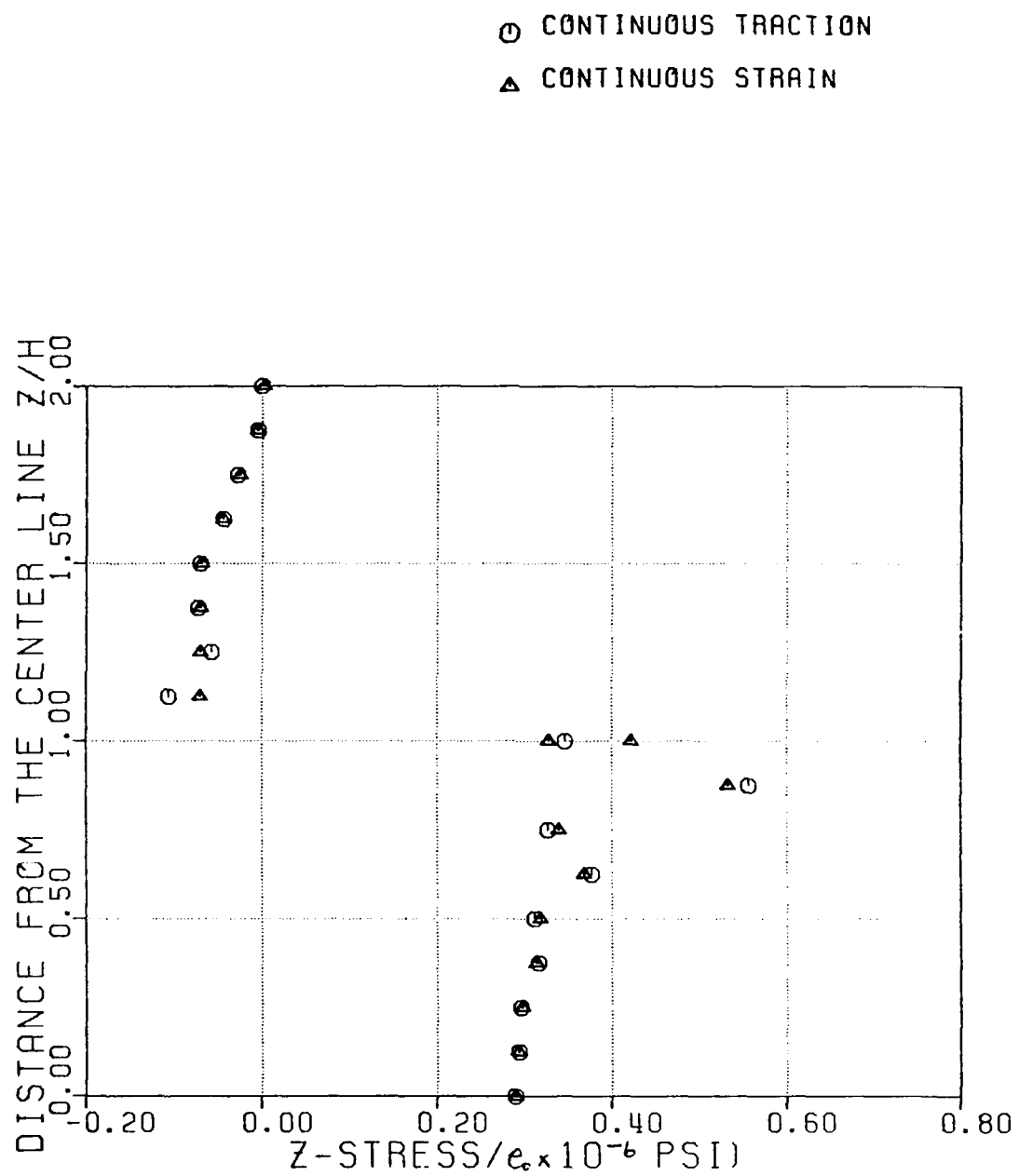


Figure 20: Through-Thickness Distribution of Z-stresss at the Free-Edge of  $[0/90]_5$  Laminate

of the 90 deg layer closer to the interface with the top layer. However, in both cases, the solutions displayed oscillatory patterns near the interface. This could be due to the finite element mesh used being not fine enough to approximate the steeply varying stresses associated with abrupt change of material properties.

Values of  $\tau_{yz}$  along the interface between the  $[0/90]_s$  layers, calculated from the continuous traction Q-23 element (Figure 21), showed satisfactory agreement with those calculated by Pagano. This is because the continuous traction Q-23 element exactly satisfies the traction-free boundary condition similar to Pagano's theory. However, an oscillatory error was observed near the free edge. Apparently, further mesh refinement along the y-direction is required near the free-edge in order to approximate the singular stress behavior. Figure (22) displays through-the-thickness stress distribution of  $\tau_{yz}$  calculated from both continuous strain and continuous traction Q-23 elements at the free-edge of the laminate. Apparently, satisfaction of the traction-free boundary condition associated with the continuous traction Q-23 element represents an improvement over the continuous strain Q-23 element.

Comparative results for the variation of transverse displacement along the top surface of the  $[0/90]_s$  laminate are shown in Figure (23). Excellent agreement was observed between results using the continuous traction Q-23 element and Pagano's N-2 solution.

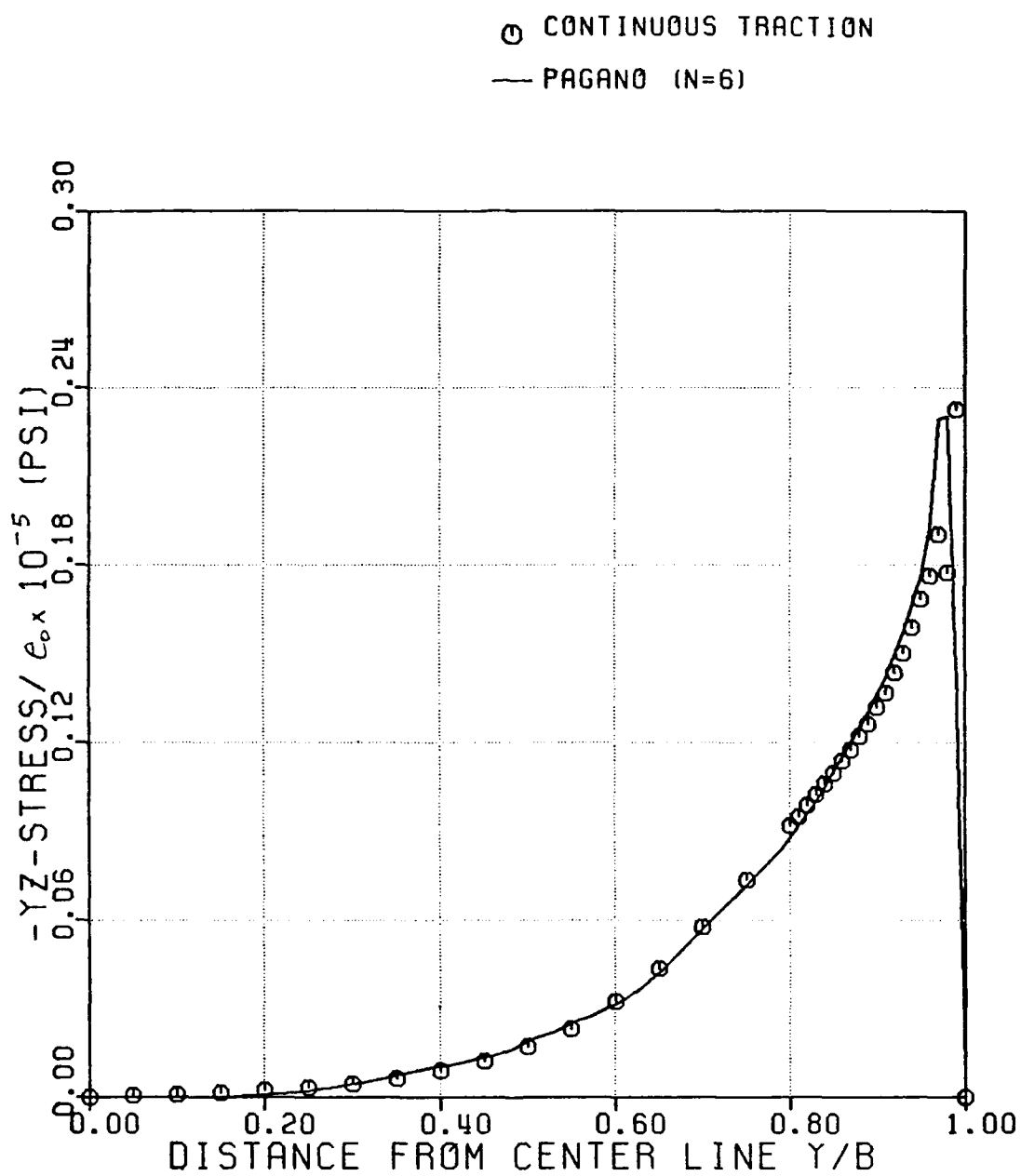


Figure 21: Distribution of YZ-stress Along the 0/90 Interface

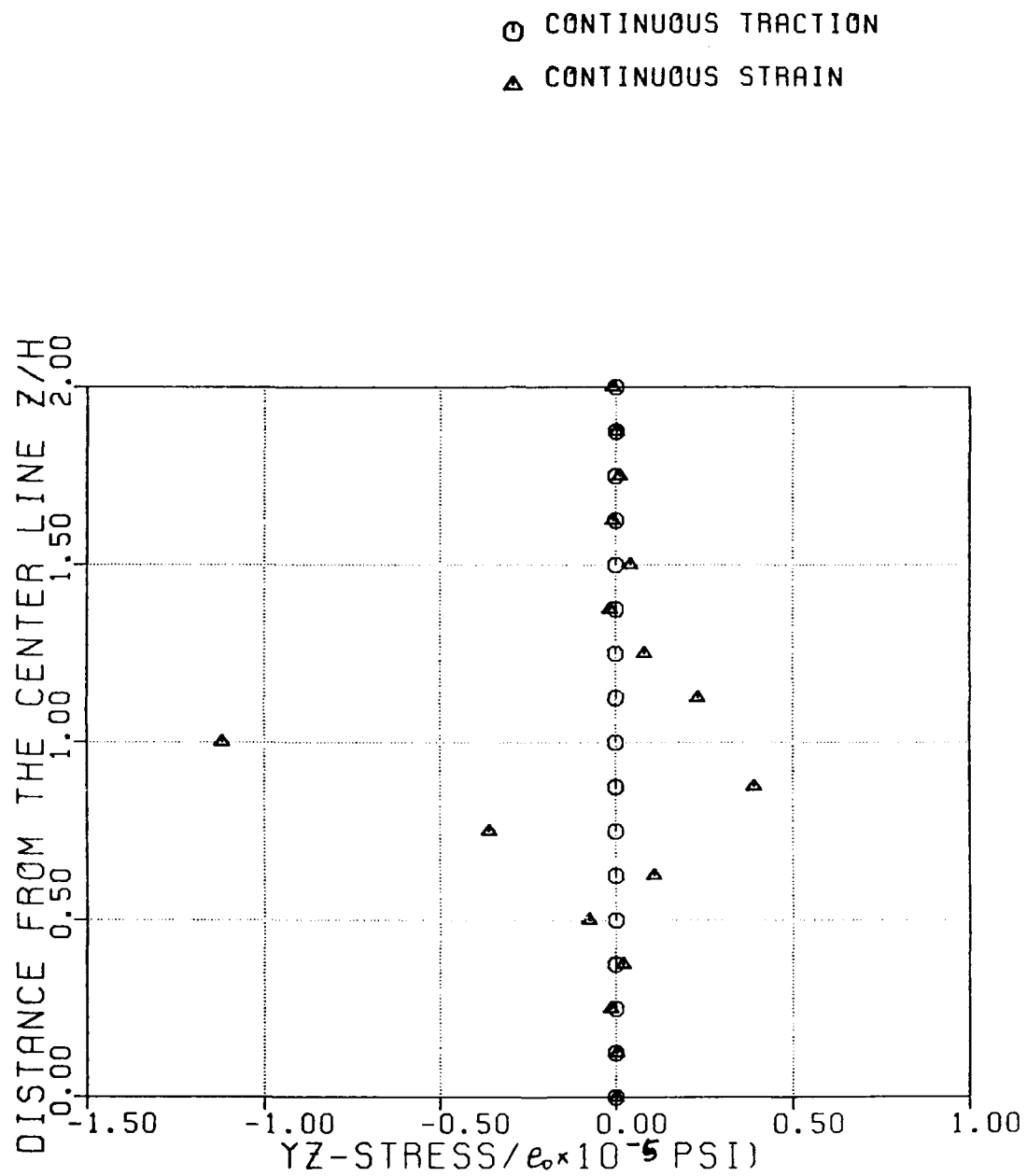
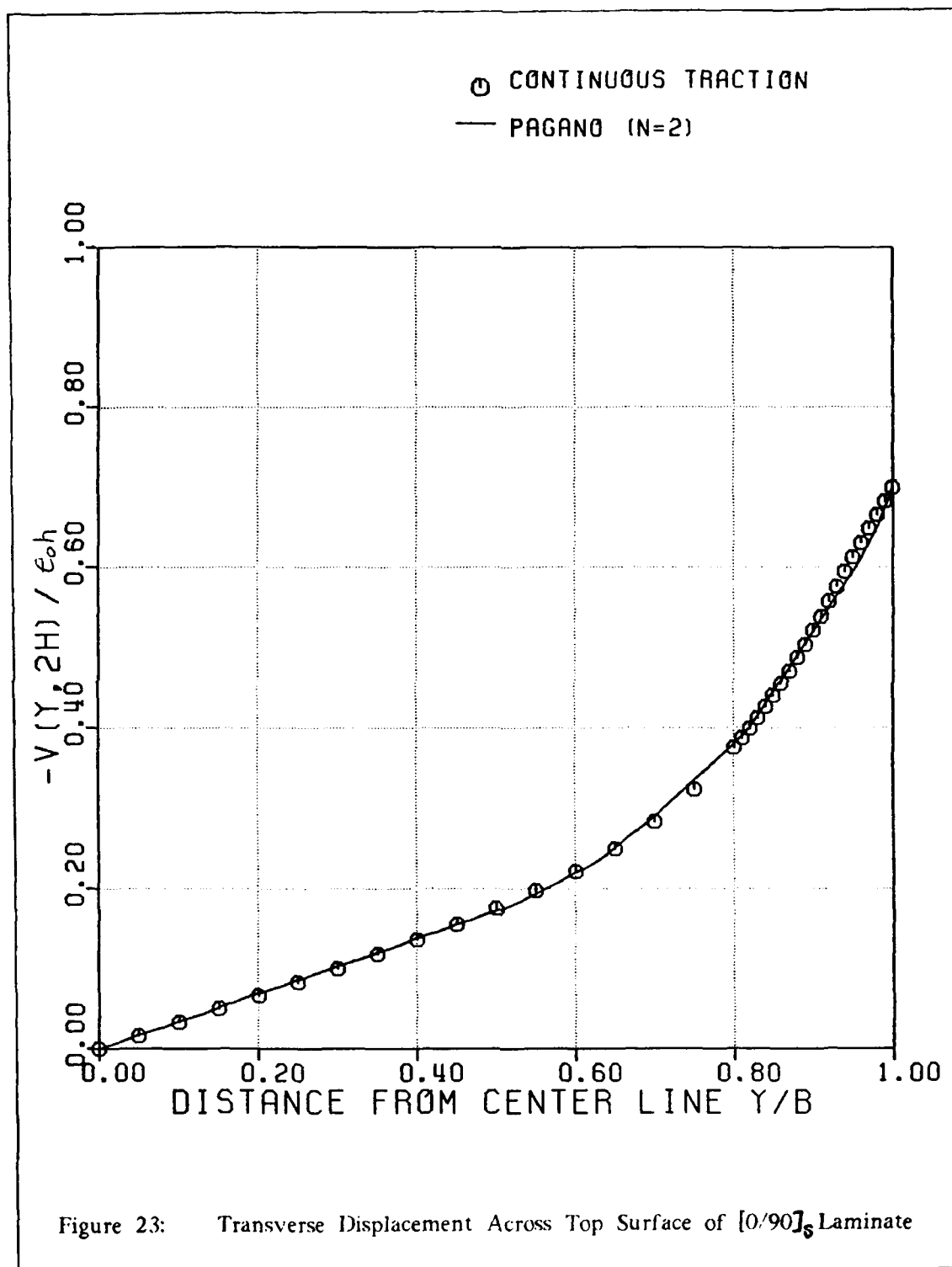


Figure 22: Through-Thickness Distribution of YZ-stress Along the Free-Edge of  $[0/90]_6$  Laminate

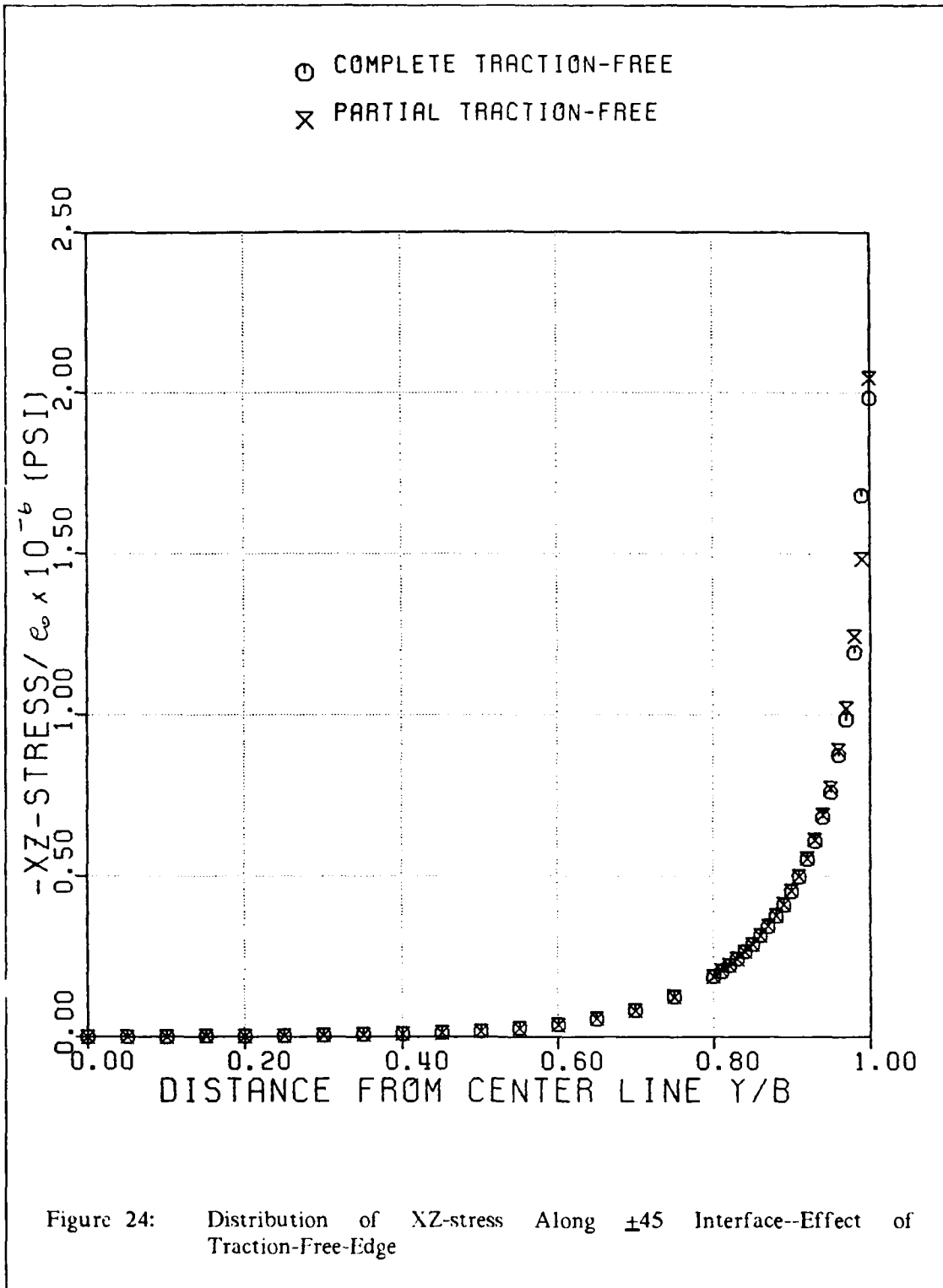


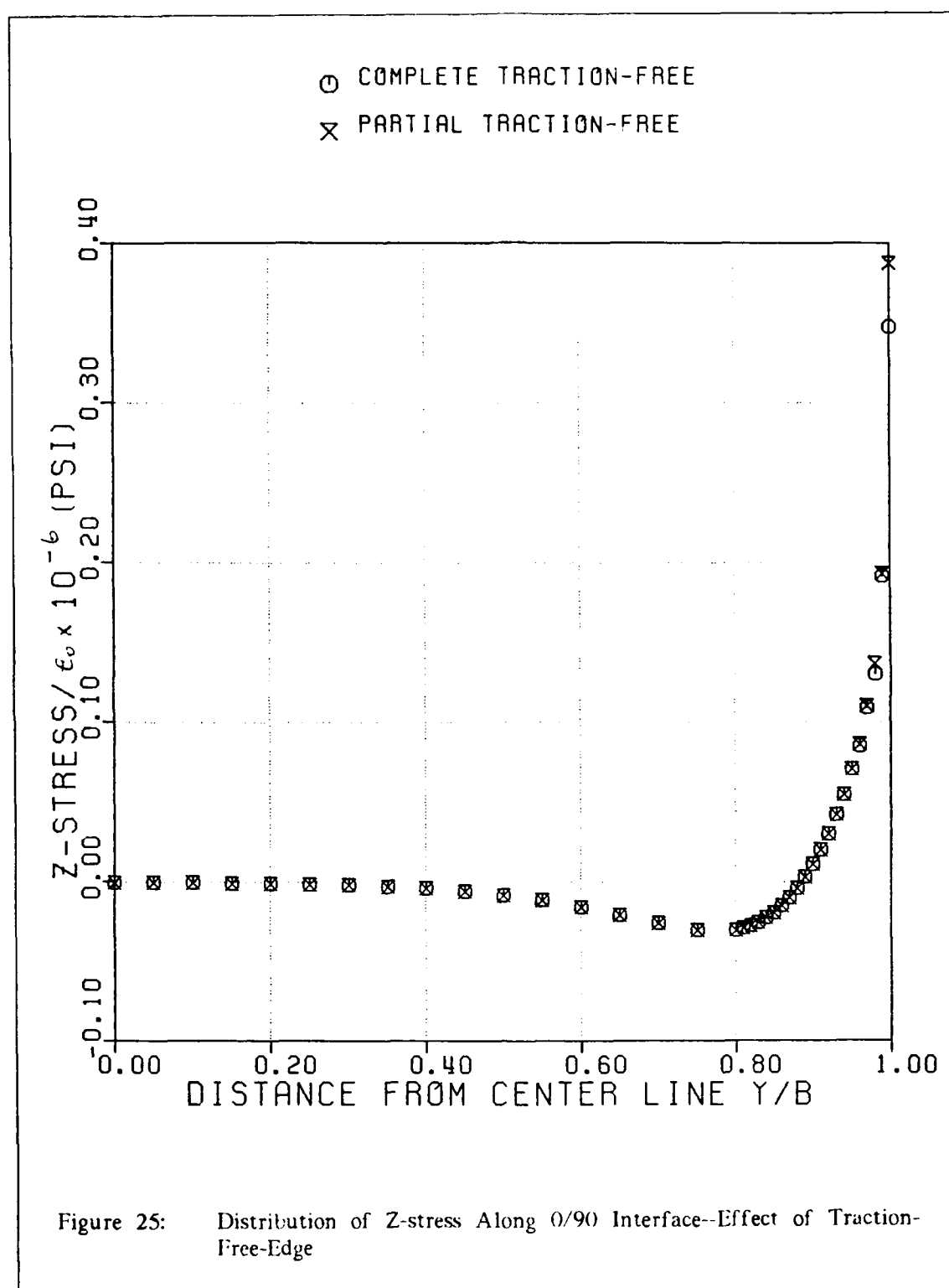


### 6.2.3 Effect of Traction-Free Edge on the Solutions

In order to investigate the effect of requiring the satisfaction of a traction-free boundary condition on the finite element solutions, the continuous traction Q-23 element was employed with only the requirement that  $\tau_{yz}=0$  along the lateral free-edge of the four-ply laminate specimens. In other words, the displacement constraint conditions developed in (188) and (189) used to specify the in-plane stress-free boundary conditions were not imposed in this model. For convenience in the following comparisons, this is designated as continuous traction (partial).

Figure (24) shows the distribution of  $\tau_{xz}$  along the interface of the 45/-45 layers. Solutions calculated from the continuous traction (partial) had a steeper gradient in the vicinity of the free-edge than that of previous continuous traction Q-23 element. A similar observation is made for the variation of  $\sigma_z$  at the interface of  $[0/90]_s$  laminate (Figure 25). Thus, it is concluded that the nonimposition of the conditions  $\sigma_y=0$  and  $\tau_{yz}=0$  would overestimate the magnitudes of the interlaminar stresses on the interface near the free-edge. However, the nonsatisfaction of these two traction-free boundary conditions had no significant effect on the displacement field in the laminate specimens. Figure (26) shows the solutions, for axial displacement distribution across the width of the top surface in the  $[45/-45]_s$  laminate, obtained from the continuous traction (partial) and from the continuous traction Q-23 element which satisfies all traction free conditions at the free-edge.





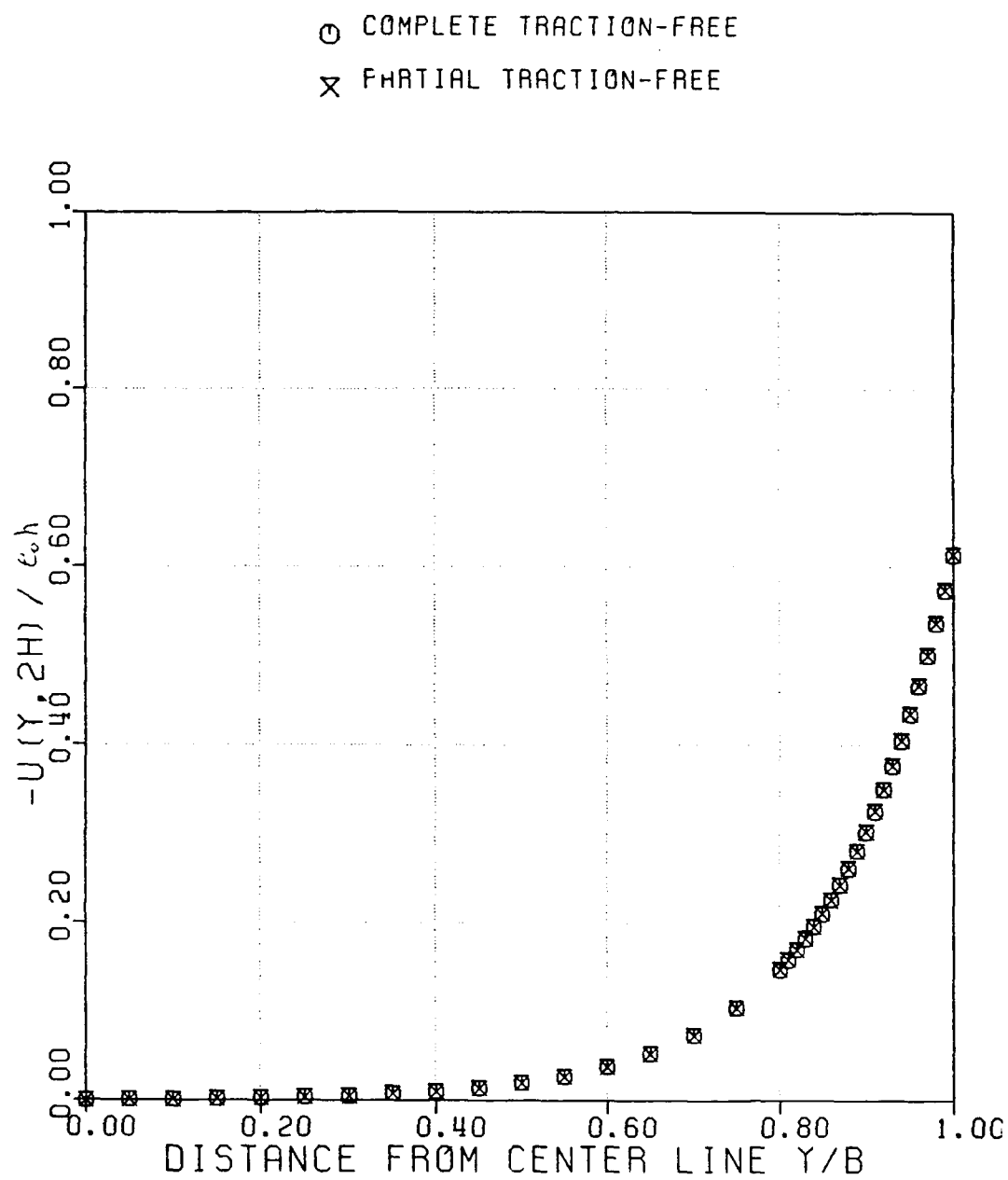


Figure 26: Axial Displacement Across Top Surface of  $[45/-45]_5$  Laminate--  
 Effect of Traction-Free-Edge

#### 6.2.4 Effect of Mesh Refinement

The analysis of the four-ply laminate specimens was originally carried out by using the continuous traction Q-23 element with a uniform 80-element model as shown in Figure (27). However, for reliability of results, the finite element mesh must be refined in regions of steeply varying stresses. This results in the present analysis using the 144-element model which indeed was obtained by dividing the two elements closest to the free-edge in the 80-element model into 10 elements along the y-direction. To study the effect of mesh refinement on the continuous traction finite element solutions, comparisons were made for the stress distributions in the four-ply laminate specimens between the uniform 80-element and the locally refined 144-element models.

Figure (28) shows the distribution of  $\tau_{xz}$  at the interface of  $[45/-45]$  laminate based on the 144-element model. A steeper gradient of  $\tau_{xz}$  was observed on the boundary as compared with the result using 80-element model. A comparison of  $\sigma_z$  distribution along the interface of the 45/-45 layers, indicates that the 144-element model had a compressive finite maximum value at the free-edge rather than a tensile quantity from the 80-element model (Figure 29). This indeed has demonstrated the inappropriate sign of  $\sigma_z$  shown in Figure (1) based on the perturbation technique as well as finite difference method. For variation of  $\sigma_z$  along the interface of  $[0/90]$  laminate, Figure (30) indicates that a singular stress behavior was properly reproduced by the 144-element model and did not show well in the results based on the 80-element mesh.

Use of 144-element model might still be insufficient to approximate the singular stress behavior. One example is the  $\tau_{yz}$  distribution, which had an oscillatory pattern near the free-edge along the interface of  $[0/90]$  laminate, as mentioned before. To

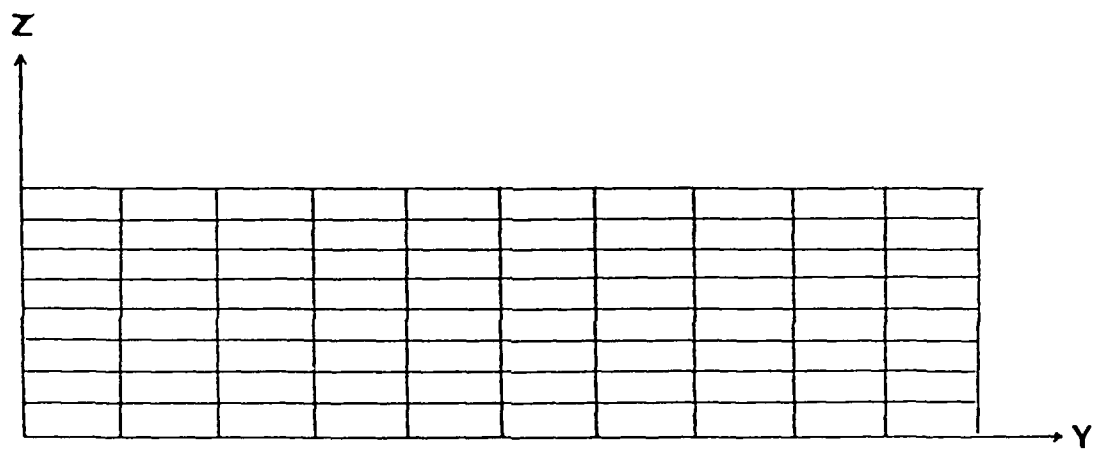
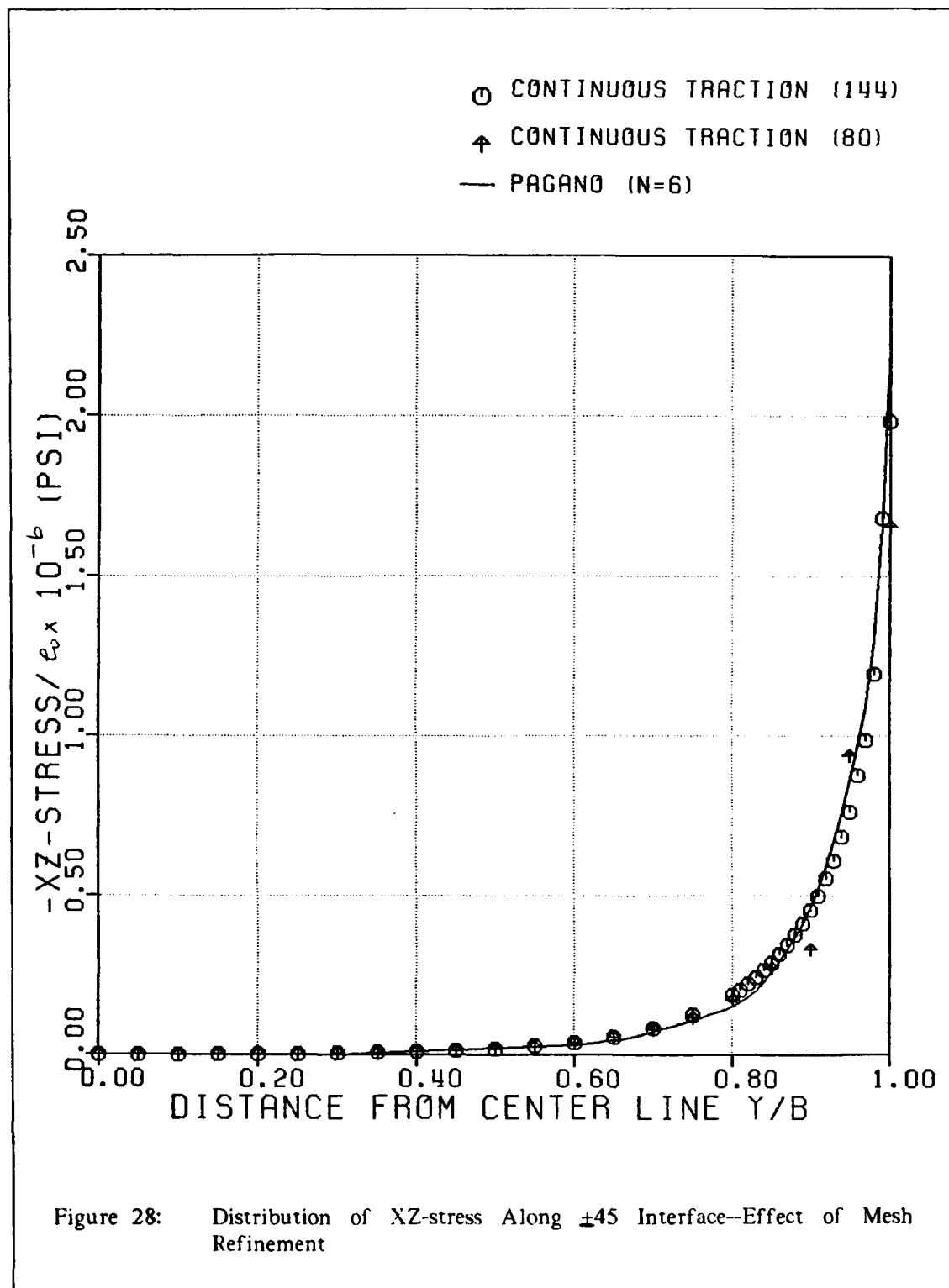
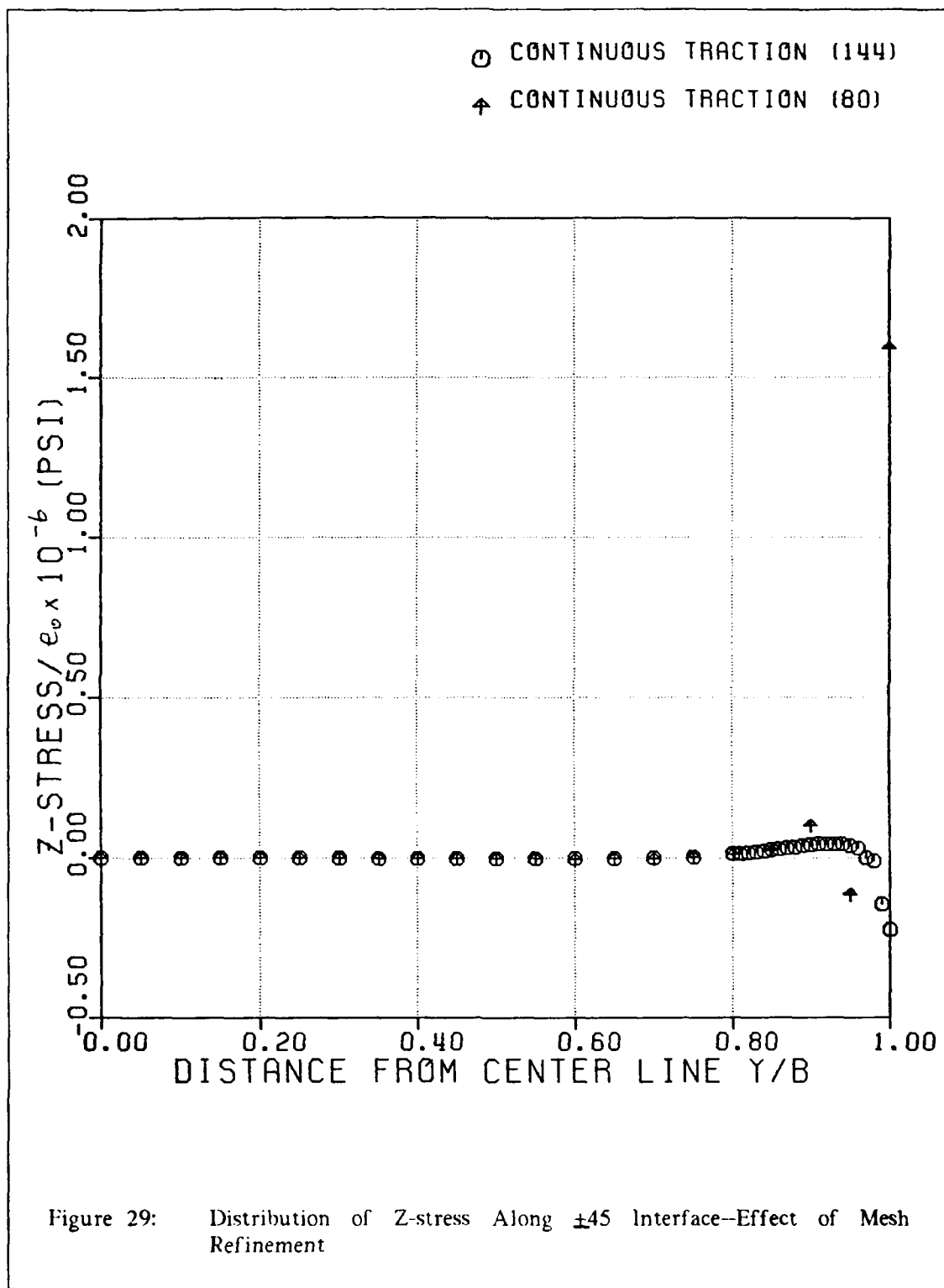


Figure 27: 80-Element Model







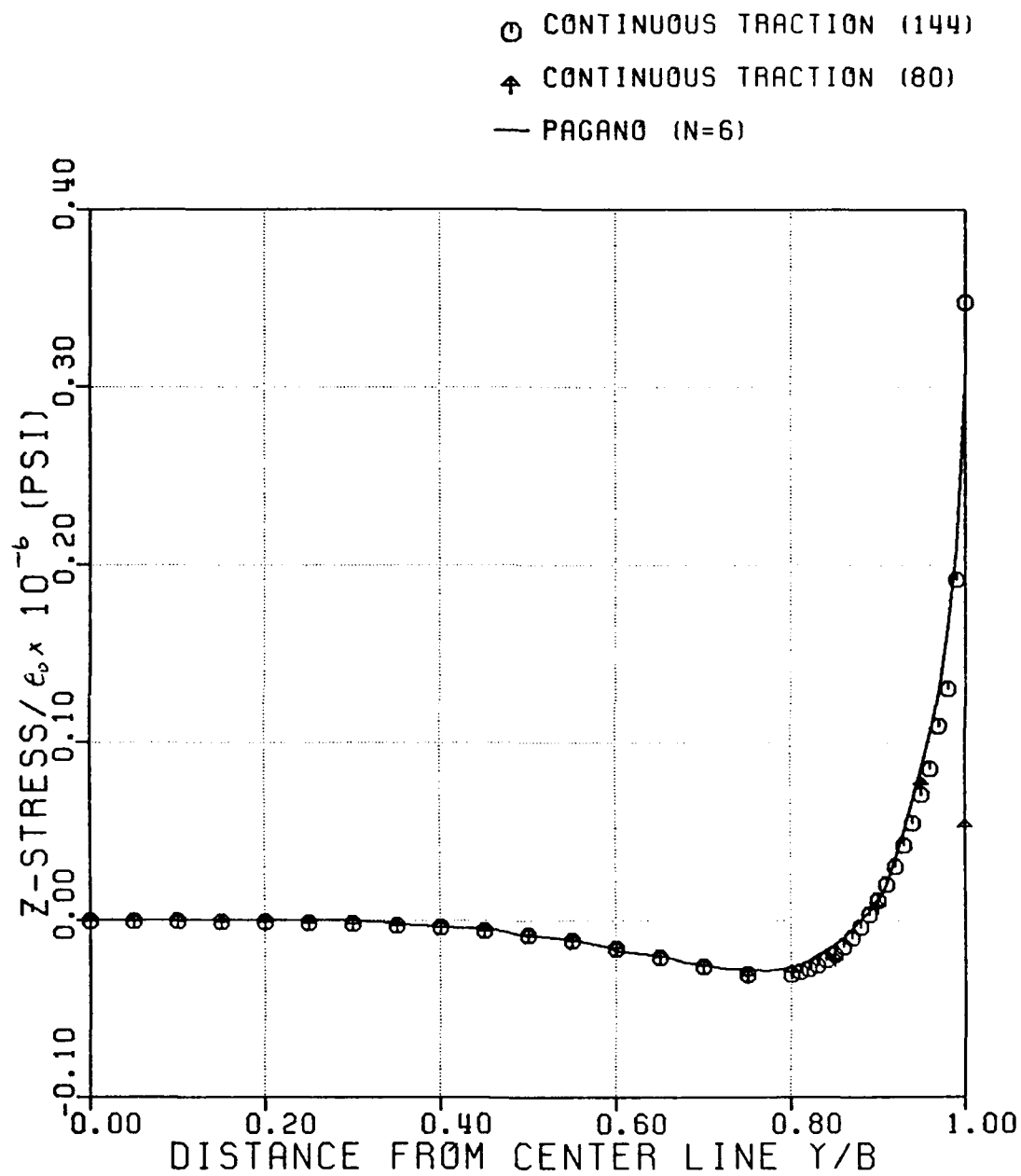


Figure 30: Distribution of Z-stress Along 0/90 Interface--Effect of Mesh Refinement

overcome this, a more refined mesh (208-element model) obtained by further dividing the two elements closest to the free-edge in the 144-element model into 10 elements, was used in the analysis. Along with the results calculated from 80- and 144-element models respectively, Figure (31) indicated the improvement of the  $\tau_{yz}$  distribution along 0/90 interface over the boundary layer region as more refined elements were used near the free-edge. However, regardless of mesh patterns used, there was an oscillatory error in  $\tau_{yz}$  in the two elements next to the free-edge.

Figure (32) shows through-the-thickness distributions of  $\sigma_x$  at the free-edge of [0/90] laminate based on the 144-element model but with finer mesh near the interface (Figure 10b) and its refinement (288-element model) in the thickness direction. It is observed that the oscillatory error near the interface was reduced by using the refined 144-element model and was nearly disappeared under more refinement over the laminate thickness. Meanwhile, the maximum value of  $\sigma_x$  within the 90-degree layer was moving closer to the 0/90 interface.

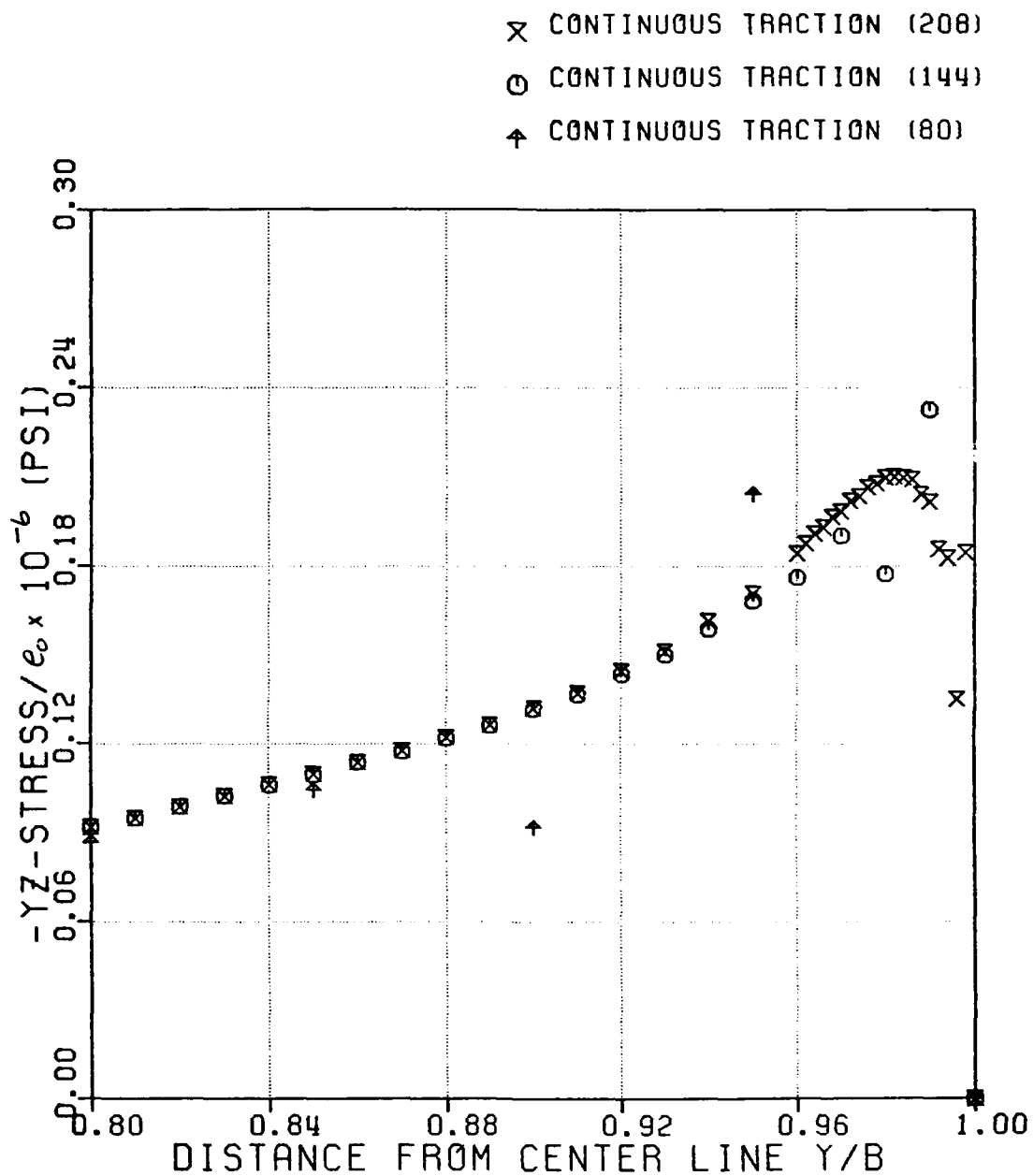


Figure 31: Distribution of YZ-stress Along 0/90 Interface--Effect of Mesh Refinement

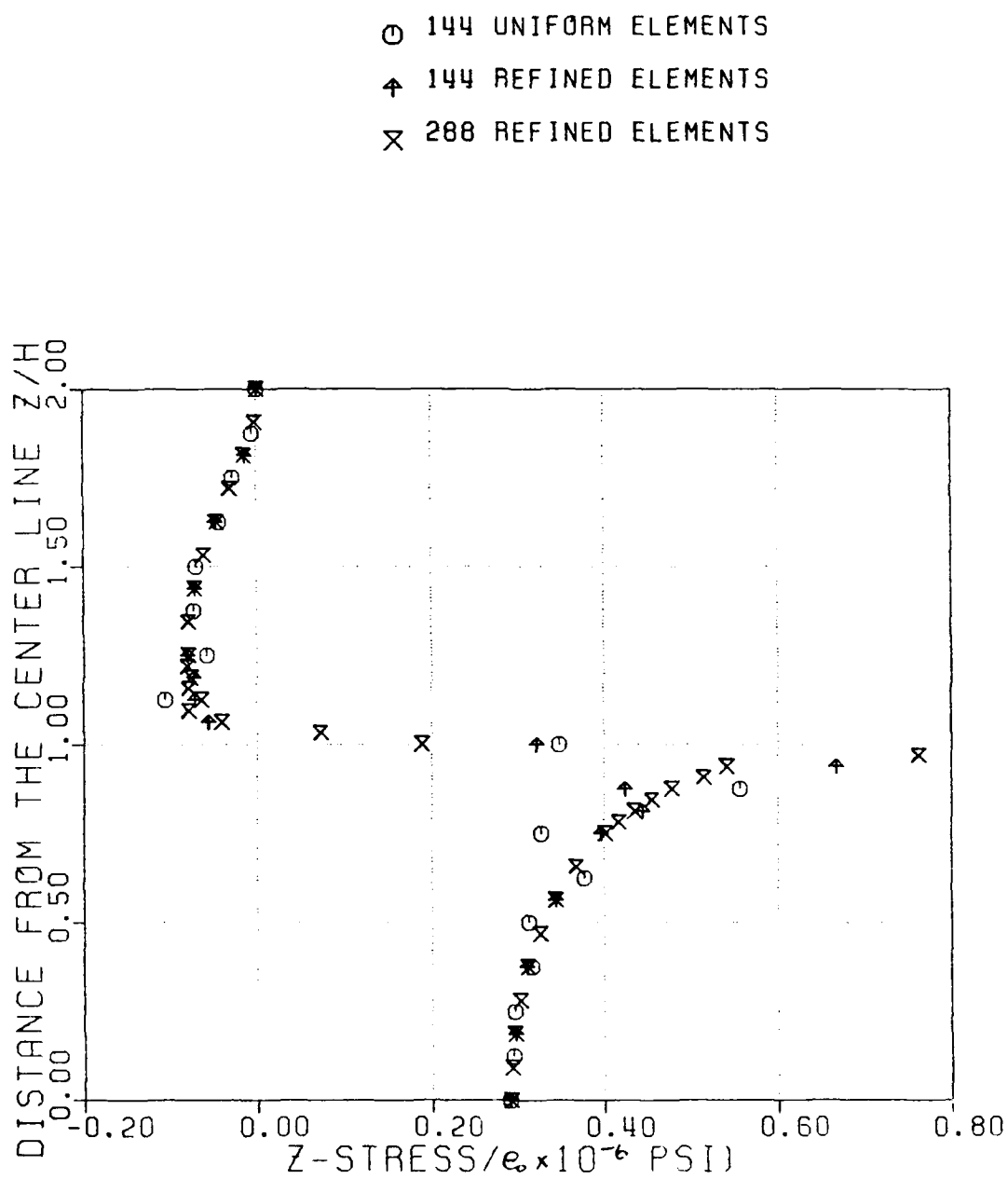


Figure 32: Through-Thickness Distribution of Z-stress at the Free-Edge of  $[0/90]_s$  Laminate--Effect of Mesh Refinement

### 6.3 Free-Edge Delamination in Multi-Ply Laminate Specimens

Analysis of the four-ply laminate specimens described in the previous section demonstrated some validity of using the proposed finite element procedures in solving free-edge effect problems. Both continuous strain and continuous traction Q-23 elements had similar prediction on the displacements and inplane stress distributions, which also compared well with Pagano's analytical solutions. However, discrepancy between continuous strain and continuous traction finite element models was apparent for the interlaminar stresses near laminate interfaces between differently oriented layers or near the traction-free boundary. Due to the fact that stress continuity across interlaminar boundary as well as traction-free boundary condition are exactly satisfied in the continuous traction Q-23 element, solutions obtained from this approach were expected to be more reliable than those from the continuous strain Q-23 element. In this section, application of the continuous traction Q-23 element to investigate the free-edge effect as well as initiation of edge delamination in the multi-ply laminates is described.

#### 6.3.1 Analysis of $[(\theta/-\theta)_m/90_{n/2}]_s$ Laminates

Four types of laminates with predetermined fiber orientations [46] were used in the present investigation. These are

Type	Stacking Sequence	Width	Ply thickness	Plies
A	$[(49.8/-49.8)_5/90]_s$	1.0 in	0.00506 in	22
B	$[(30.8/-30.8)_5/90]_s$	1.0 in	0.00508 in	22
C	$[(25.5/-25.5)_5/90]_s$	1.0 in	0.00505 in	22
D	$[(47.9/-47.9)_{10}/90]_s$	1.0 in	0.00499 in	42

The material used in the study was AS4/3501-6, graphite-epoxy, and the elastic constants were [46]

$$E_{11}=19.26 \times 10^6 \text{ psi}$$

$$E_{22}=1.32 \times 10^6 \text{ psi}$$

$$G_{12}=0.83 \times 10^6 \text{ psi}$$

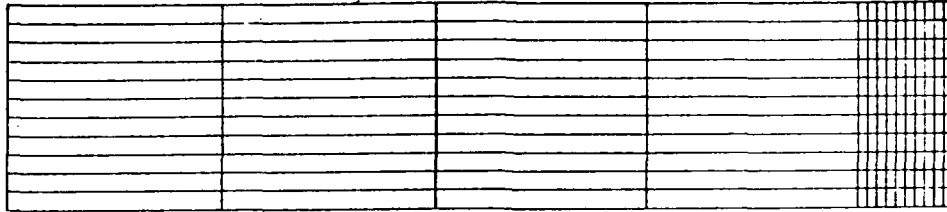
$$\nu_{12}=0.35$$

All the specimens have been investigated both analytically and experimentally at the AFWAL/AFFDL [46]. The Delamination Moment Coefficients (DMC) were derived and used to evaluate quantitatively the delamination tendency of the laminates. Also, generalized constant strain element was applied to analyze half of the width of the laminate specimens. In the experimental aspect, various techniques including Transverse Strain Gages, Cracked Silver Ink Instrumentation and Acoustic Emission Instrumentation, etc. were used to determine the onset of delamination and to validate the analytical results.

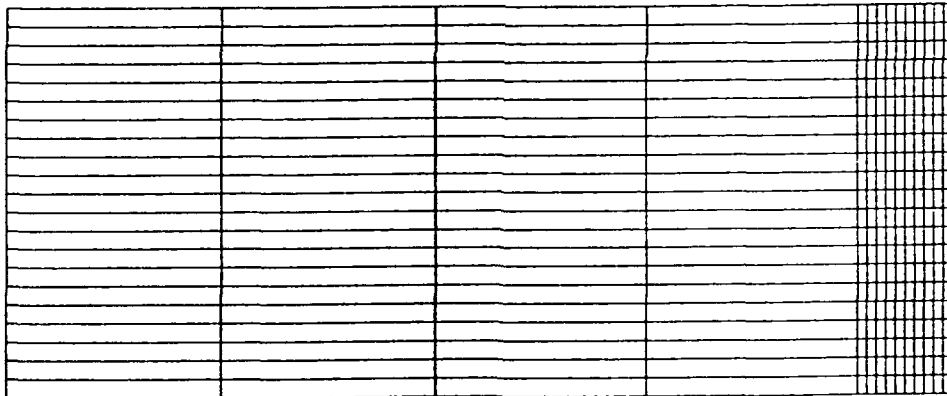
### 6.3.1.1 Numerical Evaluation

A 154-element model shown in Figure 33(a) was used to discretize one quadrant of a typical  $x=\text{constant}$  plane in the laminate specimen Types A, B, C, and a 294-element model (Figure 33(b)) was used for specimen Type D. Each ply was modeled by a single element through its thickness. Interlaminar stress field within various laminate specimens for an applied longitudinal average stress of 100 psi were computed.

Comparisons of  $\sigma_z$  distribution along the mid-plane of various multi-ply laminates, (Figures 34-37) indicate that the continuous traction Q-23 solutions had sharp rise toward the free-edge similar to constant strain element solutions [46]. Satisfactory agreement was generally observed between these two solutions for stresses in the vicinity of the free-edge except on the boundary where the stress calculated using the

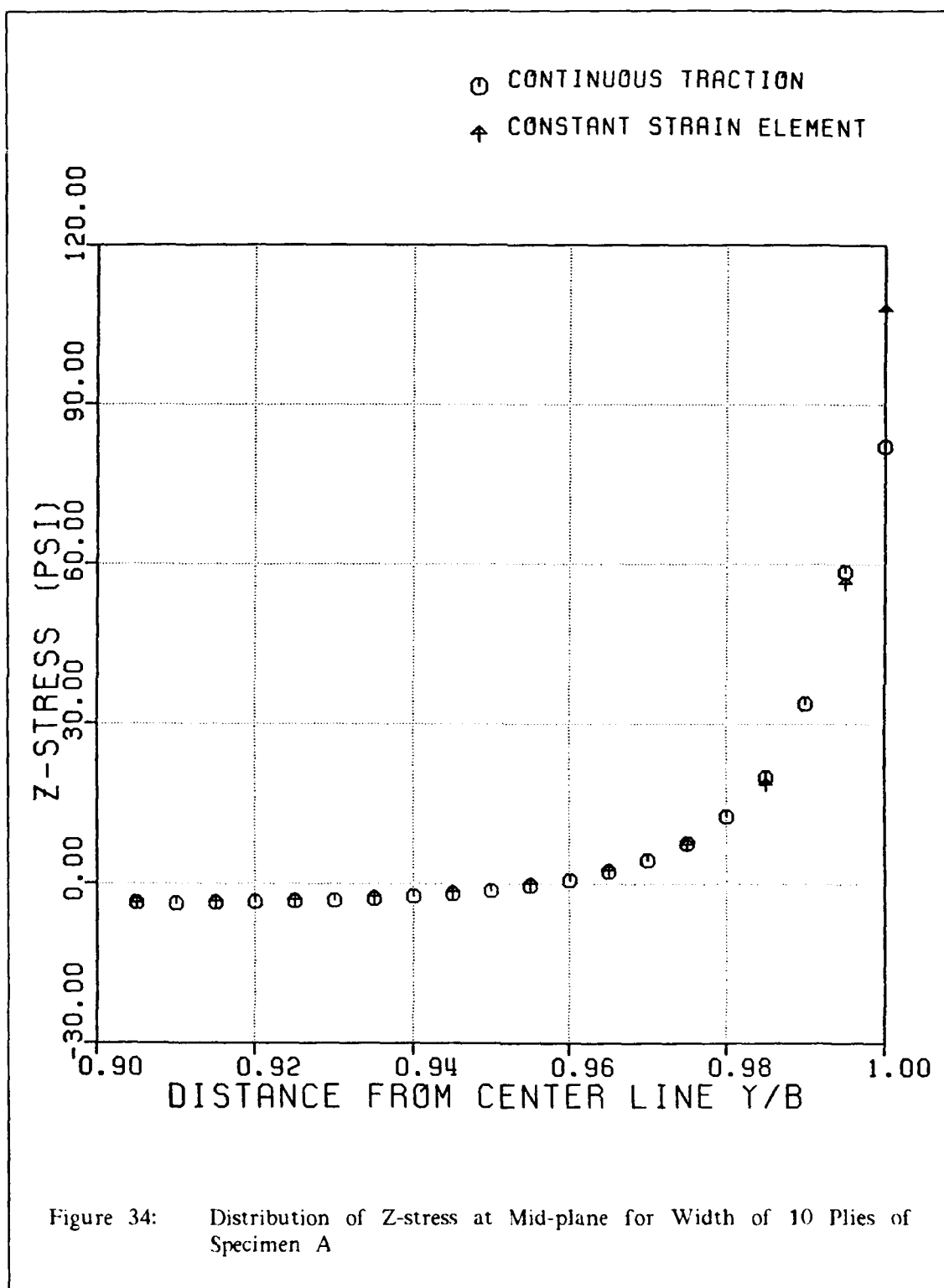


(a) 154-Element Model

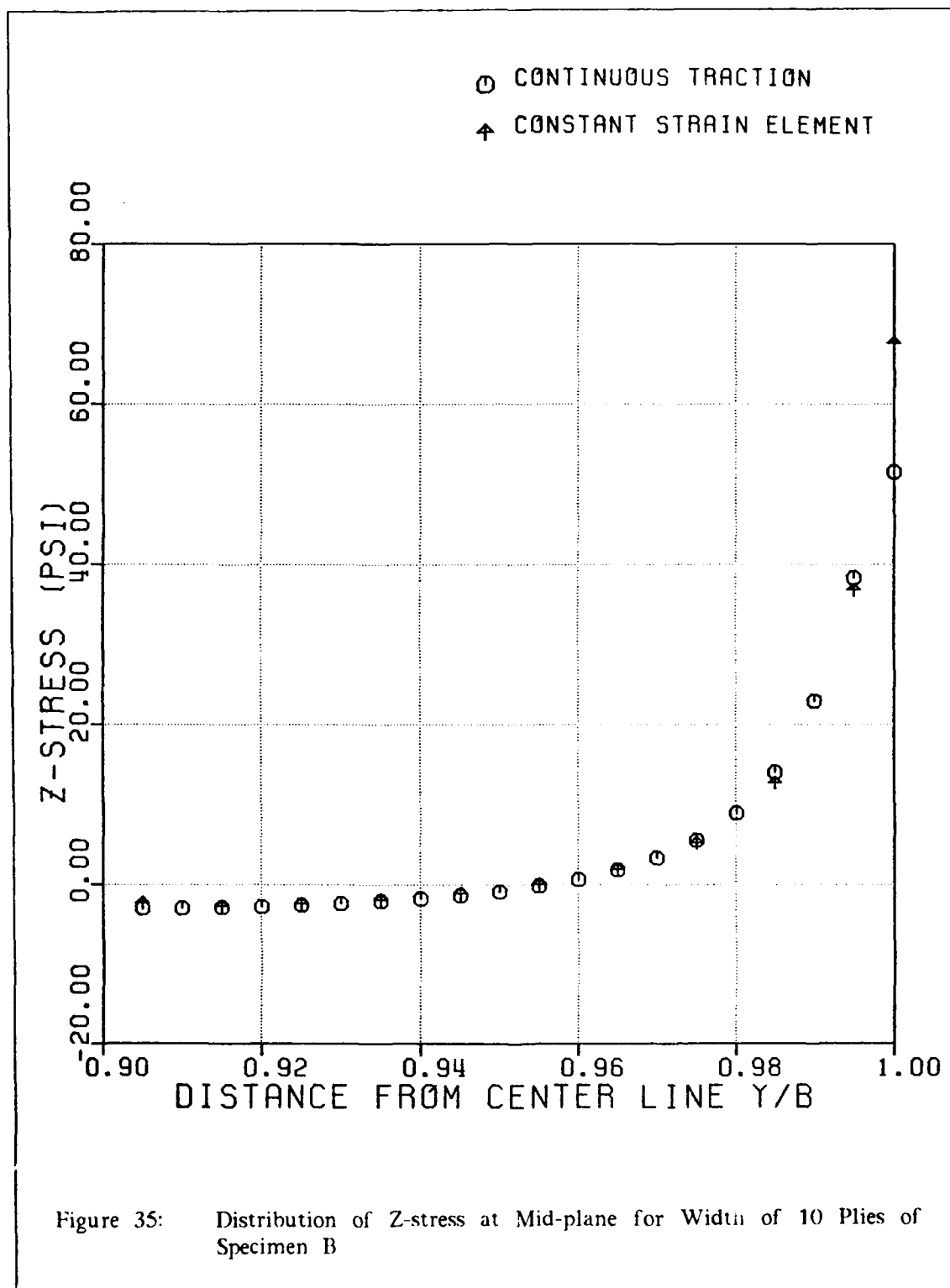


(b) 294-Element Model

Figure 33: Finite Element Meshes







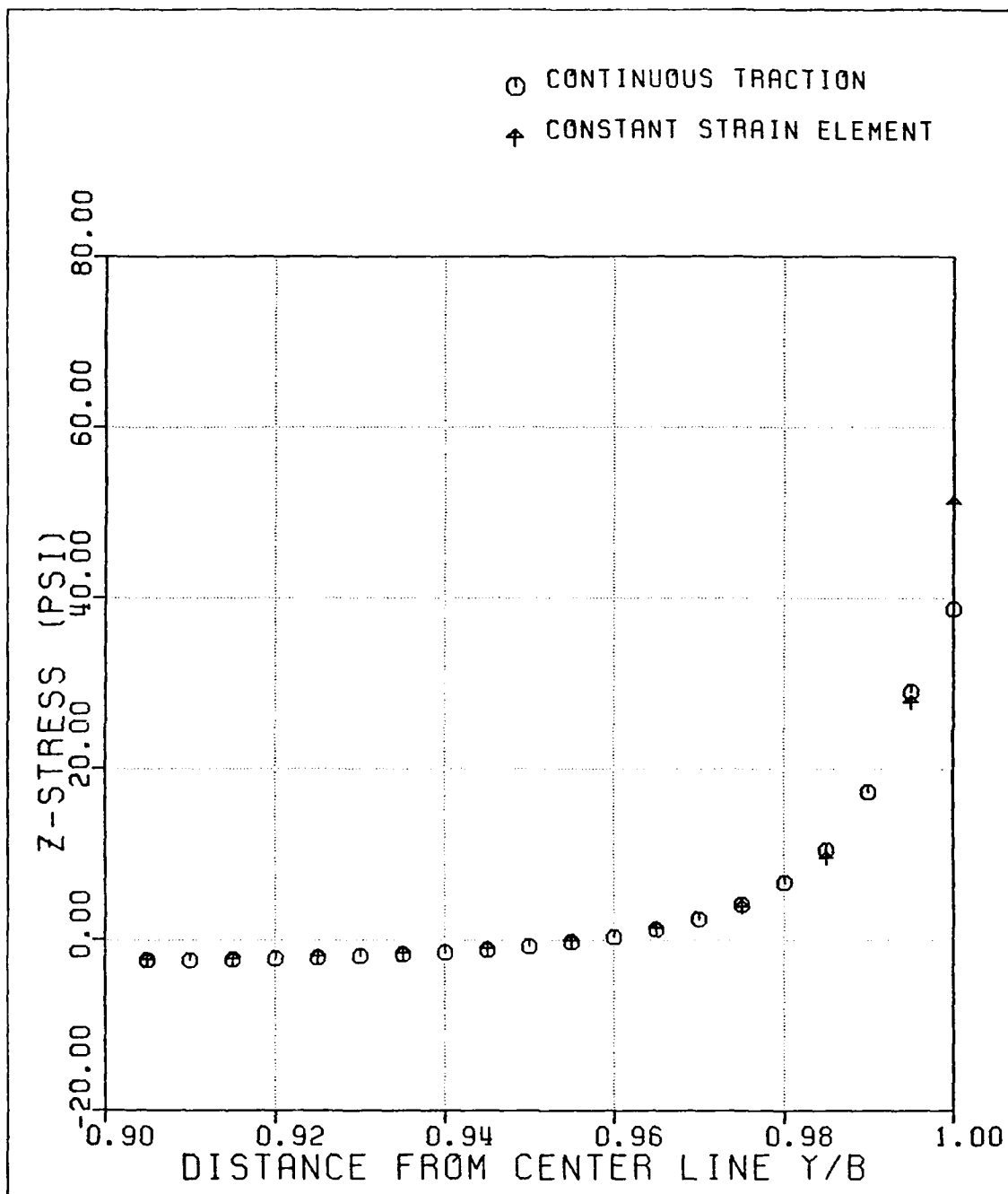
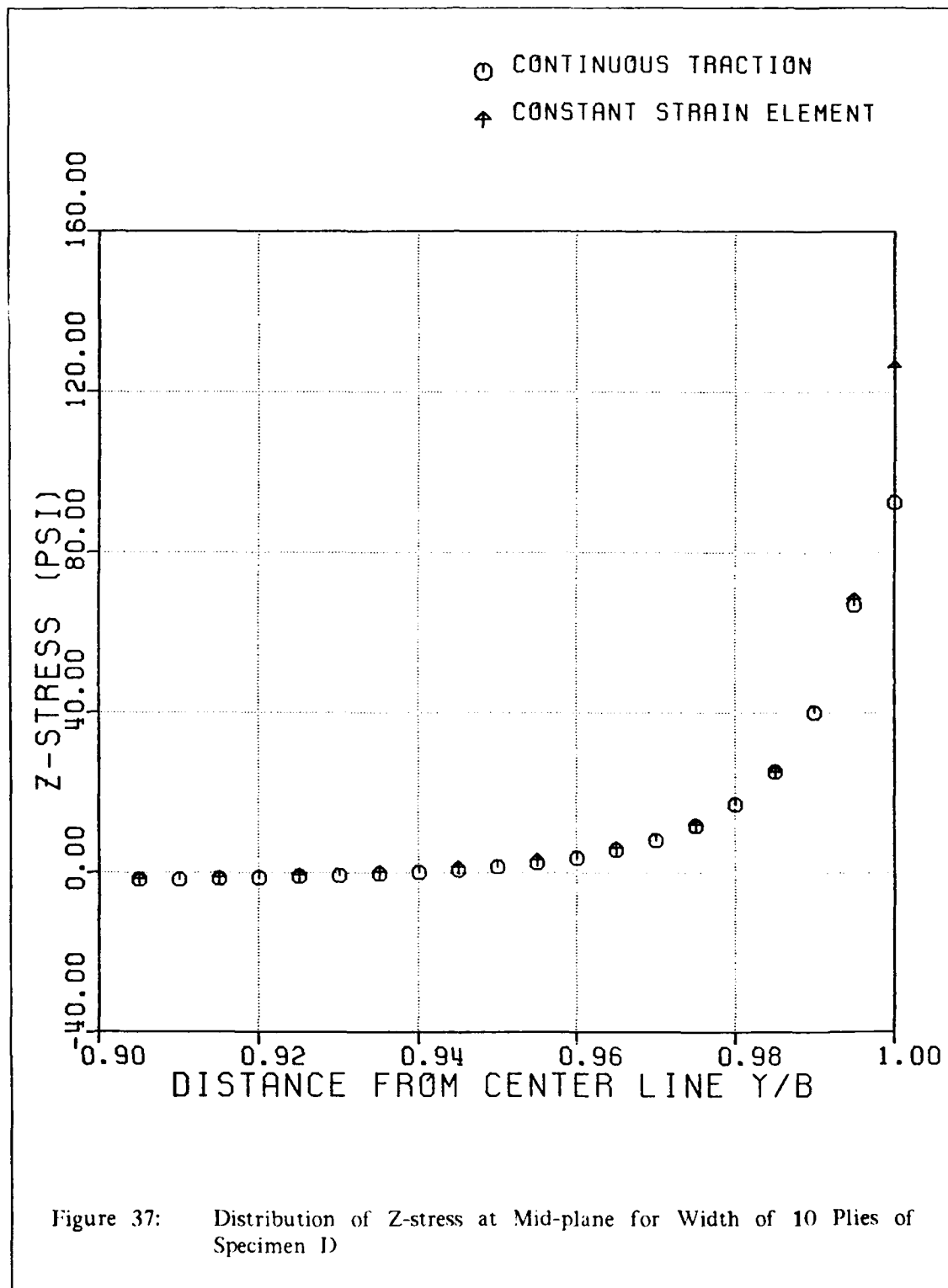


Figure 36: Distribution of Z-stress at Mid-plane for Width of 10 Plies of Specimen C



Q-23 element was distinctly less than that from the constant strain solution. However, the  $\sigma_z$  values calculated from the constant strain element were extrapolated from the interlaminar stresses at  $z=0$  obtained by Lagrangian interpolation of the  $\sigma_z$  values at the element centroids. This is unlike the continuous traction Q-23 solution where  $\sigma_z$  at the free-edge was directly calculated as nodal degree of freedom and would be expected to be more reliable.

Figures (38)-(41) show the through-the-thickness stress distributions of  $\sigma_z$  and  $\tau_{xz}$  calculated from continuous traction Q-23 element at the free-edge of various laminate specimens. It is observed that for the same applied axial stress, specimen D had the largest value of normal stress  $\sigma_z$  at the free-edge, followed by specimens A, B and C. Figure (42) illustrates this. The slope discontinuity of  $\sigma_z$  at the interfaces of the free-edge shown in Figures (38)-(41) was possibly attributed to the material as well as geometrical discontinuities in that region. Figure (43) indicates that much smoother  $\sigma_z$  distributions through the laminate thickness were recovered within the angle-ply laminae at a small distance from the free-edge. In fact, with further refinement along the free-edge, the solution of  $\sigma_z$  on the free-edge is even better. Figures (44)-(45) show the solution for  $\sigma_z$  at the free-edge and at  $y=0.495$  for specimen A with each edge element being refined into four elements along  $y$  direction. Also, figure (46) shows the functional dependence of longitudinal stress  $\sigma_x$  as well as interlaminar normal stress  $\sigma_z$  on the fiber orientation, respectively, for the  $[(\theta/-\theta)_3/90]_s$  laminate under the same applied loading. The ordinates of these curves are the respective values of  $\sigma_x$  and  $\sigma_z$  at the intersection of the mid-plane and traction-free edge of the laminate. Results obtained from the continuous traction Q-23 element indicated that both  $\sigma_x$  and  $\sigma_z$  attained their maximum values approximately in the fiber orientation

$$\theta = 30^\circ.$$

The shear stress  $\tau_{xz}$  distributions were similar for these specimens, and their magnitudes are relatively smaller than the maximum normal stress  $\sigma_z$ . However, the existence of  $\tau_{xz}$  evidently reflected a defect of the numerical model adopted in [46] in which the delamination specimen was treated as an axially symmetric problem in which  $\tau_{xz}$  was inherently assumed to be zero throughout the laminate thickness. It was noted that  $\sigma_z$  distribution had a slope discontinuity at the mid-plane surface within the 90-degree layer. This does not appear to be reasonable for the present symmetric laminate specimens. Presuming that this was associated with the use of a single element through the thickness of 90-degree layer being insufficient to accommodate the mismatch at the interface between angle-ply and cross-ply laminae, a study was carried out refining the mesh near the midplane. Figure (47) shows the dramatical improvement of  $\sigma_z$  distribution near the mid-plane surface of specimen A as increasing number of elements was used in the discretization of 90-degree layer. At the same time, the maximum value of  $\sigma_z$  in the interior of the transverse layer was observed to move closer to the interface with the angle-ply layer. Again, if both the 90-degree layer and the free-edge elements were refined, the improvement of  $\sigma_z$  was not only on the 90-degree layer but also on the entire laminate. Figures (48)-(49) show this improvement.

Comparison of the interlaminar shear stress  $\tau_{yz}$  at the center line of 90-degree layer along the width of various laminate specimens are shown in Figures (50)-(53). Solutions from both methods indicate that  $\tau_{yz}$  approached finite maximum values in the vicinity of free-edge yet the traction-free boundary condition could only be satisfied by using the continuous traction Q-23 element. The maximum values of  $\tau_{yz}$  from the

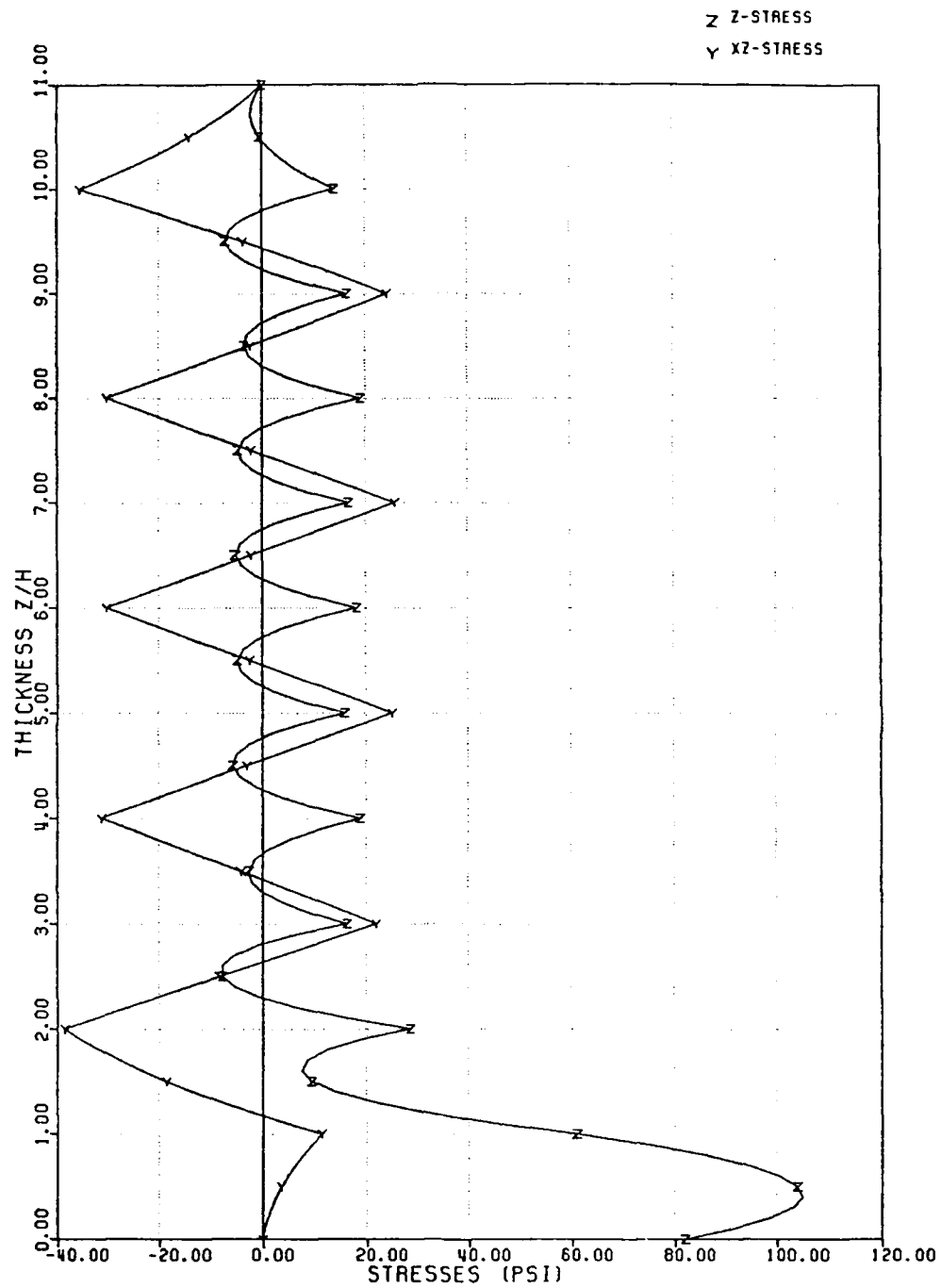


Figure 38: Through-Thickness Stress Distributions at the Free-Edge of Specimen A Based on the Continuous Traction Q-23 Element

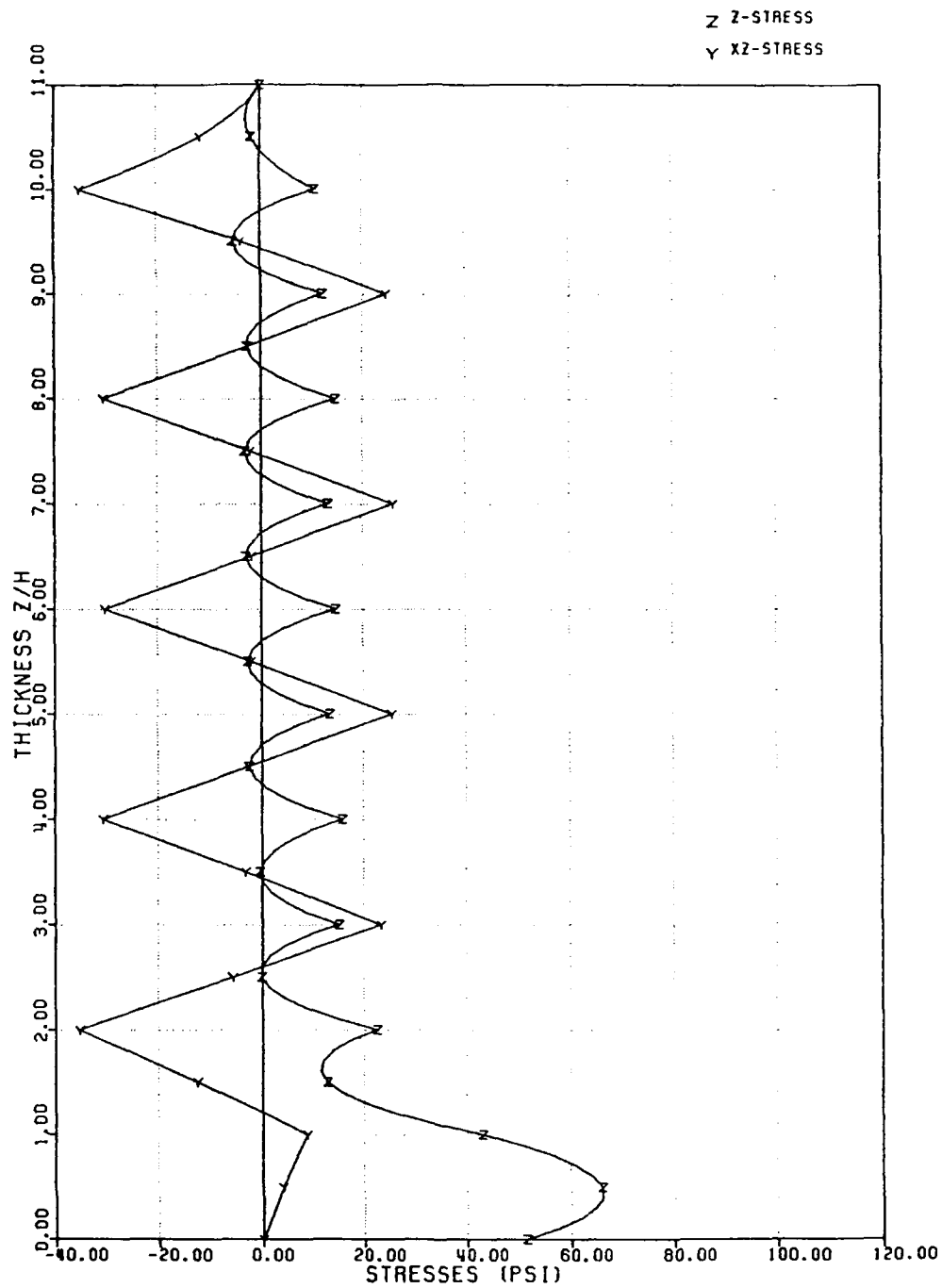


Figure 39: Through-Thickness Stress Distributions at the Free-Edge of Specimen B Based on the Continuous Traction Q-23 Element

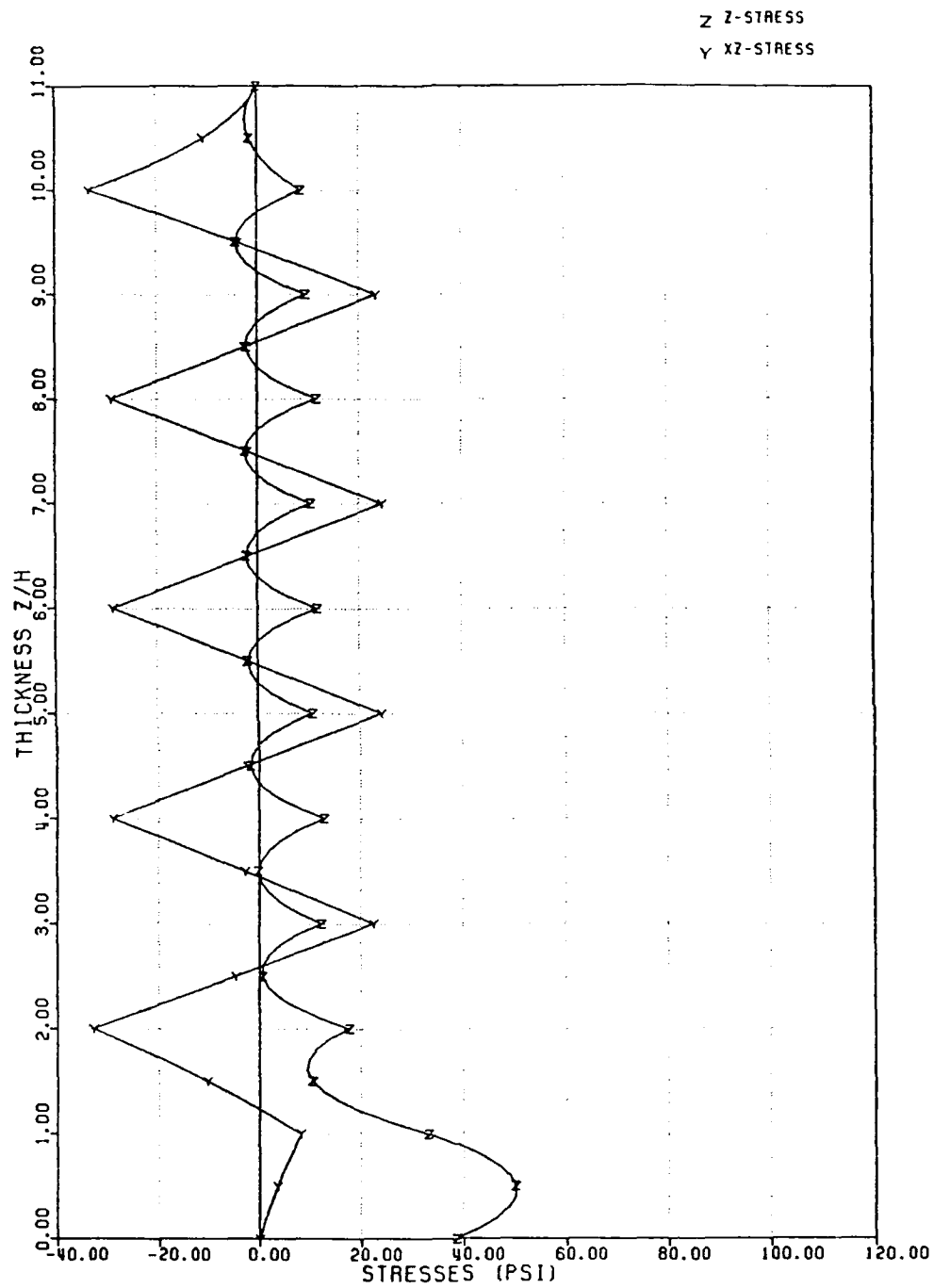
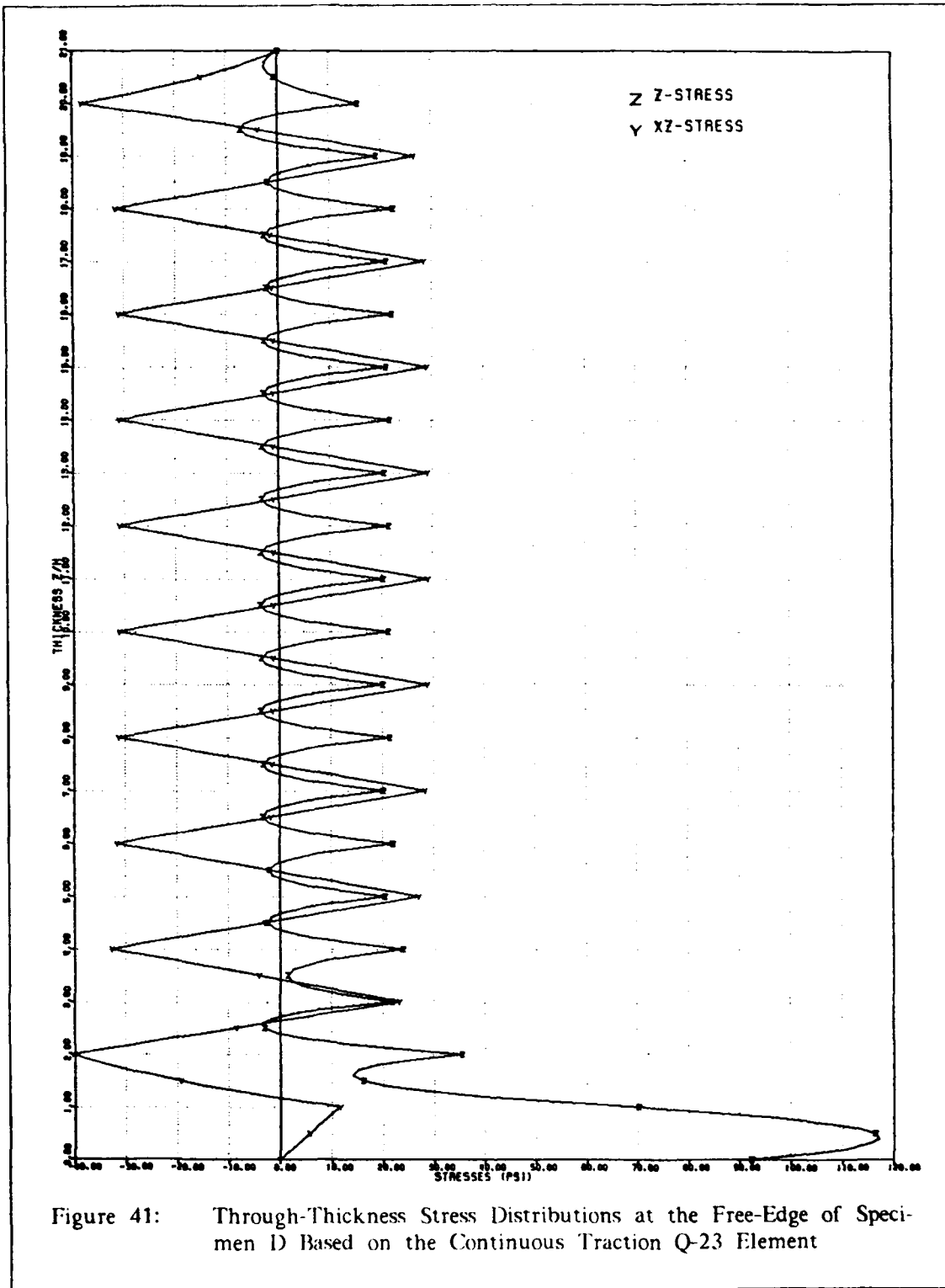
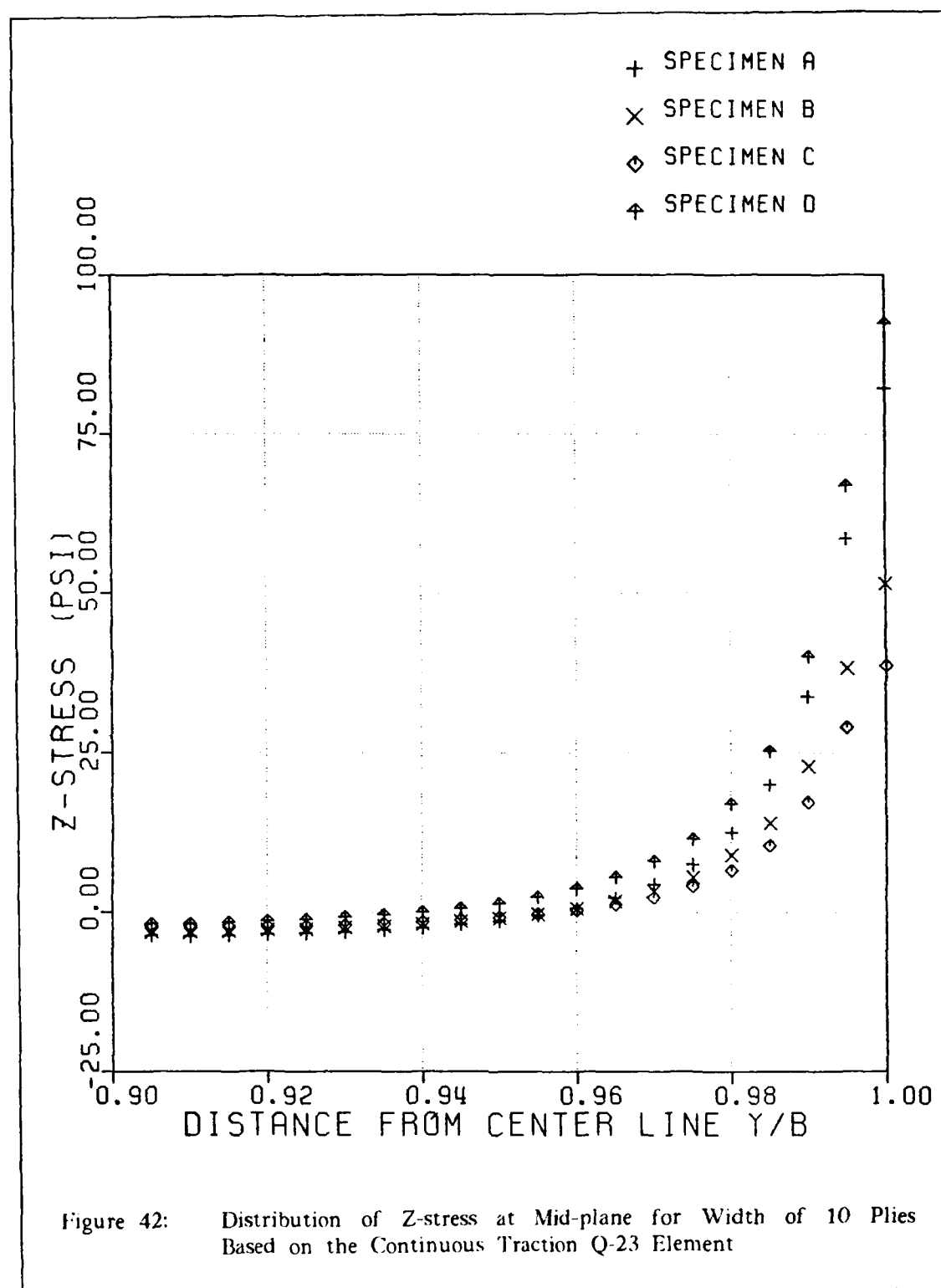
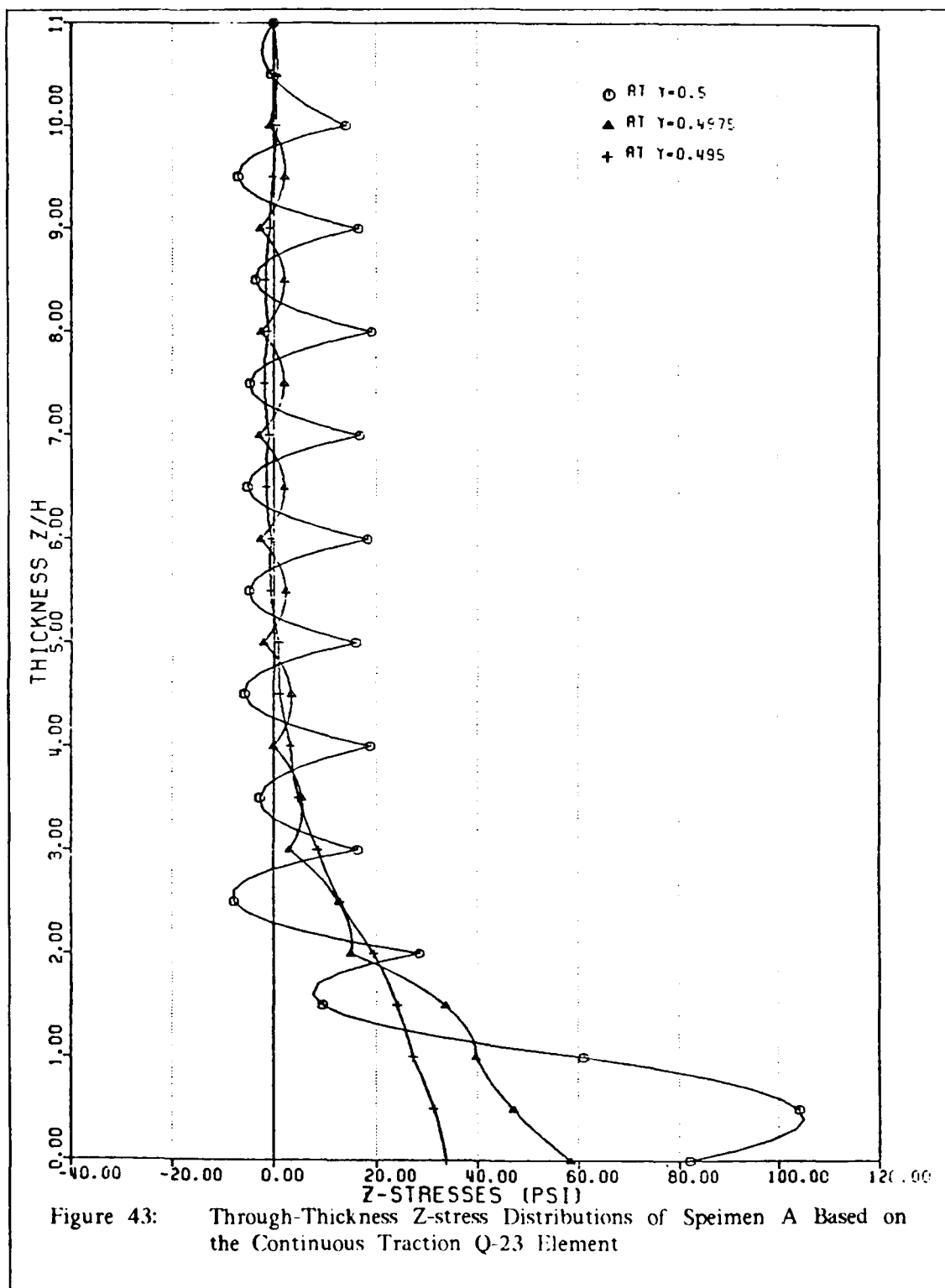


Figure 40: Through-Thickness Stress Distributions at the Free-Edge of Specimen C Based on the Continuous Traction Q-23 Element









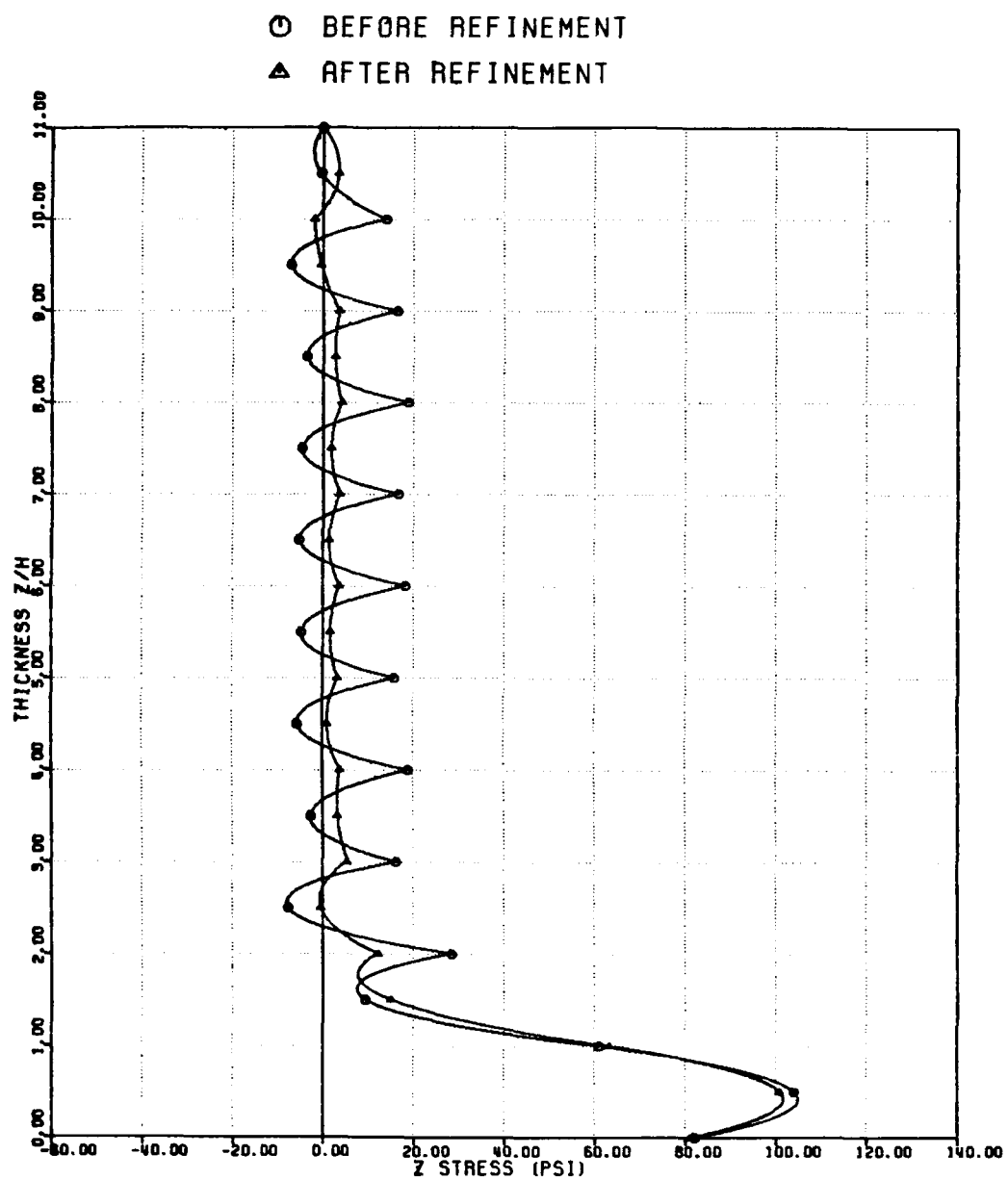


Figure 44: Through-Thickness Stress Distributions at the Free-Edge of Specimen A with Further Refinement on the Free-Edge

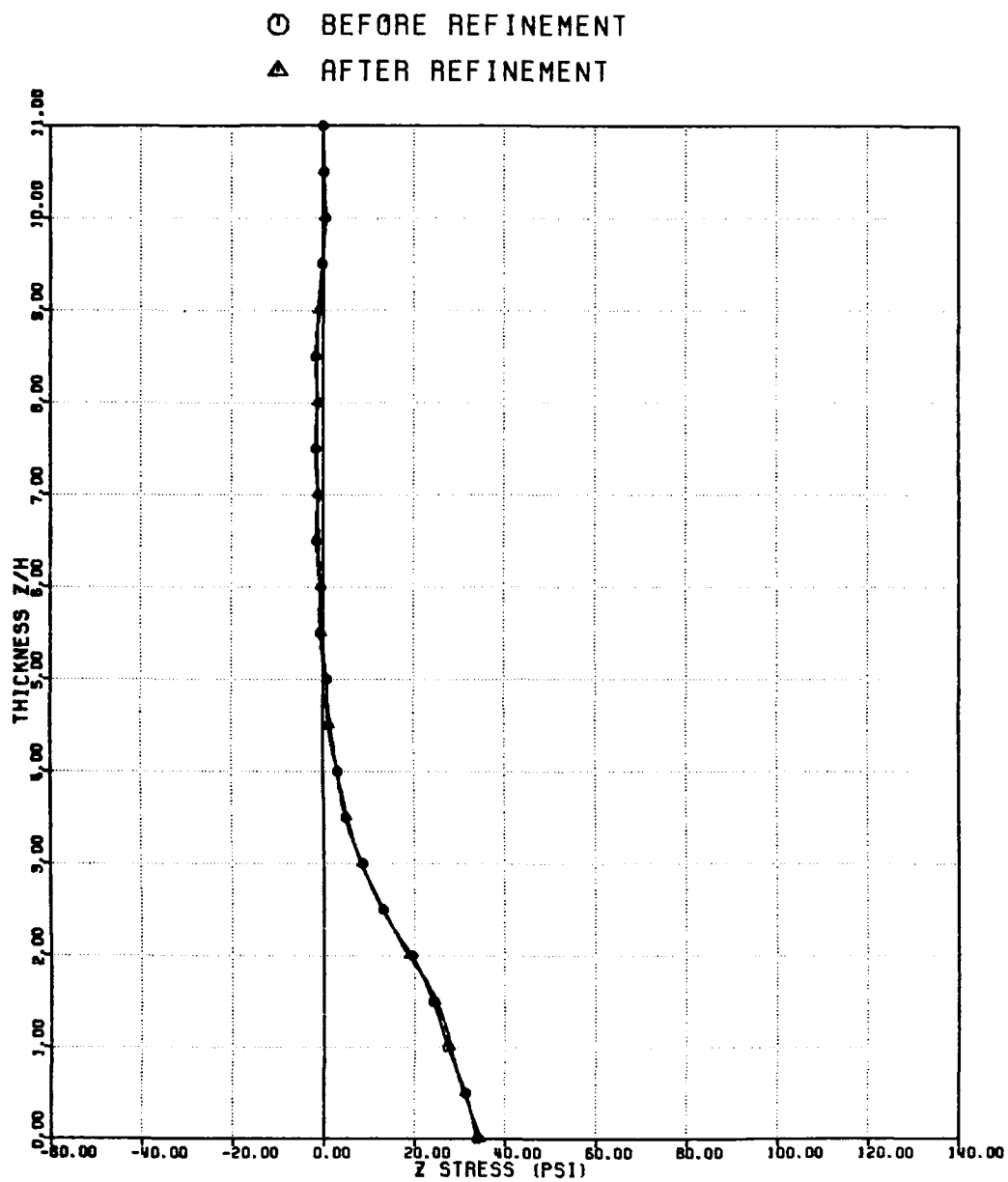


Figure 45: Through-Thickness Stress Distributions at  $y=0.495$  of Specimen A with Further Refinement on the Free-Edge

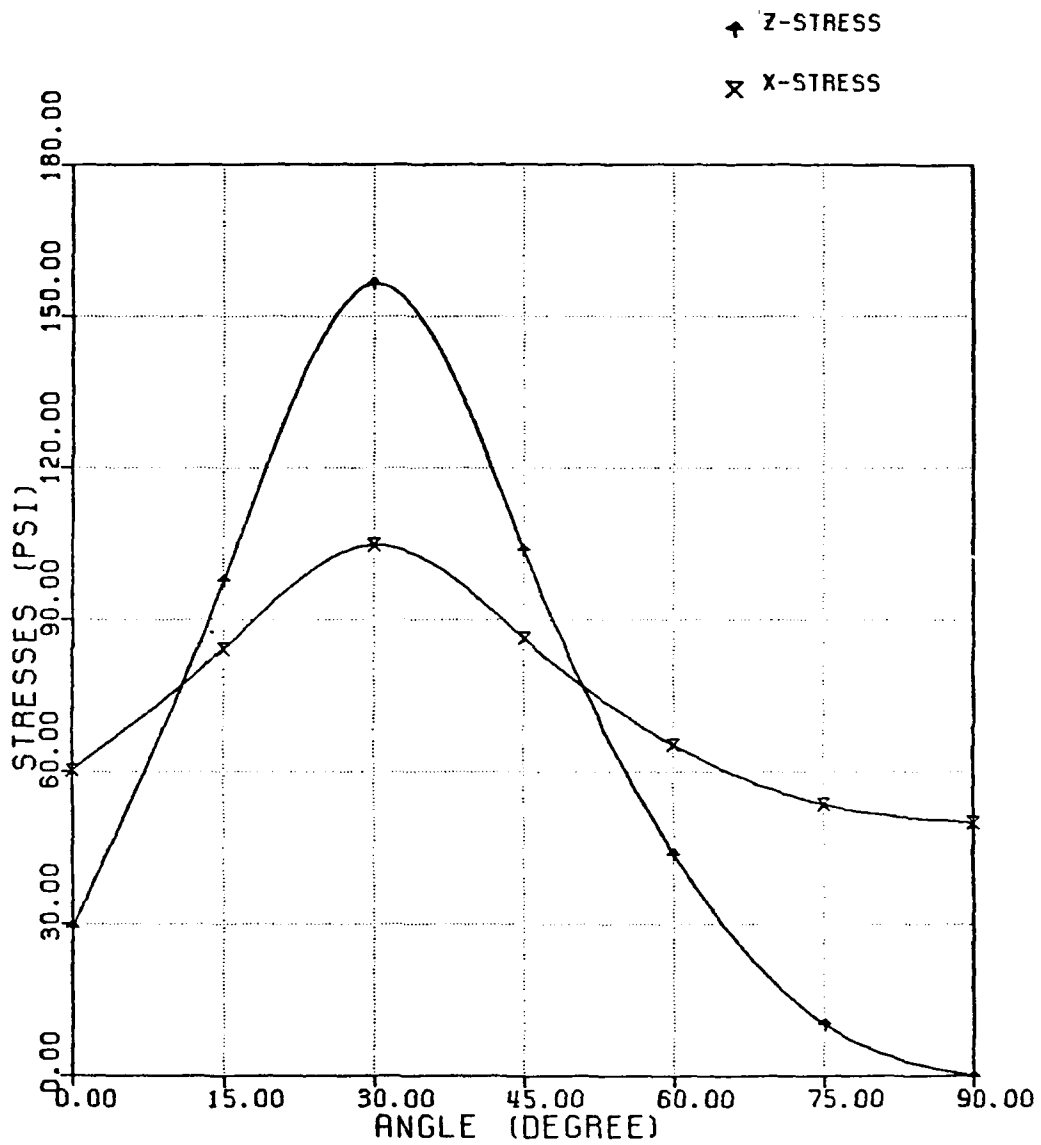


Figure 46: Stresses at the Mid-plane of the Free-Edge as a Function of Fiber Orientation for  $[(\theta/-\theta)_5/90]_S$  Laminate

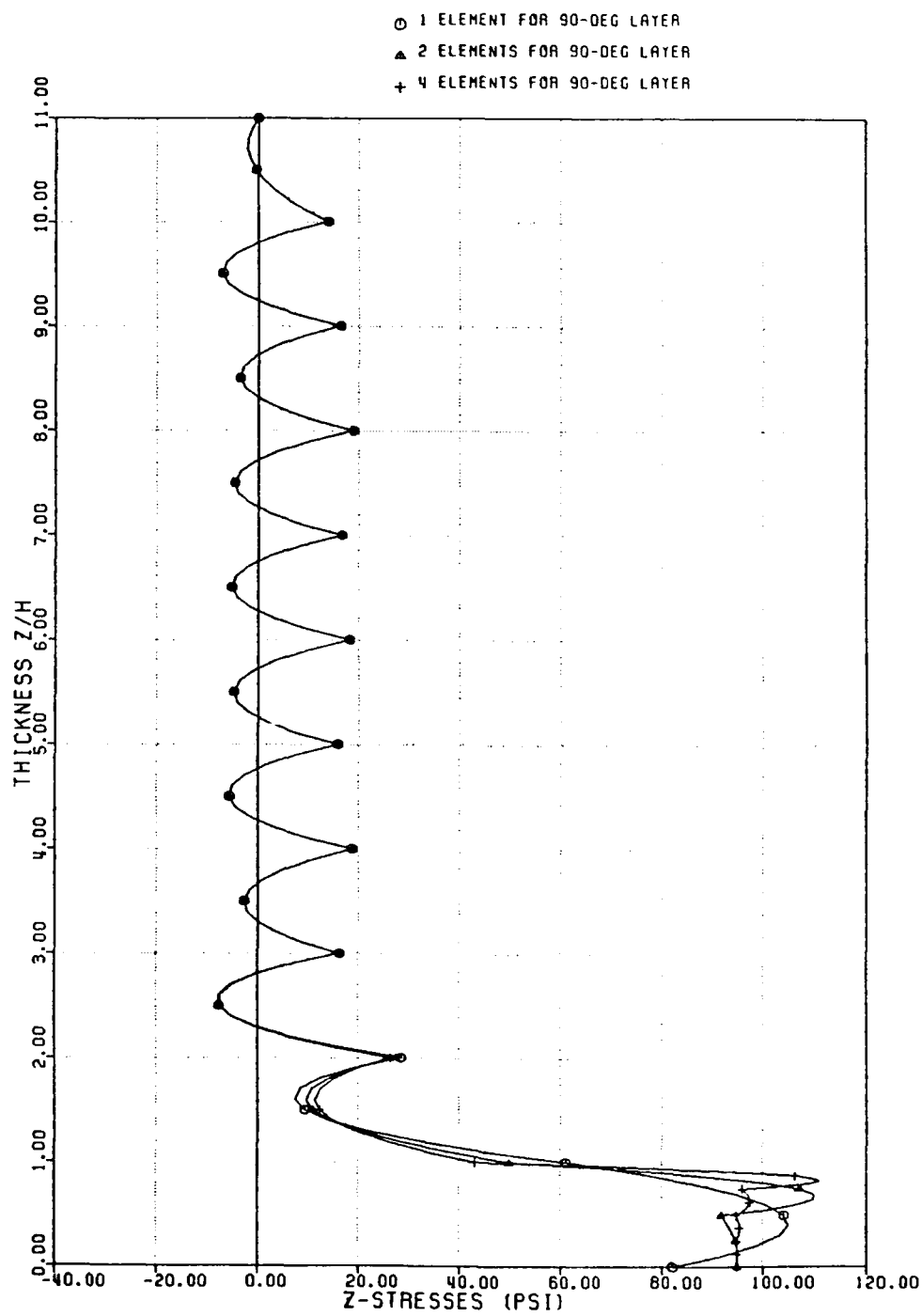


Figure 47: Through-Thickness Z-stress Distribution at the Free-Edge of Specimen A Based on the Continuous Traction Q-23 Element

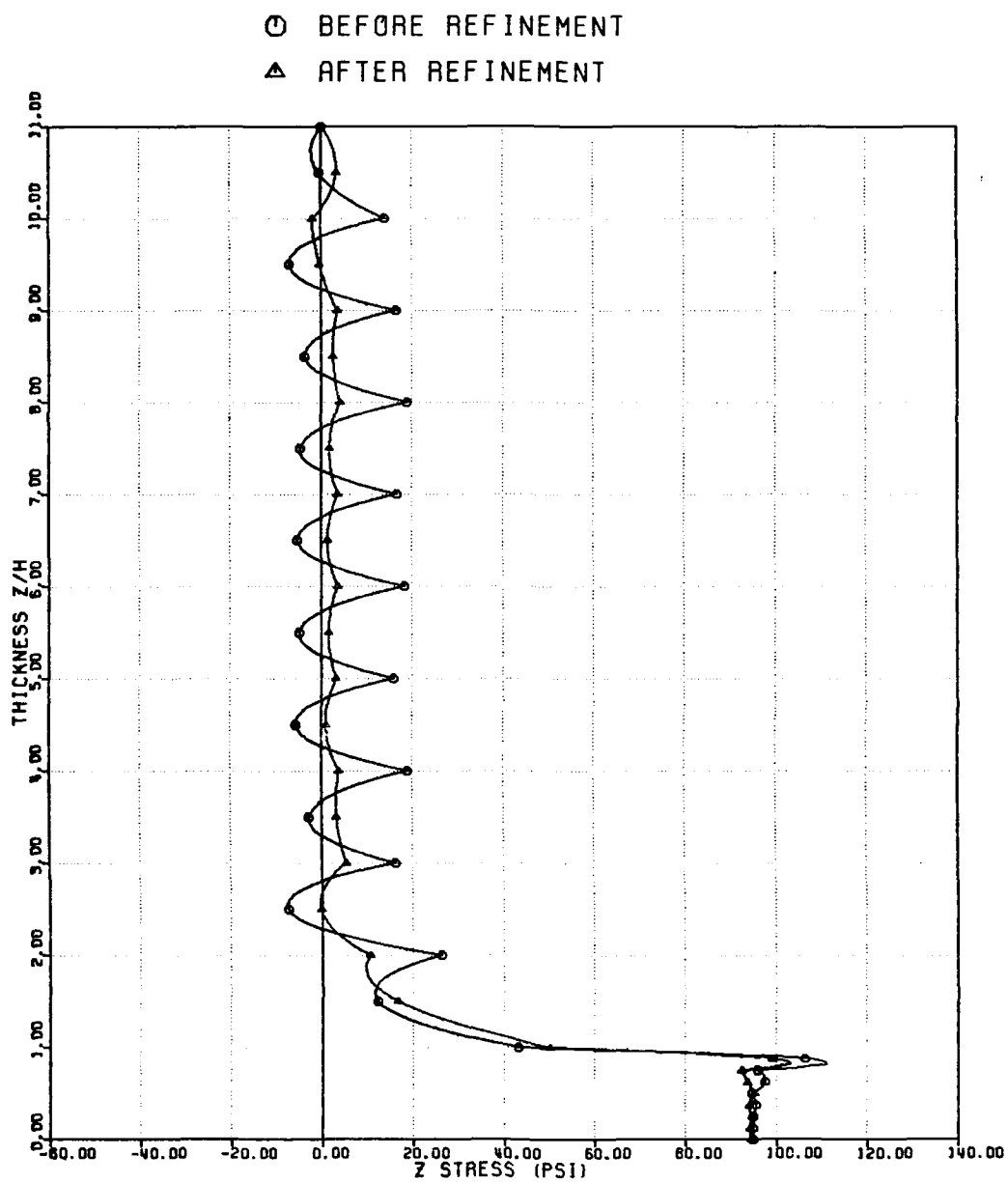


Figure 48: Through-Thickness Stress Distributions at the Free-Edge of Specimen A with Further Refinement both on the Free-Edge and on the 90-degree Layer



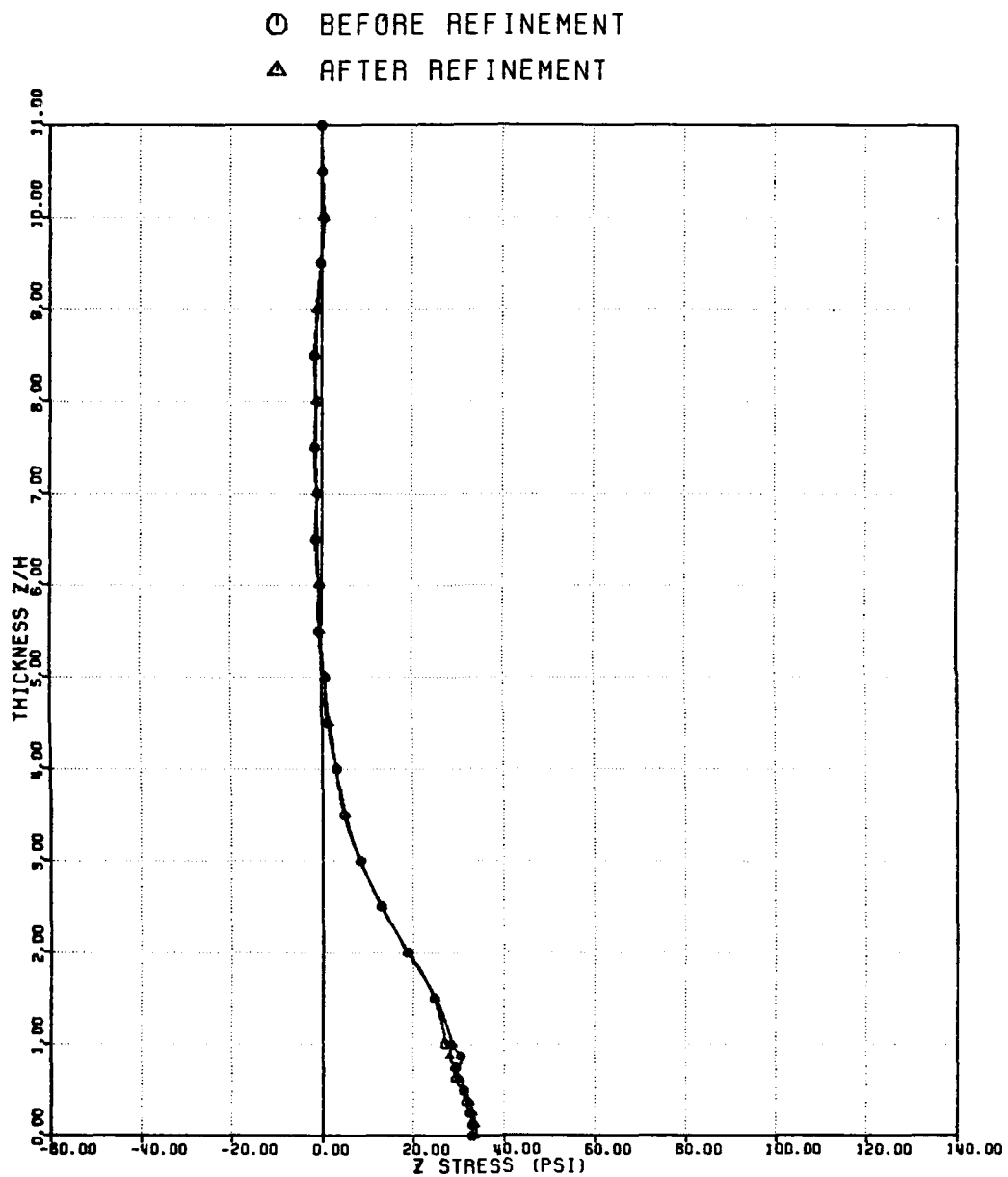


Figure 49: Through-Thickness Stress Distributions at  $y=0.495$  of Specimen A with Further Refinement both on the Free-Edge and on the 90-degree Layer

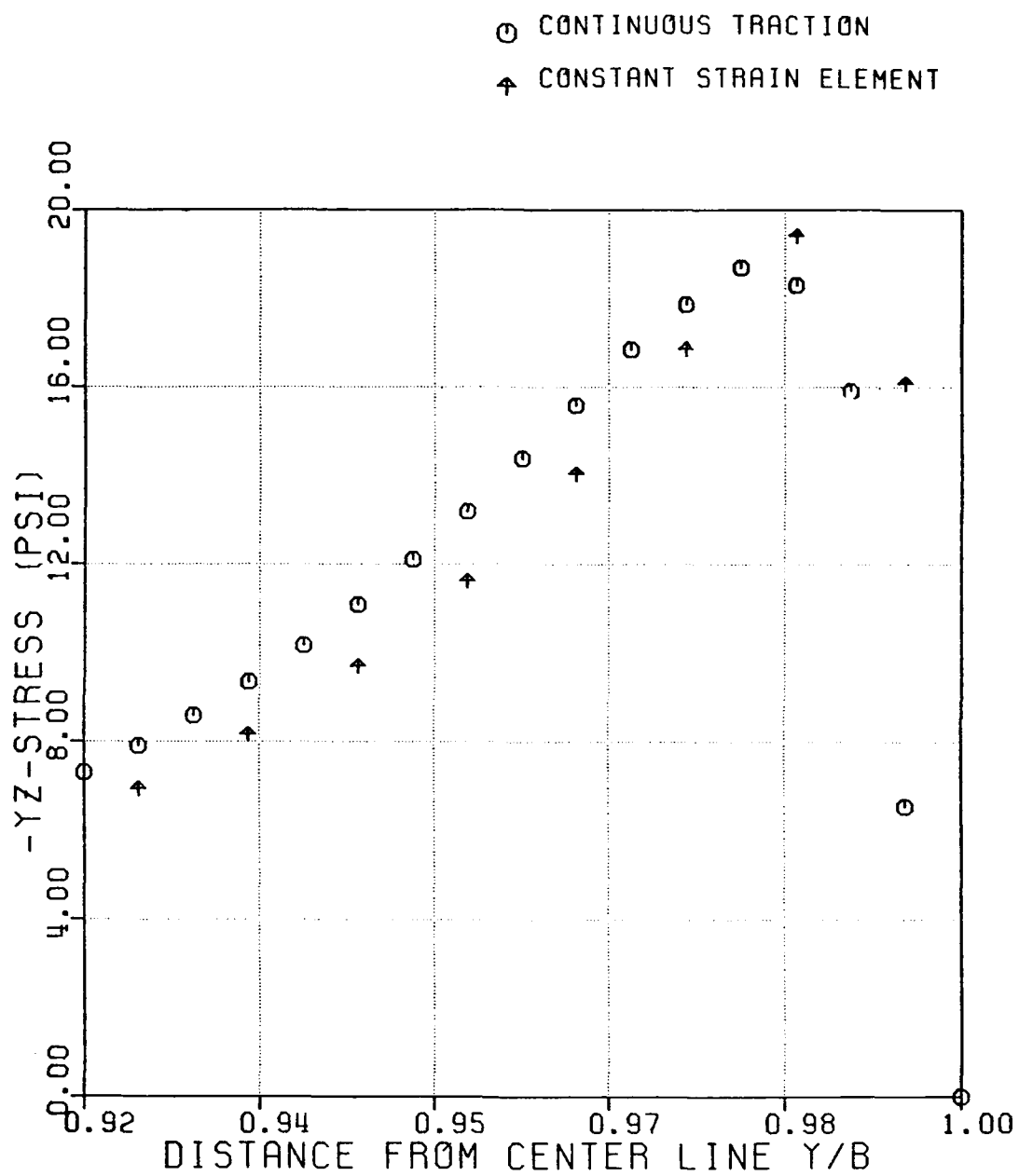
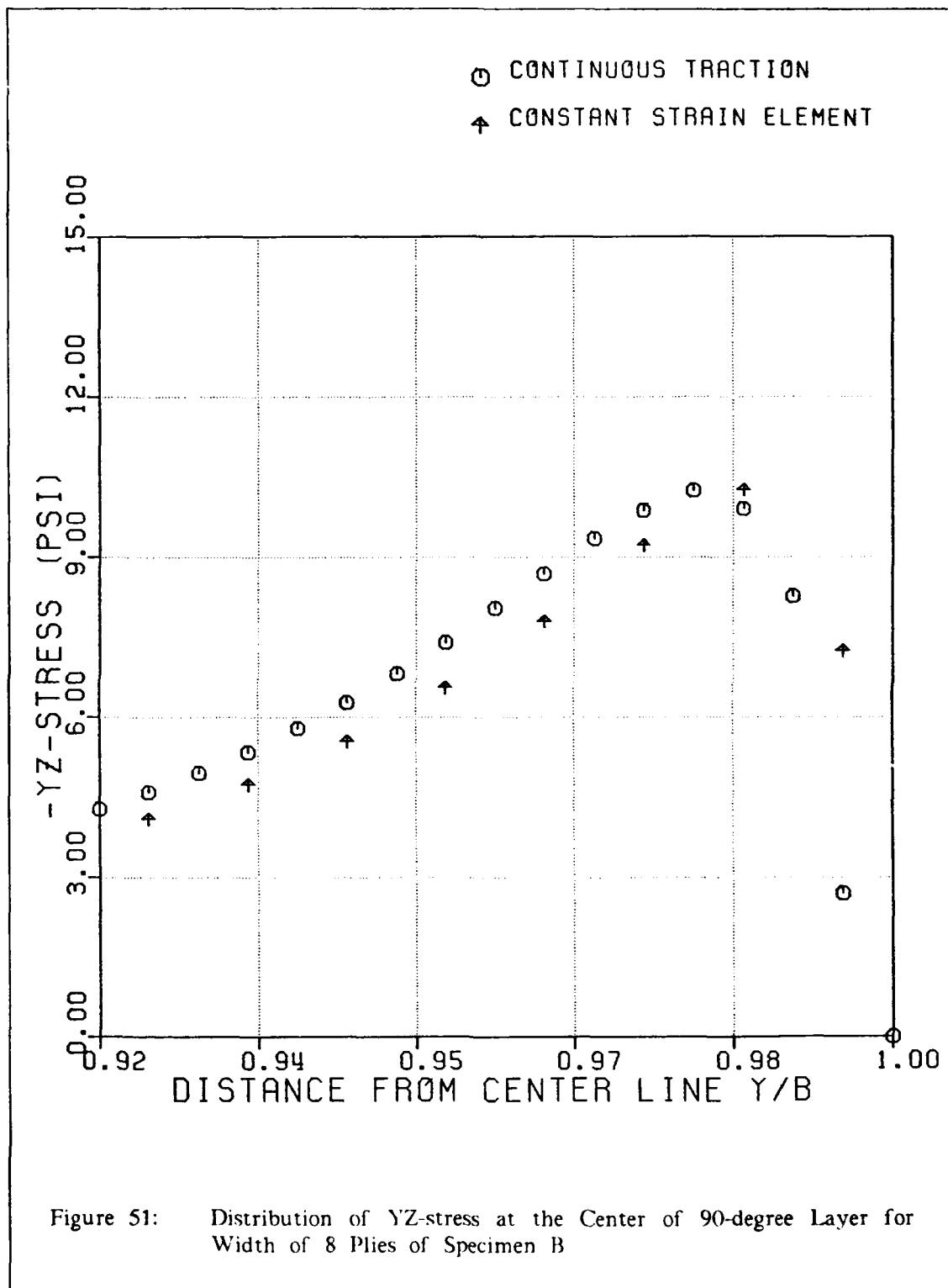
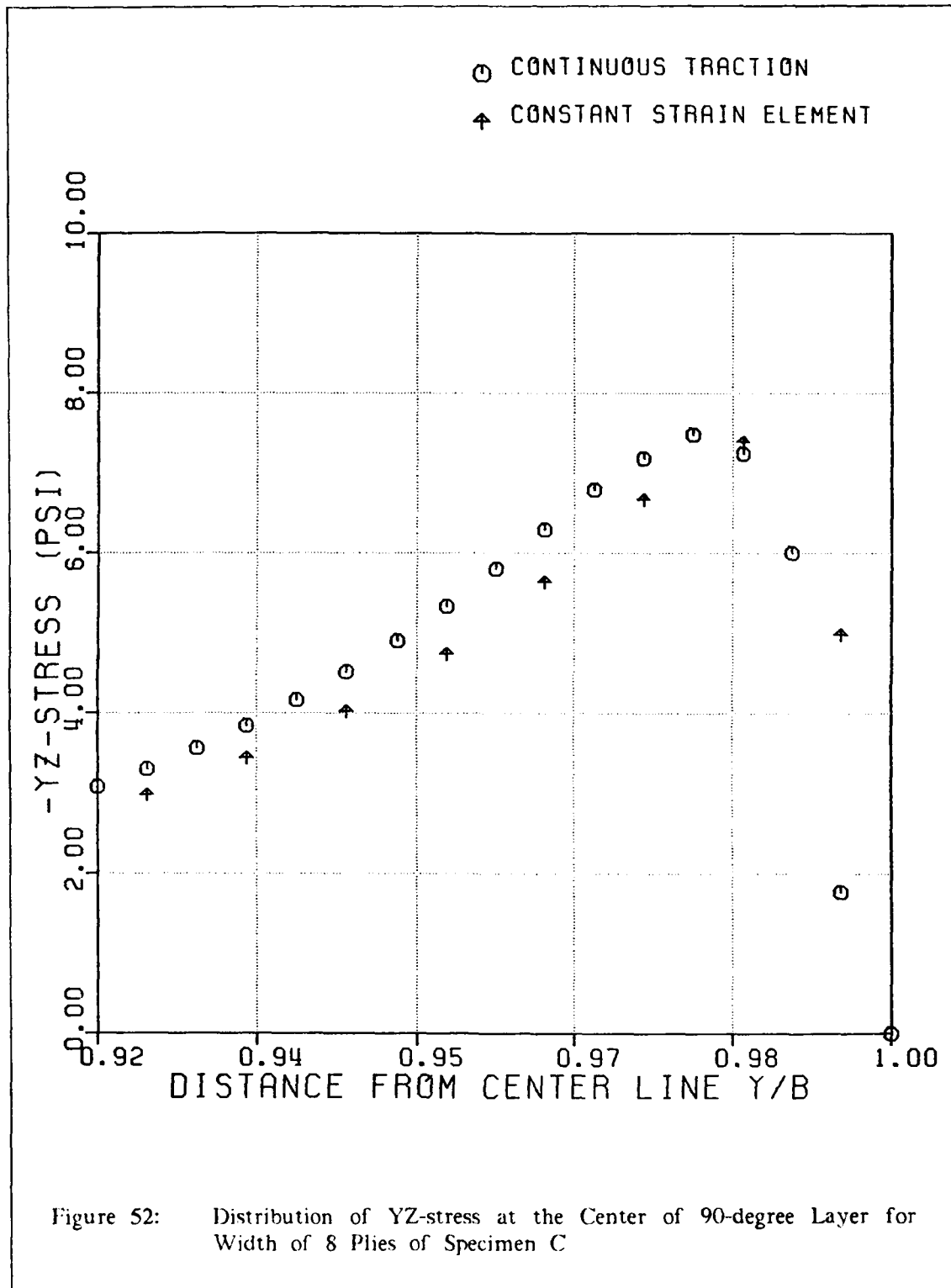
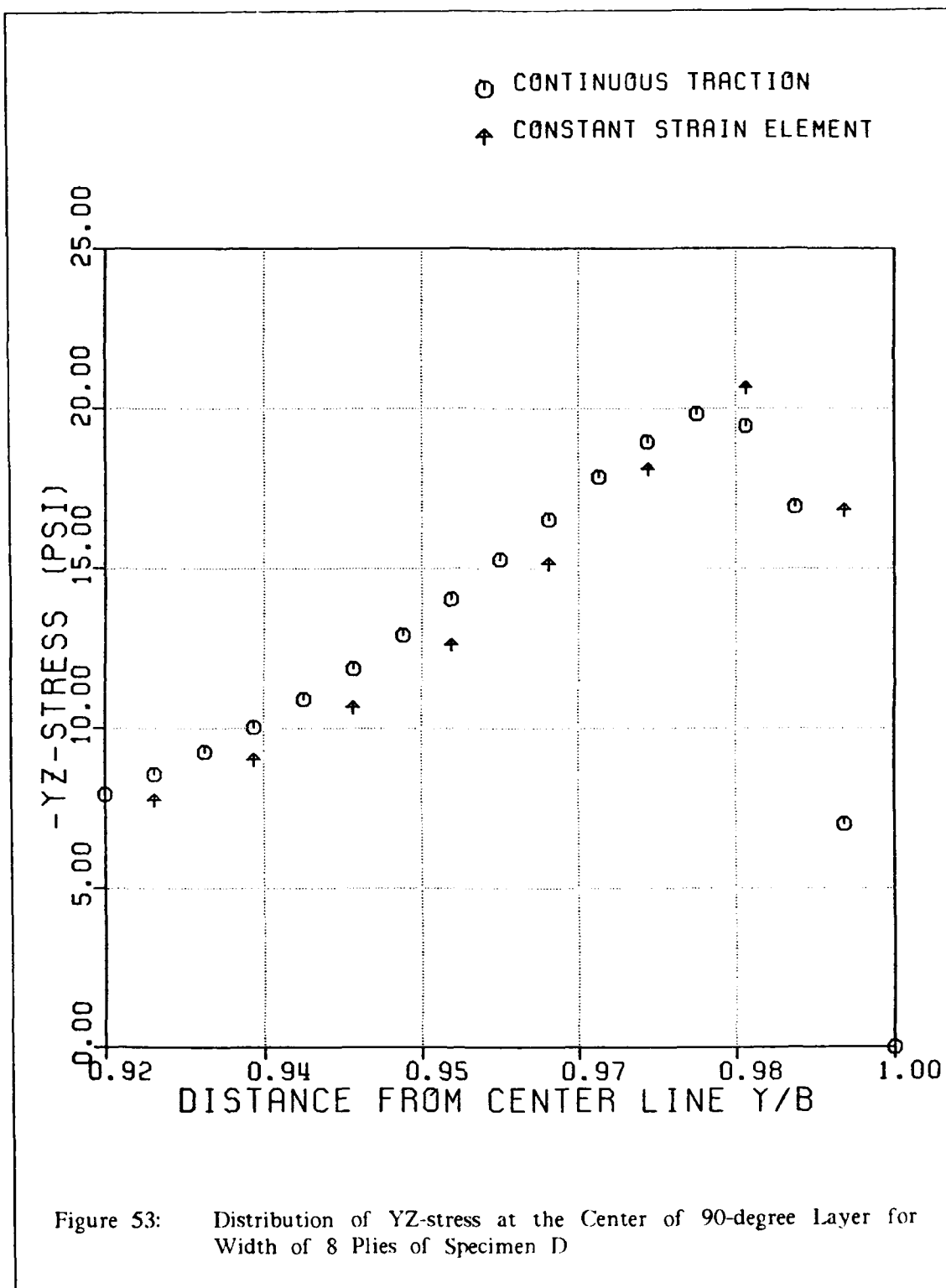


Figure 50: Distribution of YZ-stress at the Center of 90-degree Layer for Width of 8 Plies of Specimen A







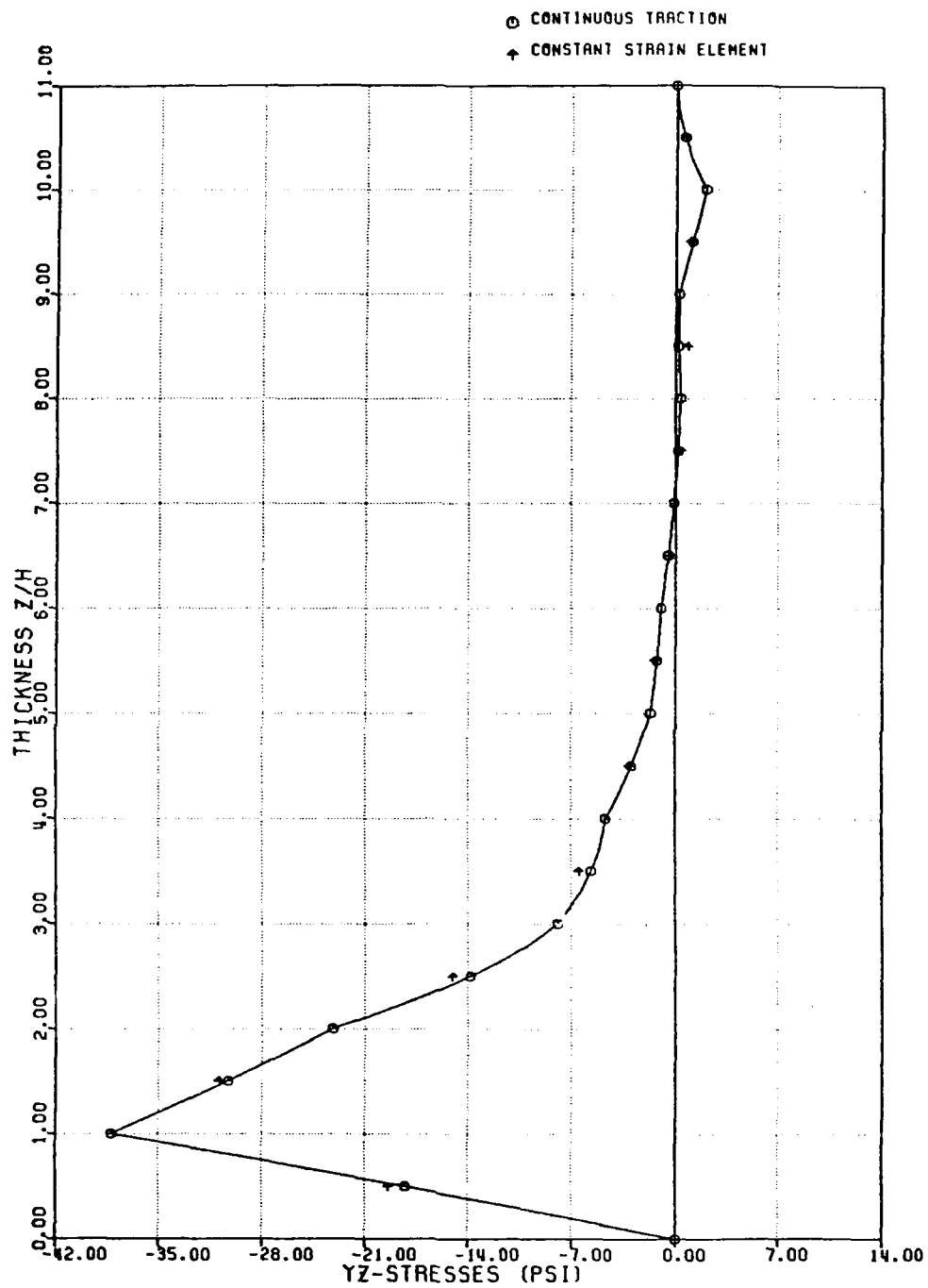


Figure 54: Through-Thickness Distribution of YZ-stress at the Center of the Second Element From the Free-Edge for Specimen A

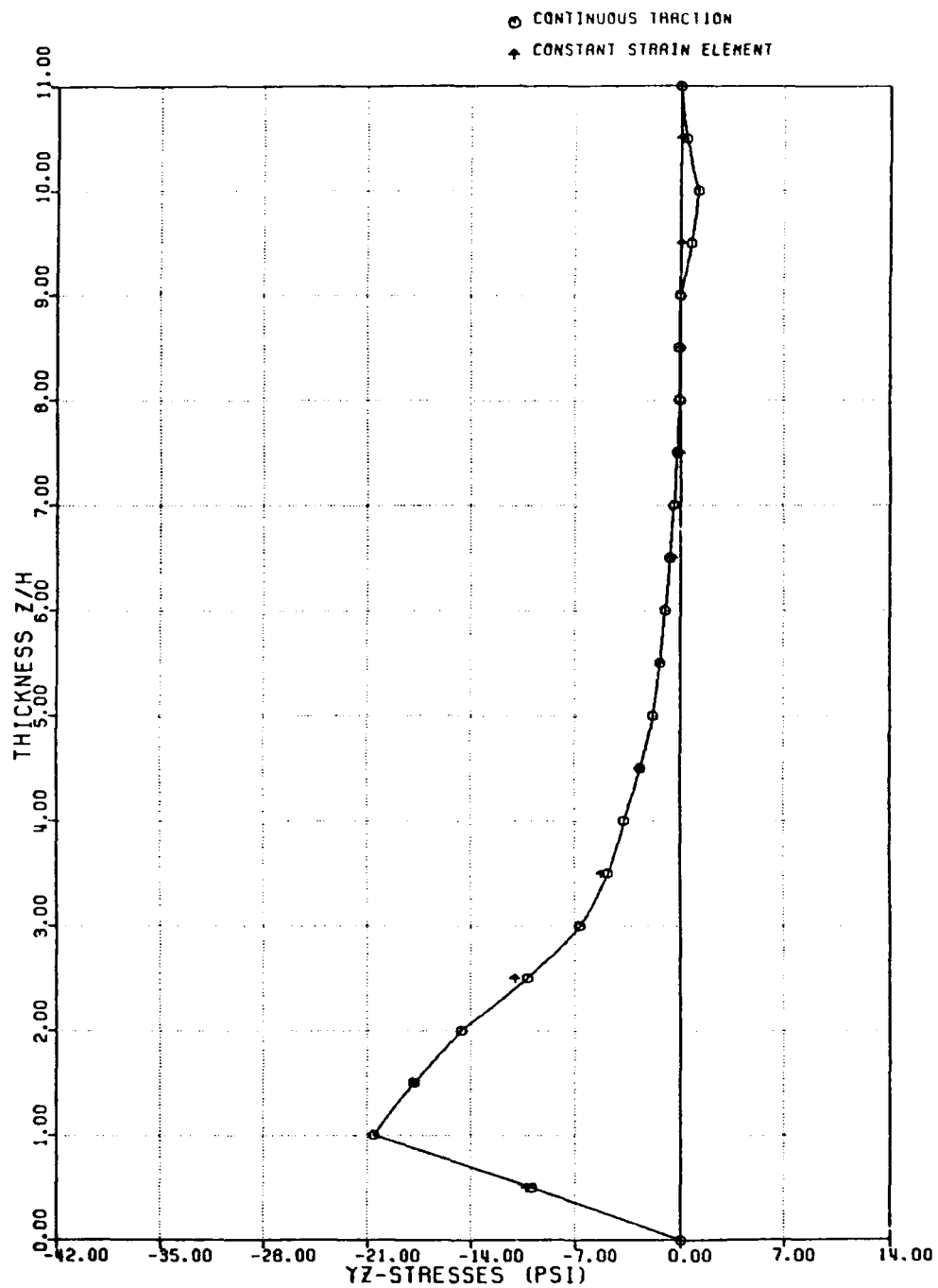


Figure 55: Through-Thickness Distribution of YZ-stress at the Center of the Second Element From the Free-Edge for Specimen B

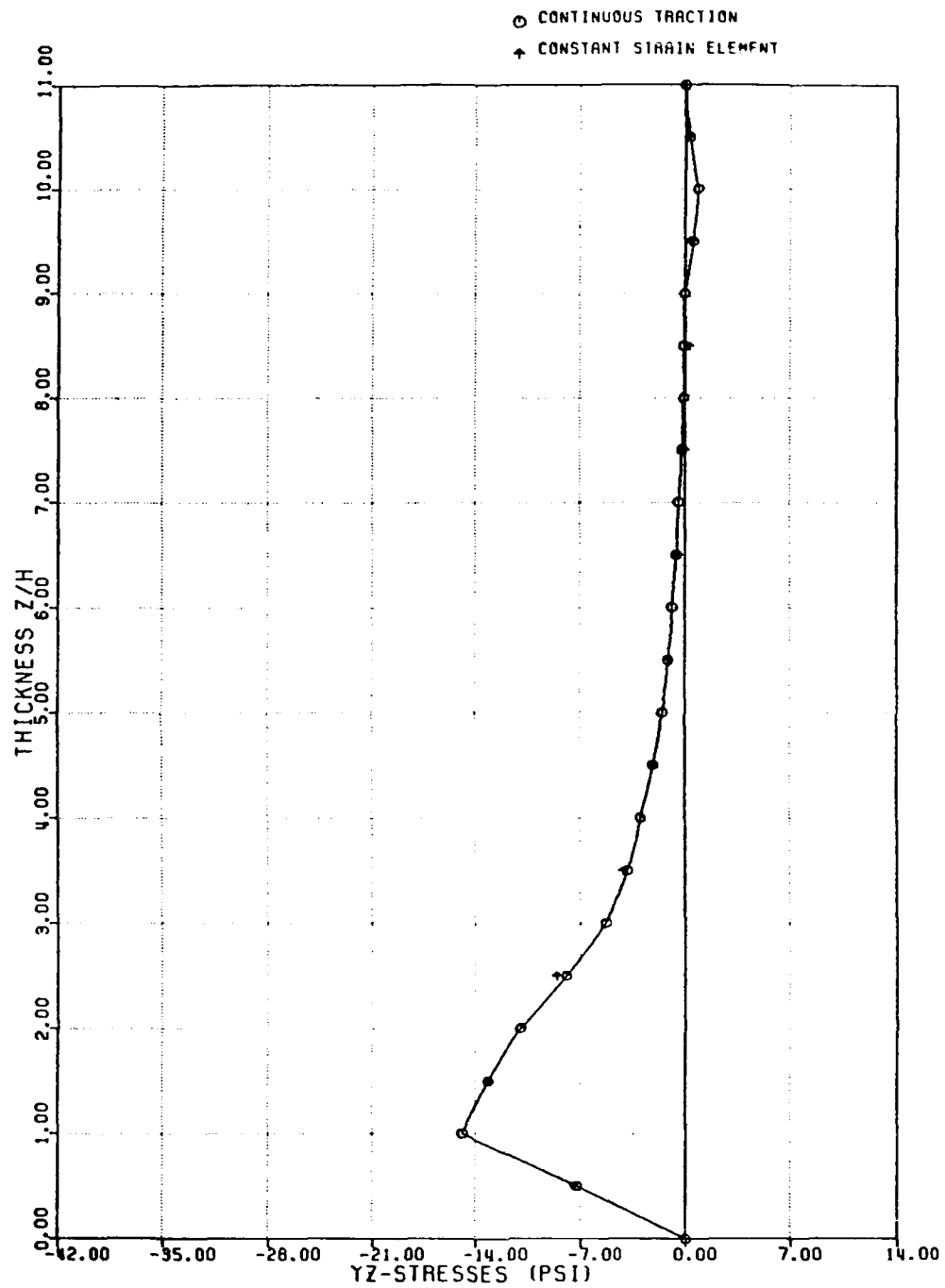
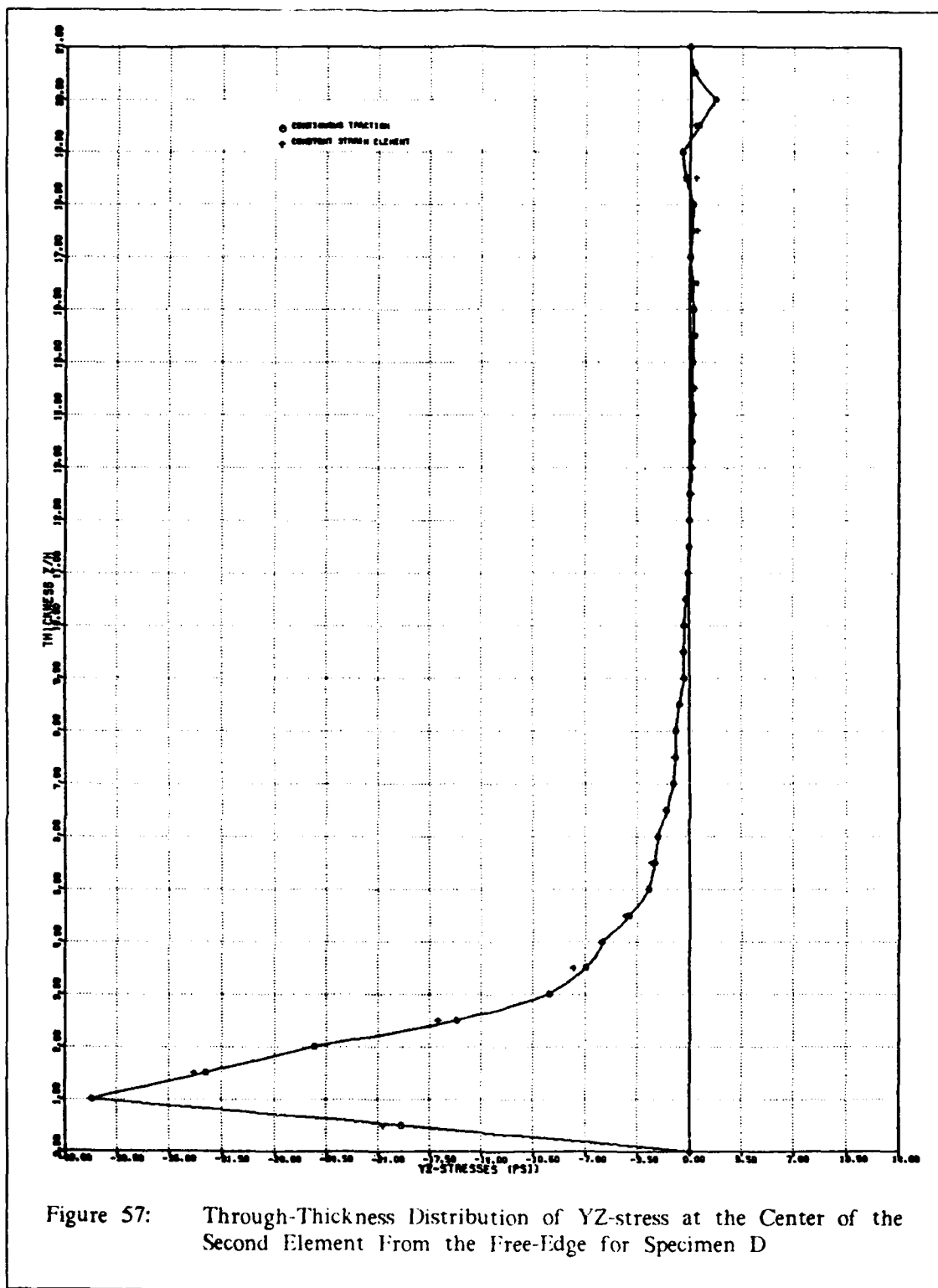


Figure 56: Through-Thickness Distribution of YZ-stress at the Center of the Second Element From the Free-Edge for Specimen C





two models were comparable. The constant strain triangular element approximation departed significantly from the Q-23 solution in the vicinity of the free-edge. This could largely be due to the nonsatisfaction of the traction-free boundary condition. Figures (54)-(57) illustrate through-the-thickness stress distribution of  $\tau_{yz}$  along center line of the second element from the free-edge for various laminate specimens. The reason to choose this site for comparison was because of the singular stress behavior being displayed in the finite element discretization for both methods (Figures 50-53). A close agreement was generally observed between these two solutions. The continuous traction Q-23 analysis show that the maximum  $\tau_{yz}$  occurred at the interface between the negative angle-ply and the 90-degree layers for all the specimens. The constant strain element does not have the capability to predict this. It is also noted that for the same applied axial stress, specimen D has the largest value of  $\tau_{yz}$ , followed by A, B and C, similar to the observation for  $\sigma_z$ .

Table (2) shows the values of interlaminar normal stress  $\sigma_z$  at the interface of the free-edge for laminate specimens A, B, C and D based on constant strain element and continuous traction Q-23 element, respectively. The ratios of the normal stresses  $\sigma_z$  to the relatively minimal value among them are 2.11 : 1.32 : 1.0 : 2.47 for constant strain element, and 2.12 : 1.33 : 1.0 : 2.39 for continuous traction Q-23 element. Thus, the normal stress ratios for specimens A, B, C and D, calculated from these two finite element schemes are comparable with each other.

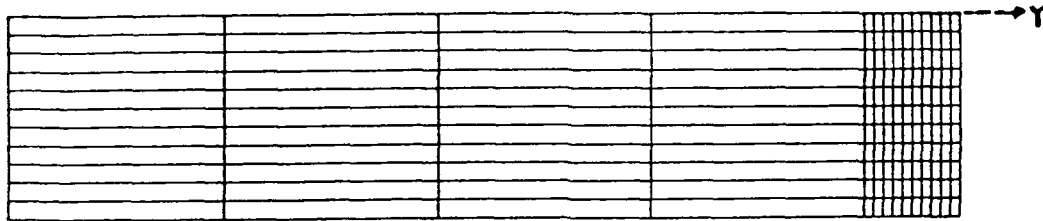
Figure (58) shows exaggerated views of the displacement fields based on the continuous traction Q-23 element in specimens A, B and C. Figure (59) shows the distortion of Specimen D. The maximum displacement in the y-direction calculated from both constant strain element and continuous traction Q-23 element shown in

Table 2: Comparisons of Delamination Tendency for Various Speimens

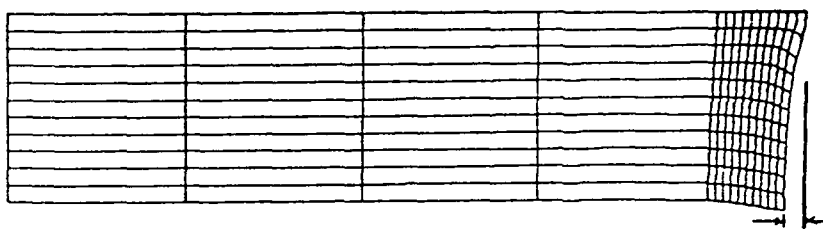
( unit : psi)

Classification	Specimen	A	B	C	D
$\sigma_z$ from Constant Strain element	Value	107.74	67.65	51.12	126.22
	Ratio	2.11	1.32	1.00	2.47
$\sigma_z$ from Continuous Stress Element	Value	82.07	51.54	38.68	92.43
	Ratio	2.12	1.33	1.00	2.39

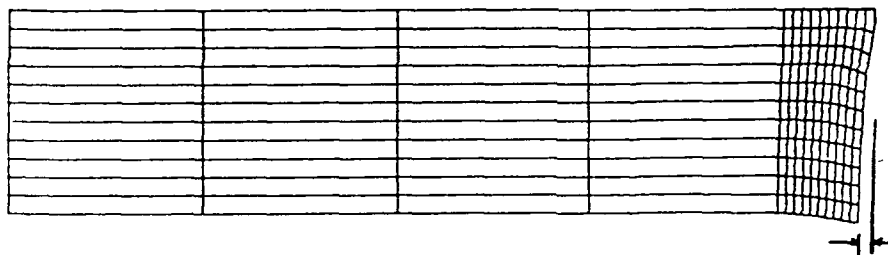
Note :  $\text{Ratio} = \frac{\sigma_z}{\sigma_{z_{\min}}}$



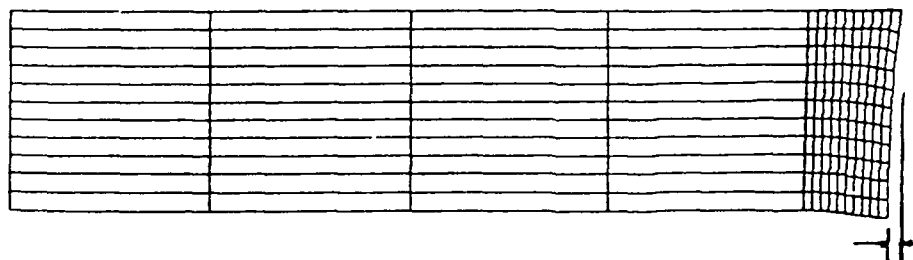
(a) Undeformed Model of A, B and C Laminates



(b) Deformed Model of A Laminate

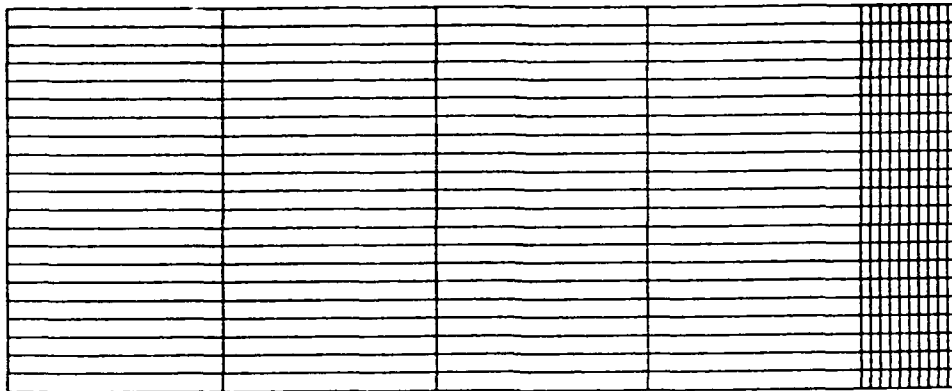


(c) Deformed Model of B Laminate

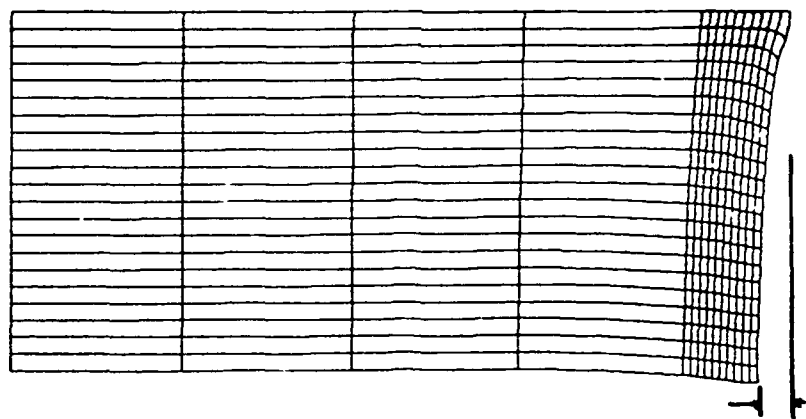


(d) Deformed Model of C Laminate

Figure 58: Finite Element Models of A, B and C Laminate Specimens



(a) Undeformed Model of D Laminate



(b) Deformed Model of D Laminate

Figure 59: Finite Element Models D Laminate Specimen

Table (3), were found to be in reasonable agreement for all these specimens. Also, from these figures, it is observed that under the same applied axial stress, specimens D had the largest distortion near the free-edge, followed by laminates A, B and C in descending order. In other words, specimen D had the greatest tendency for edge delamination among the four specimens, and the delamination would set in at the lowest applied axial stress. This again confirms the prediction based on the interlaminar normal stress  $\sigma_z$  which had the largest values for specimen D as shown in Table (2). Based upon above analysis, we conclude that both the distortions and the values of normal stress  $\sigma_z$  near the free-edge of the specimens calculated from the continuous traction Q-23 element are consistent with those of the constant strain element [46] which is much more economical to implement.

Table 3: Comparisons of Maximum Transverse Deformation for Various Specimens

(  $10^{-5}$  in)

Classification	Specimen	A	B	C	D
Constant Strain Element	Value	0.1309	0.1032	0.0829	0.1935
	Ratio	1.5789	1.2448	1.00	2.3337
Continuous Traction Element	Value	0.1171	0.0888	0.0704	0.1638
	Ratio	1.6641	1.2619	1.00	2.3274

Note :  $\text{Ratio} = \frac{v}{v_{\min}}$

### 6.3.1.2 Analytical-Experimental Correlation

An experimental study was conducted at AFWAL/AIFDL [46] to validate the analytical results. Part of the test results are summarized in Table (4), which gives the specimen type, strains, and stresses for the initiation of edge delamination determined by transverse gages, silver ink, acoustic emission and visual observation. The table also contains average axial stress for initiation of edge delamination calculated from the continuous traction Q-23 element. The average initial delamination stresses for laminates A, B, and C were found to be 19.2, 23.3 and 26.4 (ksi), respectively [45]. The corresponding finite element solutions were 15.883, 25.817 and 29.935 (ksi). To calculate these values, the nodal axial stresses within each LCCF-12 triangular element had to be recovered from the stresses calculated along the boundary of Q-23 quadrilateral. The axial loading applied on each triangular element could then be computed by integrating the nodal stress values over each triangular area. Having assembled the element axial loading over the whole system, the average axial stress was obtained by dividing the total axial loading by the total cross-sectional area.



Table 4: Experimental Results for Various Laminate Specimens

Laminate Specimen		A	B	C
Axial Strain $10^{-6}$		6099	3300	2900
Initial Matrix Cracking Stress ( ksi )		15.5	21.7	25.1
Initial Delamination Stresses ( ksi )	Gages	20.4	23.7	22.1
	Silver Ink	17.2	24.6	24.9
	Acoustic Emission	19.2	23.2	26.4
	Visual	18.1	23.5	25.9
Average Stress Calculated from Continuous traction Q-23 element (ksi)		15.883	25.817	29.935

### 6.3.2 Delamination of $[(\theta/-\theta)_2/90]_S$ Laminate

A sequence of tests had been conducted [51] to monitor the material damage in  $[(\theta/-\theta)_2/90]_S$  laminate specimens under incremental loading. The value of  $\theta$  were  $5^\circ$ ,  $15^\circ$ ,  $25^\circ$ ,  $35^\circ$ ,  $45^\circ$ . The material considered here was T300/5208 graphite epoxy with the following elastic constants:

$$E_{11}=22 \times 10^6 \text{ psi}$$

$$E_{22}=1.54 \times 10^6 \text{ psi}$$

$$G_{12}=G_{23}=0.81 \times 10^6 \text{ psi}$$

$$\nu_{12}=\nu_{23}=0.28$$

The thickness of the ten-ply laminate averaged around 0.06 inch with width equal to 1 inch. All these laminate specimens had also been analyzed [51] using the assumed stress hybrid finite element model [52] in conjunction with the quadratic tensor polynomial failure criterion [53] to predict the onset of transverse cracking and delamination. In the present study, continuous traction Q-23 element with a uniform 100 element-model shown in Figure (60) was used to analyze one quadrant of a typical  $x=\text{constant}$  plane in the laminate specimens. The calculated stresses along the traction-free edge were then substituted into the following failure criteria to determine the possible sites for initiation of transverse cracks and delamination.



### 6.3.2.1 Anisotropic Strength and Failure Criteria

With macroscopically homogeneous but orthotropic materials, development of a strength theory has been frequently accomplished by extending one of the isotropic analyses to account for anisotropy. Since strength theories are used primarily to predict onset, rather than mode of failure, the macroscopic viewpoint will predominate. It has been stated [53] that all the failure criteria are the degenerate cases of the tensor polynomial failure criterion

$$F_1\sigma_1 + F_{11}\sigma_1^2 + F_{111}\sigma_1^3 + F_{1111}\sigma_1^4 + \dots \geq 1 \quad (194)$$

or, explicitly

$$F_1\sigma_1 + F_2\sigma_2 + F_3\sigma_3 + 2F_{12}\sigma_1\sigma_2 + 2F_{13}\sigma_1\sigma_3 + 2F_{23}\sigma_2\sigma_3 + F_{11}\sigma_1^2 + F_{22}\sigma_2^2 + F_{33}\sigma_3^2 + F_{44}\sigma_4^2 + F_{55}\sigma_5^2 + F_{66}\sigma_6^2 + \dots \geq 1 \quad (195)$$

Here,  $\sigma_i$  are the stress tensor components in the material coordinates and  $F_1$ ,  $F_{11}$  and  $F_{111}$  etc. are the components of strength tensors, all components are referred to the material principle axes. In (195), terms associated with  $\sigma_4$ ,  $\sigma_5$ , and  $\sigma_6$  which are  $F_4$ ,  $F_5$ , and  $F_6$ , are taken to be zero since shear strengths are the same for positive and negative shear stress. It is also assumed that there is no interaction between shear stresses and normal stresses, thus  $F_{16}$ ,  $F_{26}$ ,  $F_{36}$  etc. become zero.

The strength and failure criteria considered in the present study include the maximum stress criterion, maximum strain criterion, Hoffman's criterion and the Tsai-Wu criterion. The reason for choosing these criteria was not only their popularity but also because they include unequal tensile and compressive failure strengths.

### Maximum stress criterion

Failure of material is assumed to occur if any one of the following conditions is satisfied [47]

$$\begin{aligned}\sigma_1 &> X_T; \sigma_2 > Y_T; \sigma_3 > Z_T \\ \sigma_4 &> R; \sigma_5 > S; \sigma_6 > T\end{aligned}\quad (196)$$

where  $\sigma_1, \sigma_2, \sigma_3$  are the normal stress components;  $\sigma_4, \sigma_5, \sigma_6$  are the shear stress components;  $X_T, Y_T, Z_T$  are the lamina normal strengths in the x, y, z directions respectively; and R, S, T are the shear strengths in the yz, xz and xy planes, respectively. When  $\sigma_1, \sigma_2, \sigma_3$  are compressive, they should be compared with  $X_C, Y_C$  and  $Z_C$ , the normal strengths in compression in the x, y and z directions. Reddy [54] stated that the maximum stress criterion could also be expressed in the form of tensor polynomial criterion as

$$\begin{aligned}(\sigma_1 - X_T)(\sigma_1 + X_C)(\sigma_2 - Y_T)(\sigma_2 + Y_C)(\sigma_3 - Z_T)(\sigma_3 + Z_C)(\sigma_4 - R)(\sigma_4 + R) \\ (\sigma_5 - S)(\sigma_5 + S)(\sigma_6 - T)(\sigma_6 + T) = 0\end{aligned}\quad (197)$$

Comparing (197) with (195) and ignoring those higher order terms, the strength tensors are [54]

$$\begin{aligned}F_1 &= \frac{1}{X_T} - \frac{1}{X_C}; F_2 = \frac{1}{Y_T} - \frac{1}{Y_C}; F_3 = \frac{1}{Z_T} - \frac{1}{Z_C} \\ F_{11} &= \frac{1}{X_T X_C}; F_{22} = \frac{1}{Y_T Y_C}; F_{33} = \frac{1}{Z_T Z_C} \\ F_{44} &= \frac{1}{R^2}; F_{55} = \frac{1}{S^2}; F_{66} = \frac{1}{T^2} \\ F_{12} &= -\frac{F_1 F_2}{2}; F_{13} = -\frac{F_1 F_3}{2}; F_{23} = -\frac{F_2 F_3}{2}\end{aligned}\quad (198)$$

and the remaining strength constants are zero.

### Maximum strain criterion

Failure is assumed to occur if one of the following conditions is satisfied [48]

$$\begin{aligned} \epsilon_1 > X_{\epsilon T}; \epsilon_2 > Y_{\epsilon T}; \epsilon_3 > Z_{\epsilon T} \\ \epsilon_4 > R_{\epsilon}; \epsilon_5 > S_{\epsilon}; \epsilon_6 > T_{\epsilon} \end{aligned} \quad (199)$$

where  $\epsilon_1, \epsilon_2, \epsilon_3$  are the normal tensile strains in the x, y, z directions respectively;  $\epsilon_4, \epsilon_5, \epsilon_6$  are the shear strains in the yz, xz and xy planes respectively;  $X_{\epsilon T}, Y_{\epsilon T}, Z_{\epsilon T}$  are the tensile strain strengths in the x, y, z directions and  $R_{\epsilon}, S_{\epsilon}, T_{\epsilon}$  are the shear strain strengths in the yz, xz and xy planes respectively. Again, expressing the criterion in the form of tensor polynomial (195),

$$\begin{aligned} (\epsilon_1 - X_{\epsilon T})(\epsilon_1 + X_{\epsilon T})(\epsilon_2 - Y_{\epsilon T})(\epsilon_2 + Y_{\epsilon T})(\epsilon_3 - Z_{\epsilon T})(\epsilon_3 + Z_{\epsilon T})(\epsilon_4 - R_{\epsilon})(\epsilon_4 + R_{\epsilon}) \\ (\epsilon_5 - S_{\epsilon})(\epsilon_5 + S_{\epsilon})(\epsilon_6 - T_{\epsilon})(\epsilon_6 + T_{\epsilon}) = 0 \end{aligned} \quad (200)$$

Expressing strains in terms of stresses via the compliance matrix for orthotropic materials, (200) can be expressed in the form of (195) and we have [54]

$$F_1 = F_1^A + \frac{S_{11}}{S_{22}} F_2^A + \frac{S_{13}}{S_{33}} F_3^A$$

$$F_2 = \frac{S_{12}}{S_{11}} F_1^A + F_2^A + \frac{S_{23}}{S_{33}} F_3^A$$

$$F_3 = \frac{S_{13}}{S_{11}} F_1^A + \frac{S_{23}}{S_{22}} F_2^A + F_3^A$$

$$F_{11} = \frac{1}{X_T X_C} + \left(\frac{S_{12}}{S_{22}}\right)^2 \frac{1}{Y_T Y_C} + \left(\frac{S_{13}}{S_{33}}\right)^2 \frac{1}{Z_T Z_C} - \frac{S_{13}}{S_{33}} F_1^A F_3^A - \frac{S_{12}}{S_{22}} F_1^A F_2^A - \frac{S_{12} S_{13}}{S_{22} S_{33}} F_2^A F_3^A$$

$$F_{22} = \frac{1}{Y_T Y_C} + \left(\frac{S_{12}}{S_{11}}\right)^2 \frac{1}{X_T X_C} + \left(\frac{S_{23}}{S_{33}}\right)^2 \frac{1}{Z_T Z_C} - \frac{S_{12}}{S_{11}} F_1^A F_2^A - \frac{S_{23}}{S_{33}} F_2^A F_3^A - \frac{S_{12} S_{23}}{S_{11} S_{33}} F_1^A F_3^A$$

$$F_{33} = \frac{1}{Z_T Z_C} + \left(\frac{S_{12}}{S_{11}}\right)^2 \frac{1}{X_T X_C} + \left(\frac{S_{23}}{S_{22}}\right)^2 \frac{1}{Y_T Y_C} - \frac{S_{13}}{S_{11}} F_1^A F_3^A - \frac{S_{23}}{S_{22}} F_2^A F_3^A - \frac{S_{13} S_{23}}{S_{11} S_{22}} F_1^A F_2^A$$

$$\begin{aligned}
F_{44} &= \frac{1}{R^2}; \quad F_{55} = \frac{1}{S^2}; \quad F_{66} = \frac{1}{T^2} \\
F_{12} &= \frac{S_{12}}{S_{11}} \frac{1}{X_T X_C} + \frac{S_{12}}{S_{22}} \frac{1}{Y_T Y_C} + \frac{S_{13} S_{23}}{S_{33}^2} \frac{1}{Z_T Z_C} \\
&\quad - \frac{1}{2} \left( \frac{S_{12}^2}{S_{11} S_{22}} + 1 \right) F_1^A F_2^A - \frac{1}{2} \left( \frac{S_{13} S_{12}}{S_{11} S_{33}} + \frac{S_{23}}{S_{33}} \right) F_1^A F_3^A - \frac{1}{2} \left( \frac{S_{12} S_{23}}{S_{22} S_{33}} + \frac{S_{13}}{S_{33}} \right) F_2^A F_3^A \\
F_{13} &= \frac{S_{13}}{S_{11}} \frac{1}{X_T X_C} + \frac{S_{13}}{S_{33}} \frac{1}{Z_T Z_C} + \frac{S_{12} S_{23}}{S_{22}^2} \frac{1}{Y_T Y_C} \\
&\quad - \frac{1}{2} \left( \frac{S_{13}^2}{S_{11} S_{33}} + 1 \right) F_1^A F_3^A - \frac{1}{2} \left( \frac{S_{12} S_{13}}{S_{11} S_{22}} + \frac{S_{23}}{S_{22}} \right) F_1^A F_2^A - \frac{1}{2} \left( \frac{S_{13} S_{23}}{S_{22} S_{33}} + \frac{S_{12}}{S_{22}} \right) F_2^A F_3^A \\
F_{23} &= \frac{S_{23}}{S_{22}} \frac{1}{Y_T Y_C} + \frac{S_{23}}{S_{33}} \frac{1}{Z_T Z_C} + \frac{S_{12} S_{13}}{S_{11}^2} \frac{1}{X_T X_C} \\
&\quad - \frac{1}{2} \left( \frac{S_{23}^2}{S_{22} S_{33}} + 1 \right) F_2^A F_3^A - \frac{1}{2} \left( \frac{S_{12} S_{23}}{S_{11} S_{22}} + \frac{S_{13}}{S_{11}} \right) F_1^A F_2^A - \frac{1}{2} \left( \frac{S_{23} S_{13}}{S_{11} S_{33}} + \frac{S_{12}}{S_{11}} \right) F_1^A F_3^A \quad (201)
\end{aligned}$$

Here,  $S_{ij}$  ( $i, j=1, 2, 3$ ) are the components of the compliance matrix, and  $F_1^A, F_2^A, F_3^A$  are the expressions given for  $F_1, F_2, F_3$  in the maximum stress criterion.

### Hoffman's criterion

Hoffman's criterion [49] is a special case of the tensor polynomial criterion for the following choice of the parameters  $F_i$  and  $F_{ij}$ :

$$\begin{aligned}
F_1 &= \frac{1}{X_T} - \frac{1}{X_C}; F_2 = \frac{1}{Y_T} - \frac{1}{Y_C}; F_3 = \frac{1}{Z_T} - \frac{1}{Z_C} \\
F_{11} &= \frac{1}{X_T X_C}; F_{22} = \frac{1}{Y_T Y_C}; F_{33} = \frac{1}{Z_T Z_C} \\
F_{44} &= \frac{1}{R^2}; F_{55} = \frac{1}{S^2}; F_{66} = \frac{1}{T^2} \\
F_{12} &= -\frac{1}{2} \left( \frac{1}{X_T X_C} + \frac{1}{Y_T Y_C} - \frac{1}{Z_T Z_C} \right) \\
F_{13} &= -\frac{1}{2} \left( \frac{1}{X_T X_C} + \frac{1}{Z_T Z_C} - \frac{1}{Y_T Y_C} \right) \\
F_{23} &= -\frac{1}{2} \left( \frac{1}{Z_T Z_C} + \frac{1}{Y_T Y_C} - \frac{1}{X_T X_C} \right)
\end{aligned} \tag{202}$$

#### Tsai-Wu criteria

The Tsai-Wu criterion is given by

$$F_i \sigma_i + F_{ij} \sigma_i \sigma_j \geq 1 \tag{203}$$

where

$$\begin{aligned}
F_1 &= \frac{1}{X_T} - \frac{1}{X_C}; F_2 = \frac{1}{Y_T} - \frac{1}{Y_C}; F_3 = \frac{1}{Z_T} - \frac{1}{Z_C} \\
F_{11} &= \frac{1}{X_T X_C}; F_{22} = \frac{1}{Y_T Y_C}; F_{33} = \frac{1}{Z_T Z_C} \\
F_{44} &= \frac{1}{R^2}; F_{55} = \frac{1}{S^2}; F_{66} = \frac{1}{T^2} \\
F_{12} &= -\frac{1}{2\sqrt{X_T X_C Y_T Y_C}} \\
F_{13} &= -\frac{1}{2\sqrt{X_T X_C Z_T Z_C}} \\
F_{23} &= -\frac{1}{2\sqrt{Y_T Y_C Z_T Z_C}}
\end{aligned} \tag{204}$$

Here, it is noted that the maximum stress and maximum strain criteria involved several separate equations, and there was no allowance for interaction of the stresses or failure modes. The Hoffman criterion and Tsai-Wu criterion, however, do provide for



interaction, and the interaction is fixed. That is, these failure expressions are not invariant with respect to coordinate system. As expressed in terms of quadratic tensor polynomial shown in (202) and (204) respectively, the only difference between these two criteria was on the determination of strength tensors  $F_{12}$ ,  $F_{13}$ ,  $F_{23}$ .

### 6.3.2.2 Onset of Material Damage

Each laminate specimen was tested individually in an electro-hydraulic, servo-controlled closed-loop testing machine [51]. The strain and nominal stress at the first sight of transverse cracking and onset of delamination are summarized in Table (5).

The measured strength (ksi) of T300/5208 graphite epoxy are given by [50]

Longitudinal tension :  $X_T = 210$   
 Longitudinal compression :  $X_C = 200$   
 Transverse tension :  $Y_T = 10$   
 Transverse compression :  $Y_C = 21$   
 Shear in 1-2 plane :  $S = 13$

It is further assumed that  $Z_T=Y_T$ ,  $Z_C=Y_C$ ,  $R=S$  and  $T=S/2$ . Substituting above information into (198), (201), (202) and (209) to calculate  $F_i$  and  $F_{ij}$ , the strength tensor for any complex stress state can then be obtained and compared with the actual stress tensor. Failure is assumed to occur when the magnitude of the actual stress tensor exceeds that of the strength tensor.

#### Transverse Cracking

Based on the stress field calculated from the continuous traction Q-23 element, the four failure criteria discussed in 6.3.2.1 were applied to every point along the traction-free edge for all five laminate specimens at the strain levels shown in Table (5), respectively, when the first sight of transverse cracking was detected. The results

Table 5: Test Results for  $[(\pm \theta)_2 90]_S$  Laminate

	$\theta$	5	15	25	35	45
Transverse cracking	Strain (%)	0.493	0.326	0.301	0.351	0.532
	Stress (ksi)	69.7	39.6	29.1	20.5	15.9
Delamination	Strain (%)	0.697	0.383	0.336	0.406	0.620
	Stress (ksi)	99.3	46.7	30.8	23.9	18.2

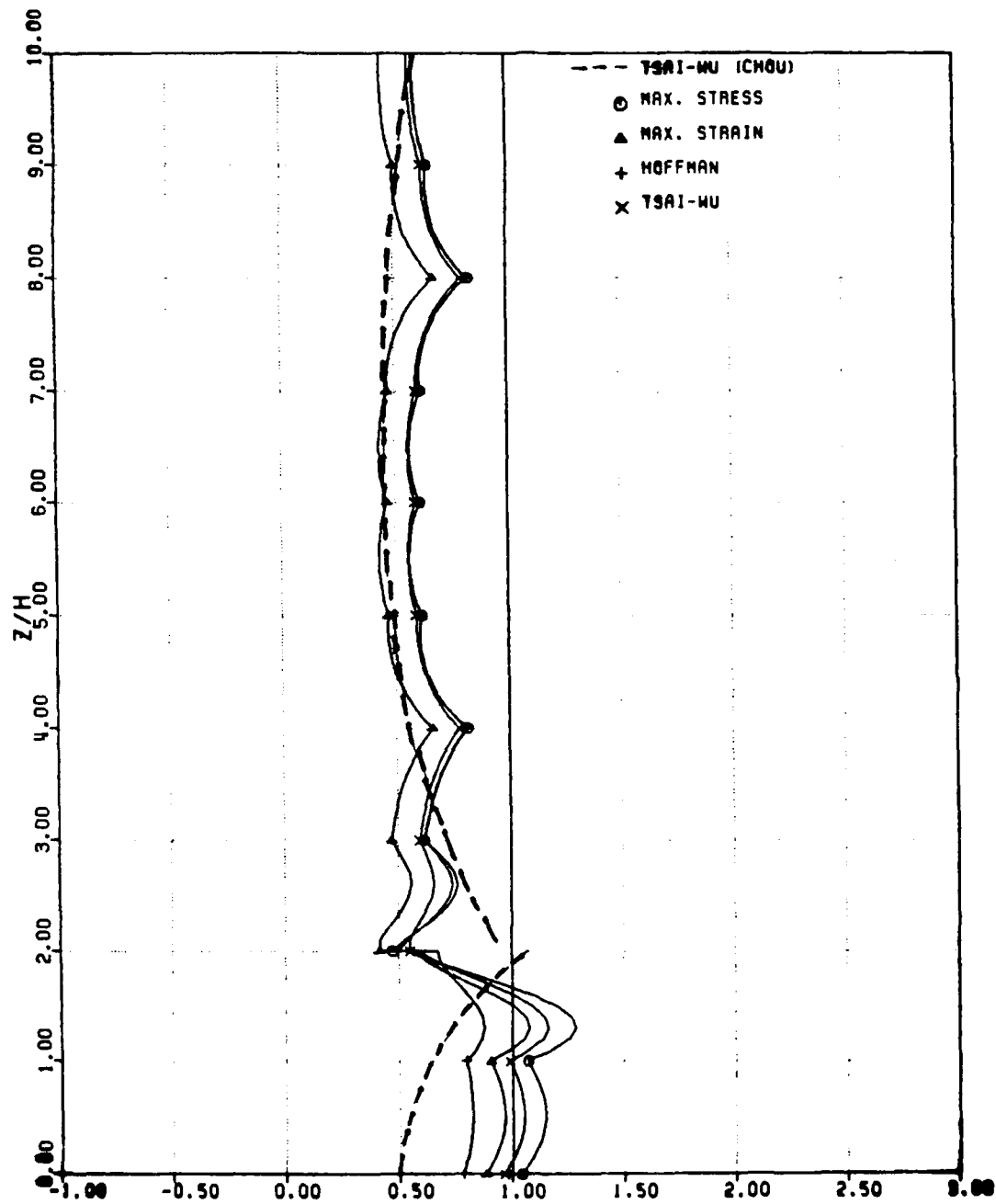


Figure 61: Ratio of Stress-to-Strength Tensor for  $[(\pm 5)_2/90]_5$  Laminate under Transverse Cracks Loading

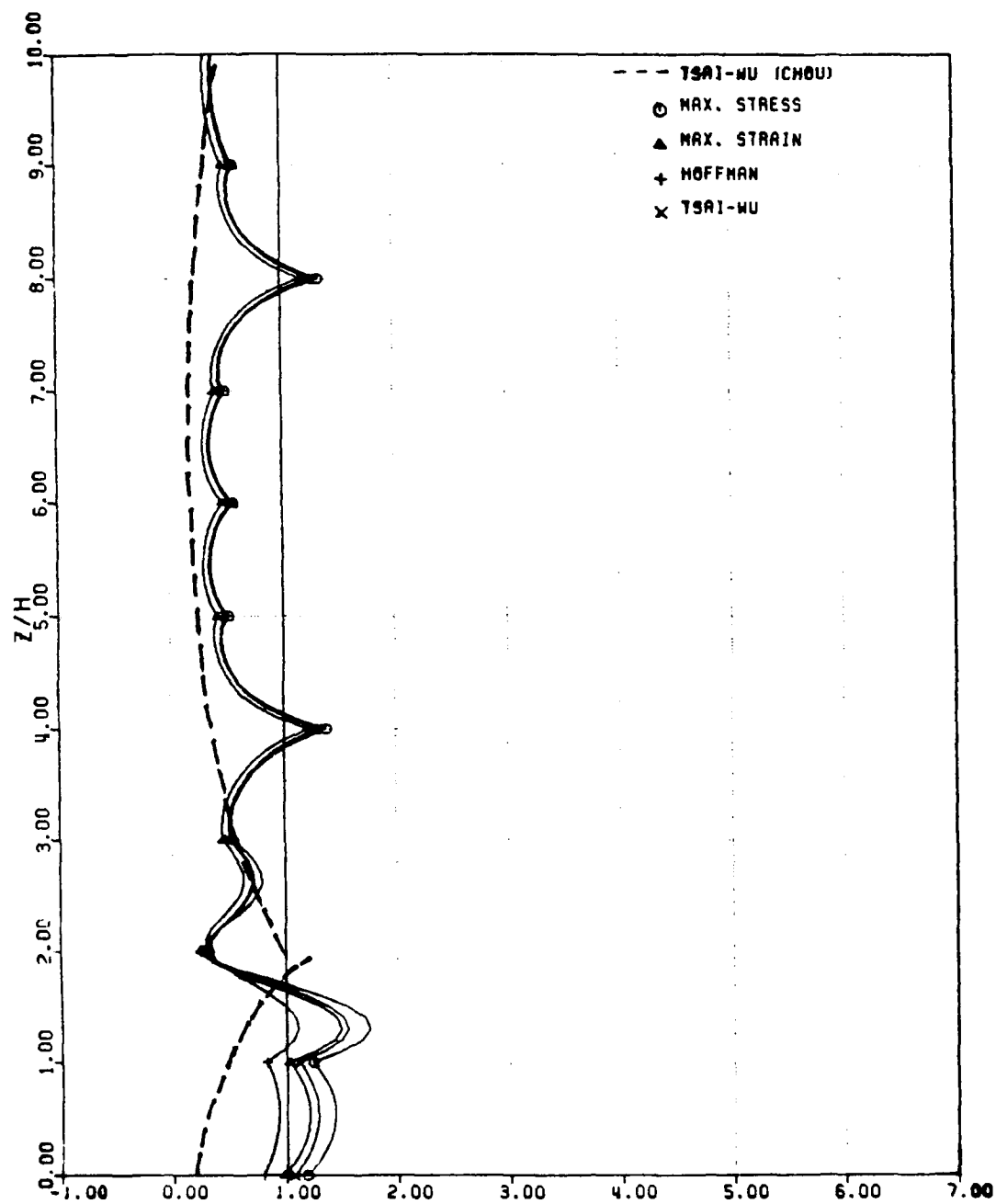


Figure 62: Ratio of Stress-to-Strength Tensor for  $[(\pm 15)_2/90]_S$  Laminate under Transverse Cracks Loading

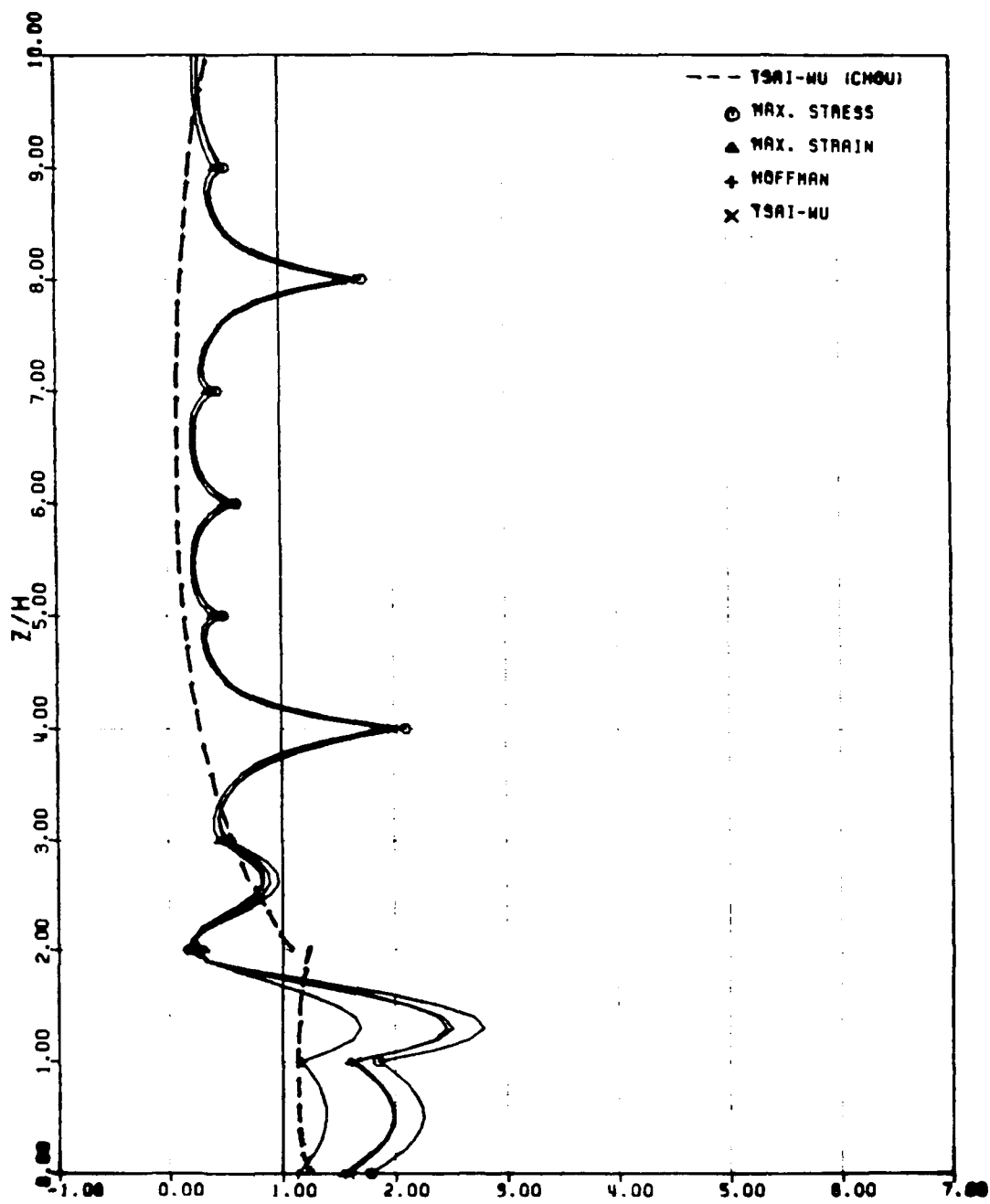


Figure 63: Ratio of Stress-to-Strength Tensor for  $[(\pm 25)_2/90]_s$  Laminate under Transverse Cracks Loading

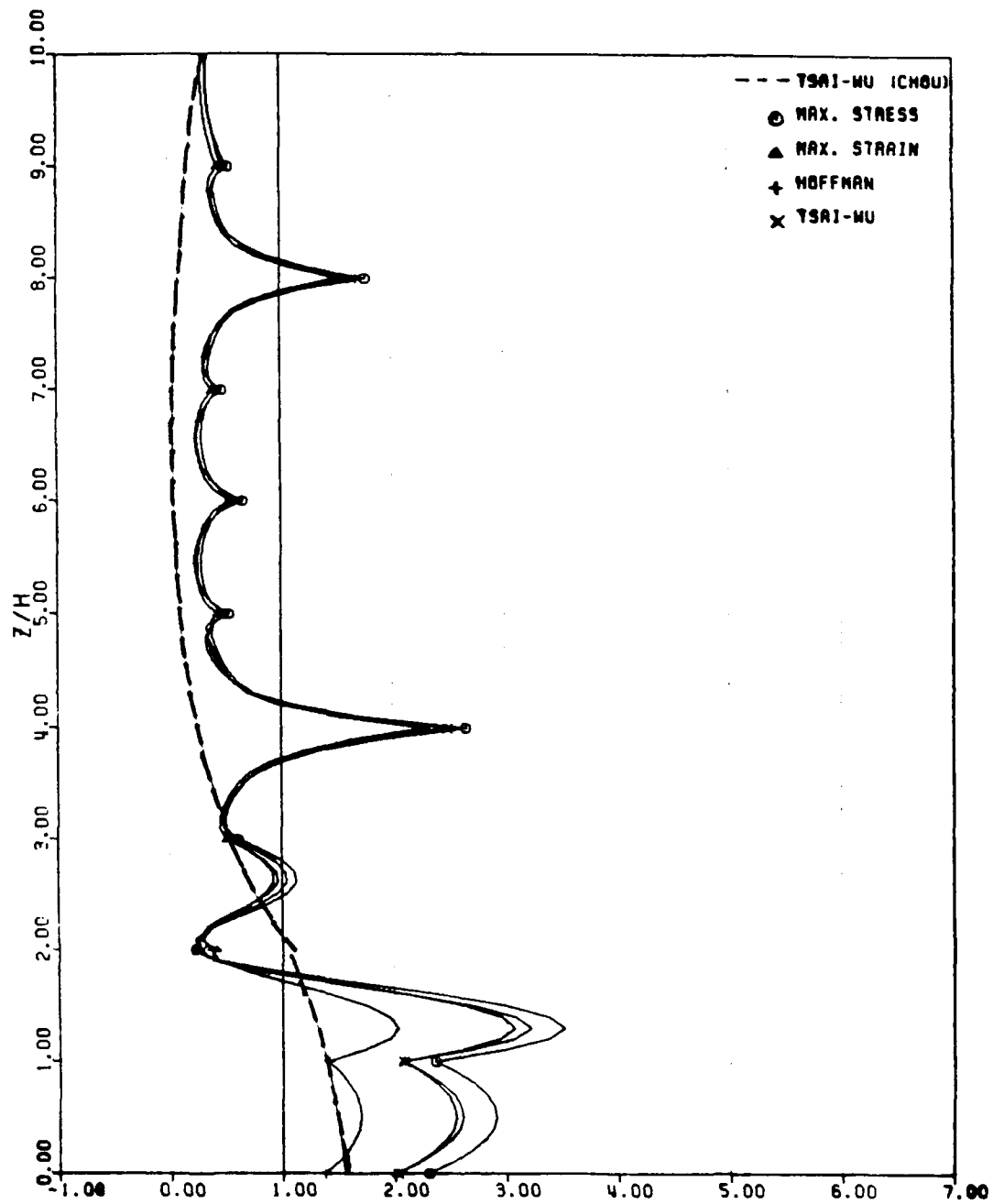


Figure 64: Ratio of Stress-to-Strength Tensor for  $[(\pm 35)_2/90]_s$  Laminate under Transverse Cracks Loading

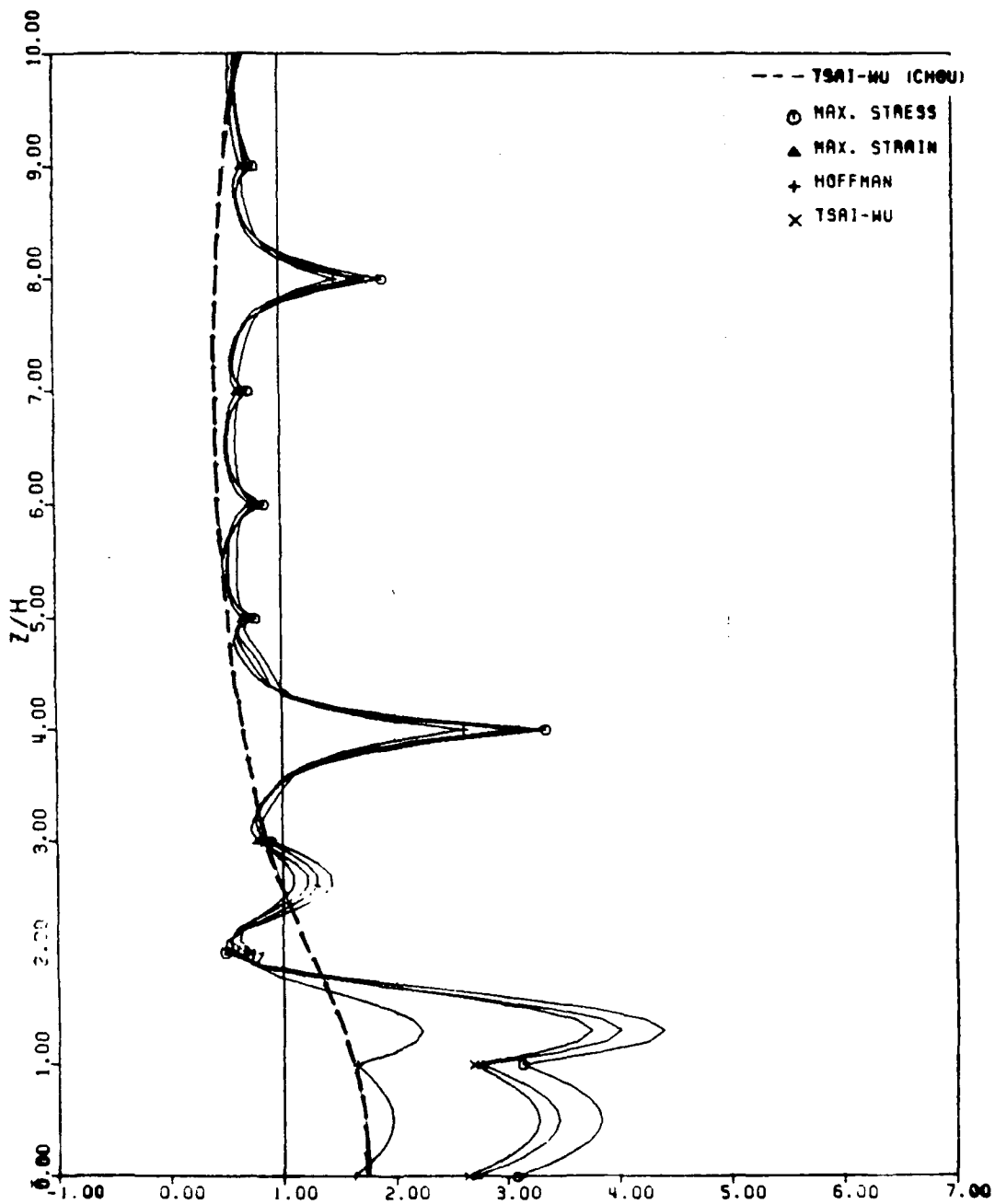


Figure 65: Ratio of Stress-to-Strength Tensor for  $[(\pm 45)_2/90]_5$  Laminate under Transverse Cracks Loading

are shown in Figures (61)-(65) along with Chou's [50] predictions. Those points that lie in the region where the actual stress-to-strength tensor ratio is greater than unity represent failure. Due to the discrepancy of the calculated stress field based on different numerical schemes, the prediction of the lamina failure surface from the same failure criterion (such as Tsai-Wu theory) varied significantly through the laminate free-edge. An obvious failure phenomenon resulting from the transverse cracking within the 90-degree layer was detected based on the continuous traction Q-23 element for all the laminate specimens. At the same time, initiation of edge delamination at the interfaces between  $\theta$  and  $-\theta$  become apparent as the value of  $\theta$  increases, which was not indicated according to Chou's analysis. However, the fact that transverse cracks always occurred prior to delamination in all cases is noticed, and this indeed matches experimental observation [51]. Here, it is noted that the magnitudes of stress-to-strength ratios shown in these figures sometimes departed significantly from unity particularly in the interior of transverse layer and near the interfaces. This could possibly be due to the inaccurate insitu transverse strength data and the inappropriate assumption of the interlaminar strengths.

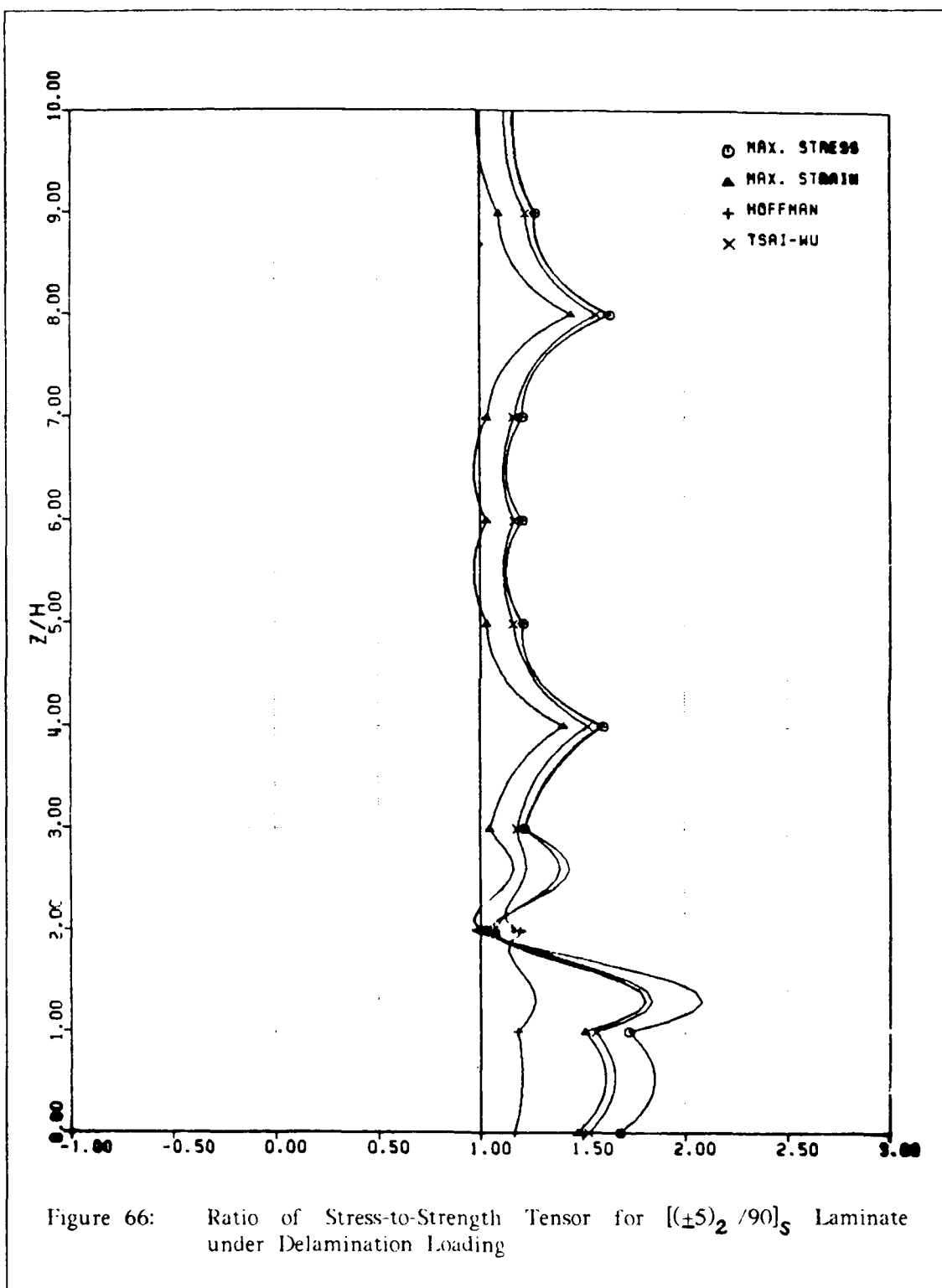
### Edge Delamination

Following the same procedure as in the prediction of transverse cracking, maximum stress, maximum strain, Hoffman and Tsai-Wu criteria were applied to every point along the free-edge of various laminate specimens at the respective strain level corresponding to the onset of delamination. For illustration, failure surfaces predicted from the continuous traction Q-23 element for  $\theta=5^\circ$  and  $\theta=25^\circ$  laminate specimens are shown in Figures (66) and (67). In the case of  $\theta=5^\circ$ , Figure (66) shows that following the transverse cracks formed in the 90-degree layer, delaminations were



developed at the interfaces between 5/-5 layers. Meanwhile, transverse cracks also extended to the angle-ply layers under incremental loading. The fact that all the failure surfaces exceeded unity shown in Figure (67) might result from the inaccurate material strength data. For the  $\theta=25^\circ$  laminate, however, transverse cracks were still confined to the 90-degree layer as delamination propagated at the 25/-25 interfaces. Based on these observations, we can infer that fiber orientations of the laminates with the same stacking sequence have played an important role on the determination of damage modes under incremental loading.

In general, the Hoffman theory had more conservative predictions than the others on the initiation of transverse cracking within the 90-degree layer, and the maximum strain criterion predicted conservatively on the subsequent edge delamination at the interfaces between angle-ply laminae. Since the materials were assumed linear elastic in the analysis, the applied strain loading corresponds to the onset of transverse cracks or delamination based on the continuous traction Q-23 model, and the failure criteria would be expected to be lower than the experimental observation. However, throughout the analysis, delamination was assumed to occur in a state of generalized plane strain without the influence of transverse cracking. In reality, this is not the case. More work needs to be done to study the interrelationships between delamination and other damage modes such as matrix cracking and fiber breakage, etc. Also, many practical composite systems actually exhibit extensive nonlinear mechanical response in shear and transverse to the reinforcement, resulting in nonlinear laminate mechanical behavior. Extension of the present continuous traction finite element procedure to include nonlinear material behavior, along with careful determination of material properties and strength data, may lead to better estimation of initiation of various damage modes under incremental loading.



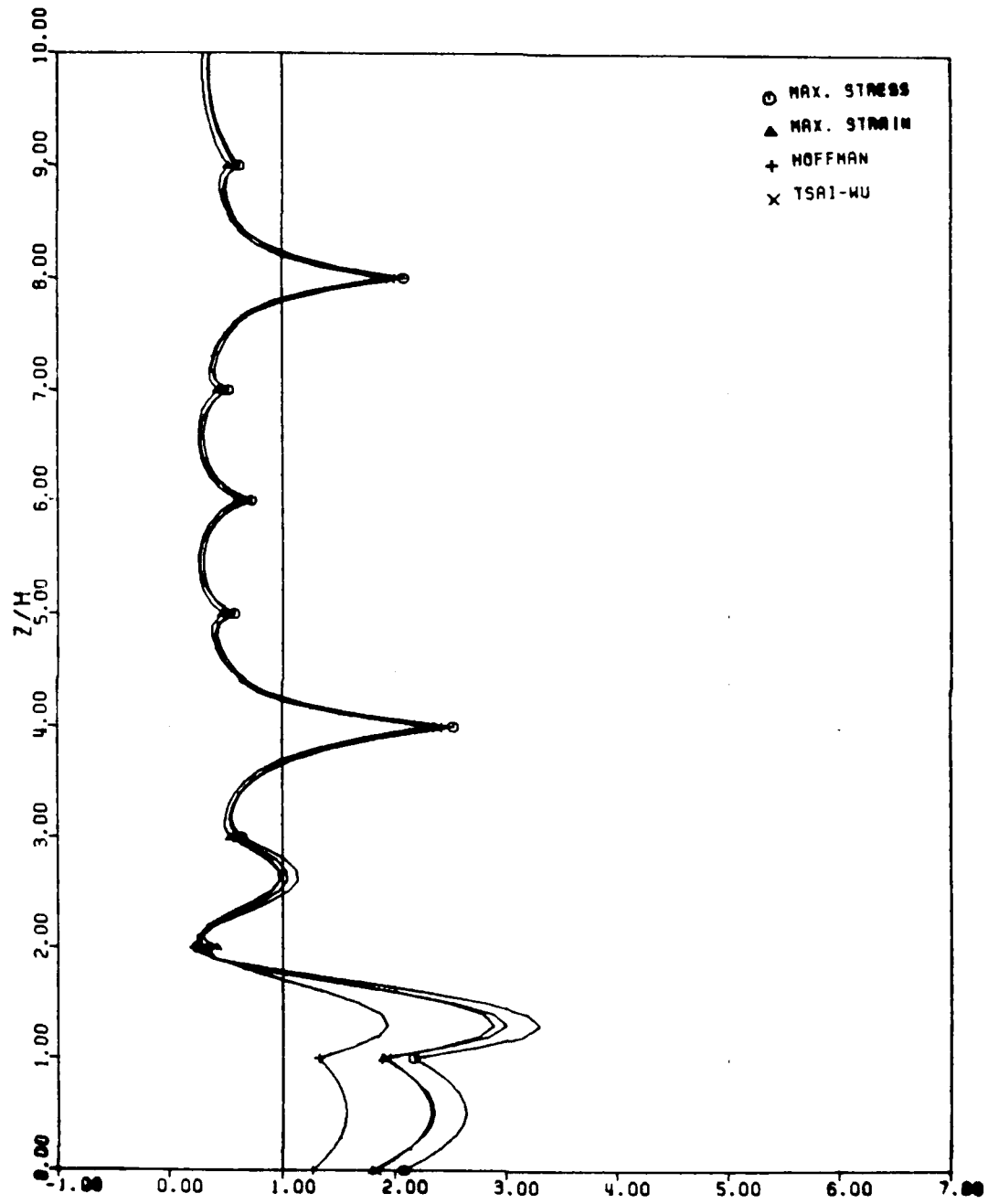


Figure 67: Ratio of Stress-to-Strength Tensor for  $[(\pm 25)_2/90]_5$  Laminate under Delamination Loading

## SECTION VII

### DISCUSSION

The problem of free-edge delamination in composite laminate coupons subjected to uniform inplane extension has been investigated. Before delamination can be predicted via a stress-based failure criterion, an accurate stress calculation within the laminate, particularly near the interfaces and traction-free boundary, is necessary. However, the stress field under this situation is highly complex in nature. Besides, the anisotropy and heterogeneity of the material system, and presence of the traction-free boundary makes the analysis difficult. Literature on this subject was abundant but an effective as well as reliable solution had not been found.

The present research effort has resulted in developement of a continuous strain finite element model in plane elasticity based on the compatible cubic interpolation function proposed by Clough and Felippa [40], in which the normal slope continuity was ensured across the interelement boundary. Extending the continuous strain model to the analysis of a pseudo two dimensional free edge delamination coupon under uniform extension, a continuous strain field along both inplane and transverse directions was obtained. However, due to material anisotropy, the stresses along the interfaces between differently oriented layers were discontinuous. Also, traction-free boundary was not satisfied. The continuous strain model was used as the basis for the developement of a continuous traction finite element procedure. Knowing the fact that the displacement field within each element is described by nodal displacement

components and their gradients, to ensure traction continuity, a transformation procedure was developed to map the gradients normal to element boundary to a mixed set of degrees of freedom through appropriate displacement-stress relationships. For global assembly, the nodal degrees of freedom of this element include interlaminar stress components at the corner nodes, as well as traction components at the mid-side nodes of each element. This ensures continuity of displacement and traction along interelement boundaries as well as across laminate interfaces providing a small deformation situation is considered. At the same time, equilibrium condition is maintained between two adjacent elements (layers). A significant aspect of this displacement based formulation is that it allows traction free boundary conditions to be specified in a point wise sense.

In the four-ply laminate analysis, numerical results calculated from the continuous traction Q-23 element generally agreed well with Pagano's analytical solutions [8] although these two schemes were based upon quite different theories. For illustration, Table (6) outlines the basic characteristics associated with each of these approaches. The approximate solutions for stress components  $\tau_{xz}$  and  $\sigma_z$ , which play an important role in delamination of composite laminates, were calculated using both approaches and found to have similar distribution. The study also revealed that the pattern of mesh refinement had significant effect on the estimates of interlaminar stress field in the vicinity of traction-free edge or near the interface between two differently oriented layers. Here, it is essential to realize that the continuous traction finite element procedure is only applicable to the Q-23 element and cannot be simplified to Q-15 and Q-19 elements. This is because the continuity of traction across laminate interface cannot be simplified in the absence of mid-side nodes at the interface between two

Table 6: Comparison of Pagano's Theory and Continuous Traction Q-23 Element

Method	Pagano	Continuous traction Q-23
Variational principle	Reissner's variational principle	Minimum potential energy principle
Type of formulation	Mixed	Displacement
Basis of field equations	Plate theory	Elastic solid
Assumed inside each layer (element)	Kinematic relations & Stress equilibrium	Kinematic relations & constitutive law
Along interlaminar boundary	Continuous traction & weighted displacement	Continuous displacement & traction
Assumed stress w.r.t. Z-axis	Inplane---linear Transverse---cubic	Quadratic
Unknowns in final equations	Weighted displacements & interlaminar stresses	Displacements & interlaminar stresses
Solution technique	Direct solving differential equations	Finite element method

adjacent layers. In comparison with the continuous strain Q-23 element, the introduction of the transformation process in the Q-23 element makes the continuous traction procedure more expensive. However, the continuous traction Q-23 element significantly improves the reliability of the stress field solution because of the interlaminar stress continuity at the interface between differently oriented fiber layers, along with satisfaction of traction-free boundary condition along specimen edges.

Application to the multiply laminate specimens with stacking sequence of  $[(0/-0)_2/90]_2$  further illustrated the potential of the continuous traction finite element procedure in the analysis of edge delamination problem. Satisfactory agreement was generally observed for interlaminar stress distributions as well as laminate displacement field between continuous traction Q-23 element and constant strain element solutions [44] except that, in the vicinity of the free-edge, the constant strain element was deficient due to nonsatisfaction of traction-free boundary condition ( $\tau_{yz}=0$ ) and the assumption of ( $\tau_{xz}=0$ ) imbedded in the axisymmetric analysis. The results from the continuous traction Q-23 element would be expected to be superior to the constant strain element (conventional assumed displacement elements) for prediction of stress field in the free-edge delamination specimens. Of course the simple axisymmetric model is economical to use.

Regarding prediction of damage initiation in laminate composite coupons,  $[(0/-0)_2/90]_2$ , under incremental loading, the continuous traction finite element procedure along with some popular anisotropic failure criteria was found to be successful in modelling some failure phenomena observed in the experiments. Basically, the laminate specimens under analysis were assumed to be made of linear elastic brittle materials. Thus, initiation of delamination directly led to catastrophic laminate failure regardless

of the damage accumulation process. Numerical experiment discussed in the last section revealed that the Hoffman criterion had a more conservative prediction on the initiation of transverse cracking within the 90-degree layer, and the maximum strain criterion on the subsequent edge delamination between the angle-ply laminae interfaces.

In summary, we conclude that the proposed continuous traction finite element scheme not only overcomes the drawback of deficient stress calculation arising in the conventional assumed displacement approach, but also provides a reliable as well as effective numerical solution procedure with a wider range of applicability to the analysis of the free-edge delamination problem. Though based on a completely different variational formulation, this model has shared the characteristic of continuous displacement as well as traction fields across laminate interface, with Pagano's approximate theory derived from a mixed formulation. Though developed for evaluation of stresses in composite laminates, the continuous traction procedure is also applicable to analysis of layered media involving material interfaces where a two-dimensional or pseudo two-dimensional representation is applicable. This would include stresses in layered airfield and highway pavements, pressures on tunnel lining, etc.



## REFERENCES

1. Pagano, N. J. and Pipes, R. B., **Some Observations on the Interlaminar Strength of Composite Laminates**, *Int. J. Mech. Sci.*, Vol. 15, 679, 1973.
2. Puppo, A. H. and Evensen, H. A., **Interlaminar Shear in Laminated Composites Under Generalized Plane Stress**, *J. Comp. Matls.*, Vol. 4, 204, 1970.
3. Pipes, R. B. and Pagano, N. J., **Interlaminar Stress in Composite Laminates - An Approximate Elasticity Solution**, *J. App. Mech.*, Vol. 41, 668, 1974.
4. Pagano, N. J., **On the Calculation of Interlaminar Normal Stress in Composite Laminate**, *J. Comp. Matls.*, Vol. 8, 65, 1974.
5. Wang, J. T. S. and Dickson, J. N., **Interlaminar Stresses in Symmetric Composite Laminates**, *J. Comp. Matls.*, Vol. 12, 390, 1978.
6. Hsu, P. W. and Herakovich, C. T., **Edge Effects in Angle-Ply Composite Laminates**, *J. Comp. Matls.*, Vol. 11, 422, 1977.
7. Tang, S. and Levy, A., **A Boundary Layer Theory - Part II: Extension of Laminated Finite Strip**, *J. Comp. Matls.*, Vol. 9, 42, 1975.
8. Pagano, N. J., **Stress Fields in Composite Laminates**, *Int. J. Solids Structures*, Vol. 14, 385, 1978.
9. Pagano, N. J., **Free-edge Stress Fields in Composite Laminates**, *Int. J. Solids Structures*, Vol. 14, 401, 1978.
10. Pagano, N. J. and Soni, S. R., **Global-Local Laminate Variational Model**, *Int. J. Solids Structures*, Vol. 19, No. 3, 207, 1983.
11. Pipes, R. B. and Pagano, N. J., **Interlaminar Stresses in Composite Laminates Under Uniform Axial Extension**, *J. Comp. Matls.*, Vol. 4, 538, 1970.
12. Altus, E., Rotem, A., and Shmueli, M., **Free-Edge Effect in Angle-Ply Laminates - A New Three-Dimensional Finite Differences Solution**, *J. Comp. Matls.*, Vol. 14, 21, 1980.
13. Wang, A. S. D. and Crossman, F. W., **Some New Results on Edge Effect in Symmetric Composite Laminates**, *J. Comp. Matls.*, Vol. 11, 92, 1977.

14. Wang, A. S. D. and Crossman, F. W., **Calculation of Edge Stresses in Multi-Layer Laminates by Substructuring**, J. Comp. Mats., Vol. 12, 76, 1978.
15. Raju, I. S. and Crews, J. H., **Interlaminar Stress Singularities at a Straight Free-edge in Composite Laminates**, Computers & Structures, Vol. 14, No. 1-2, 21, 1981.
16. Whitcomb, J. C., Raju, I. S. and Goree, J. G., **Reliability of the Finite Element Method for Calculating Free-edge Stresses in Composite Laminates**, Computers & Structures, Vol. 15, No. 1, 23, 1982.
17. Rybicki, E. F., **Approximate Three-Dimensional Solutions for Symmetric Laminate Under Inplane Loading**, J. Comp. Mats., Vol. 5, 354, 1971.
18. Spilker, R. L., **A Traction-Free-Edge Hybrid Stress Element for the Analysis of Edge Effects in Cross-Ply Laminates**, Computers & Structures, Vol. 12, 167, 1980.
19. Wang, S. S. and Yuan, F. G., **A Singular Hybrid Finite Element Analysis of Boundary-Layer Stress in Composite Laminates**, Int. J. Solids Structures, Vol. 19, No. 9, 825, 1983.
20. Rybicki, E. F. and Schmueser, D. W. and Fox, J., **An Energy Release Rate Approach for Stable Crack Growth in the Free-Edge Delamination Problem**, J. Comp. Mats., Vol. 11, 470, 1977.
21. Wang, A. S. D. and Crossman, F. W., **Initiation and Growth of Transverse Cracks and Edge Delamination in Composite Laminates - Part I: An Energy Method; Part II: Experimental Correlation**, J. Composite Materials Supplement, Vol. 14, 71, 1980.
22. O'Brien, T. K., **Characterization of Delamination Onset and Growth in a Composite Laminate**, Damage in Composite Materials, ASTM STP 775, K. L. Reifsnider Ed. 140, 1982.
23. Wilkins, D. J., Eisenmann, J. R., Camin, R. A., Margolis, W. S. and Benson, R. A., **Characterizing Delamination Growth in Graphite-Epoxy**, Damage in Composite Materials, ASTM STP 775, K. L. Reifsnider Ed. 168, 1982.
24. O'Brien, T. K., **Mixed-Mode Strain Energy Release Rate Effects on Edge Delamination of Composites**, Effect of Defects in Composite Materials, ASTM STP 836, 125, 1984.
25. Law, G. E., **A Mixed-Mode Fracture Analysis of (+25/90) Graphite/Epoxy Composite Laminates**, Effect of Defects in Composite Materials, ASTM STP 836, 143, 1984.

26. Whitney, J. M. and Browning, C. L., **Materials Characterization for Matrix-Dominated Failure Modes**, Effect of Defects in Composite Materials, ASTM STP 836, 104, 1984.
27. Pagano, N. J. and Rybicki, E. F., **On the Significance of Effective Modulus Solutions for Fibrous Composites**, J. Comp. Matls., Vol. 8, 214, 1974.
28. Whitney, J. M. and Sun, C. T., **A Higher Order Theory for Extensional Motion of Laminated Composites**, J. Sound and Vibration, Vol. 30, 85, 1973.
29. Pian, T. H. H. and Tong, P., **Basis of Finite Element Methods for Solid Continua**, Int. J. Num. Mech. Engng., Vol. 1, 3, 1969.
30. Wang, S. S. and Chou, L., **Boundary-Layer Effects in Composite - Part I. Free-edge Stress Singularities; Part II. Free-Edge Stress Solutions and Basic Characteristics**, J. App. Mech., Vol. 49, 541, 1982.
31. Sandhu, R. S., **Variational Principles for Finite Element Approximations**, Finite Elements in Water Resources Engineering, Ed. G. F. Pinder and C. A. Brebbia, Pentech Press, 1976.
32. Magri, F., **Variational Formulation for Every Linear Equation**, Int. J. Engng. Sci., Vol. 12, 537, 1974.
33. Sandhu, R. S. and Salaam, U., **Variational Formulation of Linear Problems with Non-homogeneous Boundary Conditions and Internal Discontinuities**, Comp. Methods App. Mechs. and Engng., Vol. 7, 75, 1976.
34. Sandhu, R. S., **A Note on Finite Element Approximation**, U.S.-Japan Seminar on Interdisciplinary Finite Element Analysis, Cornell University, Ithaca, New York, 1978.
35. Prager, W., **Variational Principles of Linear Elastostatics for Discontinuous Displacements, Strains and Stresses**, in Recent Progress in Applied Mechanics, The Folke Odequist Volume, 463, 1967.
36. Rai, I. S. and Sandhu, R. S., **Finite Element Analysis of Anisotropic Plate Using Q-19 Element**, Part I. Theoretical Development, Technical Report AFDDL TR-74 120, 1974.
37. Salaam, U., **Finite Element with Relaxed Continuity - An Investigation of the Variational Basis and Numerical Performance**, Ph.D. Dissertation, The Ohio State University, 1974.
38. Wilson, E. L., **The Static Condensation Algorithm**, Int. J. Num. Mech. Engng., Vol. 8, 199, 1974.
39. Strang, G. and Fix, G., **An Analysis of the Finite Element Method**, Prentice Hall, Englewood Cliffs, N.J. 1973.

40. Tocher, J. L. and Hartz, W., **A Higher Order Plane Stress Element**, J. Engng. Mech. Div., Proc., Amer. Soc. Civil Engrs., No. 5402, 149, 1967.
41. Clough, R. W. and Felippa, C. A., **A Refined Quadrilateral Element for Analysis of Plate Bending**, Proc., Second Conference on Matrix Methods in Structural Mechanics, AFFDL-TR-68-150, Wright Patterson Air Force Base, Ohio, 1968.
42. Felippa, C. A., **Refined Finite Element Analysis of Linear and Nonlinear Two-Dimensional Structures**, Ph.D. Dissertation, University of California, Berkeley, 1966.
43. Vinson, J. R. and Sierakowski, R. L., **The Behavior of Structures Composed of Composite Materials**, Martinus Nijhoff Publishers, Boston, 1986.
44. Spencer, A. J. M., **Continuum Mechanics**, Longman Inc., New York, 1980.
45. Clough, R. W., **The Finite Element in Plane Stress Analysis**, Proc., 2nd ASCE Conf. on Electronic Computation, Pittsburgh, 1960.
46. Sandhu, R. S. and Sendekyj, G. P., **On Delamination of  $[(+0_m/90_{\gamma/2})_5]$  Laminates Subjected to Tensile Loading**, AFWAL-TR-87-3058, Wright Patterson Air Force Base, Ohio, 1987.
47. Jenkins, C. F., **Report on Materials of Construction Used in Aircraft and Aircraft Engines**, Great Britain Aeronautical Research Committee, 1920
48. Waddoups, M. E., **Advanced Composite Material Mechanics for the Design and Stress Analysis**, General Dynamics, Fort Worth Division Report, 1967.
49. Hoffman, O., **The Brittle Strength of Orthotropic Materials**, J. Comp. Matls., Vol. 1, 200, 1967.
50. Tsai, S. W. and Wu, E. M., **A General Theory of Strength for Anisotropic Materials**, J. Comp. Matls., Vol. 5, 58 1971.
51. Chou, S. C., **Delamination of T300/5208 Graphite/epoxy Laminate**, Fracture of Composite Materials, G. C. Sih and V. P. Tamuzs Ed., 247, 1982.
52. Spilker, R. L. and Chou, S. C., **Edge Effects in Symmetric Composite Laminates: Importance of Satisfying the Traction-Free Edge Condition**, J. Comp. Matls., Vol. 14, 2, 1980.
53. Wu, E. M., **Phenomenological Anisotropic Failure Criterion**, **Composite Materials**, Vol. 2, G. P. Sendekyj, ed., 1974.
54. Reddy, J. N. and Pandey, A. K., **A First-Ply Failure Analysis of Composite Laminates**, Computers & Structures, Vol. 25, No. 3, 371, 1987.

## Appendix A

### DERIVATION OF COMPATIBLE CUBIC INTERPOLATION FUNCTIONS

This appendix contains a summary of Telippa's [41,42] approach in deriving the cubic compatible interpolations for in-plane displacement  $u$  in a more detailed format.

In order to derive the cubic interpolation functions for the complete triangular element, three different coordinate systems, i.e. triangular coordinate, local and global Cartesian coordinates should be defined as illustrated in Figure (A.1). The geometry of an arbitrary triangular element can be expressed in a Cartesian coordinate system by its nodal coordinates or its projected dimensions as shown in Figure (A.2), or alternately by its intrinsic dimensions as defined in Figure (A.3).

Let  $j$  and  $k$  denote the first and second cyclic permutations of  $i=1,2,3$  (i.e.  $j=2,3,1$  and  $k=3,1,2$ ), the projected dimensions may be written as

$$a_i = x_j - x_k; \quad b_i = y_j - y_k \quad (A.1)$$

Also, the intrinsic dimensions may be defined in terms of the projected dimensions. Referring to Figure (A.2), define

$$\lambda_i = \frac{d_i}{l_i} \quad (A.2)$$

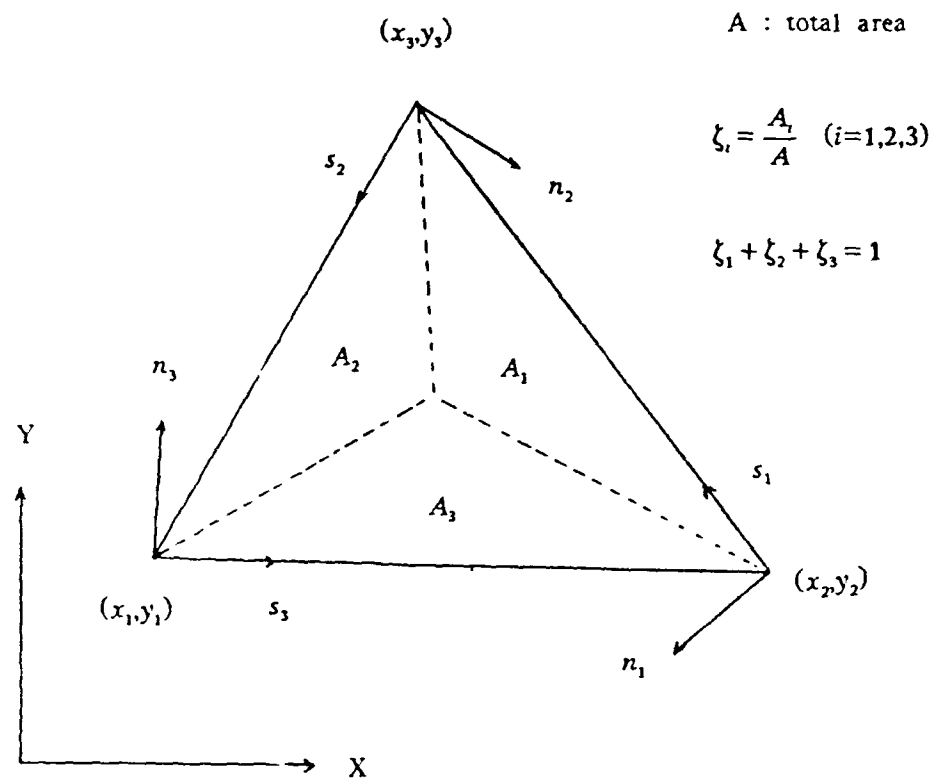


Figure A.1: Triangular, Local and Global Cartesian Coordinates

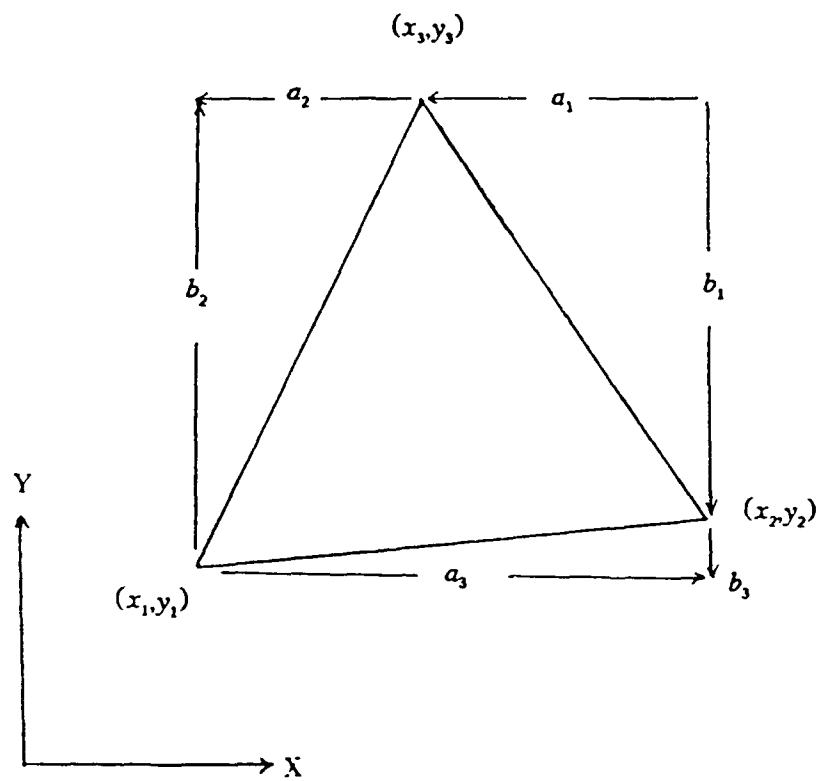


Figure A.2: X-Y Projected Dimensions

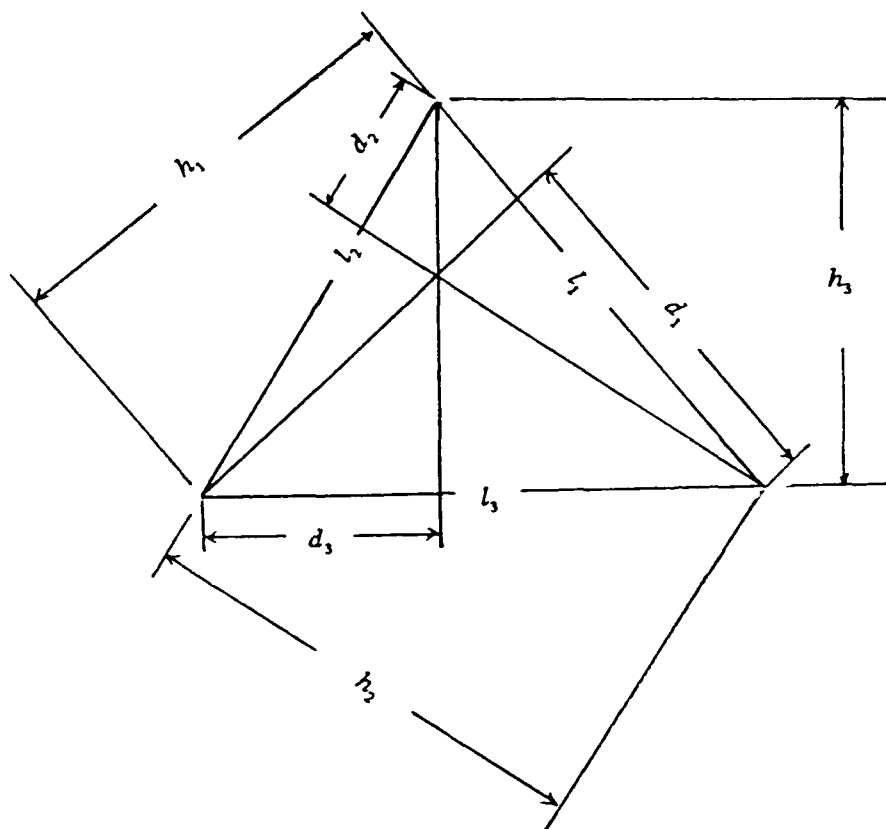


Figure A.3: Intrinsic Dimensions



$$\mu_i = 1 - \lambda_i \quad (\text{A.3})$$

$$d_i = -\frac{(a_i a_k + b_i b_k)}{l_i} \quad (\text{A.4})$$

The triangular coordinates  $\xi_i, \xi_j, \xi_k$  of any point "P" in the triangle may be defined either as the ratios of the areas  $A_i$  of the subtriangles subtended by the point to the total area  $A$  of the triangle, or as the ratios of the normal distances  $n_i$  to the height  $h$ , i.e.

$$\xi_i = \frac{A_i}{A} = \frac{n_i}{h} \quad (\text{A.5})$$

as shown in Figure (A.1). It is noted that the triangular coordinates are related by the constraining condition  $\xi_1 + \xi_2 + \xi_3 = 1$

With reference to Figure (2), the displacement interpolation functions for each subelement (i) express the relationship between the displacement  $u^{(i)}$  within the element and the ten displacement components of its nodal points  $r^{(i)}$  as follows

$$u^{(i)} = \{\phi^{(i)}\}^T \{r^{(i)}\} \quad (\text{A.6})$$

For example, the nodal displacement vector for subelement 1 is

$$\{r^{(1)}\}^T = \{u_2, u_{x_2}, u_{y_2}, u_3, u_{x_3}, u_{y_3}, u_6, u_{x_6}, u_{y_6}, u_{1,8}\} \quad (\text{A.7})$$

The corresponding ten cubic interpolation functions expressed in triangular coordinates are

$$\phi^{(1)} = \begin{bmatrix} \zeta_1^2(3-2\zeta_1)+6\mu_1^{(1)}\zeta_1\zeta_2\zeta_3 \\ \zeta_1^2(a_3^{(1)}\zeta_2-a_2^{(1)}\zeta_3)+(a_3^{(1)}\mu_3^{(1)}-a_1^{(1)})\zeta_1\zeta_2\zeta_3 \\ \zeta_1^2(b_2^{(1)}\zeta_3-b_3^{(1)}\zeta_2)+(b_1^{(1)}-b_3^{(1)}\mu_3^{(1)})\zeta_1\zeta_2\zeta_3 \\ \zeta_2^2(3-2\zeta_2)+6\lambda_3^{(1)}\zeta_1\zeta_2\zeta_3 \\ \zeta_2^2(a_1^{(1)}\zeta_3-a_3^{(1)}\zeta_1)+(a_2^{(1)}-a_3^{(1)}\lambda_3^{(1)})\zeta_1\zeta_2\zeta_3 \\ \zeta_2^2(b_3^{(1)}\zeta_1-b_1^{(1)}\zeta_3)+(b_4^{(1)}\lambda_3^{(1)}-b_2^{(1)})\zeta_1\zeta_2\zeta_3 \\ \zeta_3^2(3-2\zeta_3) \\ \zeta_3^2(a_2^{(1)}\zeta_1-a_1^{(1)}\zeta_2) \\ \zeta_3^2(b_1^{(1)}\zeta_2-b_2^{(1)}\zeta_1) \\ -4h_3^{(1)}\zeta_1\zeta_2\zeta_3 \end{bmatrix} \quad (A.8)$$

where the subscripts correspond to the renumbered nodes of the subelement, and  $\zeta_i$  are the local triangular coordinates of points in subtriangle 1. With this convention, the interpolation functions for subelements 2 and 3 are the same as (A.8) appropriately permuting the subscripts and superscripts. It should be noted, however, that the nodal displacements in (A.6) are identified by node numbers defined for the complete element assembly.

If the vector  $\{\bar{r}\}$  of all nodal displacements of the complete element assembly is written as the ordered set

$$\{\bar{r}\}^T = \{u_1, u_{s_1}, u_{v_1}, u_2, u_{s_2}, u_{v_2}, u_3, u_{s_3}, u_{v_3}, u_4, u_{s_4}, u_{v_4}, u_5, u_{s_5}, u_{v_5}, u_6, u_{s_6}, u_{v_6}\} \quad (A.9)$$

the displacement in subelement 1 can be expressed as

$$u^{(1)} = \{\phi^{(1)}\}^T \{\bar{r}\} = [\phi_c^{(1)} \phi_s^{(1)}] \begin{Bmatrix} r \\ r_o \end{Bmatrix} \quad (A.10)$$

where  $\{\bar{\phi}^{(1)}\}$  is similar to (A.8), but expanded with 5 zeros to account for the nodal displacements not associated with subelement 1, and with appropriate arrangement of terms. The vectors  $\{\phi_e^{(1)}\}$  and  $\{\phi_v^{(1)}\}$  represent the interpolation functions for the external and internal nodal displacements respectively.

Expressing the displacements in the other subelements similarly, the complete system of displacements can be written as

$$\begin{Bmatrix} u^{(1)} \\ u^{(2)} \\ u^{(3)} \end{Bmatrix} = \begin{bmatrix} \phi_e^{(1)T} & \phi_v^{(1)T} \\ \phi_e^{(2)T} & \phi_v^{(2)T} \\ \phi_e^{(3)T} & \phi_v^{(3)T} \end{bmatrix} \begin{Bmatrix} r \\ - \\ r_v \end{Bmatrix} \quad (\text{A.11})$$

(A.11) is an expression of the cubic displacement patterns in the three subelements. The displacement of two adjacent subtriangles are identical along their common boundary. The normal slope at any of these nodes (say 7 of subelement 1) is given by

$$\left( \frac{\partial u^{(1)}}{\partial n} \right)_7 = \Theta_7^{(1)} = [b_{7e}^{(1)}; b_{7v}^{(1)}] \begin{Bmatrix} r \\ - \\ r_v \end{Bmatrix} \quad (\text{A.12})$$

where  $b_{7e}^{(1)}$ ,  $b_{7v}^{(1)}$  respectively are values of  $\{\frac{\partial \phi_e^{(1)}}{\partial n}\}$ ,  $\{\frac{\partial \phi_v^{(1)}}{\partial n}\}$  at node 7 for subelement 1, and  $n$  denotes the axis normal to the element boundary. To maintain internal slope continuity, it is necessary that  $\Theta_7^{(1)} = -\Theta_7^{(3)}$ , where the negative sign results from the convention that the positive normal is directed outwards. For the three points 7, 8, 9,

$$\begin{pmatrix} \theta_7^{(1)} + \theta_7^{(3)} \\ \theta_8^{(2)} + \theta_8^{(1)} \\ \theta_9^{(3)} + \theta_9^{(2)} \end{pmatrix} = \begin{pmatrix} b_{7e}^{(1)} + b_{7e}^{(3)} & b_{7o}^{(1)} + b_{7o}^{(3)} \\ b_{8e}^{(2)} + b_{8e}^{(1)} & b_{8o}^{(2)} + b_{8o}^{(1)} \\ b_{9e}^{(3)} + b_{9e}^{(2)} & b_{9o}^{(3)} + b_{9o}^{(2)} \end{pmatrix} \begin{pmatrix} r \\ r_o \end{pmatrix} = \begin{pmatrix} 0 \\ 0 \\ 0 \end{pmatrix} \quad (\text{A.13})$$

or symbolically

$$[B_e | B_o] \begin{pmatrix} r \\ r_o \end{pmatrix} = 0 \quad (\text{A.14})$$

The values of  $r_o$  which will satisfy these compatibility conditions are obtained by solving (A.14), i.e.

$$r_o = -B_o^{-1} B_e r = L r \quad (\text{A.15})$$

Substituting the slope continuity constraint of (A.15) into (A.11), the fully compatible displacement field in the three subelements becomes

$$\begin{pmatrix} u^{(1)} \\ u^{(2)} \\ u^{(3)} \end{pmatrix} = \begin{pmatrix} \phi_e^{(1)T} \\ \phi_e^{(2)T} \\ \phi_e^{(3)T} \end{pmatrix} + \begin{pmatrix} \phi_o^{(1)T} \\ \phi_o^{(2)T} \\ \phi_o^{(3)T} \end{pmatrix} L \{r\} = \begin{pmatrix} \hat{\phi}^{(1)T} \\ \hat{\phi}^{(2)T} \\ \hat{\phi}^{(3)T} \end{pmatrix} \{r\} \quad (\text{A.16})$$

Explicit expressions of these functions for subelement 3 are

$$\hat{\phi}_{o1}^{(3)} = \zeta_1^2 (3 - 2\zeta_1) + 6\mu \zeta_1 \zeta_2 \zeta_3 + \zeta_3^2 [3(\lambda_2 - \mu_1)\zeta_1 + (2\mu_3 - \lambda_2)\zeta_3 - 3\mu_3 \zeta_2]$$

$$\begin{aligned}\hat{\Phi}_{u_{x_1}}^{(3)} &= \zeta_1^2(a_3\zeta_2 - a_2\zeta_3) + (a_3\mu_3 - a_1)\zeta_1\zeta_2\zeta_3 \\ &+ \frac{1}{6}\zeta_3^2[3(2a_1 - a_3\mu_3 - a_2\lambda_2)\zeta_1 + 3(a_1 - a_3\mu_3)\zeta_2 + (-3a_1 + 2a_3\mu_3 + a_2\lambda_2)\zeta_3]\end{aligned}$$

$$\begin{aligned}\hat{\Phi}_{u_{y_1}}^{(3)} &= \zeta_1^2(b_2\zeta_3 - b_3\zeta_2) + (b_1 - b_3\mu_3)\zeta_1\zeta_2\zeta_3 \\ &+ \frac{1}{6}[\zeta_3^2[3(-2b_1 + b_3\mu_3 + b_2\lambda_2)\zeta_1 + 3(b_3\mu_3 - b_1)\zeta_2 + (3b_1 - 2b_3\mu_3 - b_2\lambda_2)\zeta_3]\end{aligned}$$

$$\hat{\Phi}_{u_2}^{(3)} = \zeta_2^2(3 - 2\zeta_2) + 6\lambda_3\zeta_1\zeta_2\zeta_3 + \zeta_3^2[3(\mu_1 - \lambda_3)\zeta_2 + (2\lambda_3 - \mu_1)\zeta_3 - 3\lambda_3\zeta_1]$$

$$\begin{aligned}\hat{\Phi}_{u_{x_2}}^{(3)} &= \zeta_2^2(a_1\zeta_3 - a_3\zeta_1) + (a_2 - a_3\lambda_3)\zeta_1\zeta_2\zeta_3 \\ &+ \frac{1}{6}\zeta_3^2[3(a_3\lambda_3 - a_2)\zeta_1 + 3(a_1\mu_1 + a_3\lambda_3 - 2a_2)\zeta_2 + (3a_2 - a_1\mu_1 - 2a_3\lambda_3)\zeta_3]\end{aligned}$$

$$\begin{aligned}\hat{\Phi}_{u_{y_2}}^{(3)} &= \zeta_2^2(b_3\zeta_1 - b_1\zeta_3) + (b_3\lambda_3 - b_2)\zeta_1\zeta_2\zeta_3 \\ &+ \frac{1}{6}\zeta_3^2[3(b_2 - b_3\lambda_3)\zeta_1 + 3(-b_1\mu_1 - b_3\lambda_3 + 2b_2)\zeta_2 + (-3b_2 + b_1\mu_1 + 2b_3\lambda_3)\zeta_3]\end{aligned}$$

$$\hat{\Phi}_{u_3}^{(3)} = \zeta_3^2[3(1 + \mu_2)\zeta_1 + 3(1 + \lambda_1)\zeta_2 + (1 - \mu_2 - \lambda_1)\zeta_3]$$

$$\hat{\Phi}_{u_{x_3}}^{(3)} = \frac{1}{6}\zeta_3^2[3(a_1 + 3a_2 + a_3\mu_2)\zeta_1 - 3(3a_1 + a_2 + a_3\lambda_1)\zeta_2 + (a_1\lambda_1 - a_2\mu_2)\zeta_3]$$

$$\hat{\Phi}_{u_{y_3}}^{(3)} = \frac{1}{6} \zeta_3^2 [-3(b_1 + 3b_2 + b_2 \mu_2) \zeta_1 + 3(3b_1 + b_2 + b_1 \lambda_1) \zeta_2 - (b_1 \lambda_1 - b_2 \mu_2) \zeta_3]$$

$$\hat{\Phi}_{u_{n_4}}^{(3)} = -4 \frac{A}{3l_3} [6\zeta_1 \zeta_2 \zeta_3 + \zeta_3^2 (5\zeta_3 - 3)]$$

$$\hat{\Phi}_{u_{n_5}}^{(3)} = -4 \frac{A}{3l_1} [\zeta_3^2 (3\zeta_2 - \zeta_3)]$$

$$\hat{\Phi}_{u_{n_6}}^{(3)} = -4 \frac{A}{3l_2} [\zeta_3^2 (3\zeta_1 - \zeta_3)] \quad (A.17)$$

The above set of interpolants is applicable to all points lying in subtriangle 3. For points lying in subtriangle 1 and 2,  $\{\hat{\Phi}^{(1)}\}$ ,  $\{\hat{\Phi}^{(2)}\}$  can be written down by cyclic permutation of all subscripts and superscripts in (A.17). All the symbols on the right side of (A.17) relate to the complete triangle.

## LIST OF SYMBOLS

A list of the most commonly used symbols and their general meaning follows.

$a, b$	Global dimensions of a triangle
$A$	Area of triangle
$A_i$	Area of subtriangle $i$
$B_i$	Material constants
$\bar{C}_{ij}$	Components of the stiffness matrix in the global coordinate system
$C_{ij}$	Components of the stiffness matrix in the material coordinate system
$\bar{S}_{ij}$	Components of the compliance matrix in the global coordinate system
$S_{ij}$	Components of the compliance matrix in the material coordinate system
$\bar{Q}_{ij}$	Components of the transformed reduced stiffness matrix
$Q_{ij}$	Components of the reduced stiffness matrix
$d_i$	Projection of a corner of a triangle over opposite side
$D_{11}$	Inversion of $\bar{Q}_{11}$
$D_{12}, D_{21}, D_{22}$	Components of the reduced material compliance matrix
$E$	Young's moduli

$f_i$	Cartesian components of the body force vector
$h_i$	Triangle heights
$h$	Lamina thickness
$K_{ij}$	Elements of Stiffness matrix
$l_i$	Triangle side lengths
$N$	Normal to boundary
$A$	Linear operator or matrix of linear operators on a region $R$
$C$	Linear operator or matrix of linear operators on the boundary of $R$
$D$	Domain of operator $A$
$E^n$	$n$ -dimensional Euclidean space
$R$	Open connected region in $E^n$
$S$	Boundary of $R$
$S_1, S_2$	Complementary subset of $S$
$\bar{R}$	Closure of $R$
$n_i$	Local cartesian components of the unit normal to a surface
$s_i$	Local cartesian components of the unit tangential to a surface
$R_i$	Open connected subregion of $R$
$\partial R_i$	Boundary of subregion $R_i$
$\sigma_{ij}$	Cartesian components of the stress tensor
$u_i$	Cartesian components of the displacement vector
$t_i$	Cartesian components of the traction vector



$t_i$	Cartesian components of the prescribed traction vector
$\delta_{ij}$	Kronecker's delta
$E_{ijkl}$	Cartesian components of the isothermal elasticity tensor
$\phi$	Interpolation functions
$u^m$	Assumed displacements in element m
$q^m$	Assumed generalized nodal displacements at the boundary of element m
$r^m$	Assumed generalized nodal displacements internal to element m
$e^m$	Vector of strains in element m deriving from $u^m$
$K$	Stiffness matrix
$F$	Load vectors
$x, y, z$	Cartesian coordinates in $E^3$
$\nu$	Poisson's ratio
$G$	Shear moduli
$\epsilon$	Components of infinitesimal or linear strain tensor
$\xi$	Natural coordinate
$\theta'$	Rotation angle from global axis $x$ to material axis 1
$T_i$	Transformation matrix
$e_o$	Applied uniform strain loading
$u$	Displacement component in x-direction
$v$	Displacement component in y-direction
$w$	Displacement component in z-direction

$U$	Displacement function in x-direction
$V$	Displacement function in y-direction
$W$	Displacement function in z-direction
$\theta$	fiber orientation
$\lambda, \mu$	Geometric parameters
$\Omega$	Linear functional
$G$	Displacement-stress transformation matrix for corner node
$H, L$	Displacement-stress transformation matrix for mid-side node
$B_K$	Bilinear mapping on $V_K \times V_K$
$l_{ij}$	Coordinate transformation tensor